12-2010

# Design and implementation of an actively adjustable spring mechanism via redundant actuation

Eleazar Marquez
*The University of Texas Rio Grande Valley*, eleazar.marquez01@utrgv.edu

# DESIGN AND IMPLEMENTATION OF AN ACTIVELY ADJUSTABLE SPRING MECHANISM VIA REDUNDANT ACTUATION

A Thesis

by

ELEAZAR MARQUEZ

Submitted to the Graduate School of the
University of Texas-Pan American
In partial fulfillment of the requirements for the degree of

MASTER OF SCIENCE

December 2010

Major Subject: Mechanical Engineering

# DESIGN AND IMPLEMENTATION OF AN

# ACTIVELY ADJUSTABLE SPRING MECHANISM

# VIA REDUNDANT ACTUATION

A Thesis
by
ELEAZAR MARQUEZ

COMMITTEE MEMBERS

Dr. Robert A. Freeman
Co-Chair of Committee

Dr. Horacio Vasquez
Co-Chair of Committee

Dr. Javier A. Kypuros
Committee Member

Dr. Dumitru I. Caruntu
Committee Member

December 2010

## ABSTRACT

Marquez, Eleazar, Design and Implementation of an Actively Adjustable Spring Mechanism via Redundant Actuation. Master of Science (MS), December, 2010, 213 pp., 38 tables, 72 figures, references, 33 titles, 2 appendices.

This study presents the theoretical results and experimental validation of an adjustable stiffness mechanism. The use of redundant actuation is emphasized in the design of a one degree-of-freedom Watt II mechanism capable of independently controlling the effective stiffness without a change in equilibrium position. This approach is in contrast to previous spring mechanism designs unable to actively control the spring rate independent of deflection, and has potential applications in various types of suspension and assembly systems. Results indicate that driving the redundantly actuated, unidirectional, spring mechanism requires attaching two direct brush-type direct current motors on each of the two grounded revolute joints, and that the concept of adjustable springs has proven to be valid regardless of the friction effects. The torques are controlled with corresponding power amplifiers which incorporate current control loops, and the effective stiffness of the system is dependent on the redundant actuator torques of the motors.

# DEDICATION

It is an honor to dedicate this Thesis to my wonderful and lovely family who has been an inspiration in my life. Mom and Dad, you have instilled the greatest education by teaching me responsibility, discipline, hard work, respect, and integrity. These values have taken me to accomplish what I am today, thank you for your support and love, but most importantly, thank you for believing in my dreams.

The completion of this work would not have been possible without Jesus Christ, my Lord and Savior. Jesus, it is by your grace and mercy that I have reached this point in my life, thank you for all the blessings you have given me throughout the years. To you the glory, honor, and power.

# ACKNOWLEDGMENTS

As a graduate student, I had the fortune to work under the supervision of two top class Mechanical Engineers, Dr. Robert A. Freeman and Dr. Horacio Vasquez. I am deeply grateful with Dr. Freeman for giving me an opportunity to conduct research in his area of expertise and for supporting me financially. In my first semester of graduate school, he gave me a chance to continue working on one of his major projects without knowing me very well, and I must say that there are few people in this world that can trust you like that. He was also the first person that introduced me to the concept of redundant actuation, and I have to admit that every time we discussed the subject, I was amazed by his knowledge. It was just an honor to have worked with him.

In a similar manner, I would like to appreciate Dr. Vasquez for all of his hard work and dedication on this project. I must say that he is an expert in taking an idea and making it work. The first time I met with him to discuss about the project, he was able to immediately give me feedback. It was a great honor to have him as an advisor on my thesis project, I learned many techniques and ideas that helped me complete what was required. At this time, I would also like to thank the rest of the committee members that in one way or another contributed to my project and graduate education: Dr. Dumitru I. Caruntu and Dr. Javier A. Kypuros. Lastly, I want to thank the Graduate Coordinator of the Mechanical Engineering Department, Dr. Tarawneh, for being the first person to open doors for me and for being of great help throughout my graduate education.

TABLE OF CONTENTS

Page

LIST OF TABLES

Page

LIST OF FIGURES

Page

# CHAPTER I

# INTRODUCTION

The objective of this study is to model and simulate an actively adjustable, unidirectional, spring mechanism based on the concept of redundant actuation (Figure 1.1). Theoretical computations of the nonposition, dependent planar mechanism will be validated by developing, implementing, and testing a physical model. In previous research, a one degree-of-freedom Stephenson III linkage [33] has been theoretically modeled and simulated to achieve a desired effective stiffness via redundant actuation yet lacks the development and testing of a physical model to validate its performance. This accounts for research to be taken into the next phase.

In this study a one degree-of-freedom, unidirectional, Watt II linkage will be implemented instead of the Stephenson III linkage. The idea is to reduce the kinematic and kinetic equations by reducing the number of links on the mechanism and yet generate equivalent results. The linkage or kinematic chain is composed of a planar, four revolute-four bar mechanism (D111), which contains two grounded revolute joints, and by a slider-crank mechanism (D011), which contains a prismatic joint that allows the mechanism to modulate along the horizontal axis. This output linear displacement slider is used as a reference source to determine the effective stiffness of the system generated by the internal loads.

In order to obtain a desired effective stiffness from the actively adjustable spring mechanism two steps must be accomplished. First, the geometric design and motion analysis of the Watt II linkage must be determined through the incorporation of the kinematic and kinetic

equations (Basic Kinematic Relationship's). Secondly, the two input forces (torques) *must* be integrated into the system to meet the concept of redundant actuation. These two forces are applied on the spring mechanism in the form of torque and are generated in an opposite direction of each other. On the other hand, physically driving the redundantly actuated mechanism requires attaching two direct brush-type direct current (DC) motors on each of the two grounded revolute joints. The torques on the motors are controlled with corresponding amplifiers which incorporate current control loops.

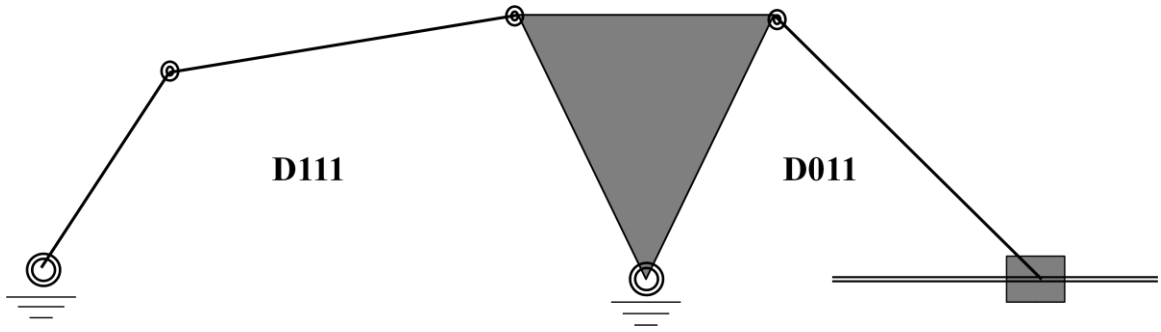


**Figure 1.1: Watt II Mechanism (Spring)**

Additionally, to achieve a desired effective stiffness of the system, an output linear displacement slider (prismatic joint) is used as a reference source, which is totally dependent on the redundant actuator torques of the DC motors. To measure such step experimentally, an external force is applied on the prismatic joint to obtain the stiffness of the mechanism according to the calculated equilibrium torques. As a result, a linear potentiometer and a force sensor will be implemented to determine the displacement of the slider element as a function of the external force acting on it and its stiffness as set by the input torques from the motors.

A distinguishing feature of implementing redundant actuation is that the Watt II linkage is capable of independently controlling the effective stiffness without a change in equilibrium

position and adjust continuously independent of position. How is this accomplished? In order to control the effective stiffness of the system without a change in (equilibrium) position, two equilibrium input torques are required. For example, consider the Watt II mechanism in Figure 1.1. If the equilibrium input torques are incremented, the configuration is going to remain intact, but the stiffness of the system is going to increase. This approach is in contrast to previous spring mechanism designs unable to actively control the spring rate independent of deflection. This is important because in many applications, the spring mechanism does not have to be replaced in order to increase or decrease the spring rate, only the input torques are modified to obtain the desired effective stiffness. However, one of the disadvantages of implementing redundant actuation is primarily the cost since more actuators are needed to drive the system and consequently, more energy is being consumed by the system. Nonetheless, redundant actuation has potential applications in various types of suspension and assembly systems. The incorporation of redundant actuation is the essence that permits the system to behave as a spring mechanism.

It is in the robotics community that redundant actuated systems have begun to receive major attention. This is due to the fact that redundantly actuated systems have more force inputs than they have kinematic degrees of freedom. For instance, the requirement of “tight” coordination of dual/multiple mechanical manipulators in numerous robotic applications has led to this interest. Such applications involve the transportation of heavy objects in such manner that load distribution among arms is targeted, to complex geometrical shape assemblies where multiple arms is favorable. Additionally, recent robotic mechanisms containing closed-loops in their structure incorporate redundant actuation as part of the design and functionality.

Applications of such fall under five technological categories according to the type of task performed by redundancy, and can be observed in Table 1.1.

The task addressed in category one is *load sharing/balancing* (LS/B) among the actuators [2, 3, 10, 15, 22]. This application is found in robotic systems that contain multiple chains or multiple linkages. For example, consider a manipulator or robotic arm. In this case, redundant actuation targets to distribute the required operational load to each of the system actuators optimally by maintaining load requirements within an operational range. Several of these include Dual Arms (DA), Walking Machines (WM), and manipulators with Direct Drive (DD) substructures.

In addition, redundant actuation has potential application *Disturbance force rejection* (DFR) [31, 30]. The goal in this case is for one actuation set to supply the required input load for the nominal task to be executed, while the redundant input set opposes the disturbance loads. For example, consider a manipulator grabbing a bowling ball. As said, one set of actuators is going to supply the necessary load to carry out the task, but once the bowling ball is grabbed, the manipulator will tend to drop due to the mass. Therefore, the redundant inputs counteract such disturbance loads. Multiple load paths to ground, Braced Arms (BA), and In-Parallel Structured Machining Arms (MA) embrace this category.

In category three redundant actuation is linked to *internal load control* [11, 18, 19, 20, 23, 27]. High internal loading is a harmful factor in spatial mechanisms, resulting in excessive joint fastening and bending of the linkages. Therefore, in robotic systems the internal loads imparted to the grasped object need to be accurately controlled for two reasons. Foremost, if such loads are well controlled the desired motion of the object is achievable and secondly,

damage to the object or system are evitable. Applications include Dual Arms (DA), Walking Machines (WM), Robotic Hands (H), and Zero-Backlash Geared Drives (GD).

**Table 1.1: Technological Needs**

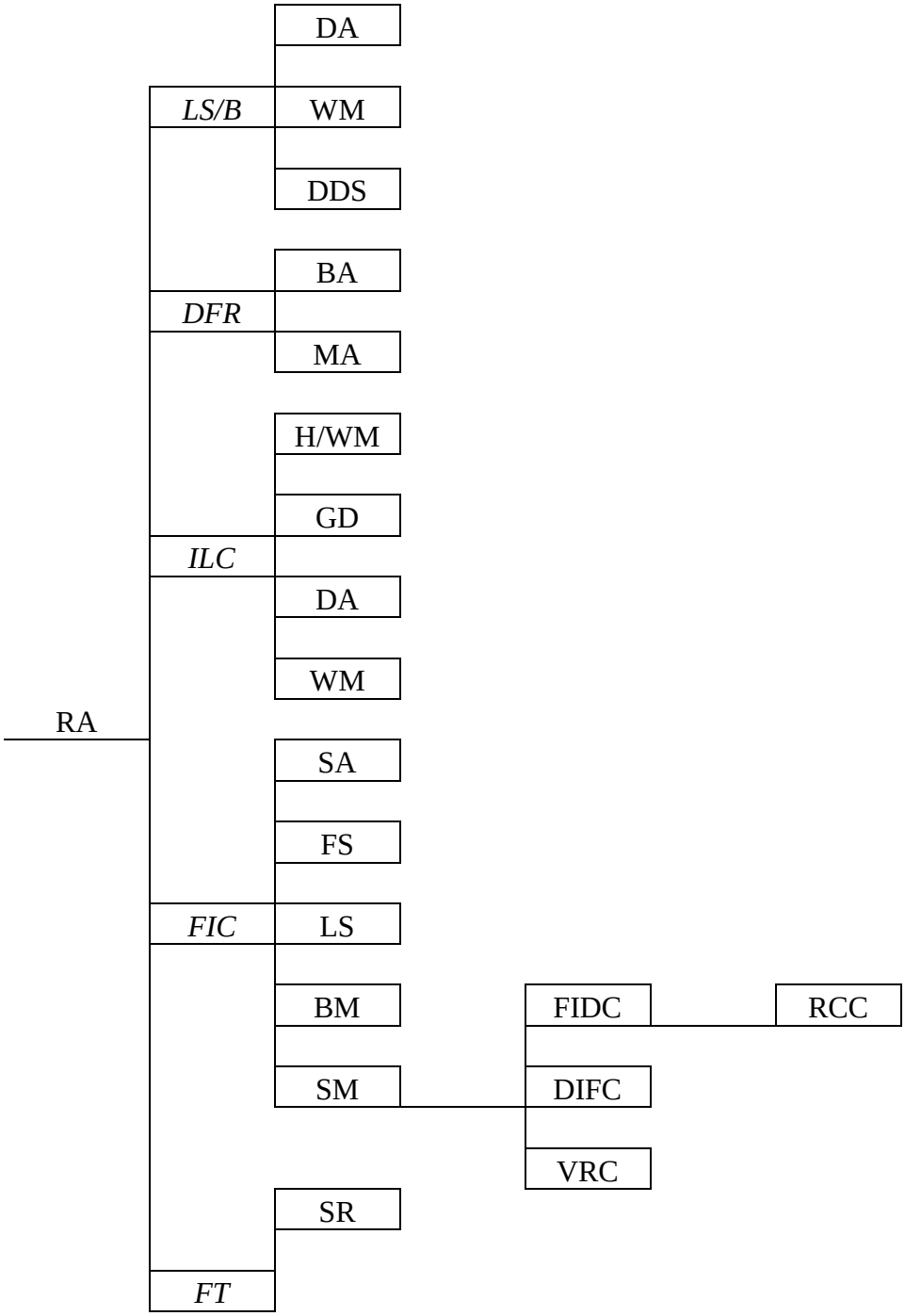

Furthermore, redundant actuation is considered in *feedforward impedance control* (FIC) in the fourth category [4, 12, 13]. The purpose of impedance control is to work with instabilities encountered in contact tasks such as multi-limbed locomotion and machining and assembly operations. Applications involucrate Serial Arms (SA), Flexible Structures (FS), Magneto and Electro-Static Levitation Systems (LS), Bio-Mechanical Prostheses (BM) and Spring Mechanisms (SM). Lastly, *Fault-tolerance* (FT) [25] is addressed in category five, where the incorporation of additional actuators is the aim in providing continuous satisfactory performance in case individual actuators fail.

Moreover, redundant actuation has potential application in the design and control of active automotive suspension systems. A research was performed by Freeman [5] on a frontal plane half-car, double A-arm, independent suspension model which was referenced to a set of global motion parameters, attached to the chassis, resulting in a two degrees-of-freedom coplanar mechanism. Results indicate that the two motion directions and three stiffness components require five actuators to effectively control the stiffness on the suspension system. This is important since a smoother ride on a vehicle can be generated without having to replace the entire suspension system. The integration of redundant actuation was validated through numerous simulations in Working Model 2D.

Although the advantage of implementing redundant actuation into several applications has been discussed, no experimental validation exists. The concept is promising in many aspects, but the question remains on how a system will behave physically. Therefore, the purpose of this study is to design, construct, and actively control a one degree-of-freedom Watt II linkage and verify the concept of redundant actuation. Theoretical computations of the nonposition dependent planar mechanism will be validated by developing and testing a physical model.

Additionally, it is important to mention that this study is of great importance for future robotic mechanisms that will be designed based on the concept of redundant actuation. The idea is that with the verification of the one degree-of-freedom mechanism, more complicated mechanisms can be generated or designed. For example, several of these mechanisms include two and three degree-of-freedom planar mechanisms, three degree-of-freedom spherical spring mechanisms, and eventually six degree-of-freedom spatial mechanisms.

With this said and understood, Chapter II will initiate by defining the concept of adjustable spring mechanisms and its applications. In a similar manner redundant actuation will be defined to comprehend its integration and the effects on the kinematics of the planar mechanism. Design and complete derivations of the unidirectional spring mechanism will embrace Chapter III with a breakdown of the two dyads composing the Watt II linkage. In particular, the design of the linkage will be divided into two phases. In phase one, the geometric design will be generated in terms of determining the equilibrium state of the mechanism, and in phase two the motion of the system will be analyzed. The implementation of redundancy to achieve the desired stiffness by means of Euler-Lagrange equations will be illustrated in Chapter IV. In Chapter V, a detailed process is devoted to the development of the physical device including set up, material and instrument selection. Additionally, a preliminary test will be conducted to observe how the system behaves in a static situation and to anticipate the behavior of the real system. Consequently, experimental results obtained will be assessed in Chapter VI and compared with the theoretical (Working Model simulation) data previously computed. In Chapter VII, lastly, conclusions will be formulated based on the comparison between the results.

# CHAPTER II

# VARIABLE STIFFNESS MECHANISM

Before attempting to arrive at a solution, it is important to define and understand the concept of adjustable springs and the idea of redundant actuation. For example, the concept of an actively adjustable, unidirectional, spring mechanism is unique for three reasons [33]. First, the device is capable of independently controlling the effective stiffness without a change in equilibrium position and adjust continuously independent of position/deflection. This means that the mechanism may be utilized for numerous applications where distinctive loads may be accounted for while the system remains at equilibrium. Second, the output stiffness is programmed and controlled prior to the operation without the measurement of external forces, reducing the control command computation required [12]. The advantage is that this feature allows the spring mechanism to react quicker than feedback based systems. For instance, a suspension system may be adjusted and controlled prior to operation to have a smoother ride. Lastly, the third distinction involves the incorporation of redundant actuation which permits the modulation of the spring mechanism.

Since the present study involves designing and analyzing a spring mechanism, five application categories will be introduced in a detailed manner in section 2.1, preceded by defining redundant actuation and its integration into the system. In section 2.3, lastly, the establishment of the equilibrium equation based on the principle of virtual work will be discussed to initiate the design process of the Watt II mechanism and consequently determine

the desired effective stiffness of the system. At this point, it is of great importance to understand the meaning of desired effective stiffness since the term will appear frequently on the next couple of chapters. The desired effective stiffness of the mechanism is the stiffness at the equilibrium position.

## 2.1 Application Categories of Spring Mechanisms

The study of springs, traditionally, has been divided into five categories according to the performance of the spring mechanism in different situations. For example, the five categories include static force balancing, inertial load balancing, energy storage, vibration resonance control (VRC) and isolation, and positioning error correction.

### 2.1.1 Category 1

Spring mechanisms are embraced for *static force balancing* in the first category. For example, spring mechanisms situated on devices such as trunk doors, automobile hoods, overhead doors, and reclining chairs have extensively been utilized to counteract the weight [9, 28]. In this case, if the spring mechanism is to be removed from such applications, the load would not be resisted at all. Similarly, under this class of spring devices lies the recognized suspension system. The springs on a suspension system allow the vehicle to ride in a smooth, clean manner. Nonetheless, a complex focus is the determination of equilibrium configuration resulted by the intricate loading situations. Moreover, load balancing has become quite difficult to understand in the human body [24]. Such implications in the musculoskeletal system are birth due to the muscles containing non-linear stiffness characteristics, and yet remain a challenge subject [8]. The compensation for gravity loads is indeed a further application resulting from static force balancing group.

### 2.1.2 Category 2

*Inertial load balancing* incorporates the second category of spring mechanisms [3, 17]. These springs are incorporated in high speed mechanisms to reduce speed fluctuations by inertial forces. One example in this category is a suspension system on any type of vehicle. When a vehicle is traveling on a bumpy road, it will tend to fluctuate vertically for quite some time. However, the suspension system on the vehicle is able to balance those inertial loads and consequently the vehicle will run smoothly again.

### 2.1.3 Category 3

Category three brings forth a diverse area of spring mechanisms implying *energy storage*. The integration of such devices is visible in mass-spring devices such as suspension systems and non-linear circuit breaker designs [14]. However, this area is in continuous research due to its complexity.

### 2.1.4 Category 4

The fourth category catalyzes spring mechanisms applied in *vibration resonance control* (VRC) *and isolation*. Previous researchers attempted to adjust frequency to approach a considerable solution; however, the use of passive springs diminished the range of testing. For instance, Lakshminaroyana and Dizioglu [16] synthesized spring restrained mechanisms maintaining a fixed natural frequency over varied amplitudes. Srinath and Karmaker [26] studied nonsinusoidally excited vibratory conveying systems while Welch [29] incorporated passive springs to accomplish special natural frequency relationships in shaking conveyor systems.

### 2.1.5 Category 5

The concept of adjustable spring mechanism, which is the focus of this study, is largely addressed under the fifth category. Springs in such class have been utilized to correct for

*positioning error* of the end-point of a robot by allowing for controlled, force induced, displacement (FIDC) of the end-point, as desired for automated insertion tasks. To achieve such task, passive spring mechanisms known as Remote Center Compliance (RCC) devices [4, 15, 32] were developed. Nonetheless, due to passive nature of these mechanisms current technology is assigned restrictly to specific designs that target minimal modulation. As a result of passive spring mechanisms, the creation of the Instrumented Remote Center Compliance (IRCC) devices have originated, however they contain a slow response.

## 2.2 Redundant Actuation in Spring Mechanisms

Until this point, the concept of redundant actuation has not been well defined and may cause confusion in the upcoming sections and chapters if not discussed. Redundant actuated linkages have more force inputs (actuators) than kinematic (motion) degrees of freedoms. For instance, the system under investigation in this study is a one degree-of-freedom mechanism, which denotes that the linear displacement slider is only allowed to modulate in one direction. This means that in order to achieve redundancy, two or more force inputs *must* be incorporated into the spring mechanism. If a two degree-of-freedom mechanism would have been used, then three or more force (torque) inputs would be needed to satisfy the concept of redundant actuation. On the other hand, if a six degree-of-freedom mechanism would have been implemented, then seven or more force input would be needed to satisfy redundancy. In this case, the two force inputs are implemented at the two grounded revolute joints of the Watt II linkage (Figure 2.2), and are represented by the output torque generated by the motors. Traditionally, in a four revolute-four bar mechanism only one force input (crank) is incorporated

to determine and analyze the behavior of the system. However, in order to create a system that behaves as a spring, this traditional approach is ineffective.

With the use of redundancy, the objective to actively control the internal load state of the mechanism can be achieved. Therefore, an effective stiffness is created similar to that of a wound metal spring as a consequence of internal loading and its association with the non-linear linkage geometry. In addition, it is significant to mention that in order to generate an effective stiffness mechanism, the two force (torque) inputs *must* be in opposite direction of each other.

The ability for the spring mechanism to be modulated prior to operation cannot take forth without redundant force inputs, disregarding the consideration of elemental springs as inputs. This, as mentioned before, portrays that the one degree-of-freedom Watt II linkage developed in the present research *must* contain at least two force inputs. In conclusion, by properly coordinating the redundant actuator efforts (force) the desired effective stiffness is created and actively adjusted.

## 2.3 Equilibrium Equation for Watt II Linkage

In this section, a mathematical equation is established based on the principle of virtual work to obtain a system that is in an equilibrium state. Another approach to such calculation is to implement Newton's second law of motion and determine the reaction forces acting on each link; however, a slight computational error in this procedure may result in an incorrect solution. Therefore, utilizing the principle of virtual work eliminates the possibility of containing an error in the equations, yet it produces an equivalent outcome.

The actively adjustable Watt II linkage under investigation is represented in Figure 2.1, and it is composed of two dyad-based planar mechanisms. The first dyad (D111) consists of a

four revolute-four bar mechanism, which contains two grounded revolute joints, and the second one (D011) consists of a slider-crank mechanism, which contains a prismatic joint. The output linear displacement slider (prismatic joint) is used as a reference source to determine the effective stiffness of the system, and is totally dependent on the torques of the motors. Driving the redundantly actuated mechanism requires attaching two motors on each of the two grounded revolute joints (point O and point C), which then generates an effective stiffness due to the internal loading of the system. Therefore, such linkage is able to independently modulate the stiffness without a change in equilibrium position. What does this mean? It means that if the equilibrium input forces (torques) are increased, the configuration is going to remain intact, but the stiffness as a result will increment.

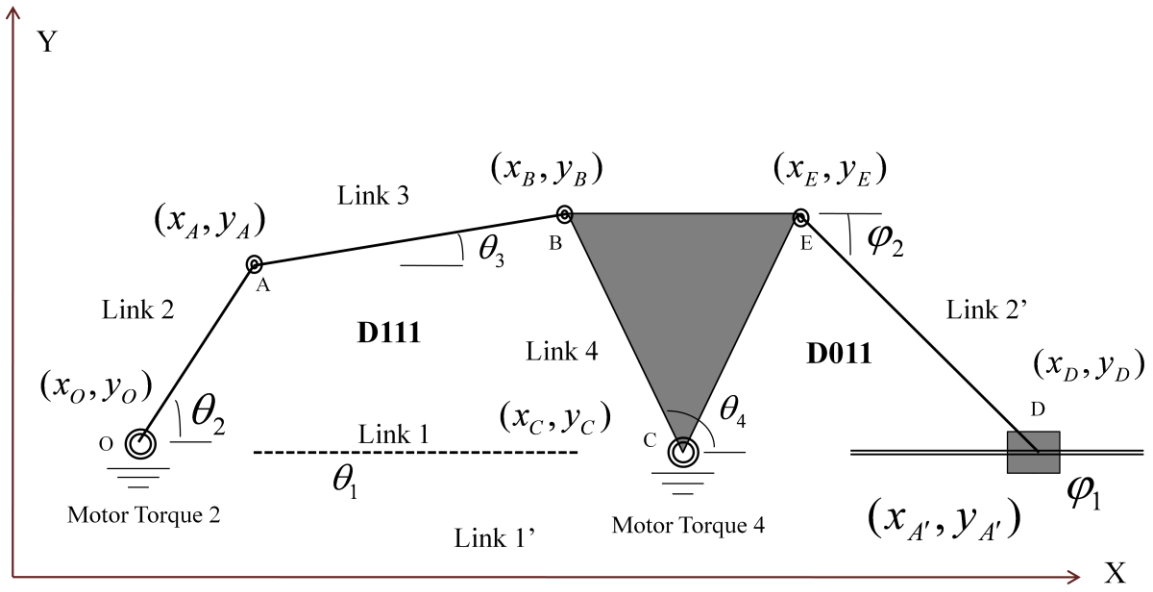


**Figure 2.1: Watt II Linkage**

Furthermore, the equilibrium state of the Watt II linkage can be obtained from the D111 four revolute-four bar mechanism (Figure 2.2), as it contains the two force (torque) inputs

necessary for redundancy. As mentioned, the two input forces (torques) *must* be incorporated in opposite direction of each other to generate a redundantly actuated system. However, these forces *must* be applied in the adequate direction or else the system will not create the internal loading necessary to produce an effective stiffness mechanism. Therefore, the force generated at $\theta_2$ must be applied in a counterclockwise direction, and the force generated at $\theta_4$ must be applied in a clockwise direction. If such forces are applied in the opposite direction, the system will generate a substantial amount of force on Link 3 that causes the mechanism to buckle.

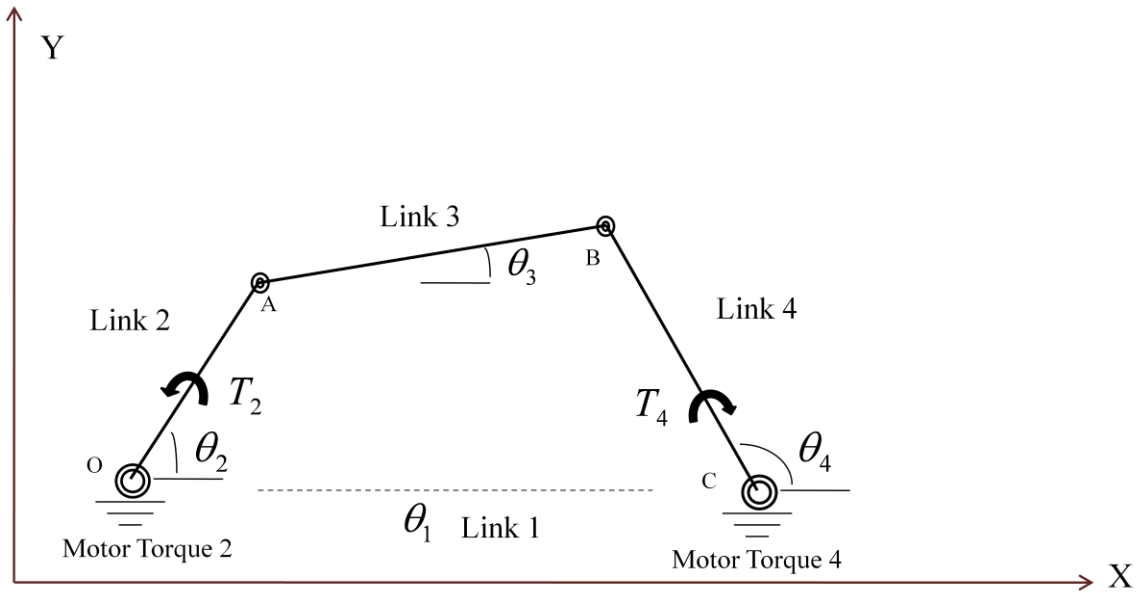


**Figure 2.2: Dyad-111**

Since the four revolute-four-bar mechanism has a one degree-of-freedom of motion, its kinematic state is completely defined by a single parameter $\theta_2$, meaning that a single motor can control the equilibrium state. Nonetheless, if a non-zero input torque is applied, the mechanism will move according to its dynamics and will not be able to be in static equilibrium. Therefore, such setback calls for the implementation of redundant actuation in which the system contains

more force inputs than kinematic freedoms. The addition of a second motor at $\theta_4$ permits the linkage to sustain internal loads while remaining in static equilibrium.

### 2.3.1 Equilibrium of Watt II Linkage

Static equilibrium is determined by setting the effective load $T_{\theta 2}{}^*$ at the selected "minimum" joint set $\theta_2$ equal to zero and assuming gravity acts normal to the plane of the four revolute-four bar mechanism. In the previous sections, the term 'effective' has appeared frequently referring to the stiffness of the mechanism and it will continue to emerge from this point forward in terms of load and inertial. For example, what is meant by the term 'effective load' is the load 'felt' at the input due to all of the applied loads. Therefore, the equilibrium equation requires that

$$T_{\theta 2}{}^* = T_2 + (g_{42}) \cdot T_4 = 0 \tag{2.1}$$

where $g_{42}$ relates the angular velocity of Link 4 to that of Link 2, and $T_2$ and $T_4$ are the efforts (torque) of the actuated joints. Since the target is to control the effective stiffness without a change in equilibrium position, the effective load due to all loads *must* be zero, which means that the system is not changing with respect to time. Therefore, equation (2.1) *must* be equal to zero to incorporate a steady-state condition on the spring mechanism. According to such equation, an arbitrarily effort at either joint can be selected and place in equilibrium by providing a balancing effort (torque) on the opposite joint. Therefore, the internal load state of the linkage can be actively adjusted independent of its motion by controlling the redundant efforts.

The equilibrium equation (2.1) is obtained by equating the virtual work done by the effective load/generalized force $T_{\theta 2}{}^*$ at $\theta_2$ to that done by the externally applied loads. The general equation yields

$$T_{\theta 2}{}^{*} \cdot \delta_{\theta 2} = \sum_{P} \left( T_P \cdot \delta\theta_P + F_{PX} \cdot \delta X_P + F_{PY} \cdot \delta Y_P \right) \tag{2.2}$$

where the moment component $T_P$ and force components $F_{PX}$ and $F_{PY}$ are a set of *P* loads acting on motion parameters $\theta_P$, $X_P$, and $Y_P$. The effective load is then acquired by cancelling like terms and substituting for the displacements in terms of their g-functions.

In this study, it is important to point out that the velocity and acceleration components are expressed in terms of *g* and *h* function, respectively. These functions are known as the *Kinematic Influence Coefficient's* (KIC's) and represent the rate of change of the system with respect to time [1, 6, 7, 21]. For instance, consider the symbol *u* represent any/all dependent parameters and $\theta_i$ represent the independent reference/input parameter. The velocity of *u* is obtained by applying the Chain Rule and taking the first derivative with respect to time

$$\frac{d}{dt}u = \left( \frac{d}{d\theta_i}u \right) \cdot \frac{d}{dt}\theta_i \tag{2.3}$$

where the derivative of *u* with respect to $\theta_i$ is referred as the first order KIC, *g*-function, and is defined by

$$g_{ui} = \frac{d}{d\theta_i}u \tag{2.4}$$

and the velocity is represented as

$$\dot{u} = g_{ui} \cdot \dot{\theta}_i \tag{2.5}$$

Hence, the function $g_{42}$ in the equilibrium equation (2.1) represents the change in position (velocity) of Link 4 relative to the change in position of Link 2.

### 2.3.2 Concept of Effective Stiffness

Considering the four revolute-four bar mechanism in Figure 2.2, a set of equilibrium loads are necessary to determine the equilibrium position of the system. Once these loads are applied and the system is at an equilibrium state, the mechanism forms an internal load within. As a result of this internal load created, a desired effective stiffness can be generated as a function of an external disturbance (force or displacement) applied. However, if a disturbance is applied to the system the effective load will not be in equilibrium ($T_{\theta 2}{}^{*} \neq 0$), and the linkage configuration will change according to its dynamics as referred to $\theta_2$

$$\Delta\left(T_{\theta 2}{}^{*}\right) = \Delta\left(T_2 + g_{42} \cdot T_4\right) = T_4 \cdot \Delta\left(g_{42}\right) \tag{2.6}$$

This phenomenon relates to a force induced by an imposed displacement in a coil metal spring. Nonetheless, the desired effective stiffness is accomplished by the enforcement of redundant actuation.

### 2.3.3 Analytical Solution for Effective Stiffness

Thus far, only the concept of effective stiffness has been covered in terms of achieving it by means of the internal loads. On the other hand, in terms of an analytical solution, the effective stiffness is determined by the change in the effective load at $\theta_2$ as a consequence of the change in $g_{42}$

$$\Delta\left(T_{\theta 2}{}^{*}\right) \cong T_4 \cdot \left(\frac{dg_{42}}{d\theta_2}\right) \cdot \Delta\theta_2 \tag{2.7}$$

The change in effective load is taken from the differential change in force due to a differential change in displacement of the unidirectional spring (seen in Figure 2.3)

$$\Delta\left(F^{*}\right) = -K \cdot \Delta x \tag{2.8}$$

$\Delta x$ is the deflection and is represented by

$$x = x_{actual} - x_{freelength} \tag{2.9}$$

and *K* is the spring rate of the system. The initial position of the spring mechanism is referred as $x_{freelength}$ and the final position is referred as $x_{actual}$. The spring rate of the mechanism in this equation, as referenced to $\theta_2$, stands out from Equation (2.7) and yields

$$K_{\theta 2} = -T_{\theta 4} \cdot \left( \frac{dg_{42}}{d\theta_2} \right) = -T_{\theta 4} \cdot h_{42} \tag{2.10}$$

where $h_{42}$ is the constitutive relationship between effort and stiffness, and is a function of position.

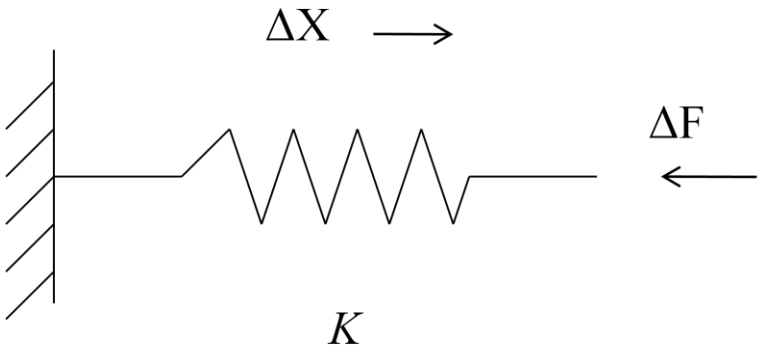


**Figure 2.3: Unidirectional Spring**

Mentioned earlier was the characterization of the velocity of the spring mechanism in terms of its KIC (g-function). The *h*-function resembled in Equation (2.10) also represents a KIC, and characterizes the acceleration of the Watt II linkage. For instance, the acceleration component is obtained by taking the second derivative of *u* with respect to $\theta_i$ from equation (2.3)

$$\frac{d^2}{dt^2}u = \left( \frac{d}{d\theta_i}u \right) \cdot \frac{d^2}{dt^2}\theta_i + \left( \frac{d^2}{d\theta_i^2}u \right) \cdot \left( \frac{d}{dt}\theta_i \right)^2 \tag{2.11}$$

where the acceleration component is represented as

$$\ddot{u} = g_{ui} \cdot \ddot{\theta}_i + h_{ui} \cdot \dot{\theta}_i^{\,2} \tag{2.12}$$

Consequently, the *h*-function known as the second order KIC is defined as

$$h_{ui} = \frac{d^2}{d\theta_i} u \tag{2.13}$$

where $h_{42}$ represents the acceleration of Link 4 with respect to the acceleration of Link 2. Obtaining this result, by means of applying the Chain Rule, indicates that the effective stiffness of the Watt II linkage is a non-linear function of displacement. Therefore, KIC are fundamental in the design process of the actively adjustable, unidirectional, spring mechanism and will be expressed in terms of position.

In summary, the implementation of redundant actuation into the Watt II linkage allows the system to behave as a spring mechanism by creating an effective stiffness. This is due to the internal loads generated when the equilibrium torques are applied on the motors placed at the two grounded revolute joints. As a result, the mechanism is capable of independently controlling the effective stiffness without a change in equilibrium position and adjust continuously independent of deflection. This approach is in contrast to previous spring mechanisms unable to effectively control the spring rate independent of deflection. In terms of analytically determining the effective stiffness of the system, the change in the effective load at $\theta_2$, as a consequence of the change in the $g_{42}$ function, is the primary factor for generating a non-linear spring mechanism. Therefore, the effective stiffness is achieved by specifying a desired spring rate and obtaining the necessary effort (torque) at $\theta_4$. Similarly, the efforts can be specified initially and then the effective stiffness can be determined based on the dynamic equations. With such information the torque required at $\theta_2$ is computable from the equilibrium equation.

# CHAPTER III

## DESIGN OF WATT II LINKAGE

In Chapter II, the concept of an actively adjustable, one degree-of-freedom, spring mechanism via redundant actuation was illustrated through the distinct categories developed as a consequence of diverse applications. Likewise, the effective stiffness of a four revolute-four bar mechanism was achieved as a result of the internal loading generated by the equilibrium motor torques. Nonetheless, until this point the equilibrium equation to determine the effective stiffness of the system has been obtained only in general terms, meaning that the lengths, angles, and position of the links have been omitted. Therefore, in this chapter the kinematic and kinetic equations will be implemented to determine the geometric design of the Watt II linkage and estimate its non-linear behavior. It is essential to point out that the design phase of the active spring mechanism is a two step process. First, the design of the four revolute-four bar (D111) is generated in terms of determining the equilibrium state of the system, then a new point is created to connect the D011 planar mechanism and form the linkage.

The target in these facets is to describe the motion of the dependent parameters in terms of position, velocity, and acceleration. Therefore, in order to obtain a mathematical expression for such case, a relationship between the dependent parameter and the torque inputs must be generated in terms of the KIC. Important to mention is the fact that the velocity and acceleration of a link can be computed in terms of its center of mass or relative to the ends of the rigid body. In this study, the g and h functions of the dependent parameters such as the links, joints, and link

angles will be calculated relative to the center of mass and described in terms of time.

Four sections embark the design of the Watt II linkage. In section 3.1, the geometric design of the four revolute-four bar mechanism is developed by implementing the kinematic and kinetic equations, and the motion of each link is described. Once the D111 has been developed, a new point will be created on the local reference frame of Link 4 to form a dyad plate design the rest of the kinematic chain, and the same process as the previous section is carried out. Based on the design parameters obtained from the mathematical expressions, a simulation in Working Model software will be generated to further analyze the behavior of the system when redundant actuation is applied. Lastly, a Pro-Engineer sketch is developed in section 3.4 that serves as a reference guide to fabricate the physical model of the spring mechanism.

## 3.1 D111 Design

### 3.1.1 Unsprung Position Analysis for the Four Revolute-Four Bar Mechanism

Before attempting to kinematically describe the motion of the four revolute-four bar mechanism, the first step is to determine the position of the links relative to each other as illustrated in Figure 3.1. For this process, it is vital to specify a two-dimensional global coordinate system (XY) that references the horizontal and vertical directions of the system. Initially, the position analysis of the D111 consists of specifying several design parameters such as the length of the links, the position of the two grounded revolute joints, and the initial angle of the input crank angle $\theta_2$. These parameters, as illustrated in Table 3.1, are not determined mathematically, instead they are arbitrarily considered by having in mind a reasonable size to fabricate the physical spring mechanism. In Figure 3.1, $(u_2, v_2), (u_3, v_3), (u_4, v_4)$ are a set of

reference frames established on each link to symbolically represent the distance of center of mass, however such calculations will be covered later on the chapter.

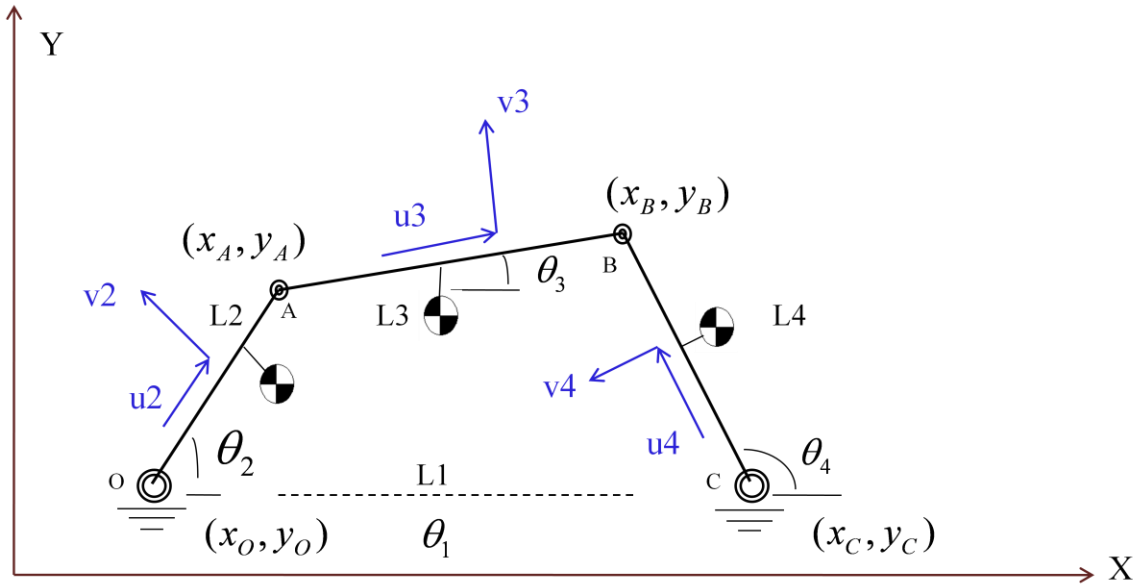


**Figure 3.1: Design Dyad**

In this case, there are three unknowns that must be solved once the design parameters have been specified on the four revolute-four bar mechanism. The length and angle of Link 1 must be determined first before solving for angles $\theta_3$ and $\theta_4$ known as the coupler angle and output angle, respectively, of the four revolute-four bar mechanism.

**Table 3.1: D111 Design Parameters**

| Units (m) | Units (m) | Units (m) | Units (m) |
|---|---|---|---|
| $X_O = 0$ | $X_C = 0.250$ | $L_2 = 0.102$ | $L_4 = 0.102$ |
| $Y_O = 0$ | $Y_C = 0$ | $L_3 = 0.153$ | $\theta_2 = 45^\circ$ |

Therefore, solving for length 1 involves considering point O and point C on the fixed frame (Figure 3.1). Determining the distance between revolute joint O and revolute joint C is simply calculating the magnitude of the two-dimensional vector as

$$L_1 = \sqrt{\left(Y_C - Y_O\right)^2 + \left(X_C - X_O\right)^2} \tag{3.1}$$

Once the length of Link 1 has been expressed, the relative angle of such link is simply determined by specifying the slope of the link using the trigonometric function

$$\tan\left(\theta\right) \tag{3.2}$$

where $\theta_i$ is calculated according to the position of the revolute joints in terms of their X and Y coordinates. It is significant to point out that such step to determine angle 1 is not necessary since the angle, according to the previously specified design parameters, is equal to zero as a consequence of the similarity in position between the two grounded joints along the Y direction. Nonetheless, each result obtained in the design process must be validated and expressed mathematically; therefore, rearranging equation (3.2) yields the desired angle

$$\theta_1 = \tan^{-1}\left(\frac{Y_C - Y_O}{X_C - X_O}\right) \tag{3.3}$$

The next phase of the unsprung position analysis is to determine the angles of Link 3 (coupler angle) and Link 4 (output angle) by implementing the method of *position loop equations*. In order to solve angle three and angle four, an initial condition must be specified to establish a relationship between the output angle and the input angle. Thies condition states that pivot A and pivot B must remain at a fixed distance throughout the motion of the system. In another words, the length of Link 3 must be constant throughout the motion of the system

$$\left(B - A\right)\cdot\left(B - A\right) - {L_3}^2 = 0 \tag{3.4}$$

Therefore, satisfying the initial condition involves implementing and expressing a series of constraint equations that define the position of the pivot B along its X and Y direction. In order to generate a *position loop equation* along the X direction of the linkage, the criteria requires a balance of links on each side of the pivot by equating $X_B = X_B$

$$X_O + L_2\cos(\theta_2) + L_3\cos(\theta_3) = X_O + L_1\cos(\theta_1) + L_4\cos(\theta_4) \tag{3.5}$$

In a similar manner, the *position loop equation* along the vertical direction is obtained by equating $Y_B = Y_B$ and implementing the adequate trigonometric functions as

$$Y_O + L_2\sin(\theta_2) + L_3\sin(\theta_3) = Y_O + L_1\sin(\theta_1) + L_4\sin(\theta_4) \tag{3.6}$$

Therefore, by cancelling $X_O$ and $Y_O$ from the respective expressions, the desired two equations and two unknowns are generated

$$L_2\cos(\theta_2) + L_3\cos(\theta_3) = L_1\cos(\theta_1) + L_4\cos(\theta_4) \tag{3.7}$$

and

$$L_2\sin(\theta_2) + L_3\sin(\theta_3) = L_1\sin(\theta_1) + L_4\sin(\theta_4) \tag{3.8}$$

Once attaining these constraints, the idea is to solve for $\theta_3$ , consequently, one approach to solve for such angle is to eliminate $\theta_4$ from the equations. Hence, what is done is that the terms that contain $\theta_4$ , from the *loop equations*, are isolated on the left hand side of the equation, and the other terms are written on the right hand side. As a result, equations (3.7) and (3.8) are rearranged to

$$L_4\cos(\theta_4) = L_2\cos(\theta_2) + L_3\cos(\theta_3) - L_1\cos(\theta_1) \tag{3.9}$$

and

$$L_4\sin(\theta_4) = L_2\sin(\theta_2) + L_3\sin(\theta_3) - L_1\sin(\theta_1) \tag{3.10}$$

To simplify these equations and further calculations, the symbol $S_i$ will represent $\sin(\theta_i)$, and the symbol $C_i$ will represent $\cos(\theta_i)$. This procedure is accomplished by expanding the expressions to form a single equation that will eliminate the output angle $\theta_3$, and allow for the solution of the coupler angle $\theta_4$. Therefore, such step involves combining and substituting the *position loop equations* into the initial condition. The end result yields a second-order polynomial or what is known as the Law of Cosines along the X and Y direction as

$$L_4^{\,2}C_4^{\,2} = L_2^{\,2}C_2^{\,2} + L_3^{\,2}C_3^{\,2} + L_1^{\,2}C_1^{\,2} + 2L_2L_3C_2C_3 - 2L_2L_1C_2C_1 - 2L_3L_1C_3C_1 \tag{3.11}$$

and

$$L_4^{\,2}S_4^{\,2} = L_2^{\,2}S_2^{\,2} + L_3^{\,2}S_3^{\,2} + L_1^{\,2}S_1^{\,2} + 2L_2L_3S_2S_3 - 2L_2L_1S_2S_1 - 2L_3L_1S_3S_1 \tag{3.12}$$

The single equation is then generated by adding both expressions as

$$\begin{aligned} L_4^{\,2}\left(S_4^{\,2} + C_4^{\,2}\right) &= L_2^{\,2}\left(S_2^{\,2} + C_2^{\,2}\right) + L_3^{\,2}\left(S_3^{\,2} + C_3^{\,2}\right) + L_1^{\,2}\left(S_1^{\,2} + C_1^{\,2}\right) + \\ &2L_3C_3\left(L_2C_2 - L_1C_1\right) + 2L_3S_3\left(L_2S_2 - L_1S_1\right) - 2L_2L_1\left(C_2C_1 + S_2S_1\right) \end{aligned} \tag{3.13}$$

where the outcome, as mentioned, is a second-order polynomial, which is expected since the equation for the effective stiffness in Chapter II is non-linear as well. In order to reduce this equation, two identities must be considered first: the Cosine Angle Sum and Difference Identity

$$\cos\theta_i \cos\theta_i \pm \sin\theta_i \sin\theta_i = \cos(\theta_i \pm \theta_i) \tag{3.14}$$

and the Pythagorean Trigonometric Identity

$$\cos^2\theta_i + \sin^2\theta_i = 1 \tag{3.15}$$

Therefore, implementing the identities gives the necessary equation to solve for the unknown angle $\theta_3$

$$L_4^{\,2} = L_2^{\,2} + L_3^{\,2} + L_1^{\,2} + 2L_3C_3\left(L_2C_2 - L_1C_1\right) + 2L_3S_3\left(L_2S_2 - L_1S_1\right) - 2L_2L_1C_{2-1} \tag{3.16}$$

With this equation at hand, the process of attaining a solution becomes tedious as a result of the number of terms involved. Therefore, to solve this second-order polynomial expression, the coefficients of $\sin\theta$ and $\cos\theta$ are gathered and a new constraint equation must be established to solve for the two roots. Solving for the two roots involves establishing the new constraint equation to represent $\sin\theta$ and $\cos\theta$ in terms of new variables and constants. Such constraint equation yields

$$PS_3 + QC_3 + R = 0 \tag{3.17}$$

where the constant coefficients are represented by *P*, *Q*, and *R* as

$$P = 2L_3\left(L_2S_2 - L_1S_1\right) \tag{3.18}$$

$$Q = 2L_3\left(L_2C_2 - L_1C_1\right) \tag{3.19}$$

and

$$R = {L_2}^2 + {L_3}^2 + {L_1}^2 - {L_4}^2 - 2L_2L_1C_{2-1} \tag{3.20}$$

Once the constant coefficients (*P*, *Q*, and *R*) have been specified, the next step is to represent the trigonometric functions $\sin\left(\theta_3\right)$ and $\cos\left(\theta_3\right)$ in terms of variables. This is accomplished by implementing the historical "Tangent Half-Angle" approach (Table 3.2), which allows for the trigonometric functions to be expressed in a quadratic form. The benefit of having a quadratic expression is that two possible roots are calculated for the unknown $\theta_3$. What is done since both Tangent Half-Angle identities contain $\tan\left(\frac{\theta_3}{2}\right)$, is to simplify them by expressing the respective trigonometric function in terms of a variable. Accordingly, the variable is denoted by $X = \tan\left(\frac{\theta_3}{2}\right)$ and yields

$$S_3 = \frac{2X}{1+X^2} \tag{3.21}$$

and

$$C_3 = \frac{1-X^2}{1+X^2} \tag{3.22}$$

**Table 3.2: Tangent Half-Angle Identity**

| | |
|---|---|
| $\cos 2\theta = \cos^2\theta - \sin^2\theta$<br>$= 2\cos^2\theta - 1$<br>$= 1 - 2\sin^2\theta$<br>$\cos(\theta_3) = \frac{1-\tan^2\left(\frac{\theta_3}{2}\right)}{1+\tan^2\left(\frac{\theta_2}{2}\right)}$ | $\sin 2\theta = 2\sin\theta\cos\theta$<br>$\sin(\theta_3) = \frac{2\tan\left(\frac{\theta_3}{2}\right)}{1+\tan^2\left(\frac{\theta_3}{2}\right)}$ |

Substituting these trigonometric functions into equation (3.17) gives a polynomial equation of second degree as

$$P\left(\frac{2X}{1+X^2}\right) + Q\left(\frac{1-X^2}{1+X^2}\right) + R = 0 \tag{3.23}$$

Now is only a matter of multiplying each term by its common denominator $1+X^2$ to simplify the equation

$$P(2X) + Q(1-X^2) + R(1+X^2) = (1+X^2) \tag{3.24}$$

Distributing each coefficient (P,Q, and R) and combining like terms results in the expression

$$(R-Q)X^2 + (2P)X + (Q+R) = 0 \tag{3.25}$$

Once the polynomial has been established, the roots $X_a$ and $X_b$ are generated by the implementation of the Quadratic Equation in terms of

$$X_a = \frac{-P + \sqrt{P^2 + Q^2 - R^2}}{R - Q} \tag{3.26}$$

and

$$X_b = \frac{-P - \sqrt{P^2 + Q^2 - R^2}}{R - Q} \tag{3.27}$$

With these roots, $\theta_3$ is calculated using the previously specified variable $X = \tan\left(\frac{\theta_3}{2}\right)$ from the Tangent Half-Angle approach

$$\theta_{3a} = 2\tan^{-1}(X_a) \tag{3.28}$$

and

$$\theta_{3b} = 2\tan^{-1}(X_b) \tag{3.29}$$

Key to mention is that from these calculated angles only the one that lies in quadrant one will be implemented as part of the spring mechanism design. The reason for this is that the unsprung position of Link 3, as illustrated in Figure 3.1, reclines between 0° and 90° relative to the horizontal axis. However, it must be clarified that only in this particular design the angles are located in such quadrants. In other designs, the angles can vary location according to the specifications of the links or the restrictions of the system.

Once the coupler angle $\theta_3$ of the four revolute-four bar has been determined, the unknown output angle $\theta_4$ can be obtained in a one step process. What is done is that both values of $\theta_3$ are substituted into the *position loop equations* of the X and Y direction, and are placed in a fraction form to calculate the necessary angle. Therefore, this requirement involves implementing the trigonometric function

$$\tan\theta = \frac{\Delta Y}{\Delta X} \tag{3.30}$$

which divides equation (3.8) by (3.9)

$$\frac{L_4 S_4}{L_4 C_4} = \frac{L_2 S_2 + L_3 S_3 - L_1 S_1}{L_2 C_2 + L_3 C_3 - L_1 C_1} \tag{3.31}$$

Rearranging the equation and substituting the respective angles, results in two expressions

$$\theta_{4a} = \tan^{-1}\left( \frac{L_2 S_2 + L_3 S_{3a} - L_1 S_1}{L_2 C_2 + L_3 C_{3a} - L_1 C_1} \right) \tag{3.32}$$

and

$$\theta_{4b} = \tan^{-1}\left( \frac{L_2 S_2 + L_3 S_{3b} - L_1 S_1}{L_2 C_2 + L_3 C_{3b} - L_1 C_1} \right) \tag{3.33}$$

It is significant to point out that from these values, the one that reclines in quadrant II will be implemented as part of the four revolute-four bar mechanism. This is due to the position of the system assumed initially, which demonstrates that the output angle *must* be positioned between 90° and 180° relative to the horizontal axis. Again, only in this particular design does the output angle lie in that particular quadrant.

The last step of the geometric analysis of the four revolute-four bar mechanism involves determining the position of the pivots A and B in terms of their global X and Y direction. It is important to clarify that in the design parameters specified earlier, the coordinates (X and Y components) of the two grounded revolute joints (O and C) were included as part of the constraints, and for such reason they do not have to be calculated. Therefore, with this understood, the position of pivot A is defined by adding the position of the grounded revolute joint C and the distance of Link 2 as

$$X_A = X_O + L_2 \cos(\theta_2) \tag{3.34}$$

and

$$Y_A = Y_O + L_2 \sin(\theta_2) \tag{3.35}$$

In a similar manner, the components (coordinates) for pivot B along the global X and Y direction are defined by adding the position of pivot A and the length of Link 3 as

$$X_B = X_A + L_3 \cos(\theta_3) \tag{3.36}$$

and

$$Y_B = Y_A + L_3 \sin(\theta_3) \tag{3.37}$$

Before moving into the next section, one factor in the analysis is that each derived equation is expressed in general terms, meaning that the specified design parameters are not substituted to obtain a value once an equation is generated. The basis behind this process is to prevent long, tedious, revisions in case an analytical error is formulated during the design phase. Therefore, Table 3.2 illustrates the values obtained from substituting the respective parameters into each expression and solving for the unknowns of the mechanism. Additionally, these values will be implemented in the latter sections and chapters to generate a simulation of the Watt II linkage (Working Model 2D software) and fabricate the physical model.

Determining the position of pivot A and pivot B concludes the unsprung position analysis of the four revolute-four bar mechanism illustrated in Figure 3.1. Therefore, the design of such mechanism was obtained by determining the geometric analysis of each link. The length of Link 1 was calculated by considering point O and point C on the fixed frame. Once the length of Link 1 was determined, a condition was specified to establish a relationship between the output angle $\theta_4$ and the input angle $\theta_2$. In order to satisfy this condition, the *position loop equations* about pivot B were implemented and consequently a second-order polynomial was obtained. Then, the Tangent Half-Angle approach was used to establish a new constraint equation and solve for the two roots. After the roots were calculated, the *position loop equations* were used to solve for the respective angles.

**Table 3.3: Unsprung Position Analysis Parameters**

| Parameters | Units (m) |
|---|---|
| $L_1$ | 0.25 |
| $P$ | 0.022 $m^2$ |
| $Q$ | -0.054 $m^2$ |
| $R$ | 0.05 $m^2$ |
| $X_a$ | 0.086 |
| $X_b$ | -0.51 |
| $\theta_{3a}$ | 9.86° |
| $\theta_{3b}$ | -54.003° |
| $\theta_{4a}$ | 105.428° |
| $\theta_{4b}$ | -149.571° |
| $X_A$ | 0.072 |
| $Y_A$ | 0.072 |
| $X_B$ | 0.223 |
| $Y_B$ | 0.098 |

### 3.1.2 Motion Analysis of Four Revolute-Four Bar Mechanism

Once the unsprung position analysis of the four revolute-four bar mechanism has been determined, the next step is to kinematically describe the motion of the system by deriving the *g*

and *h* function of each link. This is accomplished by expressing a geometric relationship between the parameter in question (dependent) and the input of the mechanism (independent). Significant to mention is that the dependent parameters of the dyad are the links, revolute/pivot joints, and link angles, and will be calculated relative to the center of mass and described in terms of time. As mentioned earlier, the motion of the system can be described relative to the center of mass or about the ends of a rigid body. In this case, the motion will be described relative to the center of mass.

The idea behind describing the behavior of the mechanism, in terms of the KIC's, is to determine four major parameters that will allow for the effective stiffness to be generated. These include: *Effective Inertia*, *Effective Stiffness due to Gravity Loads*, *Inertial Power*, and *Stiffness Generation via Redundant Actuation*. In order for such equations to be formulated, the implementation of Hamilton's Principle is considered in the general form of

$$S = \int_{t_0}^{t_1} L\left(t, x(t), \dot{x}(t)\right) dt \tag{3.38}$$

where $x(t)$ is the position of the particle at time *t*, $\dot{x}(t)$ is the velocity of the particle, and *L* is the difference between the kinetic energy and potential energy (Lagrangian). Nonetheless, before describing the motion of the four revolute-four bar mechanism in terms of its velocity and acceleration, it is important to understand how these four parameters are generated.

For instance, the first parameter *Effective Inertia* is obtained by equating the model kinetic energy with the system kinetic energy [2]. The general equation gives

$$\frac{1}{2}\left(I_{si}\right)\left(\frac{d}{dt}\phi_i\right)^2 = \sum_L \left[\frac{1}{2}\cdot M_L\left[\left(v_L{}^x\right)^2 + \left(v_L{}^y\right)^2\right] + \frac{1}{2}\cdot I_L\,\omega_L{}^2\right] \tag{3.39}$$

where the velocities are about the center of mass of link *L* and the inertia $I_1$ is about the center of mass of link *L* as well. This equation states that the *Effective Inertia* of the mechanism is determined by adding the translational kinetic energy ( $\frac{1}{2}mv^2$ ) with the rotational kinetic energy ( $\frac{1}{2}I\omega^2$ ). Therefore, what is done is that the translational and rotational velocities are written in terms of their respective *g*-function, and the like terms are cancelled to yield the *Effective Inertia* $I_{si}$ of the system

$$I_{si} = \sum_1 \left[ M_1 \cdot \left[ \left( g_{li}{}^x \right)^2 + \left( g_{li}{}^y \right)^2 \right] + I_1 g_{li}{}^2 \right] \tag{3.40}$$

where $g_{li}$ represents the velocity of the link with respect to the input. As a result, the *g*-functions, are obtained due to the change in position of the center of mass of each link with respect to the input.

Moreover, describing the motion of the system, in terms of the *Effective Stiffness due to Gravity Loads*, can be generated by equating the virtual work done by the effective load/generalized force at the input, to the virtual work done by the externally applied loads. This concept has been previously illustrated in equation (2.2) and can be expressed in terms of its *g*-function by substituting the respective virtual displacements and cancelling like terms as

$$\left( T_{si} \right)^L = \sum_P \left( T_p \cdot g_{pi} + F_P{}^X \cdot g_{pi}{}^X + F_P{}^Y \cdot g_{pi}{}^Y \right) \tag{3.41}$$

As a result, since the force of gravity acts in the vertical reference frame, the first two terms of the equation are cancelled and the expression yields

$$T_{si} = \sum_1 -\left[ \left( -M_1 \cdot g \right) \cdot g_{li}{}^y \right] \tag{3.42}$$

where $g$ is the gravitational constant acting on the system, $M$ is the mass of link $L$, and $g_{li}$ is the velocity of link $L$ about the center of mass along its Y direction.

Furthermore, kinematically describing the motion of the four revolute-four bar mechanism involves determining the *Inertial Power* of the system. This procedure is accomplished by setting the *Inertial Power* equal to the time rate of change of the kinetic energy of the system. In other words, the *Inertial Power* is the result of differentiating the *Effective Inertia* of the system (equation 3.39) with respect to the input $\theta_2$ and obtaining the respective KIC's as

$$P_{si} = \frac{1}{2}\frac{d}{d\phi_i} I_{si} = \sum_1 \left[ M_1 \left[ \left( g_{li}{}^x \cdot h_{li}{}^x \right) + \left( g_{li}{}^y \cdot h_{li}{}^y \right) \right] + I_1 g_{li} h_{li} \right] \tag{3.43}$$

where $I_1$ is the inertia about the center of mass, and the *h*-function is the acceleration about the center of mass of link $L$.

Having discussed the attainment of the *Inertial Power* of the system wraps up the argument on how the four major parameters are essential to generate the desired effective stiffness. Therefore, the target of the motion analysis is to determine the angular velocity and acceleration of each link with respect to the center of mass, and the translational velocity and acceleration of each link, along the X and Y direction, with respect to the center of mass as well.

However, before initiating the analysis, it is vital to point out which parameters will remain constant throughout the motion of the mechanism and which parameters will vary. Table 3.4 illustrates that the lengths of the links as well as the angle of Link 1 remain constant, while the angles of Link 2, Link 3, and Link 4 vary with time as the mechanism moves according to its dynamics. As a result, with these constants and variables specified the necessary geometric

relationships can be generated by means of knowing which parameters are dependent and which are independent.

**Table 3.4: Constant and Variable Parameters for D111**

| | |
|---|---|
| **Constant** | $L_2, L_3, L_4, \theta_1$ |
| **Variable** | $\theta_2, \theta_3, \theta_4$ |

With this understood, the first step in finding the angular velocities of Link 3 and Link 4 is obtained by implicitly differentiating the *position loop equations* (3.9) and (3.10) with respect to $\theta_2$. Why with respect to $\theta_2$? The reason for differentiating with respect to the $\theta_2$ is that such angle represents the input of the system, which means that the change in position of Link 3 and Link 4 depend on the change in position of Link 2. Therefore, this procedure generates two expressions that contain the unknown parameters $g_{32}$ and $g_{42}$, one along the X direction of the links and the other along the Y direction of the links. The result yields

$$-L_4 S_4 g_{42} = -L_2 S_2 g_{22} - L_3 S_3 g_{32} \tag{3.44}$$

and

$$L_4 C_4 g_{42} = L_2 C_2 g_{22} + L_3 C_3 g_{32} \tag{3.45}$$

where the KIC's are defined as

$$g_{32} = \frac{d\theta_3}{d\theta_2} \tag{3.46}$$

and

$$g_{42} = \frac{d\theta_4}{d\theta_2} \tag{3.47}$$

These KIC equations state that the change in angular rotation of the dependent parameters with respect to the change in angular rotation of the input, results in the angular velocity of the links. However, it is significant to clarify that the angular velocity of Link 2 $g_{22}$ is neglected from the equations (3.44) and (3.45) due to a constant geometric relationship generated as a result of implicit differentiation. This means that the angular velocity of Link 2 with respect to $\theta_2$, is simply one, and consequently can be removed from the expressions. As a result, this procedure reduces the derived equations into

$$-L_4 S_4 g_{42} = -L_2 S_2 - L_3 S_3 g_{32} \tag{3.48}$$

and

$$L_4 C_4 g_{42} = L_2 C_2 + L_3 C_3 g_{32} \tag{3.49}$$

The following step once these equations have been established is to determine the angular velocity of the respective links by solving simultaneously. This is accomplished by first obtaining a general expression for $g_{42}$ from equation (3.48) and substituting it into equation (3.49) to obtain the angular velocity of Link 3 as

$$g_{32} = \frac{L_2 \sin(\theta_4 - \theta_2)}{L_3 \sin(\theta_3 - \theta_4)} \tag{3.50}$$

In a similar manner, the angular velocity of Link 4 is determined by substituting this equation into the previously developed general expression for $g_{42}$ to obtain

$$g_{42} = \frac{L_2 \sin(\theta_3 - \theta_2)}{L_4 \sin(\theta_3 - \theta_4)} \tag{3.51}$$

Critical to mention is that these *g*-functions were simplified using the trigonometric identity

$$\sin\alpha\cos\beta - \cos\alpha\sin\beta = \sin(\alpha - \beta) \tag{3.52}$$

Once the angular velocity of each link has been established, the following calculation of the motion analysis involves determining the angular acceleration of each link relative to the center of mass. The computation initiates by differentiating the previously specified equations (3.48) and (3.49) with respect to the input of the mechanism and obtaining

$$-L_4 C_4 {g_{42}}^2 - L_4 S_4 h_{42} = -L_2 C_2 - L_3 C_3 {g_{32}}^2 - L_3 S_3 h_{32} \tag{3.53}$$

and

$$-L_4 S_4 {g_{42}}^2 + L_4 C_4 h_{42} = -L_2 S_2 - L_3 S_3 {g_{32}}^2 + L_3 C_3 h_{32} \tag{3.54}$$

where the KIC's are defined as

$$h_{32} = \frac{dg_{32}}{d\theta_2} \tag{3.55}$$

and

$$h_{42} = \frac{dg_{42}}{d\theta_2} \tag{3.56}$$

Before continuing the analysis, these second-order KIC's state that the change in angular velocity of Link 3 and Link 4 with respect to the change in angular rotation of the input, results in the angular acceleration of the links. Likewise, it is important to mention that the angular acceleration of Link 2 (equal to zero) has been neglected from the equations since its previously derived angular velocity resulted in a constant value. With this said, solving for the angular acceleration of Link 3 is accomplished by obtaining a general expression for $h_{42}$ from equation (3.53) and substituting it into equation (3.54) to get

$$h_{32} = \frac{L_4 {g_{42}}^2 - L_3 {g_{32}}^2 \cos(\theta_4 - \theta_3) - L_2 \cos(\theta_4 - \theta_2)}{L_3 \sin(\theta_4 - \theta_3)} \tag{3.57}$$

In addition, solving simultaneously to determine the angular acceleration of Link 4 requires substituting this equation into the previous general expression for $h_{42}$ to obtain

$$h_{42} = \frac{L_4 g_{42}{}^2 \cos(\theta_4 - \theta_3) - L_3 g_{32}{}^2 - L_2 \cos(\theta_3 - \theta_2)}{L_4 \sin(\theta_4 - \theta_3)} \tag{3.58}$$

As before, these two *h*-functions were simplified implementing the following justified trigonometric identity

$$\cos(\alpha - \beta) = \cos\alpha \cos\beta + \sin\alpha \sin\beta \tag{3.59}$$

Having solved for the angular velocity and angular acceleration of each link concludes the first phase of the motion analysis on the four revolute-four bar mechanism. The second and last phase in analyzing the behavior of the system involves determining the translational velocity and acceleration of each link, along their X and Y direction, and with respect to the center of mass. The first step in this process is to symbolically represent the distance of the center of mass on each link in terms of a new local reference frame (Figure 3.1) as

$$u_2 = \frac{L_2}{2} \tag{3.60}$$

$$v_2 = 0 \tag{3.61}$$

and

$$u_3 = \frac{L_3}{2} \tag{3.62}$$

$$v_3 = 0 \tag{3.63}$$

and

$$u_4 = \frac{L_4}{2} \tag{3.64}$$

$$v_4 = 0 \tag{3.65}$$

where $u_i$ is represented along the X direction and $v_i$ is represented along the Y direction and perpendicular to the link. By specifying these values, the motion analysis on Link 2 initiates by determining the location/position of the center of mass along the X and Y direction of the link as

$$X_2 = X_O + u_2 \cos(\theta_2) - v_2 \sin(\theta_2) \tag{3.66}$$

and

$$Y_2 = Y_O + u_2 \sin(\theta_2) + v_2 \cos(\theta_2) \tag{3.67}$$

Before obtaining the translational velocity of these expressions, it is essential to understand which parameters remain constant and which parameters vary (differentiable) as the mechanism fluctuates. Table 3.4 indicates that the only parameter differentiable in this case is the input angle $\theta_2$ , while the rest of the parameters remain constant; therefore the expressions along both directions yield

$$g_{22x} = -(u_2 \sin(\theta_2) - v_2 \cos(\theta_2)) \tag{3.68}$$

and

$$g_{22y} = u_2 \cos(\theta_2) + v_2 \sin(\theta_2) \tag{3.69}$$

In a similar manner, the translational acceleration of the link along its horizontal and vertical direction is generated by explicitly differentiating these two expressions with respect to the input (independent) parameter $\theta_2$ and obtaining

$$h_{22x} = -(u_2 \cos(\theta_2) - v_2 \sin(\theta_2)) \tag{3.70}$$

and

$$h_{22y} = -(u_2 \sin(\theta_2) + v_2 \cos(\theta_2)) \tag{3.71}$$

On the other hand, the next segment of the motion analysis is to determine the behavior of Link 3. This is accomplished by adding the inclined length of Link 2 with the location of the center of mass of Link 3 along both directions as

$$X_3 = L_2 \cos(\theta_2) + u_3 \cos(\theta_3) - v_3 \sin(\theta_3) \tag{3.72}$$

and

$$Y_3 = L_2 \sin(\theta_2) + u_3 \sin(\theta_3) + v_3 \cos(\theta_3) \tag{3.73}$$

Once the position has been determined, the translational velocity of the link (relative to the center of mass) is calculated by differentiating these two expressions with respect to the input parameter $\theta_2$ to obtain

$$g_{32x} = -L_2 \sin(\theta_2) - (u_3 \sin(\theta_3) + v_3 \cos(\theta_3)) \cdot g_{32} \tag{3.74}$$

and

$$g_{32y} = L_2 \cos(\theta_2) + (u_3 \cos(\theta_3) - v_3 \sin(\theta_3)) \cdot g_{32} \tag{3.75}$$

where $g_{32}$ is the angular velocity of Link 3. This means that having the $g_{32}$ function as part of the expressions confirms that the translational velocity of the link is related to the angular velocity of the system. In a similar manner, the motion analysis continues by differentiating these two *g*-functions with respect to $\theta_2$ to obtain the translational acceleration of the link (relative to the center of mass) as

$$h_{32x} = -L_2 \cos(\theta_2) - \left[(u_3 \sin(\theta_3) + v_3 \cos(\theta_3)) \cdot h_{32} + (u_3 \cos(\theta_3) - v_3 \sin(\theta_3)) \cdot {g_{32}}^2\right] \tag{3.76}$$

and

$$h_{32y} = -L_2 \sin(\theta_2) - \left[(u_3 \cos(\theta_3) - v_3 \sin(\theta_3)) \cdot h_{32} - (u_3 \sin(\theta_3) + v_3 \cos(\theta_3)) \cdot {g_{32}}^2\right] \tag{3.77}$$

where the $g_{32}$ and $h_{32}$ represent the angular velocity and angular acceleration of the link, respectively.

The last link to analyze from the four revolute-four bar mechanism is Link 4, but before this process is accomplished, it is important to understand how the motion analysis performed on the previous links was determined. The process was characterized by finding an equivalent point (pivot B) on the mechanism that would separate the kinematic equations generated for Link 2 and Link 3, from those kinematic equations developed for Link 1 and Link 4 (*loop-equations*). This is why the previously derived translational velocity and translational acceleration do not contain any parameters regarding Link 1 and Link 4.

With this approach discussed, the behavior of Link 4 initiates by adding the length of Link 1 with the location/position of the center of mass of Link 4 along the X and Y direction as

$$X_4 = L_1 \cos(\theta_1) + u_4 \cos(\theta_4) - v_4 \sin(\theta_4) \tag{3.78}$$

and

$$Y_4 = L_1 \sin(\theta_1) + u_4 \sin(\theta_4) + v_4 \cos(\theta_4) \tag{3.79}$$

Table 3.4 indicates that the only parameter that is differentiable with respect to the input in this case is $\theta_4$ , while the rest remain constant. Therefore, the translational velocity of the link yields

$$g_{42x} = -(u_4 \sin(\theta_4) + v_4 \cos(\theta_4)) \cdot g_{42} \tag{3.80}$$

and

$$g_{42y} = (u_4 \cos(\theta_4) - v_4 \sin(\theta_4)) \cdot g_{42} \tag{3.81}$$

where the $g_{42}$ function is the angular velocity of the link. Taking the second derivative of these two expressions results in the translational acceleration of the link as

$$h_{42x} = -(u_4 \sin(\theta_4) + v_4 \cos(\theta_4)) \cdot h_{42} - (u_4 \cos(\theta_4) - v_4 \sin(\theta_4)) \cdot g_{42}{}^2 \tag{3.82}$$

and

$$h_{42y} = (u_4 \cos(\theta_4) - v_4 \sin(\theta_4)) \cdot h_{42} - (u_4 \sin(\theta_4) + v_4 \cos(\theta_4)) \cdot g_{42}{}^2 \tag{3.83}$$

where the $g_{42}$ and $h_{42}$ represent the angular velocity and angular acceleration of Link 4, respectively.

The last phase of the motion analysis involves determining the mass moment of inertia of the system in order to solve for the rotational kinetic energy (*Effective Inertia*). This process initiates by taking into account the general (scalar) moment of inertia equation

$$\sum m_i r_i^{\,2} \tag{3.84}$$

where *m* is the mass and *r* is the distance to the axis of rotation. With such general equation established, the target is to compute the mass moment of inertia of each link and the mass moment of inertia of the two grounded revolute joints. Therefore, considering the geometry of the links and the parameters involved, allows for the inertia of each link to be calculated as

$$I_2 = \frac{1}{12} m_2 L_2^{\,2} \tag{3.85}$$

$$I_3 = \frac{1}{12} m_3 L_3^{\,2} \tag{3.86}$$

and

$$I_4 = \frac{1}{12} m_4 L_4^{\,2} \tag{3.87}$$

where $m_2, m_3, m_4$ and $L_2, L_3, L_4$ the masses and lengths of the links, respectively. On the other hand, solving for the mass moment of inertia of the grounded revolute joint O includes adding the inertia of the Link 2 by the center of mass location of the link. To achieve this, the following equation is implemented

$$I = \frac{1}{12} m\left(u_i^{\,2} + v_i^{\,2}\right) \tag{3.88}$$

where $u_i$ and $v_i$ represent the distance of the center of mass along the link and perpendicular to it. Therefore, implementing this equation and substituting the respective parameters yields the inertia of the grounded revolute joint as

$$I_O = I_2 + m_2\left(u_2{}^2 + v_2{}^2\right) \tag{3.89}$$

where such expression is obtained from the Parallel Axis Theorem (Statics). In a similar manner, the mass moment of inertia of the grounded revolute joint C is determined by adding the inertia of Link 4 with the center of mass location of the link as

$$I_C = I_4 + m_4\left(u_4{}^2 + v_4{}^2\right) \tag{3.90}$$

As in the unsprung position analysis, these previously derived equations are expressed in general terms to avoid long, tedious revisions in case an analytical error occurs during the design process. However, after substituting the specified design parameters into each generated equation, the respective values attained are illustrated in Table 3.5.

In conclusion, the geometric design of the four revolute-four bar mechanism was generated by specifying several design parameters that led to the determination of the position of each link, joint, and angle. Once the geometric design of the system was completed, the behavior was analyzed through the implementation of the kinematic and kinetic equations, and relative to the center of mass of each link. The target, in such case, was to describe the motion of the dependent parameters in terms of position, velocity, and acceleration. The process initiated by differentiating the *position loop equations* (about pivot B) to determine the *g* and *h* functions of Link 3 and Link 4 with respect to the input. Similarly, the translational velocity and acceleration of each link, relative to the center of mass, was calculated by first determining the position of the center of mass, and then differentiating twice to obtain the respective *g* and *h* functions along the X and Y directions.

**Table 3.5: Position and KIC Values**

| Position | g-function | h-function |
|---|---|---|
| $u_2 = 0.051m$ | $g_{22} = 1$ | $h_{22} = 0$ |
| $u_3 = 0.077m$ | $g_{32} = -0.583$ | $h_{32} = -0.073$ |
| $u_4 = 0.051m$ | $g_{42} = 0.578$ | $h_{42} = -1.366$ |
| $X_2 = 0.036m$ | $g_{22x} = -0.036m$ | $h_{22x} = -0.036m$ |
| $Y_2 = 0.036m$ | $g_{22y} = 0.036m$ | $h_{22y} = -0.036m$ |
| $X_3 = 0.147m$ | $g_{32x} = -0.064m$ | $h_{32x} = -0.097m$ |
| $Y_3 = 0.085m$ | $g_{32y} = 0.028m$ | $h_{32y} = -0.082m$ |
| $X_4 = 0.236m$ | $g_{42x} = -0.028m$ | $h_{42x} = 0.072m$ |
| $Y_4 = 0.049m$ | $g_{42y} = -0.007846m$ | $h_{42y} = 0.002088m$ |

## 3.2 D011 Design

### 3.2.1 Unsprung Position Analysis for Slider-Crank Mechanism

Before determining the unsprung position of the D011 planar mechanism, the first step involves specifying a new point (joint) on Link 4 that will couple both mechanisms and create the desired Watt II linkage. This point (E) is obtained by specifying a new local reference frame ( $u_E, v_E$ ) on the link and arbitrarily choosing the coordinates to determine its position in space (Figure 3.2). To avoid confusion, it is significant to clarify that in this case the new coordinate

system is only used as a reference guide along the incline, and does not represent the location of the center of mass as in the previous section. Therefore, the arbitrarily coordinates yield

$$u_E = L_4 - 0.032m \tag{3.91}$$

and

$$v_E = -0.080m \tag{3.92}$$

where $L_4$ is the length of Link 4.

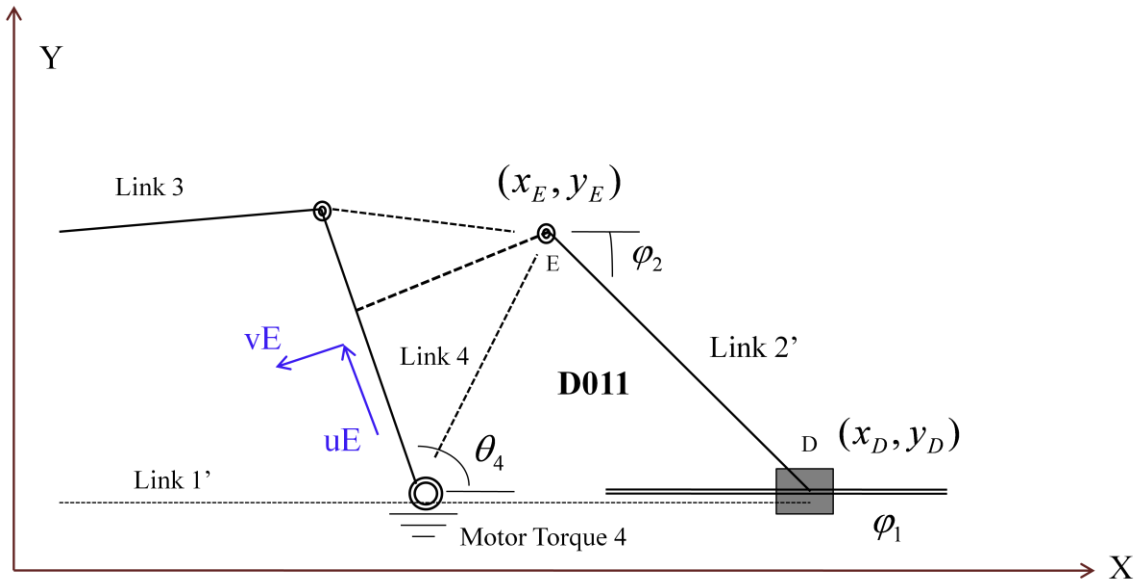


**Figure 3.2: D011 Mechanism**

Once the point (joint) has been referenced on Link 4, the unsprung position analysis of the mechanism initiates by specifying several design parameters such as the dyad type, angle of sliding, and the length of Link 2' (Table 3.6). As specified, the angle $\psi_1$ is zero, which means that the spring mechanism only modulates along the horizontal axis. With these parameters, the objective is to solve for the length of Link 1' and for the angle of Link 2' (Figure 2.1), however to accomplish this procedure the position of point E must be determined first. Therefore, using

$\theta_4$ as the relative angle, allows for the position of point E to be calculated along the horizontal and vertical direction (global) as

$$X_E = X_C + u_E \cos(\theta_4) - v_E \sin(\theta_4) \tag{3.93}$$

and

$$Y_E = Y_C + u_E \sin(\theta_4) + v_E \cos(\theta_4) \tag{3.94}$$

where $X_C$ and $Y_C$ represent the constraint on the grounded revolute joint C.

**Table 3.6: D011 Design Parameters**

| | | |
|---|---|---|
| $X_{A'} = 0m$ | $\theta_{4'} = \theta_4$ | $L_{2'} = 0.127m$ |
| $Y_{A'} = 0m$ | $\psi_1 = 0^\circ$ | $Type = 1$ |

With the position of the new point calculated, the unsprung length of Link 1' and the unsprung angle of Link 2' are determined specifying an initial condition to establish a relationship between the angle $\psi_1$ and the angle $\psi_2$. This condition states that the length of Link 2' must remain constant throughout the motion of the system, which makes sense

$$(D-E)\cdot(D-E) - L_{2'} = 0 \tag{3.95}$$

Therefore, in order to satisfy the initial condition, the method of *position loop equations* is implemented about point D. This method involves expressing a series of constraint equations that define the position of the output displacement slider (equivalent point) along its X and Y direction. Therefore, the position of the equivalent point along the horizontal coordinate is obtained by equating $X_D = X_D$ as

$$X_{A'} + L_{1'}\cos(\psi_1) = X_E + L_{2'}\cos(\psi_2) \tag{3.96}$$

where $\psi_1$ and $\psi_2$ are the relative angles of Link 1' and Link 2' respectively. In a similar manner, the *position loop equation* along the vertical coordinate is obtained by equating $Y_B = Y_B$ and implementing the adequate trigonometric functions as

$$Y_{A'} + L_{1'}\sin(\psi_1) = Y_E + L_{2'}\sin(\psi_2) \tag{3.97}$$

With these expressions defined, the next step is to isolate the terms that contain trigonometric functions on one side, and the rest on the other side as

$$L_{1'}\cos(\psi_1) - L_{2'}\cos(\psi_2) = X_E - X_{A'} \tag{3.98}$$

and

$$L_{1'}\sin(\psi_1) - L_{2'}\sin(\psi_2) = Y_E - Y_{A'} \tag{3.99}$$

The idea of rearranging the equations is to simplify the terms on the right hand side by representing them symbolically using a single constant as

$$a = X_E - X_{A'} \tag{3.100}$$

and

$$b = Y_E - Y_{A'} \tag{3.101}$$

Therefore, introducing the respective constants into the *position loop equations* (3.98) and (3.99) yields

$$L_{2'}\cos(\psi_2) = L_{1'}\cos(\psi_1) - a \tag{3.102}$$

and

$$L_{2'}\sin(\psi_2) = L_{1'}\sin(\psi_1) - b \tag{3.103}$$

It is significant to point out that by using this approach the long, tedious procedure of determining the unknown parameters $L_{1'}$ and $\psi_2$ is reduced to a two step process. For example,

step one involves expanding both of these expressions to form a single equation that will eliminate $\psi_2$ and allow for the length of Link 1' to be solved. This is first accomplished by applying the Law of Cosines along both directions as

$$L_{2'}{}^2 C_2{}^2 = L_{1'}{}^2 C_1{}^2 + a^2 - 2L_{1'}C_1 a \tag{3.104}$$

and

$$L_{2'}{}^2 S_2{}^2 = L_{1'}{}^2 S_1{}^2 + b^2 - 2L_{1'}S_1 b \tag{3.105}$$

where $S_i = \sin(\psi_i)$ and $C_i = \cos(\psi_i)$. The single equation is then generated by adding the two non-linear expressions and obtaining

$$L_{2'}{}^2\left(S_2{}^2 + C_2{}^2\right) = L_{1'}{}^2\left(S_1{}^2 + C_1{}^2\right) + a^2 + b^2 - 2L_{1'}\left(aC_1 + bS_1\right) \tag{3.106}$$

which is expected since the effective stiffness equation is non-linear as well (Chapter II). Once this equation is formulated, it can be simplified using the Cosine Angle Sum and Difference Identity (3.14) and the Pythagorean Trigonometric Identity (3.15) to eliminate $\psi_2$ as

$$L_{1'} = \left(aC_1 + bS_1\right) + Type \cdot \left[\left(aC_1 + bS_1\right)^2 + L_{2'}{}^2 - \left(a^2 + b^2\right)\right]^{\frac{1}{2}} \tag{3.107}$$

Step two, on the other hand, involves solving for the angle of Link 2'. This calculation is simply generated by forming a relationship between the *position loop equations* (3.102) and (3.103) as

$$\frac{L_{2'}S_2}{L_{2'}C_2} = \frac{L_{1'}S_1 - b}{L_{1'}C_1 - a} \tag{3.108}$$

where

$$\psi_2 = \tan^{-1}\frac{L_{1'}S_1 - b}{L_{1'}C_1 - a} \tag{3.109}$$

Furthermore, the final calculation of the analysis involves determining the position of the output displacement slider (point D) in terms of its X and Y coordinates. This requires that the length of Link 1' and the constraint on the slider are taken into consideration as

$$X_D = X_{A'} + L_{1'}C_1 \tag{3.110}$$

and

$$Y_D = Y_{A'} + L_{1'}S_1 \tag{3.111}$$

where the angle of sliding is equal to zero. Once the position for the output element is determined, each of the previously derived expression is calculated through substituting the respective parameters (Table 3.7)

**Table 3.7: D011 Analytical Values**

| Units (m) | Units (m) | Units (m) |
|---|---|---|
| $u_E = 0.07$ | $a = 0.308$ | $b = 0.089$ |
| $X_E = 0.308$ | $X_D = 0.399$ | $L_{1'} = 0.399$ |
| $Y_E = 0.089$ | $Y_D = 0$ | $\psi_2 = 134.339^\circ$ |

### 3.2.2 Motion Analysis of the Slider-Crank Mechanism

Once the unsprung position analysis of the D011 mechanism has been established, the next phase is to kinematically describe the motion of the system by obtaining the KIC's of each link. This process is accomplished by expressing a geometric relationship between the parameter in question (dependent) and the input of the mechanism (independent). Therefore, the target is to determine the angular velocity and acceleration of each link with respect to the center of mass, and the translational velocity and acceleration of each link along the X and Y coordinates and with respect to the center of mass as well.

Before analyzing the behavior of the system, it is vital to point out which parameters will remain constant throughout the motion of the mechanism and which parameters will vary. Table 3.8 illustrates that the length of Link 2' and the angle of Link 1' remain constant, while the length of Link 1', the angle of Link 2' and point E vary with time as the mechanism fluctuates. As a result, with these constants and variables the necessary geometric relationships can be generated by means of knowing which parameters are dependent and which are independent.

**Table 3.8: Constant and Variable Parameters for D011**

| | |
|---|---|
| **Constant** | $\psi_1, L_{2'}$ |
| **Variable** | $L_{1'}, \psi_2, X_E, Y_E$ |

With this understood, the first step in finding the angular velocities of Link 1' and Link 2' is obtained by implicitly differentiating the *position loop equations* with respect to the input $\theta_2$ ((3.96) and (3.97)). This procedure generates two expressions that contain the unknown parameters $g_{2'2}$ and $g_{L_1'/2}$, one along the X direction and the other along the Y direction as

$$g_{L_1'/2}\cos(\psi_1) = g_{E2x} - L_{2'}\sin(\psi_2)\cdot g_{2'2} \tag{3.112}$$

and

$$g_{L_1'/2}\sin(\psi_1) = g_{E2y} - L_{2'}\cos(\psi_2)\cdot g_{2'2} \tag{3.113}$$

where the KIC's are defined as

$$g_{2'2} = \frac{d\psi_2}{d\theta_2} \tag{3.114}$$

and

$$g_{L_{1'}/2} = \frac{dL_{1'}}{d\theta_2} \tag{3.115}$$

These KIC equations state that the change in angular rotation of the dependent parameters with respect to the change in angular rotation of the input, results in the angular velocity of the links. Important to observe from the differentiated *loop equations* is the integration of the angular velocity of point E, which must be solved first before calculating for the unknown parameters. This procedure involves differentiating its position (equations (3.93) and (3.94)) with respect to the input of the mechanism $\theta_2$ to obtain

$$g_{E2x} = -\left(u_E \sin\left(\theta_4\right) + v_E \cos\left(\theta_4\right)\right) \cdot g_{42} \tag{3.116}$$

and

$$g_{E2y} = \left(u_E \cos\left(\theta_4\right) - v_E \sin\left(\theta_4\right)\right) \cdot g_{42} \tag{3.117}$$

where $g_{42}$ is the angular velocity of Link 2 previously calculated.

Once the angular velocity of point E has been attained, the unknown parameters can be determined in a one step process instead of solving the differentiated equations simultaneously. This is accomplished by understanding that the angular velocity of Link 1' is defined by its change in length over time (3.113), which means that the exact same result can be produced by the displacement on the output slider (point D). Therefore, the velocity of the slider along its X and Y directions is obtained by differentiating its position ((3.110) and (3.111)) with respect to the input $\theta_2$ as

$$g_{D2x} = g_{L_{1'}/2} \cdot \cos\left(\psi_1\right) \tag{3.118}$$

and

$$g_{D2y} = g_{L_{1'}/2} \cdot \sin\left(\psi_1\right) \tag{3.119}$$

where $\psi_1 = 0$ from the specified design parameters (Table 3.6). By simplifying these expressions, it is determined that the angular velocity of Link 1' is equivalent to the horizontal translational velocity of point D as

$$g_{D2x} = g_{L_{1'}/2} \tag{3.120}$$

and

$$g_{D2y} = 0 \tag{3.121}$$

This indicates that the respective angular velocities of the D011 mechanism can be resolved by substituting equations (3.118) and (3.119) into the differentiated *loop equations* as

$$g_{D2x} = g_{E2x} - L_{2'} \sin(\psi_2) \cdot g_{2'2} \tag{3.122}$$

and

$$g_{D2y} = g_{E2y} - L_{2'} \cos(\psi_2) \cdot g_{2'2} \tag{3.123}$$

where the $g_{L_1'/2}$ and $g_{2'2}$ yield

$$g_{L_{1'}/2} = g_{E2x} - L_{2'} \sin(\psi_2) \cdot g_{2'2} \tag{3.124}$$

and

$$g_{2'2} = \frac{g_{E2y}}{L_{2'} \cos(\psi_2)} \tag{3.125}$$

After the angular velocity of Link 1' and Link 2' has been computed, the next procedure of the motion analysis involves determining the angular acceleration of each link. This computation initiates by differentiating the previous expressions ((3.124) and (3.125)) with respect to the input of the mechanism and obtaining two non-linear equations that give

$$h_{L_{1'}/2} = h_{E2x} - L_{2'} \cos(\psi_2) \cdot g_{2'2}{}^2 - L_{2'} \sin(\psi_2) \cdot h_{2'2} \tag{3.126}$$

and

$$h_{2'2} = \frac{h_{E2y} - L_{2'} \sin(\psi_2) \cdot g_{2'2}{}^2}{-L_{2'} \cos(\psi_2)} \tag{3.127}$$

where the KIC's are defined as

$$h_{L_{1'}/2} = \frac{dg_{L_{1'}/2}}{d\theta_2} \tag{3.128}$$

and

$$h_{2'2} = \frac{dg_{2'2}}{d\theta_2} \tag{3.129}$$

Important to observe from these non-linear equations is the integration of the angular acceleration of the new point E along the global horizontal and vertical direction. This h-function amongst the angular velocity of Link 1' and Link 2'must be calculated to prevent having more unknowns than equations. Therefore, the second-order KIC of point E is computed by differentiating its velocity (equations (3.116) and (3.117)) with respect to the input of the mechanism and obtaining

$$h_{E2x} = -\left(u_E \sin(\theta_4) + v_E \cos(\theta_4)\right) \cdot h_{42} - \left(u_E \cos(\theta_4) - v_E \sin(\theta_4)\right) \cdot g_{42}{}^2 \tag{3.130}$$

and

$$h_{E2y} = \left(u_E \cos(\theta_4) - v_E \sin(\theta_4)\right) \cdot h_{42} - \left(u_E \sin(\theta_4) + v_E \cos(\theta_4)\right) \cdot g_{42}{}^2 \tag{3.131}$$

where $h_{42}$ is the angular acceleration of Link 4 previously calculated.

Having solved for the angular velocity and angular acceleration of each link concludes the first phase of the motion analysis. The second phase in analyzing the behavior of the system involves determining the translational velocity and acceleration of Link 2', along its X and Y coordinates, with respect to the center of mass. As accomplished in the previous section, the first

step in this process is to symbolically represent the distance of the center of mass on Link 2' in terms of a new local reference frame (Figure 3.3) as

$$u_{2'} = \frac{L_{2'}}{2} \tag{3.132}$$

and

$$v_{2'} = 0 \tag{3.133}$$

where $u_i$ represents the horizontal distance along the incline and $v_i$ represents the normal distance of the link. With such values specified, the motion analysis on Link 2' initiates by determining the location/position of the center of mass along the X and Y direction of the link as

$$X_{2'} = L_{1'}\cos(\psi_1) + u_{2'}\cos(\psi_2) - v_{2'}\sin(\psi_2) \tag{3.134}$$

and

$$Y_{2'} = L_{1'}\sin(\psi_1) + u_{2'}\sin(\psi_2) - v_{2'}\cos(\psi_2) \tag{3.135}$$

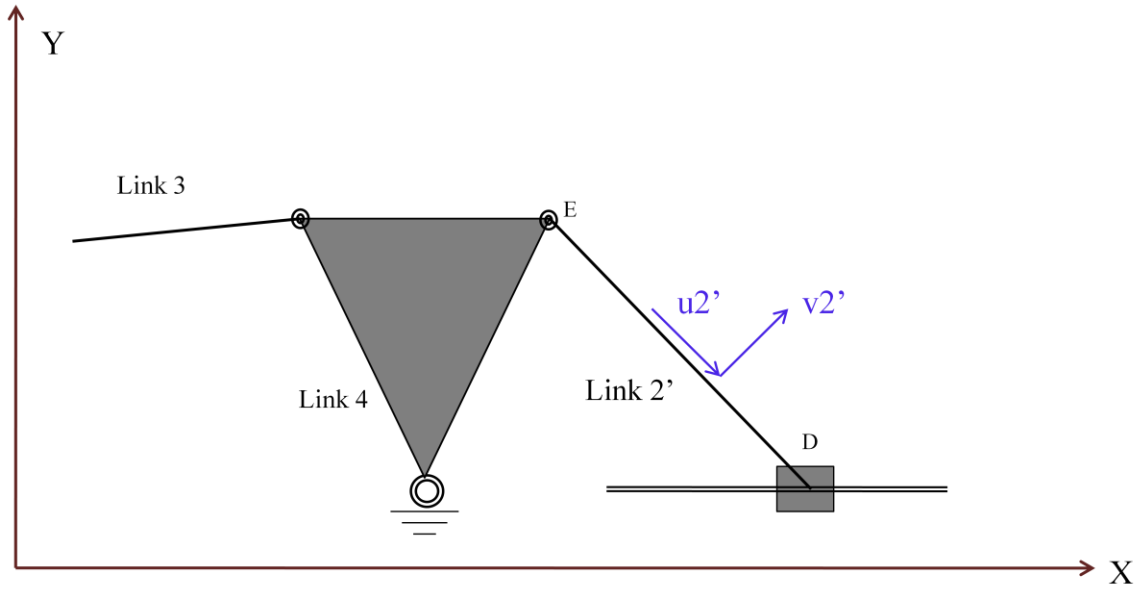


**Figure 3.3: Local Coordinate System D011**

Once the position has been identified, the velocity of the link can be obtained by simply differentiating the expressions, however, it is necessary to first understand which parameters will remain constant and which will change as the mechanism fluctuates. Table 3.8 indicates that the parameters that change in this case are the length of Link 1', the angle of Link 2', and point E, while the rest of the parameters remain constant; therefore, the translational velocity of the link yields

$$g_{2'2x} = -\left(u_{2'}\sin\left(\psi_2\right) + v_{2'}\cos\left(\psi_2\right)\right)\cdot g_{2'2} \tag{3.136}$$

and

$$g_{2'2y} = \left(u_{2'}\cos\left(\psi_2\right) - v_{2'}\sin\left(\psi_2\right)\right)\cdot g_{2'2} \tag{3.137}$$

In a similar manner, the translational acceleration Link 2' relative to the center of mass is generated by differentiating these two expressions with respect to the input $\theta_2$ and obtaining

$$h_{2'2x} = -\left(u_{2'}\sin\left(\psi_2\right) + v_{2'}\cos\left(\psi_2\right)\right)\cdot h_{2'2} - \left(u_{2'}\cos\left(\psi_2\right) - v_{2'}\sin\left(\psi_2\right)\right)\cdot g_{2'2}{}^2 \tag{3.138}$$

and

$$h_{2'2y} = \left(u_{2'}\cos\left(\psi_2\right) - v_{2'}\sin\left(\psi_2\right)\right)\cdot h_{2'2} - \left(u_{2'}\sin\left(\psi_2\right) + v_{2'}\cos\left(\psi_2\right)\right)\cdot g_{2'2}{}^2 \tag{3.139}$$

where $g_{2'2}$ and $h_{2'2}$ represent the angular velocity and acceleration of Link 1' and Link 2', respectively.

The last phase in analyzing the behavior of the system involves determining the mass moment of inertia of the links in order to solve for the rotational kinetic energy (*Effective Inertia*). In this case, it is important to distinguish that Link 2' is the only link that contains a mass, and therefore is the only one to be computed. With this understood, the inertia is calculated by taking into account the geometry of the link and the distance to the axis of rotation as

$$I_{2'} = \frac{1}{12} m_{2'} L_{2'}{}^2 \tag{3.140}$$

where $m_{2'}$ is the mass of the link and $L_{2'}$ is the respective length. Since Link 2' is the only link to be analyzed from the system, this calculation finalizes the design phase of the D011 mechanism in terms of its geometry and motion analysis. Once the expressions formulated from these analyses were written in general terms, each and one of them were calculated by substituting the respective parameters and obtaining the desired values (Table 3.9).

**Table 3.9: Analytical Results**

| **Mass (*kg*)** | **Inertia ( $kgm^2$ )** | **Position (*m*)** | **g-function (*m*)** | **h-function (*m*)** |
|---|---|---|---|---|
| $m_2 = 0.0255$ | $I_2 = 2.211\times10^{-5}$ | $X_{D2x} = 0.399$ | $g_{D2x} = -0.086$ | $h_{D2x} = 0.24$ |
| $m_3 = 0.0348$ | $I_3 = 6.789\times10^{-5}$ | $Y_{D2x} = 0$ | $g_{D2y} = 0$ | $h_{D2y} = 0$ |
| $m_4 = 0.0605$ | $I_4 = 5.245\times10^{-5}$ | $X_{E2x} = 0.308$ | $g_{E2x} = -0.051$ | $h_{E2x} = 0.102$ |
| $m_{2'} = 0.0469$ | $I_O = 8.843\times10^{-5}$ | $Y_{E2x} = 0.089$ | $g_{E2y} = 0.034$ | $h_{E2y} = -0.110$ |
| | $I_C = 2.098\times10^{-4}$ | $X_{2'2} = 0.355$ | $g_{2'2x} = -0.017$ | $h_{2'2x} = 0.069$ |
| | $I_{2'} = 6.304\times10^{-5}$ | $Y_{2'2} = 0.045$ | $g_{2'2y} = -0.017$ | $h_{2'2y} = 0.055$ |
| | | | $g_{2'2} = 0.381$ | $h_{2'2} = -1.383$ |

In conclusion, it is necessary to emphasize that the geometric design of the mechanism in this section was generated by specifying several design parameters that led to the determination of the position of each link, joint, and angle. After the unsprung position was determined, the behavior of the system was analyzed by implementing the kinematic and kinetic equations, relative to the center of mass, that determined the KIC of each parameter in question. In order to accomplish such procedures, an initial condition had to be specified first to establish a

relationship between the angles $\psi_1$ and $\psi_2$. Then, the *position loop equations* (about point D) were implemented to determine the KIC's of the system.

Important to recall, before closing, is that the design of the one degree-of-freedom Watt II linkage was accomplished in two steps. Phase one, as seen in the previous section, involved determining the unsprung position of a four revolute-four bar mechanism and analyzing its behavior in terms of position, velocity, and acceleration (relative to the center of mass). In phase two, a geometric design and motion analysis was generated for the D011 mechanism to describe its behavior and complete the structure of the unidirectional linkage.

### 3.3 Working Model Simulation

Once the design of the Watt II linkage has been completed, the next step is to use the attained parameters and create a simulation in Working Model 2D that will assist in visually understanding the appearance and behavior of the one degree-of-freedom spring mechanism. In particular, this process allows the previously calculated analytical values to be compared with those generated by the model and verify if they match. Nonetheless, it is significant to mention that the target in this section is to only develop the unsprung model and leave the comparison of motion parameters for the next chapter, once the spring mechanism is redundantly actuated by implementing the required equilibrium motor torques.

Before attempting to model the spring mechanism, the first step is to arbitrarily choose a coordinate system on the workspace that will reference the starting point (grounded revolute joint O) and allow for the system to be fully constrained as the links are assembled (Figure 3.4). This point of reference will start at the coordinates (0,0) to be on the same page with the global

coordinate system specified earlier (design of linkage ) and facilitate the process of generating a model.

After determining the initial reference point on the workspace, the process begins by using the tools offered in Working Model to create and position each link according to the calculated constraints (Table 3.1 and Table 3.2). For example, the length of Link 2 is drawn to scale using a *rectangular element* and is placed at a 45° angle from its fixed end referenced at (0,0). Before continuing, it is necessary to clarify that Working Model measures the angles in units of radians and not in units of degrees. This means that the 45° angle of Link 2 together with all the angles specified and determined in sections 3.1 and 3.2, *must* be converted to radians (3.139) in order for a fully constraint model to be generated.

$$radians = \deg \cdot \left( \frac{2\pi}{360} \right) \tag{3.141}$$

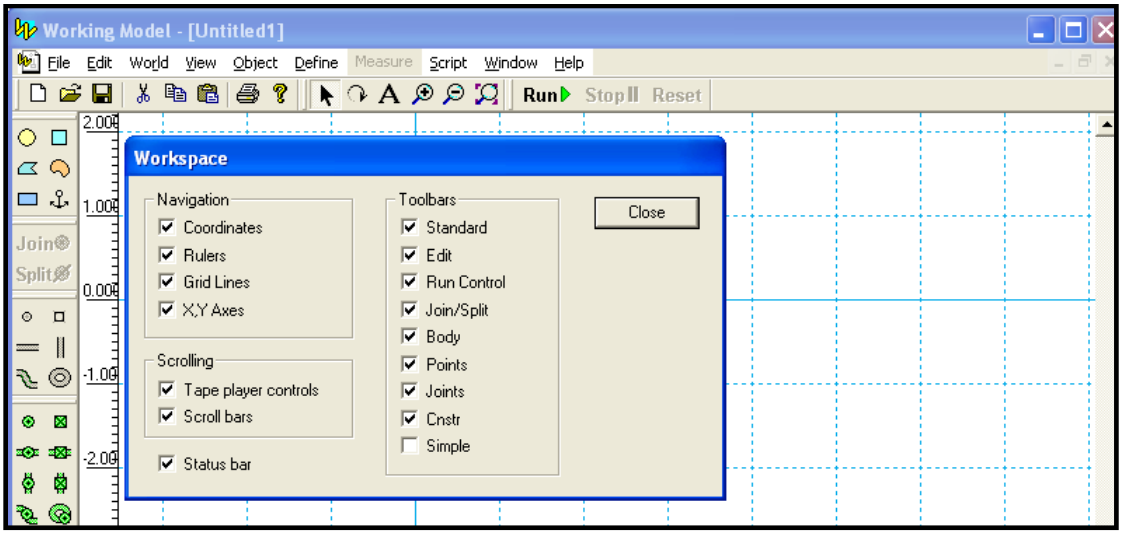


**Figure 3.4: Working Model Reference Frame**

With this said, the process continues by placing a *motor* on the grounded (fixed) end to simulate one of the two input forces required to have a redundantly actuated system, however its mode

*must* be modified to ‘torque’ from the default settings. If this change is not made, the software will assume that the motor is in ‘velocity’ mode and the dynamics of the mechanism will be altered, making the results different from the ones computed. In a similar manner, the mechanical properties of Link 2 such as the mass and mass moment of inertia also need to be modified from the default settings to prevent an automatic material selection from the software.

The next step is for the length of Link 3 to be created (*rectangular element*) and positioned about the free-end of Link 2 through a *point element*. Once the links are connected and the angle is specified in radians, the mechanical properties of the link are modified to prevent an automatic parameter selection from the software that would produce inconsistencies on the system as a result of the change in dynamics.

With these two links fully constrained, the process of modeling the Watt II linkage continues by finding a way of coupling Link 4 and revolute joint E to avoid having additional links on the system. This problem is solved by incorporating a triangular plate on the free-end of Link 2 that references and unites each of the three revolute joints involved (B,C, and E). With such solution established, the solid plate is generated by using a *polygon shape element* in Working Model to specify the position of each revolute joint in terms of their X and Y coordinates (Figure 3.5). Once these parameters have been defined and the dyad plate has been assembled, a ‘torque’ motor is implemented at the grounded (fixed) revolute joint C to simulate a second input force that is required to have a redundantly actuated system.

The last segment to complete the assembly of the linkage involves creating Link 2’ and the output linear displacement slider. Before continuing, it is important to recall that the output element slider is used as a reference source to determine the effective stiffness of the system and is totally dependent on the motor torques.

With this concept emphasized from the previous chapter, the length of Link 2' is drawn to scale using a *rectangular element* and placed at a 134.339° angle relative to the horizontal of point E. Once the assembly between these two points is completed, the mechanical properties such as the mass and mass moment of inertia are modified from the default settings to prevent an automatic selection from the software.

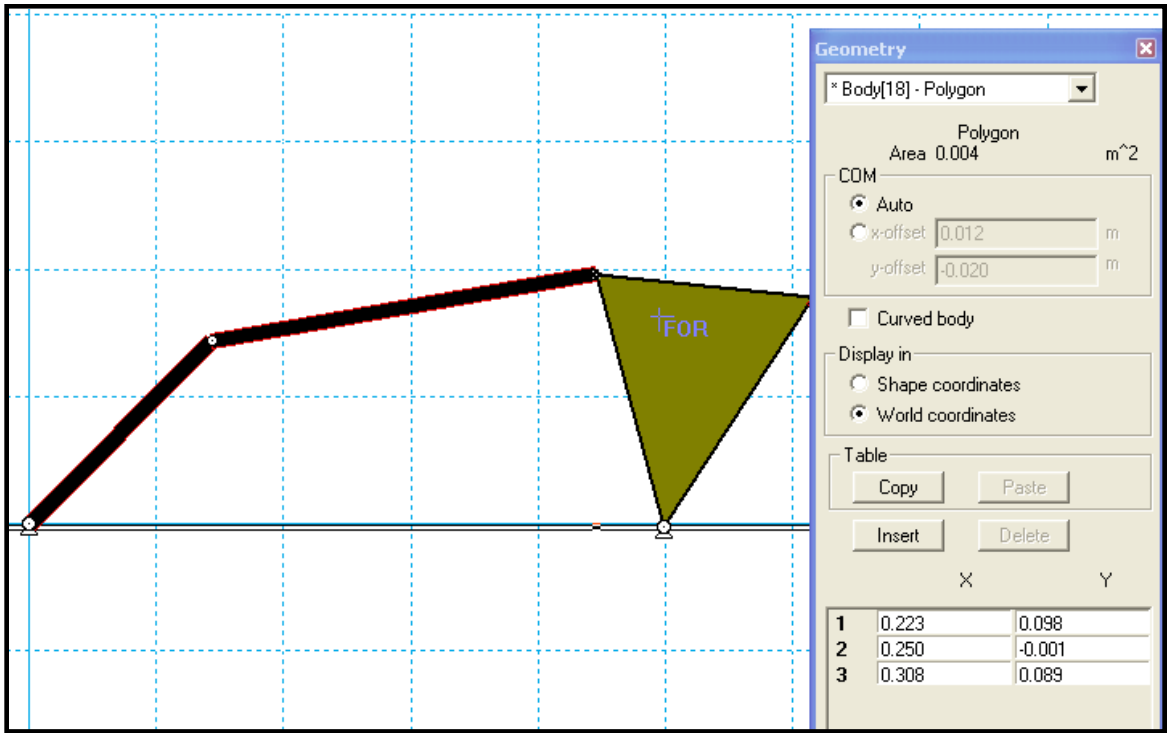


**Figure 3.5: Coupling Dyads**

In a similar manner, the output linear displacement element is generated and assembled using the same tools in Working Model as before. This time, however, once the default settings have been modified, a *key slot joint* is implemented along the horizontal axis of the output element to allow for the spring mechanism to modulate as a force is applied (Figure 3.6).

In conclusion, with the parameters attained from the design phase of the spring mechanism, a simulation was created in Working Model 2D to visualize the appearance and behavior of the system. However, the target in this section was to only develop the unsprung linkage model and leave the comparison of motion parameters for the next chapter. As a result, the process began by utilizing the tools offered in the software to create the linkage and generate a fully constrained system. After the links were created and assembled, the calculated mechanical properties of the links were specified on the default settings. This modification was done to prevent an automatic material selection from the software that would alter the dynamics of the system.

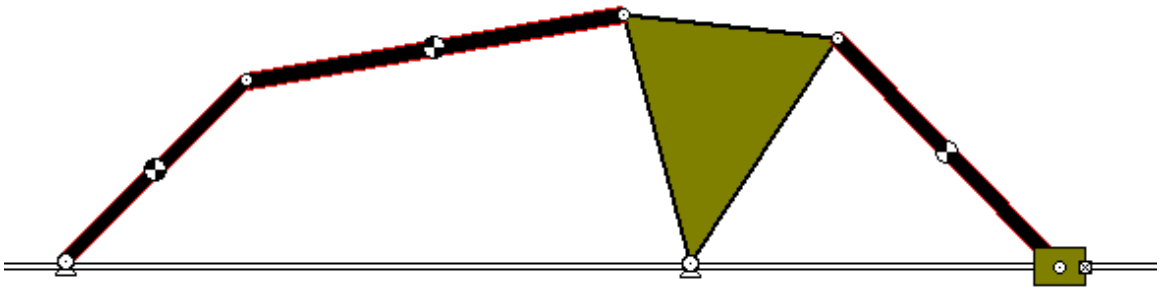

**Figure 3.6: Watt II Spring Mechanism**

### 3.4 Pro-Engineer Model

One of the advantages of using Pro-Engineer software is that a three dimensional model of the spring mechanism can be generated. With this sketch, details such as the development of each component and the assembly of the linkage can be foreseen before the manufacturing process begins. However, the greatest challenge in the drawing is to find a way to mount the mechanism on the shafts of the two DC motors to obtain a precise, horizontal motion on the

output displacement slider. For these reasons, the target in this section is to create a computer-aided design (CAD) drawing of the actively adjustable spring mechanism that will serve as a reference guide during the process of fabricating the physical model. Such drawing is completed in two steps; first, each individual component will be created according to the specified or calculated parameters, and secondly the components and the respective motors will be assembled to generate the one degree-of-freedom mechanism.

Before initiating the design of each component, it is vital to point out several parameters that will allow for the spring mechanism to be created in three dimensions. These parameters are not determined mathematically, instead they are arbitrarily considered by having in mind a reasonable size of fabricating the physical spring mechanism. For instance, Table 3.10 demonstrates that each link has a cross-sectional length of 0.0127 *m* and a cross-sectional width of 0.00635 *m*, while the dyad plate that connects the D111 and D011 mechanisms has a thickness of 0.003175 *m*. Additionally, the table indicates that the holes of the revolute joints are to be extruded using a diameter of 0.00635 *m*, this dimension is regarded to be consistent with the diameter of the motor shafts.

**Table 3.10: Dimensions for Physical Model**

| Parameters | Units (m) |
|---|---|
| Cross-sectional Length | 0.0127 |
| Cross-sectional Width | 0.00635 |
| Hole Diameter | 0.00635 |
| Plate Thickness | 0.003175 |

With these parameters defined, the next step involves specifying the correct unit system (SI) in Pro-Engineer to be on the same page with the units specified in the design phase (Figure 3.7). If this change is not made, the default units (English System) on the software will remain activated, and the overall size of the sketch generated will be smaller than the original design.

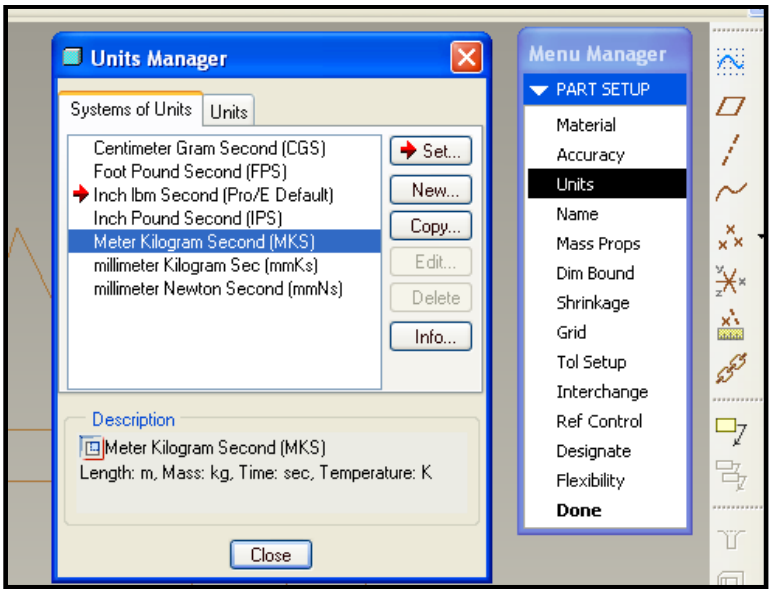


**Figure 3.7: Pro-Engineer Units Specification**

Once the parameters have been specified and the correct unit system has been incorporated, the process initiates by using the tools offered in the software to create each link. For example, Link 2 is sketched using an *extrusion* tool that permits the cross-sectional dimensions (Table 3.10) and the depth (length) of the link to be designated. In this case, the depth that is to be specified *must* exceed the original depth (Section 3.1) in such manner that the extruded holes on the link have a substantial margin at the end. Therefore, such problem is solved by leaving the distance between the center of the holes intact (original length), while the length outside of the holes is extended (Figure 3.8). If this length is not modified, it is impossible to create a drawing that matches the

previously designed mechanism, and consequently the desired effective stiffness will not be generated. With this requirement understood, a total length of 0.01905 *m* is not only added to this link, but to every link on the linkage. After specifying the necessary depth on Link 2, the procedure continues by *extruding* a hole on the end where the DC motor is to be mounted, and another hole on the respective end where Link 3 is to be connected. Once the holes are *extruded*, it is necessary to add a new *axis* of rotation, perpendicular to the center of each hole, to specify that the link can pivot about those references. If this *axis* is not specified, the software does not have a source of reference to align the two joints that are to be coupled, and as a result the assembly process becomes tedious or impossible to achieve.

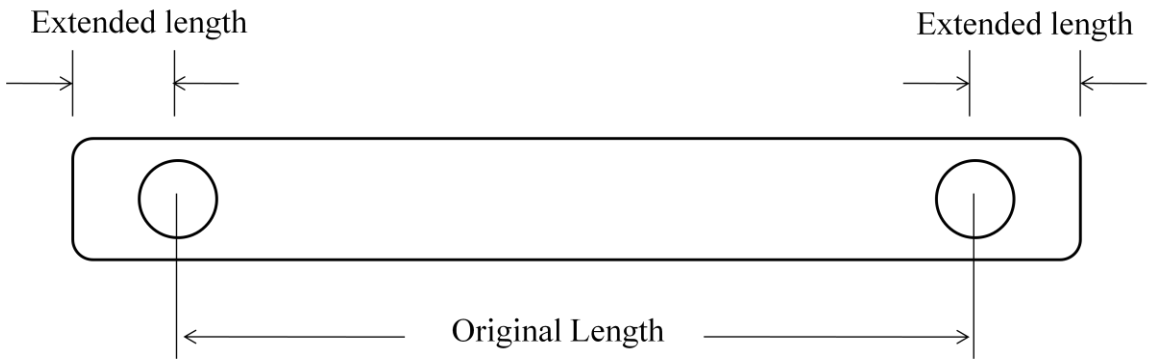


**Figure 3.8: Extended Length in Links**

This procedure implemented on Link 2 is applied to the development of Link 3 and Link 2' as well. Therefore, the next component of the linkage to be sketched using Pro-Engineer is the dyad plate that couples the D111 and D011 mechanisms. In this case, sketching the plate can be accomplished by either specifying the relative angles between the revolute joints (B, C, and E), or by specifying the position of each of the three joints in terms of their X and Y coordinates. The quickest approach is to specify the respective coordinates by implementing several reference

lines on the workspace and drawing the appropriate diameter on the points to *extrude* the holes (Figure 3.9). Once the revolute joints have been created, the dyad plate is completed by sketching a substantial amount of space on the outside of the pivots to keep the specified parameters intact and allow for the mechanism to function according to the calculated values.

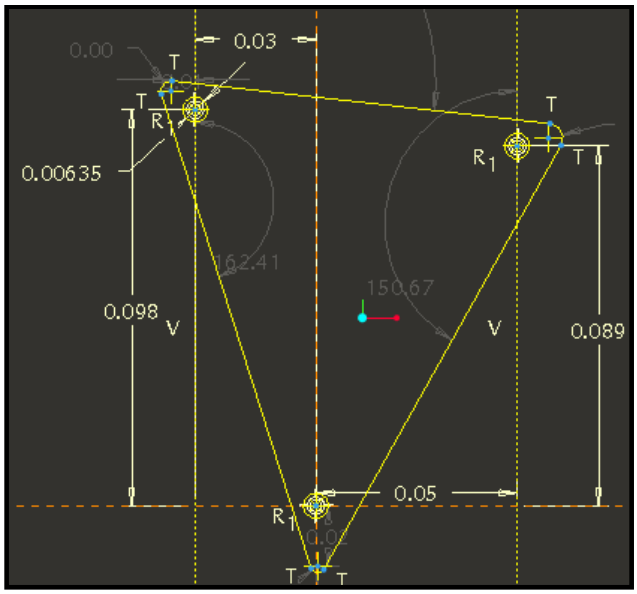


**Figure 3.9: Dyad Plate**

Furthermore, the next component to be sketched is the output displacement element. In this case, the challenge is to develop a slider element that is able to adapt to the three-dimensional parameters of Link 2' without the need to remove material from the component. The solution to the problem lies in creating a rail system that contains a pair of sliding blocks and allows for the link to be mounted in between (Figure 3.10). Once this design is well defined, it can easily be sketched on the software with the tools available. However, it is essential to point out that the most important factor in this procedure is for the holes to be *extruded* right on the center of the

element to prevent misalignment with the revolute joint C, and as a result achieve a smooth horizontal motion.

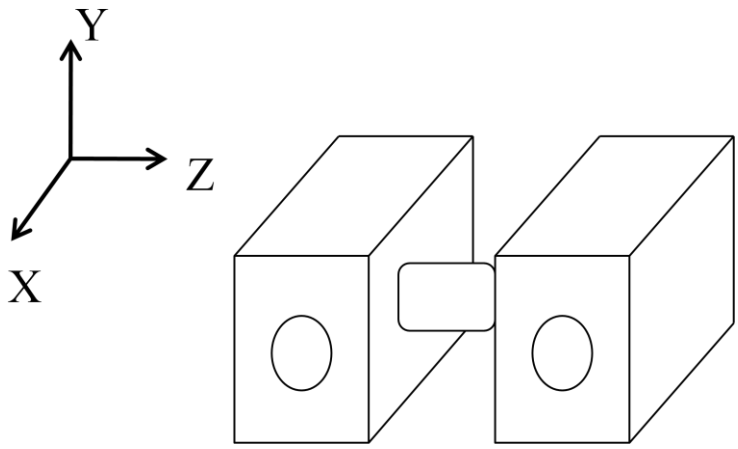


**Figure 3.10: Linear Displacement Element**

Having sketched the displacement element concludes one of the two steps required to develop a CAD drawing for the actively adjustable spring mechanism. The second and last step involves generating the assembly of the linkage with the previously generated components. However, as mentioned earlier, the greatest challenge in generating a drawing is finding a way to mount the mechanism on the shafts of the motors and satisfy all of the parameters determined in the design phase. This process can be accomplished by sketching a pair of motors to visually understand how the assembly of the mechanism can be adapted to the rotating devices, and to see what other components may be needed to obtain a smooth modulation from the slider. Once the motors have been generated in Pro-Engineer, they are mounted on a base according to their specified distance ($L_1$: Table 3.2) and each of the links are assembled using a pin connection (Figure 3.11). Before continuing, it is important to mention that this pin is sketched 0.00635 *m* in diameter to meet each hole requirement, and 0.0127 *m* in length to satisfy the distance across the

connected links. If these dimensions are not suited to employ a tight fit across the links, then the mechanism will be unstable and will not be able to modulate according to the predicted dynamics.

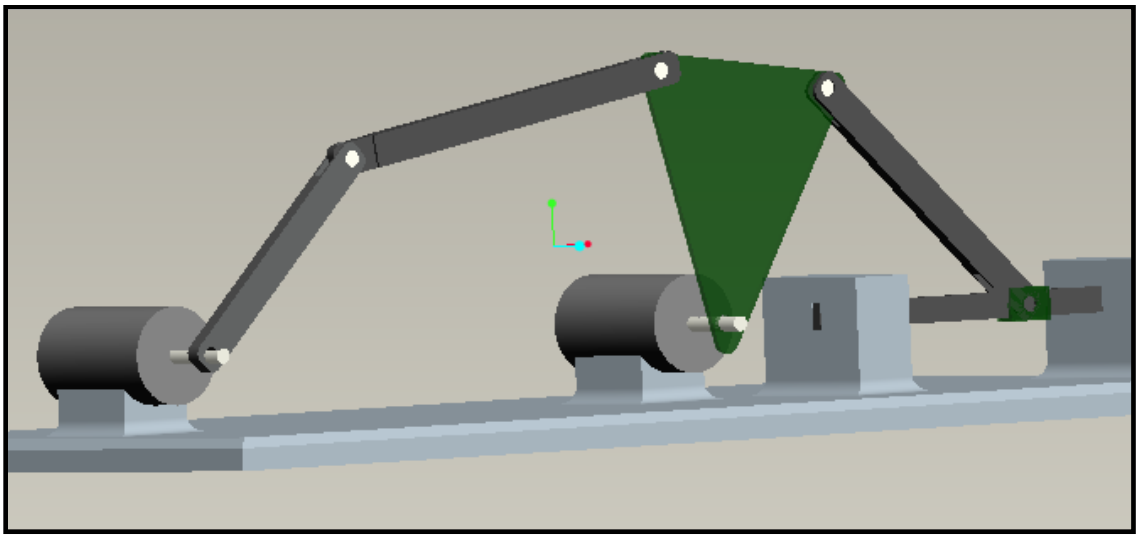

**Figure 3.11: Assembly of Spring Mechanism (Pro-Engineer)**

With this said and understood, one issue to notice from the figure is that the motor shafts are located a certain distance from the bottom of the base. This means that assembly of the output displacement element *must* be elevated to that distance in order to create a system that is aligned with the grounded revolute joints. To solve this problem, two walls are placed in between the slider element to support the rail system that is to be mounted horizontally. As a result, the three-dimensional assembly of the Watt II linkage can be completed with all of the details needed to fabricate a physical device.

In conclusion, a computer-aided design drawing of the designed spring mechanism was created (Pro-Engineer) to serve as a reference guide during the process of fabricating a physical model. With this sketch, one of the advantages is that details such as the development of each

component and the assembly of the linkage can be foreseen before the manufacturing process begins. For example, some of these details included specifying the adequate dimensions on each component (X, Y, and Z direction) to have a functional mechanism, determining the size of the holes on the links to connect each component and the two grounded DC motors, finding an approach to assemble the revolute joints (pins, screws, etc.), and making sure that the dimensions on the assembly matched the dimensions of the previously designed mechanism in order to obtain a precise, one degree-of-freedom motion along the horizontal axis. With such details considered, the fabrication process of the linkage is simplified in two ways. First, with all the dimensions specified on the drawing, the process of purchasing a material with the exact dimensions is facilitated. Secondly, the fabrication process is simplified by knowing exactly what machinery and tools to use when manufacturing each component of the spring mechanism.

# CHAPTER IV

## MOTOR TORQUES AND DESIRED EFFECTIVE STIFFNESS

In the previous chapter, kinematic and kinetic equations were implemented to determine the geometric design and behavior of the Watt II linkage. Part of the analysis required describing the motion of the mechanism in terms of position, velocity, and acceleration. However, in no case were the two nonlinear input forces, required to drive the redundantly actuated system, incorporated as part of the design process. Therefore, in this chapter the two equilibrium forces (torques) needed to satisfy the concept of redundant actuation and consequently create an effective stiffness on the linkage will be calculated using the principle of virtual work (power in = power out). The goal in this process is to substitute the previously calculated *g* and *h* functions and solve for the *Effective Inertia*, *Inertial Power*, and *Effective Stiffness due to Gravity Loads* to obtain the required forces and the desired effective stiffness of the system.

Three sections constitute the process of attaining the nonlinear two input forces (torques) needed for the spring mechanism to be at its equilibrium state. In section 4.1, the principle of virtual work will be implemented to generate the necessary equations that will allow for the motor torques at $\theta_2$ and $\theta_4$ to be solved. As a result, the *model* kinetic energy will be equated with the *system* kinetic energy to solve for the Effective Inertia of the system and consequently attain the respective effort at $\theta_2$. Once the motor torque at the grounded revolute joint O has been determined, the motor torque at $\theta_4$ is obtained by solving the system equilibrium equation

calculated in Chapter II (section 2.2), and the desired effective stiffness is determined as well. At this point, it is necessary to review what desired effective stiffness means. As mentioned earlier, the desired effective stiffness of the actively adjustable spring mechanism represents the stiffness at equilibrium position. In the final section, the two generated forces (torques) will be implemented in Working Model to verify that the analytical results match the parameters created by the simulation.

### 4.1 Motor Torque at Theta Two

In the present section, three major equations are generated during the process of solving the two nonlinear input forces. For example, the purpose of generating equation one (*Effective Inertia*) is to account for the generalized mass of the system in terms of calculating the angular and translational velocity and of each link relative to the center of mass. On the other hand, equation two (*Inertial Power*) is developed in order to consider the forces acting on the spring mechanism in terms of calculating the angular velocity and acceleration of each link relative to the center of mass, and the translational velocity and acceleration of each link relative to the center of mass. Lastly, equation three is generated during the process of finding the two efforts (*Effective Stiffness due to Gravity Loads*) to determine the gravity loads acting on the system in terms of calculating the translational velocity of each link along the vertical direction. However, before these three equations can be attained, it is important to understand how the principle of virtual work is generated and how can it benefit the calculation process.

As briefly mentioned, the principle of virtual work is generated by equating the ‘input power’ of the system with the ‘output power’ of the system. This power balance implies that as the (equilibrium) spring mechanism is subject to a displacement along the horizontal axis, the total virtual work of all external forces is equal to zero. Therefore, the advantage of using the

principle of virtual work is that the unknowns, in this case the forces acting on the system, can be solved using an energy approach (4.1) instead of the traditional approach (Newton's second law). Using the traditional approach, on the other hand, can certainly solve for the equilibrium torques of each motor, but the process will take longer and the possibility of making an error is greater.

$$L = KineticEnergy - PotentialEnergy \tag{4.1}$$

With the principle of virtual work understood, the first major equation (*Effective Inertia*) is obtained by equating the *model* kinetic energy with the *system* kinetic energy as

$$K.E._{Model} = K.E._{System} \tag{4.2}$$

From this equation, one important detail to point out is that the kinetic energy is the only source of energy regarded from the Lagrangian equation (4.1). The potential energy, on the other hand, is totally neglected based on the fact that the output linear displacement element only modulates along the global horizontal direction and not along the vertical direction. For this reason the generalized mass of the Watt II linkage is obtained by adding the translational kinetic energy (X and Y direction) with the rotational (angular) kinetic energy. Such terms are equivalent to

$$K.E._{Model} = \frac{1}{2} I_{si} \dot{\phi}_i^{\,2} \tag{4.3}$$

and

$$K.E._{System} = \sum_l \left( \frac{1}{2} I_l \dot{\theta}_l^{\,2} + \frac{1}{2} M_l \left( \dot{x}_l^{\,2} + \dot{y}_l^{\,2} \right) \right) \tag{4.4}$$

where

$I_{si} =$ Effective mass

$\dot{\phi}_i =$ Input speed

$l =$ Link

$I_l$ = Mass moment of inertia of the link relative to the center of mass

$\dot{\theta}_l$ = Absolute angular speed of the link relative to the center of mass

$M_l$ = Mass of link

$\dot{x}_l, \dot{y}_l$ = Absolute velocity components of link with respect to the center of mass

Once these two equations are combined (see equation 3.40), the next step is to calculate the terms in the expression by means of calculating the angular and translational velocity of each link relative to the center of mass. However, it is significant to mention that this process has already been accomplished in Chapter III and there is no need to repeat it. The only step that is needed to solve the *Effective Inertia* of the system involves substituting all of the calculated parameters into equation (3.40). Therefore, after the substitution has been made, the final expression yields

$$\begin{aligned} I_{2s} = I_2 \cdot g_{22}{}^2 + m_2 \cdot \left(g_{22x}{}^2 + g_{22y}{}^2\right) + I_3 \cdot g_{32}{}^2 + m_3 \cdot \left(g_{32x}{}^2 + g_{32y}{}^2\right) + \\ I_4 \cdot g_{42}{}^2 + m_4 \cdot \left(g_{42x}{}^2 + g_{42y}{}^2\right) + I_{2'} \cdot g_{2'2}{}^2 + m_{2'} \cdot \left(g_{2'2x}{}^2 + g_{2'2y}{}^2\right) + I_O + I_C \end{aligned} \tag{4.5}$$

where $I_{2s}$ is calculated in terms of position.

Furthermore, *Inertial Power* is the second major equation that is generated during the process of solving for the two, nonlinear, equilibrium motor torques. As said before, the purpose of deriving the *Inertial Power* is to solve for the forces acting on the system using an energy approach instead of the traditional approach. However, before this expression can be generated, it is important to see how the energy approach relates to the Newton's second law of motion.

The process is formulated by considering the energy produced by a single particle moving along a path as

$$K.E. = \frac{1}{2} m v^2 \tag{4.6}$$

where *m* represents the mass of the particle and *v* represents the velocity of the particle. With such equation considered, the course of finding the *Inertial Power* of the system is initiated by simply differentiating with respect to time as

$$\frac{d}{dt}\left(K.E\right)=\frac{d}{dt}\left(\frac{1}{2}mv^{2}\right)=\frac{1}{2}m\left(2v\dot{v}\right) \tag{4.7}$$

where the end result states that the change in kinetic energy of the particle is equivalent to the product between the velocity and the rate of change of momentum

$$\frac{d}{dt}\left(K.E.\right)=mav \tag{4.8}$$

From this result, the relationship between the energy and Newton's second law of motion can be identified. For example, Newton's second law of motion (4.9) states that the summation of forces acting on the system is equivalent to the rate of change of momentum. This indicates that the amount of motion (momentum) on a body is the product between the mass and the velocity, which is *exactly* the same case presented in equation (4.8). However, the process does not end here, there is one more step that needs to be taken into consideration before the *Inertial Power* of the mechanism can be calculated.

$$\sum F=ma \tag{4.9}$$

This step involves writing the energy equation (4.8) in terms of Newton's second law. For instance, since the product between the mass and the acceleration can be found in both equations, it can be represented in terms of an effort $\left(F=ma\right)$ as

$$\frac{d}{dt}\left(K.E\right)=Fv \tag{4.10}$$

where the right-hand side of the expression can also be written as the product between the inertial load (or mass) $T_i^{\,l}$ and the input speed (or velocity) $\dot{\phi}_i$

$$\frac{d}{dt}(K.E.) = T_i^{\,I}\,\dot{\phi}_i \tag{4.11}$$

With this relationship formulated between the energy and Newton's second law of motion, the idea is to first solve for the *Inertial Load* of the system before obtaining the *Inertial Power*. Therefore, the calculation initiates by implementing the Chain Rule to differentiate equation (4.11) with respect to time as

$$\frac{d}{dt}\left(\frac{1}{2} I_{is}\dot{\phi}_i^{\,2}\right) = T_i^{\,I}\,\dot{\phi}_i \tag{4.12}$$

and obtaining the expression

$$T_i^{\,I} = I_{is}\ddot{\phi}_i + P_{is}\dot{\phi}_i^{\,2} \tag{4.13}$$

where $\ddot{\phi}_l$ represents the angular acceleration of each link relative to the center of mass, and $\dot{\phi}_l^{\,2}$ represents the angular velocity of each link relative to the center of mass. From this equation, additionally, the term $P_{is}$ represents the *Inertial Power* of the system and is a result of differentiating the previously calculated *Effective Inertia* with respect to the input as

$$P_{is} = \frac{1}{2}\frac{dI_{is}}{d\phi_i} = \sum_l \left(I_l \cdot g_{li} \cdot h_{li} + M_l \cdot \left[g_{lix} \cdot h_{lix} + g_{liy} \cdot h_{liy}\right]\right) \tag{4.14}$$

where the KIC's represent the angular velocity and acceleration of each link relative to the center of mass, and the translational velocity and acceleration of each link relative to the center of mass. These values have also been computed in the previous chapter and there is no need to repeat the procedure. Therefore, substituting the computed values into the equation yields the *Inertial Power* of the Watt II mechanism as

$$\begin{aligned} P_{2s} &= I_2 \cdot g_{22} \cdot h_{22} + m_2 \cdot \left(g_{22x}h_{22x} + g_{22y}h_{22y}\right) + I_3 \cdot g_{32} \cdot h_{32} + \\ & m_3 \cdot \left(g_{32x}h_{32x} + g_{32y}h_{32y}\right) + I_4 \cdot g_{42} \cdot h_{42} + m_4 \cdot \left(g_{42x}h_{42x} + g_{42y}h_{42y}\right) + \\ & I_{2'} \cdot g_{2'2} \cdot h_{2'2} + m_{2'} \cdot \left(g_{2'2x}h_{2'2x} + g_{2'2y}h_{2'2y}\right) \end{aligned} \tag{4.15}$$

where $I_i$ represents the mass moment of inertia of each link, $g_{22}$ represents the angular velocity of Link 2 with respect to $\theta_2$, which is equal to one (Chapter III), and $m_i$ represents the mass of each link.

The last major equation developed before the input force at $\theta_2$ can be calculated, is the *Effective Stiffness due to Gravity Loads*. This process, as evaluated in Chapter II, initiates by equating the virtual work done by the effective load/generalized force at the input, to the virtual work done by externally applied loads as

$$T_{\theta 2}{}^{*} \cdot \delta_{\theta 2} = \sum_{P} \left( T_P \cdot \delta\theta_P + F_{PX} \cdot \delta X_P + F_{PY} \cdot \delta Y_P \right) \tag{4.16}$$

where the moment component ($T_P$) and force components ($F_{PX}$ and $F_{PY}$) are a set of *P* loads acting on motion parameters $\theta_P$, $X_P$, and $Y_P$. From such general condition, it is important to observe the development of the equilibrium force ($T_{\theta 2}$) needed to create an effective stiffness on the system and consequently drive the actively adjustable spring mechanism. However, before this force (torque) can be obtained, the first step is to divide the expression by the virtual displacement $\delta_{\theta 2}$ to cancel the displacements done by the externally applied loads and create an equation that is written in terms of KIC's. Once the KIC's are implemented, all of the externally applied loads are substituted in general terms as

$$\sum_{A} \left( T_a g_{ai} \right) = I_{is} \frac{d^2}{dt^2} \left( \phi_i \right) + P_{is} \left( \frac{d}{dt} \phi_i \right)^2 - \left( T_{is} \right)^k - \left( T_{is} \right)^g - \left( T_{is} \right)^L - \left( T_i \right)^m \tag{4.17}$$

where

$T_{is}{}^{k}$ = Effective loads

$T_{is}{}^{g}$ = Gravity loads with respect to the center of mass

$T_{is}^{\ L}$ = Externally applied loads

$T_i^{\ m}$ = Motor torque

However, not all of these loads are needed to determine the effort at the grounded revolute joint. For example, the necessary loads *only* include the motor torque and the gravity loads, while the externally applied loads and the effective loads are totally neglected. Having explained this allows for the expression of the required motor torque to be attained as

$$T_{2m} = \left(I_{2s} \cdot \alpha_2 + P_{2s} \cdot \omega_2^{\ 2}\right) - \left(T_{2s}\right)^g \tag{4.18}$$

where the first term in parenthesis represents the *Inertial Load* ($T_i^{\ I}$) and $\left(T_{2s}\right)^g$ represents the gravity loads acting on the system in a downward direction. Since the *Inertial Load* has already been determined in the previous paragraph, only the gravity loads of the linkage need to be computed to complete the process. For instance, the procedure involves implementing Newton's second law of motion to determine the translational velocity of each link along the vertical direction as

$$\sum F = ma \Rightarrow F_{ly} = -M_l g \Rightarrow \sum_l \left(g_{liy}\right) \cdot -M_l g \tag{4.19}$$

where gravity is assumed to act in the negative-Y direction (Figure 4.1)

$$g = gravity \tag{4.20}$$

and the load is represented by the change in position

$$g_{liy} = \frac{dy_l}{d\phi_i} \tag{4.21}$$

However, it is significant to point out that such calculation has been accomplished in Chapter III and there is no need to repeat the process. Therefore, substituting the calculated *g*-functions into equation (4.19) yields the third major equation as

$$T_{2s} = g_{22y} \cdot (-m_2 \cdot g) + g_{32y} \cdot (-m_3 \cdot g) + g_{42y} \cdot (-m_4 \cdot g) + g_{2'2y} \cdot (-m_{2'} \cdot g) \tag{4.22}$$

where the minus sign represents the gravity of the system acting in a downward direction (Figure 4.1).

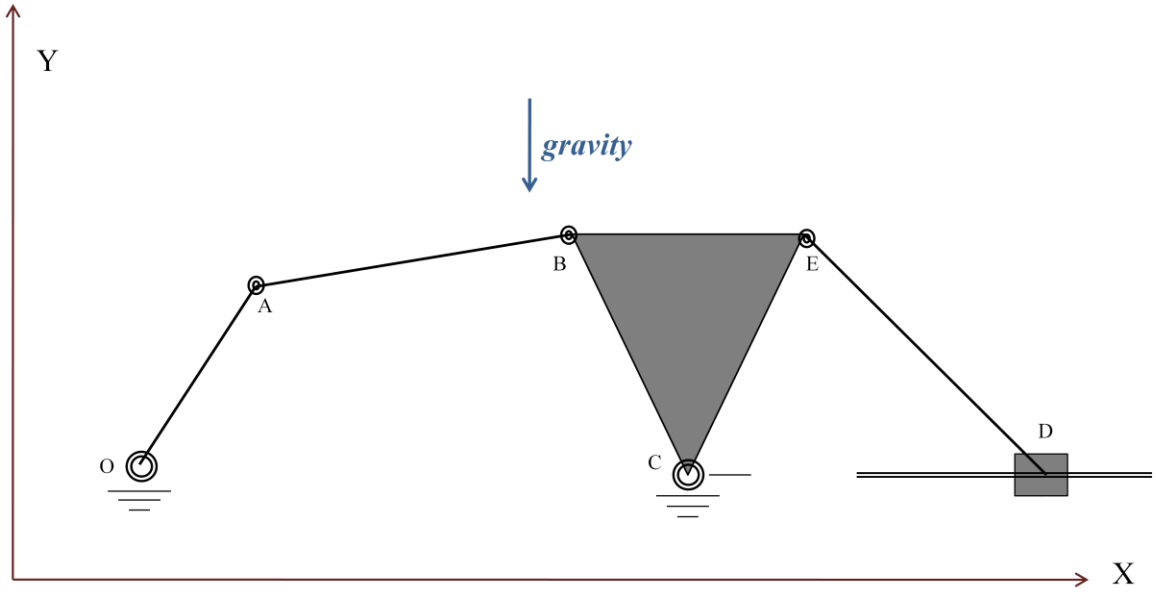


**Figure 4.1: Gravity in Spring Mechanism**

With this equation at hand, the motor torque at $\theta_2$ is easily calculated by means of expanding equation (4.18) and obtaining

$$T_{2m} = \left(I_{2s} \cdot \alpha_2 + P_{2s} \cdot \omega_2{}^2\right) - \begin{pmatrix} g_{22y} \cdot (-m_2 \cdot g) + g_{32y} \cdot (-m_3 \cdot g) + \\ g_{42y} \cdot (-m_4 \cdot g) + g_{2'2y} \cdot (-m_{2'} \cdot g) \end{pmatrix} \tag{4.23}$$

where $I_{2s}$ represents the *Effective Inertia*, $P_{2s}$ represent the *Inertial Power*. At this point, however, it is necessary to emphasize the direction of the force. In Chapter II it was said that a certain condition needed to be met in order for the mechanism to create the necessary internal loading. The condition stated that the force generated at $\theta_2$ *must* be applied in a counterclockwise direction, and the force generated at $\theta_4$ *must* be applied in a clockwise

direction in order to produce an effective stiffness on the mechanism. If such forces (torques) are applied in the opposite direction, the concept of redundant actuation is useless and the system will not behave as a spring mechanism. Therefore, the value of this force (torque) *must* be a positive value in order to produce the adequate direction.

In conclusion, three major equations were generated prior to the attainment of the nonlinear input force (torque) at $\theta_2$ (*Effective Inertia*, *Inertial Power*, and *Effective Stiffness due to Gravity Loads*). These equations were generated based on the principle of virtual work and were derived using an energy balance approach that related to Newton's second law of motion. After each expression was developed, the process of solving all of the terms (KIC's) did not have to be implemented since they had been calculated in the previous chapter. This allowed for the attainment of the effort at the input to be easily computed without the need to repeat any calculation (Table 4.1) and consequently the effort at the output angle. As in the previous chapters, the analytical expressions generated in this chapter were represented in general terms to avoid any mistakes when computing.

**Table 4.1: Motor Torque Two Parameters**

| Parameters | Values |
|---|---|
| $I_{2s}$ | $5.493\times10^{-4}\,m^2\cdot kg$ |
| $P_{2s}$ | $-3.249\times10^{-4}\,m^2\cdot kg$ |
| $T_{2s}$ | $-6.213\times10^{-3}\,N\cdot m$ |
| $T_i^I$ | $2.244\times10^{-4}\,N\cdot m$ |
| $T_{2m}$ | $6.437\times10^{-3}\,N\cdot m$ |

### 4.2 Motor Torque at Theta Four

In Chapter II, it was said that since the Watt II mechanism has a one degree-of-freedom motion along the horizontal axis, its kinematic state is completely defined by a single parameter $\theta_2$, meaning that a single motor can control the equilibrium state of the system. However, the problem in implementing a single motor is that if a non-zero input torque is applied, the mechanism will move according to its dynamics and the static equilibrium condition will be lost. The solution to this problem, as a result, was to implement a second force (redundant actuation) that would sustain the internal loading of the linkage and at the same time keep the system in static equilibrium.

Up to this point, however, such force has not been calculated. Therefore, the target in this section is to compute the effort at $\theta_4$ with the help of the previously calculated torque (at joint O). In this process, it is important to mention that there is no need to manipulate multiple equations to obtain a solution, only a single equation is required to solve for the unknown.

For example, the process initiates by taking the equilibrium equation of the mechanism (Chapter II: equation (2.1)) and isolating the unknown on one side of the equation and the rest of the parameters on the other side. Once this expression has been rearranged, the end result states that the motor torque is equivalent to the ratio between the motor torque at $\theta_2$ and the angular velocity of Link 4 as

$$T_4 = \frac{-T_2}{g_{42}} \tag{4.24}$$

where $g_{42}$ is the velocity of Link 4 with respect to Link 2. From this equation, it is seen that a negative value is obtained for $T_4$, what this means is that the direction of the force is to be

applied in a clockwise manner. Such result certainly validates the condition that states that the force generated at $\theta_4$ *must* be applied in a clockwise direction in order to produce an effective stiffness on the mechanism.

Moreover, once the second force has been computed and the system has reached an equilibrium position, the next step is to formulate a relationship that will be useful during the testing of the physical model and will allow for any motor torque to be solved in a one step process. The idea is to avoid repeating the entire calculation process to find a set of equilibrium torques. With this relationship at hand, for example, an arbitrarily or desired torque can be specified and the other one can easily be computed. Therefore, what is done is that the calculated value of $T_4$ is written over the calculated value of $T_4$ to obtain a dependent integer as

$$\frac{T_4}{T_2} = -1.729 \tag{4.25}$$

where any of the two forces can be specified first.

### 4.2.1 Desired Effective Stiffness at Equilibrium State (K*)

Having solved for the equilibrium input forces (torques) required to satisfy the concept of redundant actuation and consequently drive the actively adjustable spring mechanism, the next step is to determine the desired effective stiffness of the system at its equilibrium state (as mentioned in Chapter II). This calculation is obtained by the following process:

$$\left(T_d{}^*\right)^K, K_d{}^* \tag{4.26}$$

where $K_d{}^*$ is the desired effective stiffness of the system.

$$\left(T_i{}^*\right)^K = g_{di}\left(T_d{}^*\right)^k \tag{4.27}$$

Therefore,

$$\left(T_d{}^*\right)^K = \frac{1}{g_{di}}\left(T_i{}^*\right)^k \tag{4.28}$$

Consequently,

$$K_d{}^* = \frac{d\left(T_d{}^*\right)^k}{d\phi_d} \tag{4.29}$$

$$= -\left[\frac{d}{d\phi_i}\left(T_d{}^*\right)^k\right]\frac{d\phi_i}{d\phi_d} \tag{4.30}$$

$$= -\left[\frac{d}{d\phi_i}\frac{\left(T_d{}^*\right)^k}{g_{di}}\right]\frac{1}{g_{di}} \tag{4.31}$$

$$= -\left[\frac{\left\{\frac{d\left(T_i{}^*\right)^k}{d\phi_i}\right\}g_{di} - \left(T_i{}^*\right)^k\left\{\frac{d\left(g_{di}\right)}{d\phi_i}\right\}}{g_{di}{}^2}\right]\frac{1}{g_{di}} \tag{4.32}$$

and

$$= -\frac{1}{g_{di}{}^3}\left[\left(-K_i{}^*\right)g_{di} - \left(T_i{}^*\right)^k h_{di}\right] \tag{4.33}$$

Therefore, the desired effective stiffness at point D (Figure 4.1) is represented as

$$K_D{}^* = \frac{1}{\left(g_{D2X}\right)^3}\left[g_{D2X}\cdot K_2{}^* + h_{D2X}\cdot\left(T_2{}^*\right)^K\right] \tag{4.34}$$

where $T_2{}^*$ is equal to zero due to the equilibrium state of the system, $K_2{}^*$ represents the effective stiffness at the input (equation (2.9)), and consequently the final expression yields

$$K_D{}^* = \frac{K_2{}^*}{\left(g_{C2X}\right)^2} \tag{4.35}$$

In conclusion, the input forces (torques) required to satisfy the concept of redundant actuation were calculated in this section. The process initiated by using the equilibrium equation of the mechanism to substitute the previously calculated effort and obtain the necessary torque at $\theta_4$. After the system reached its static equilibrium state, a relationship between the two forces was generated to facilitate the process of attaining another set of equilibrium torques. In addition, the desired effective stiffness of the system due its equilibrium state was determined. This procedure, as a result, wraps up the entire theoretical calculations in the present study.

### 4.3 Working Model Verification

Before the physical model can be generated, it is important to verify that all of the computed, theoretical values are correct. This verification is accomplished by implementing the values of the two motor torques into the previously generated Working Model simulation. Within the simulation, there are two major observations that need to be considered. For example, the first observation is to validate that the Watt II linkage remains in static equilibrium as the motor torques are applied. If the system modulates with these parameters, then a computational error occurred on the analyses and should be fixed as soon as possible. However, if the system remains in its equilibrium state, then the second observation involves verifying that the KIC's generated in the simulation match those theoretically calculated.

With these observations in mind, the verification process initiates by implementing the respective motor torques on each of the grounded revolute joints (Figure 4.2). After running the simulation, results indicate that the model remains in static equilibrium and the motion parameters (*g*-functions) of each link are equivalent to the predicted values (see Table 3.5)! The percent error on the g-functions is 0.7% and 1.2%, which means that the results are accurate.

This outcome demonstrates that the entire analysis is correct and that indeed, the system will behave as a spring mechanism as a result of the internal loading created.

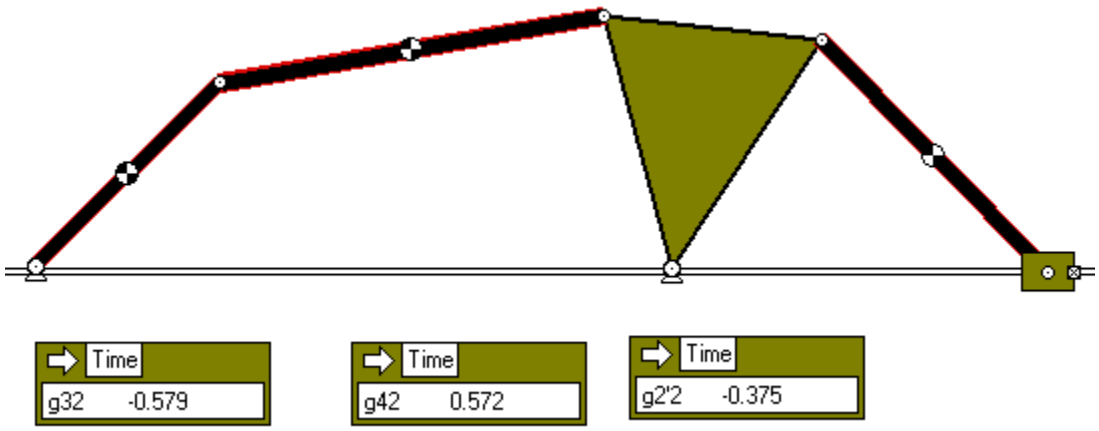


**Figure 4.2: Working Model Verification**

Before continuing, however, it is great significance to mention that the computed, theoretical values also need to be validated using a 'DC motor' on each of the grounded revolute joints. The reason for this is that the spring mechanism will be physically driven using two direct brush-type DC motors. Not only this, but with the incorporation of the DC motors several motor parameters (physical) can be implemented to closely simulate the behavior of the real system. In the previous simulation, for example, the two input forces (torques) needed for the system to be at an equilibrium state were generated with a 'torque' motor, but in reality, a torque value cannot be directly specified on a brush-type DC motor. What is done, in reality, is that the required motor torque is applied in terms of a current or voltage. In this case, for instance, the software requires that the two input torques of the system are specified in terms of an input voltage.

Not only is the input voltage required to have a good sense of how the Watt II linkage is going to behave, but there are several other parameters that need to be specified on each motor as

well. For example, these parameters include the resistance of the motor amature, the inductance, the speed constant, and the motor constant, which is also defined as the torque constant (Table 4.2). It is important to clarify that such parameters are not calculated or arbitrarily considered; rather they are obtained from the specifications of the 5A direct brush-type DC motor. However, before specifying the parameters into Working Model, it is important to recall that the software only accounts for SI units. This means that, in this case, the speed constant and the motor constant are the only parameters that need to be converted from English units to SI units in order to be consistent with all of the design parameters. Therefore, the conversion process for such parameters is accomplished as follows:

$$Speed\_const. = \frac{10.2V\ \min}{KRPM}\ x\ \frac{60s}{1\min}\ x\ \frac{1rev}{2\pi \cdot rad}\ x1000 = 0.0974Vs \qquad (4.26)$$

and

$$Motor\_const. = \frac{13.7oz \cdot in}{1Amp}\ x\ \frac{1lb}{16oz}\ x\ \frac{4.448N}{1lb}\ x\ \frac{1m}{39.37in} = 0.0967Km \qquad (4.27)$$

**Table 4.2: DC Motor Parameters specified in Working Model**

| Parameters | Motor 2 | Motor 4 |
|---|---|---|
| Resistance | 1.041 Ohm | 1.040 Ohm |
| Inductance | 0.004 Henry | 0.004 Henry |
| Speed Constant | 0.097 Kv | 0.097 Kv |
| Motor Constant | 0.097 Km | -0.097 Km |
| Input Voltage | 1.00 V | 1.729 V |

Once these parameters have been specified and the simulation in Working Model has been generated, results indicate that the model remains in static equilibrium and the motion parameters (*g*-functions) of each link are equivalent to the predicted values (Table 3.5). This result indicates that the computed values are correct and that the next phase of the project can be considered.

# CHAPTER V

## MANUFACTURING AND ASSEMBLY OF THE SPRING MECHANISM

Up to this point, the concept of redundant actuation has been incorporated to theoretically design an actively adjustable spring mechanism (Watt II linkage). Not only has the theoretical design of the linkage been completed, but most importantly, the calculated values have been validated via Working Model simulation. This accomplishment certainly allows for the next phase of the project to be considered. However, before continuing into the next phase, it is of great importance to briefly summarize how such process has been achieved.

The process began in Chapter II by determining the equilibrium equation of the spring mechanism. Such expression was accomplished by equating the virtual work done by the effective load, to that done by the externally applied loads. Based on this expression, consequently, kinematic and kinetic equations were implemented in Chapter III to determine the geometric design of the one degree-of-freedom mechanism and estimate its non-linear behavior. After describing the motion of the mechanism in terms of position, velocity, and acceleration, the two equilibrium forces (torques) needed to create an effective stiffness on the linkage were calculated in Chapter IV. These equations were generated based on the principle of virtual work and were derived using an energy balance approach that relates to Newton's second law of motion.

With this brief summary, the process of developing and testing a physical model can be taken into consideration. Therefore, the target of the present chapter is to carry out the

fabrication and assembly process of the actively adjustable spring mechanism according to the parameters generated on the Pro-Engineer drawing.

As mentioned earlier, one of the advantages of using the computer-aided design drawing is that it allows for each component of the mechanism to be fabricated to scale. This, in particular, will eliminate any speculating scenarios that can be unnecessary and time consuming during the fabrication process. However, before such process can be carried out, several details must be regarded first in order for the manufacturing mechanism to have a sequential order.

Specifically, there are four sections that embellish this chapter. In section 5.1, a material selection will be made based on the identification of different types of conditions that affect the fabrication and functionality of the linkage. Once the material has been selected, the process of manufacturing the spring mechanism will initiate (in section 5.2) by using the tools and machines needed to fabricate each component according to the design specifications (Department of Mechanical Engineering at The University of Texas-Pan American). A preliminary test will then be conducted (in section 5.3) using a mechanical link, a direct drive DC motor, and a power amplifier to observe how the system behaves in a static situation, and consequently anticipate how the real system will be driven. This procedure is important because since there is no experimental validation, the behavior of the system is not known. Based on the results, the idea is to determine what electronic components (power amplifier, power supply, etc.) will be required to drive the redundantly actuated system and carry out the necessary experiments. In the last section of the chapter, the Watt II linkage will be mounted and assembled using all of the equipment purchased (section 5.4). With the setup completed, a series of experiments will be planned out and conducted to validate the concept of adjustable springs (Chapter VI).

## 5.1 Material Selection

The target of the present section is to decide on two materials (preferably a metal) that will be implemented during the fabrication phase of the spring mechanism. The first material will be selected on the basis of fabricating the components of the Watt II linkage, and the second material will be selected on the basis of fabricating the rail system (in which the linear displacement element modulates). However, before these selections can be made, it is important to identify several types of conditions and environments in which the spring mechanism will be exposed during the manufacturing process, or during the actual testing. If these circumstances are not taken into consideration, the chances of *not* meeting the design specifications increase and consequently, there is a possibility of developing a system that will not function properly.

With these consequences in mind, the first condition is found in the machining process. For example, one characteristic that the selected materials must have is the feasibility to be machined under high temperatures and high cutting speeds. Under these circumstances, first of all, the materials must possess sufficient toughness (ductility) to avoid fracture during plastic deformation. If this characteristic is very minimal or is not found, the components will fracture as soon as a small force is applied to the (brittle) surface. This, in particular, must be avoided in order for the machines to perform smooth, clean cuts. On the other hand, the materials should not be too tough that the machines cannot penetrate and create the specified design parameters. If the strength of the materials is too high, the tools and machines can be damaged or ruined by trying to achieve something beyond their capability. Therefore, the most important factor to satisfy both of these cases is to consider the mechanical properties of the materials, such as coefficient of thermal expansion, modulus of elasticity, and yield strength.

Moreover, a second issue to keep in mind is that the spring mechanism will be in constant contact with the atmosphere and with a lubricant (fluid) that is to be applied on the revolute joints and the output sliding element to minimize friction. The problem, in both cases, is that *corrosion* can develop on the metal in a matter of days and can cause rapid degradation. For example, the type of corrosion that forms when the metal comes in contact with the atmosphere is *atmospheric corrosion*. This type of corrosion forms due to the chemical reaction between the metal and the salt (NaOH) present in the atmosphere. What happens, in particular, is that the material looses excess amount of electrons during the anodic reaction and as a result is not able to create a protective layer. On the other hand, the type of corrosion that forms when the metal comes in contact with the lubricant is *erosion corrosion*. This phenomena occurs when the passive layer of the metal is removed (due the shear stress of the fluid) and the surface is exposed to the oxygen atoms.

The effect of having these types of corrosion is that they can jeopardize the functionality and aesthetics of the spring mechanism. This means that if the system is not functioning properly, the experimental data will not be able to match the theoretical values.

However, it is significant to mention that corrosion not only forms as a result of the contact between the metal and the atmosphere, or between the metal and the fluid. Corrosion will also form in the areas where two metals come in contact with each other (*galvanic corrosion*). For example, in this case the (anodic) chemical reaction can occur as a result of machining the material with a different type of metal, or as a result of coupling the links with a bolt or pin. During the reaction, what happens is that the difference of (voltage) potential between the two metals causes most of the electrons to be transferred to one metal. In this particular metal, a cathodic protection will form due to the excess of electrons transferred from the other metal, and

as a result corrosion will not occur. The metal with the weaker charge, however, will only retain a small amount of electrons, and consequently corrosion will take effect. Therefore, a non-corrosive material that produces a greater charge during the potential difference must be kept in mind as well.

### 5.1.1 Material for Linkage

After these major circumstances have been identified, the material that compensates the fabrication of the spring mechanism is *Aluminum alloy 6061-T6*. Specifically, there are two main reasons for selecting this material. The most important reason, particularly, is that the alloy contains the mechanical properties and physical properties needed to withstand all of the specified circumstances (Table 5.1). The grouping of these properties allows the material to produce several characteristics that facilitate the process of fabricating the spring mechanism. For example, such characteristics include the following:

- Medium to high strength
- Good toughness
- Good surface finish
- Excellent corrosion resistance to atmospheric condition
- Good corrosion to sea water
- Can be anodized
- Good weldability and brazability
- Good workability
- Lightweight

With these features, machining each component will be carried out in a feasible manner and the Watt II linkage will be able to function properly.

**Table 5.1: Physical and Mechanical Properties**

| Property | Value |
|---|---|
| Ultimate tensile strength | $260-310\ MPa$ |
| Density | $2.7\ g/cm^3$ |
| Melting point | $\approx 580^\circ C$ |
| Modulus of elasticity | $70-80 MPa$ |
| Poisson's ratio | 0.33 |
| Coefficient of thermal expansion | $20-100^\circ C$ |

The second reason for selecting the aluminum alloy (Table 5.2) is that it is a common material in the marketplace and its cost is relatively low in comparison with other materials (Stainless Steel, Nickel, etc.). For example, there are materials that contain the required properties, but are not common in the marketplace, and there are materials that common in the marketplace, but are too expensive to purchase. This material, however, not only contains the necessary mechanical properties and physical properties, but it is common in the marketplace and the cost is remarkably affordable. Having explained the basis of selecting the *Aluminum alloy 6061-T6*, allows for the material to be purchased. In this case, however, there are two different types of sizes that need to be selected. For example, the first size of material contains the dimensions needed to fabricate all of the links of the mechanism (0.0127 x 0.00635 x 1.8288 *m*), and the second type of size contains the dimensions needed to fabricate the dyad plate (0.3048 x 0.3048 x 0.003175 *m*). Once these sizes are determined, a pair of each is purchased.

The reason for acquiring an extra set of material is in case of making an error during the fabrication of each component. For instance, if only the needed material is purchased and an error is made, the ordering process has to be repeated and the project will be on hold for at least a week.

**Table 5.2: Aluminum Alloy 6061-T6 Composition**

| Element | Weight % |
|---|---|
| Aluminum | Balance |
| Magnesium | 0.8 – 1.2 |
| Silicon | 0.4 – 0.8 |
| Iron | Max. 0.7 |
| Copper | .015 – 0.40 |
| Zinc | Max. 0.25 |
| Titanium | Max. 0.15 |
| Manganese | Max. 0.15 |
| Chromium | 0.04 – 0.35 |
| Other | 0.05 |

### 5.1.2 Material for Rail System (Track)

The following step involves choosing a material for the fabrication of the rail system (track). However, before this decision can be made, it is of major importance to identify an additional type of condition in which the material will be exposed during the testing of the device.

For example, the most important issue to consider formulates from the contact that will be generated between the material and linear displacement element. Under this circumstance, the selected material must have the ability to operate under the presence of shear forces created on the surfaces. If such characteristic is not found, the shear forces will deteriorate the surface of each component and the spring mechanism will not be able to modulate in a precise fashion. As a result of the deterioration, the components will have to be fabricated a second time to restore the functionality of the system. The problem with repeating this process is that a good amount of time will be consumed and at the mean time, the project will remain inactive. Therefore, the selected material for the rail system must be wear-resistant to eliminate the possibility of having these types of miscues.

With this type of condition identified, the material selection for the rail system can be made. For example, the material that best suits the fabrication of the rail system is a *copper-zinc alloy* (*brass*). This particular material is selected based on the mechanical and physical properties needed to operate under all the mentioned conditions and circumstances. The combination of these properties allows for the *copper-zinc alloy* to produce several characteristics that facilitate the fabrication process of the spring mechanism, and at the same time helps conserve the aesthetics. For example, such characteristics include:

- High corrosion resistance
- High tensile strength
- Good machining qualities
- Good ductility
- Surface smoothness
- Good hardness

- Good Workability
- Lightweight

Not only is the fabrication process facilitated and the aesthetics conserved with these features, but also the modulation of the system can be precisely generated along the global horizontal direction. Furthermore, the material was also selected for being common in the marketplace and for being relatively low in price. Certainly, this important factor allows the process of purchasing the alloy (brass) to be simplified.

In conclusion, a material selection was made based on the identification of different types of conditions that affected the fabrication and functionality of the linkage. *Aluminum alloy 6061-T6*, for example, was selected on the basis of fabricating each component of the spring mechanism, and *copper-zinc alloy* (brass), on the other hand, was selected on the basis of fabricating the rail system. Both of these materials were selected based on their excellent mechanical properties and their relative low cost on the marketplace.

## 5.2 Fabrication Process

With the material selection made, the target of the present section is to fabricate the components of the Watt II linkage using the parameters specified on the Pro-Engineer drawing. Specifically, the spring mechanism will be generated in three phases. The idea behind separating the fabrication into phases is to manufacture the components that use the same machinery in one phase, and leave the components that require different machinery on the other phases. Separating the components into phases, first of all, avoids having the trouble of resetting the machines each time a new component is fabricated, and secondly, it reduces the time of the entire process.

For example, in the first phase the components that will be machined are Link 2, Link 3, and Link 2'. In this case, the only parameter that is different is the length, but such problem can be solved by using the same machine to create all the links and by simply adjusting the material to obtain the respective components. Other than that, the process of fabricating the holes and the rounding on the edges remains identical, and can be generated using the same machines. Moreover, the second phase of the fabrication process involves machining the dyad-plate that combines the D111 and D011 mechanisms. In this case, the process is quite challenging since the plate has a triangular shape and most of the machines are set to fabricate rectangular shapes. However, by modifying the settings on the machines, the adequate shape and specifications can be generated. In the last phase of fabricating the spring mechanism, the component that will be machined is the linear displacement element. The most important factor, in this procedure, is for the hole to be precisely drilled on the center of the element in order to prevent misalignment once the rail system is mounted. However, by using the adequate features on the machines and taking every detail into consideration, the hole can be generated on the center of the element without a problem.

With this said, it is significant to identify what kind of machines will be implemented during the fabrication process: Horizontal Band Saw, Vertical Band Saw, Belt Sander, Lathe, and Vertical Milling Machine. Nonetheless, in order to operate these machines successfully and without any setbacks, all of the safety measures and procedures *must* be followed strictly.

### 5.2.1 Phase I

Therefore, phase one initiates by using a measuring device to mark the required length of each link on the material (0.0127 x 0.00635 x 1.8288 *m*). Once the three lengths have been marked in a subsequent manner, the Horizontal Band Saw is utilized to cut each component.

Before attempting to continue with the fabrication process, however, it is important to explain and understand why this particular machine is being utilized. In particular, there are two main reasons. The first reason is that the Horizontal Band Saw generates smooth, clean cuts with a high level of precision. There are machines, on the other hand, that can perform the same task, but their level of precision is not very high. For example, one case is the Vertical Band Saw. This machine can easily cut the lengths of the three components in a matter of seconds, but the major problem is that uneven surfaces are generated since the material is being hand-guided through the blade. Therefore, the advantage of using the Horizontal Band Saw is that it allows for the material to be locked during the cutting process and the blade is able to penetrate smoothly through the surface. Moreover, the second reason for implementing such particular machine is that it minimizes the time of operation drastically. For example, the Vertical Milling Machine is one machine that can indeed generate the three links, but the process of operation requires implementing several steps that can be tedious and time consuming. Alternatively, the Horizontal Band Saw only involves a single step to obtain the desired cut, and the time of operation takes a couple of seconds.

With this said, the process of fabricating the links (phase one) continues by removing the edge burrs with an electric Belt Sander. Removing the edge burrs is an extremely important procedure that *must* be applied every time a material has been machined. In particular, there are two main reasons for applying this procedure. The first reason of removing the edge burrs is to avoid any kinds of injury that may rise during the handling of the material or during the assembly process of the linkage. For instance, the burrs are extremely sharp that they can easily cause an accident if any small contact is made. On the other hand, the removal of the edge burrs allows for the aesthetics of each component and the functionality of the system to be conserved.

For example, if the extra material is not grinded off, it will interfere during the assembly of the links and consequently, the spring mechanism will not be able to modulate smoothly along any direction. Therefore, removing the burrs is an extremely important procedure that *must* be taken into consideration.

Furthermore, drilling the (0.00635 *m*) holes on each of the three links is the next procedure that needs to be accomplished. Before continuing, however, it is significant to mention that drilling the holes into the components is one of the most important procedures in the fabrication process. If the holes are not drilled on their exact location, for example, the mechanism will not behave as an adjustable spring and consequently, the experimental values will not match the computed theoretical values. Therefore, drilling the holes on the plate is best accomplished by using the Vertical Milling Machine. The advantage of using this particular machine, first and foremost, is that it is capable of perforating with a high level of precision along the vertical direction. However, in order to accomplish such precision, there are two particular steps that must be accounted first.

For example, step one involves mounting a point master on the machine to determine the *x* and *y* coordinates on the link. The objective in using the point master is to establish a reference frame along the edges of the component that will facilitate the positioning of the drill. What is done, in particular, is that the X and Y travelers (digital scales) are zeroed out from the edges of the component in order to specify the distance of the hole from that respective location. However, if the reference frame is not generated, it will be impossible to predict or find the specific location of the hole with simply using the naked eye. Therefore, not using the point master is certainly a disadvantage in obtaining the calculated design parameters and consequently, the dynamics of the system will be altered.

Step two, in addition, involves removing the point master from the machine and replacing it with a center drill. With the incorporation of the center drill, for example, the goal is to initiate the perforation process by simply marking the surface of the material. Such marking/indentation will serve as a channel for the taper drill to be used afterwards. However, if this step is omitted, it will be impossible to drill the hole with simply using the taper drill. What will happen, in such case, is that the taper drill will be constantly rotating on the surface without any penetration and the material will be damaged. Therefore, a center mark is created on each component where a hole is to be drilled. Once this mark has been completed, the (0.00635 $m$) taper drill is mounted on the Vertical Milling Machine and the perforation process of each hole is completed.

With the holes created on each component, the final step (in phase one) is to round the ends of the three links with the Belt Sander. Rounding the edges of a component is another important factor that has to be considered each time the fabrication process comes to a completion. For example, in this case rounding will eliminate the possibility of having large stress concentrations on the ends of the material, which in the long run can cause damage to the spring mechanism, or failure in other cases.

### 5.2.2 Phase II

Consequently, phase two of the fabrication process initiates by hand sketching a reference frame on the square plate (0.3048 x 0.3048 x 0.003175). The idea of having a coordinate system is to have a reference when hand sketching the triangular dyad in terms of the X and Y coordinates. However, when sketching the dyad, it is important to label each point precisely on the material in order to avoid developing an unconstraint mechanism. If these three points are not drawn to scale, what will happen is that when the assembly of the spring mechanism is completed and the testing begins, the behavior of the system will not be in

accordance to the calculated parameters. Consequently, the plate will have to be fabricated a second time. Therefore, all of the precautions must be taken into consideration during the sketching of the dyad plate.

Once the 0.003175 *m* thickness dyad has been sketched according to the design specifications, the Vertical Band Saw is used to cut the triangular shape. Before attempting to continue, nonetheless, it is necessary to explain why this particular machine is best suited for this task. The main reason for using the Vertical Band Saw is that the components can be hand-guided through the blade without any supports, which means that any desired pattern or shape can be generated. However, the only problem with this is that the edges will not be created in a uniform manner due to the unstable motion of the material. Therefore, what is done to solve the problem is that the component is cut slightly beyond the required dimensions to allow for the uneven sides to be straightened with the Belt Sander. With the implementation of the Belt Sander, not only are the edges straightened, but all of the burrs that can cause injury during handling or during the assembly process are removed. Moreover, a second reason for using the Vertical Band Saw is that it is very practical and efficient. Even though the use of the Belt Sander is needed to straighten the edges, the process of fabricating the plate is quick. On the other hand, the Horizontal Band Saw and the Vertical Milling Machine are machines that can generate the dyad plate as well, but they are not practical enough to perform the task in a one step process.

Moreover, using the Milling Machine to drill the three (0.00635 *m*) holes on the dyad plate is the next step that needs to be completed. In this case, however, extra precautions need to be made when using the X and Y travelers since the edges are not perpendicular to each other. Nonetheless, the process is generated by using the same tools as before. For example, a master

point is mounted on the machine and a reference frame is created on the digital scales with the use of the *x* and *y* axes. Once digital scales are zeroed out at the respective ends and the dyad plate is centered, a mark/indentation is made at the surface with a center drill. This starting mark allows for the holes to be fully perforated with a taper drill. Therefore, having drilled the holes wraps up the second phase of fabricating the actively adjustable spring mechanism.

### 5.2.3 Phase III

Moreover, phase III involves fabricating the linear displacement element which is composed of two, attached rectangular elements (Figure 3.10). However, it is important to mention that in order fabricate the linear displacement element, there are three steps that must be completed. For example, the first step involves using a measuring device to mark the required length (of each block) on the aluminum alloy. Once the two lengths have been marked in a subsequent manner, the piece of material is taken to the Horizontal Band Saw and the respective blocks are generated. Nonetheless, as mentioned earlier, each time a material is subject to a cutting blade, edge burrs are generated on the surface. This means that the sharp burrs on the surface of the blocks have to be removed in order to avoid any kinds of injury during the material handling or during the assembly process of the mechanism. Therefore, in order to prevent these scenarios, and in addition help maintain the aesthetics and functionality of the system, the electric Belt Sander machine is utilized.

Step two, furthermore, involves drilling a hole along the *x*-axis of the output element (Figure 5.1). The purpose of extruding the hole on the output element is to implement a rail component that will serve as a sliding guide on the spring mechanism. This procedure, however, is extremely important and must be done in a very precautious manner. For example, such procedure is important in the sense that if a hole is not extruded specifically on the center of the

surface, misalignment will be created between the blocks. What will happen, consequently, is that the rail system and the two blocks will not be parallel with each other and a large amount of friction will be generated as the slider modulates along the horizontal axis. This phenomena, as a result, will not allow the output element to modulate in a smooth, clean manner, and the stiffness generated from the spring mechanism will be incorrect. Therefore, what is done to avoid this type of scenario is that a point master is mounted on the Vertical Milling Machine to determine the coordinates along the edges of the component. The advantage of implementing such procedure is that the X and Y travelers will place the drill on any desired location and the hole will be extruded with a very high precision. Once the travelers have been zeroed out, a center drill is mounted on the machine and a starting mark is made on the surface, where the extrusion is to be generated. This process allows for the hole along the *x*-axis to be extruded with a 0.003175 *m* taper drill.

Before continuing, however, it is important to mention that the hole along the *x*-axis is not the only hole that needs to be extruded from the linear displacement element. The other hole, in particular, needs to be extruded along the *z*-axis of the displacement element (Figure 5.1). The main reason for extruding the hole along the *z*-direction is that a cylindrical component (length: 0.015875 *m*; diameter: 0.00635 *m*) will be implemented between the rectangular blocks to assemble the sliding element and connect Link 2'. If the hole is not drilled along such particular direction, for example, it will be impossible to assemble the respective components. Therefore, the process of drilling the hole is generated by using the same machine and tools as before.

Once the holes have been precisely generated along the *z*-direction and the edges of each block have been rounded with the Belt Sander, the next step (three) is to assemble the sliding element. This is accomplished in two steps. The first step involves taking one of the ends of Link

2’ and placing it on the center of the cylindrical component. Once Link 2’ has been placed, each rectangular element is mounted and pasted (aluminum epoxy) at the ends of the cylindrical component with a certain margin. With the assembly completed, the two rectangular elements remain fixed on the ends and the link in the middle is able to rotate about the shaft.

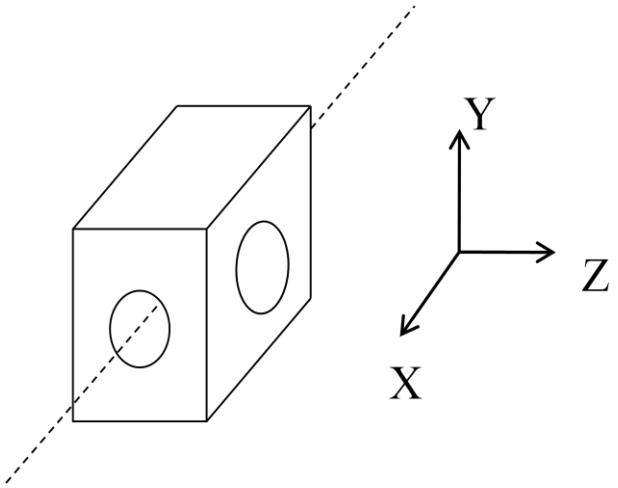


**Figure 5.1: Slider Output Element**

Up to this point, each component of the spring mechanism has been precisely fabricated using various types of machines and tools. However, there is one more issue that has to be addressed before a preliminary test can be performed. This issue involves finding a way to mount/attach the dyad plate and Link 2’ onto the shafts of the brush-type DC motors. If these are not attached properly, the motor shafts will rotate freely without the links of the mechanism and consequently, the internal loads will not be generated. Therefore, what is done is that a hole is drilled besides each link and a set screw is placed.

For example, the hole on Link 2’ is generated similarly as those in other components, the only difference is that a 0.003175 *m* taper drill is used to make the extrusion. Once the extrusion

is completed, the female thread on the hole is created by implementing a tap and rotating it smoothly in a clockwise direction. If the tap is rotated without precaution, the thread will not develop properly and the hole will not be useful. On the other hand, generating a hole on the dyad represents a greater challenge since the thickness of the plate is too small. What is done to increment the thickness is that a (0.0127 x 0.00635 x 0.0254 *m*) link is pasted on the rear side of the plate with an aluminum epoxy. This allows for the 0.003175 *m* hole to be generated on the link similarly as the one on Link 2'.

In conclusion, each component of the Watt II linkage was precisely fabricated according to the specifications on the Pro-Engineer drawing. Several machines such as the Horizontal Band Saw, Vertical Band Saw, and Vertical Milling Machine were implemented to create the specific parameters on the components. However, the precision of these machines was accomplished by mounting the adequate tools and by taking the necessary precautions.

### 5.3 Preliminary Test

In this section, there are several questions that need to be addressed before mounting and driving the redundantly actuated mechanism. One of these questions is in regards to the amount of torque that can be generated from a 5A brush-type DC motor. In particular, finding the maximum amount of torque on the motor can facilitate the process of generating a (test) plan to determine the desired effective stiffness on the mechanism. For example, a certain range of minimum and maximum values can be specified to generate different equilibrium loads on the spring mechanism. However, in order to determine the maximum torque, an experimental setup must be developed first. In particular, the experimental setup involves mounting a link on the shaft and positioning a load cell at a certain distance to measure the force exerted as the motor

intends to rotate. The torque will then be calculated using two quantities: the force exerted on the load cell and the length of the arm.

Another question that *must* be addressed before driving the redundantly actuated mechanism is obtaining a relationship between the torque and current. As mentioned in the previous chapter, a set of equilibrium torques cannot be directly specified on the brush-type DC motor, it must be specified in terms of current. Therefore, what will be done experimentally is that a certain amount of (current) values will be applied on the motor, and the force exerted on the load cell will be taken to measure the respective torque. These current values will be generated in steps of 0.25A to obtain a precise correlation between the two parameters.

With these cases defined, the objective of the present section is to perform a preliminary test that will address such types of questions and anticipate how the spring mechanism will be driven. This is process is important because since there is no experimental validation, the behavior of the real system is unknown. Based on the results attained, all of the electrical components needed to assemble and drive the redundantly actuated mechanism will be determined as well.

Therefore, the process initiates by selecting several electronic devices that will allow for the shaft of the brush-type DC motor to rotate in a clockwise direction. For example, such devices include:

- 5A brush-type DC motor with continuous stall torque of 55 oz-in
- DC servo amplifier with analog input
- 24 Voltage power supply
- Load cell
- Digital multimeter

- Potentiometer, 10K ohm
- MB-800 breadboard system with power supply (5 Volts)
- Fuse / Fuseholder
- Wire / 3 POS Power cord
- System link

Once the devices are selected, the next step is to connect them in a careful manner and obtain the desired motion on the shaft (Figure 5.2). However, it is important to emphasize that if the necessary precautions are not implemented at this stage and as a result the devices are connected incorrectly, two major setbacks that will be experienced. The first one is that certain components will get damaged due to an overcharge, and consequently, the questions that need to be addressed before driving the mechanism will not be answered at all. This phenomena, in addition, will delay the process of testing as those devices damaged will have to be replaced with new ones. The second setback that will be experienced, on the other hand, is that a major accident will occur due to the electricity involved. Therefore, what is done to avoid these types of scenarios is that all of the devices are carefully wired and connected one step at a time.

With this understood, the process initiates by connecting a 3POS power cord into the 24V power supply that provides the necessary voltage to the system. However, before any connection can be made, it is important to use a digital multimeter and determine the positive, neutral, and ground of each conductor on the power cord. If this simple procedure is not taken into consideration and it is assumed that a certain color represents a particular phase, what will happen is that the conductors will be mounted on a different terminal and the 24V power supply will overcharge. Consequently, the electronic device will get damaged and there will no voltage provided.

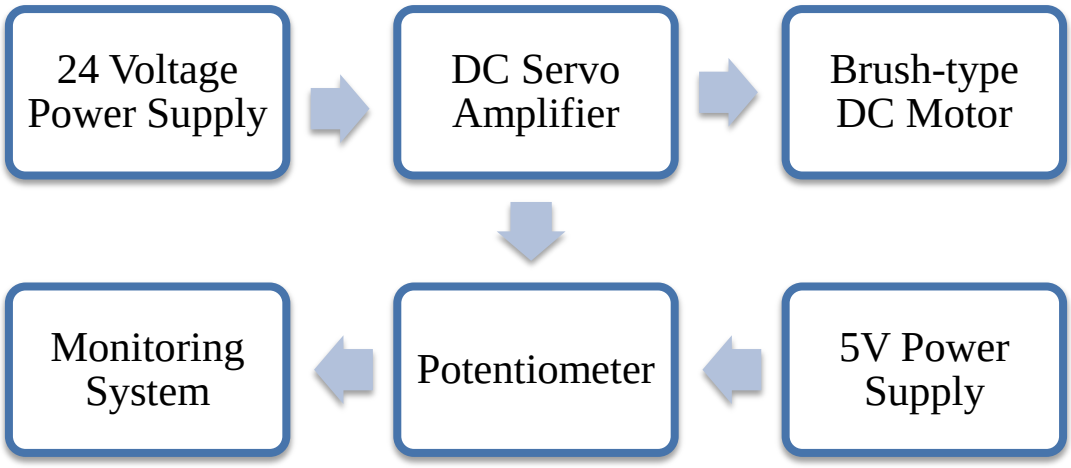


**Figure 5.2: Preliminary Test Configuration**

After the correct phases are determined for each conductor on the power cord, the next step on the experimental setup is to supply power to the DC servo amplifier. Nonetheless, it is important to clarify that the DC servo amplifier needs to be supplied with two sources of power, one that powers the brush-type DC motor and the other one that powers the potentiometer. For example, the first source is obtained from the 24V power supply and is used to drive the brush-type DC motor. In particular, the connection is accomplished by grounding the DC servo amplifier with the negative terminal of the 24V power supply, and by wiring the positive terminals to generate the voltage. However, it is important to mention that a cable with a fuse holder is also placed in between the positive terminals to ensure that only a maximum voltage can be generated. The idea behind this action is to burn the fuse in case the current exceeds its rating and therefore, eliminate the possibility of damaging the 24V power supply.

Once the DC servo amplifier has been powered to connect the brush-type DC motor, the next step is to actually connect the motor. This step is accomplished by taking the positive and negative wires from the motor and connecting them to the respective terminals on the servo amplifier. In addition, a digital multimeter is inserted in between the positive terminals to measure the amperes generated by the motor. This way the correlation between the torque and current can be obtained in a precise manner.

The second source of power, on the other hand, is obtained from a 5V MB-800 breadboard and is implemented to power the potentiometer. The connection initiates by inserting a piece of wire in all the pins located on the *input and control* section (amplifier). After the wires are placed accordingly, the pins that contain ground (-) are grouped and soldered to a single wire to avoid having multiple connections on the power supply. This, in addition, allows for the device to be connected to the negative terminal on the 5V MB-800 power supply and to the reference input (amplifier) to be connected on the positive terminal. Once this step is completed, the potentiometer is mounted and connected to the 5V power supply. In addition, a digital multimeter is placed in between the positive terminals to measure the voltage generated from the DC motor.

Therefore, powering the DC servo amplifier completes the wiring needed for the shaft of the brush-type DC motor to rotate in a clockwise direction. At this point, however, it is important to conduct a simple test and verify that all the wires are connected properly, and observe if the speed of the motor shaft is controlled with the potentiometer. After the test has been conducted, results indicate that indeed, the wiring of the system is correct and the speed of the shaft is controlled with the potentiometer. For example, as the potentiometer is rotated in a clockwise direction, the speed of the motor shaft increases, on the other hand, as the potentiometer is

rotated in a counterclockwise direction, the speed of the motor shaft decreases. From this simple test, the digital multimeters also give the respective voltage and current generated by the DC motor, which means that every connection is correct.

Nevertheless, there are several details that need to be taken care of before the actual testing begins. One of them is to strap the motor onto the base where the electronic devices are mounted. This simple task is accomplished by extruding (cordless-hand drill) four holes on the plywood and using cable ties to attach the motor. By doing so, the motor will not be able to slide as the speed of the shaft increases. In a similar manner, the DC servo amplifier and the 24V power supply are also fixed to the plywood, but in this case, a screw is used instead. Furthermore, a second detail that needs to be taken care of is mounting a fabricated link (length: 0.1016 $m$) onto the shaft of the motor with the use of a set screw. In such circumstance, nonetheless, it is extremely important that the set screw is well-tighten with the shaft of the motor. If the set screw is not well-tighten, what will happen is that there will be loose components as the shaft rotates, and consequently, inaccurate results will be generated from the experiment. Another task that needs to be addressed is to place a load cell that will measure the force exerted on the link as the motor intends to rotate (Figure 5.3).

This procedure is accomplished by taking an extra piece of plywood (0.0254 x 0.0254 x 0.254 m) and making a small extrusion (Vertical Milling Machine) on its surface to place the link. Once the extrusion is generated, the piece of plywood is strapped onto the workspace with a pair of cable ties, and the load cell is placed on the top surface in such manner that the sensor is located perpendicular to the link. From this setup, it is important to point out that the load cell is connected to DataStudio-Activity software that measures the force exerted. Furthermore, the last detail that needs to be addressed, before initiating the actual testing, is to set the DC servo

amplifier to a torque mode application. If the amplifier is set to a different mode, the system will behave differently and the desired output will not be generated. Therefore, what is done is that the reference manual of the amplifier is obtained and the respective mode is implemented. According to the manual, the typical current (torque) mode application is obtained by simply modifying the potentiometer functions/pins on the amplifier. In particular, the REF GAIN pin *must* be fully turned clockwise and the LOOP GAIN pin *must* be fully turned counterclockwise.

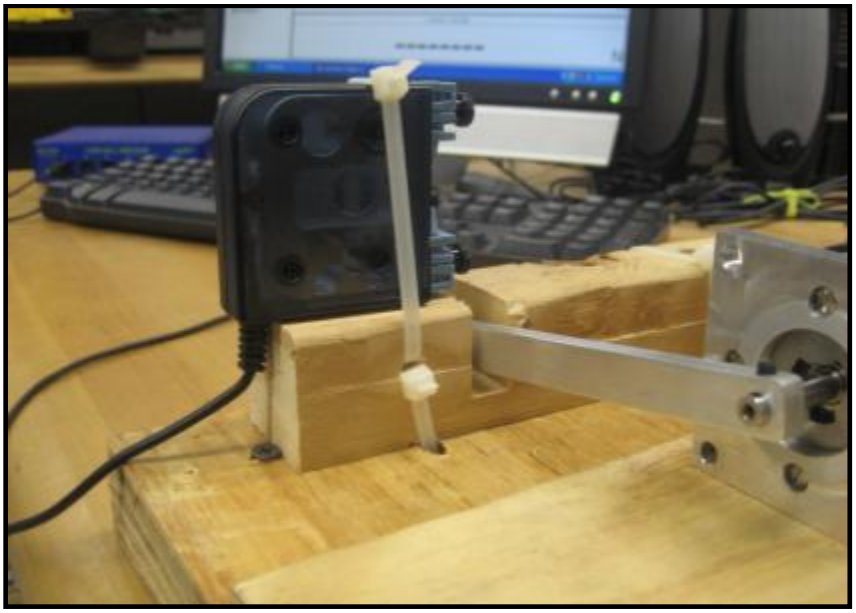

**Figure 5.3: Load Cell and Brush-Type DC Motor**

### 5.3.1 Preliminary Test Results

With these details taken care of and the experimental setup completed, the next step is to conduct the preliminary test. As mentioned earlier, the goal in such test is to begin by generating 4A on the brush-type DC motor and progressively decrease to 0.5A in steps of 0.25A. This will allow for the maximum amount of torque on the motor to be attained, as well as the relationship between the torque and current.

Therefore, after conducting such experiment and obtaining information on DataStudio, three major observations are made. For example, the first major observation is that the force exerted on the load cell remains constant throughout each (current) interval, meaning that when the shaft of the motor is not moving, a constant torque is being generated (Figure 5.4). This result, as expected, is favorable in the sense that the torque on each motor will not vary as the spring mechanism is placed in static equilibrium. However, if the force had varied with respect to time, equilibrium would have never been reached and the experimental data would have been inaccurate in every aspect. Consequently, a different type of motor would have been required to carry out the experiment.

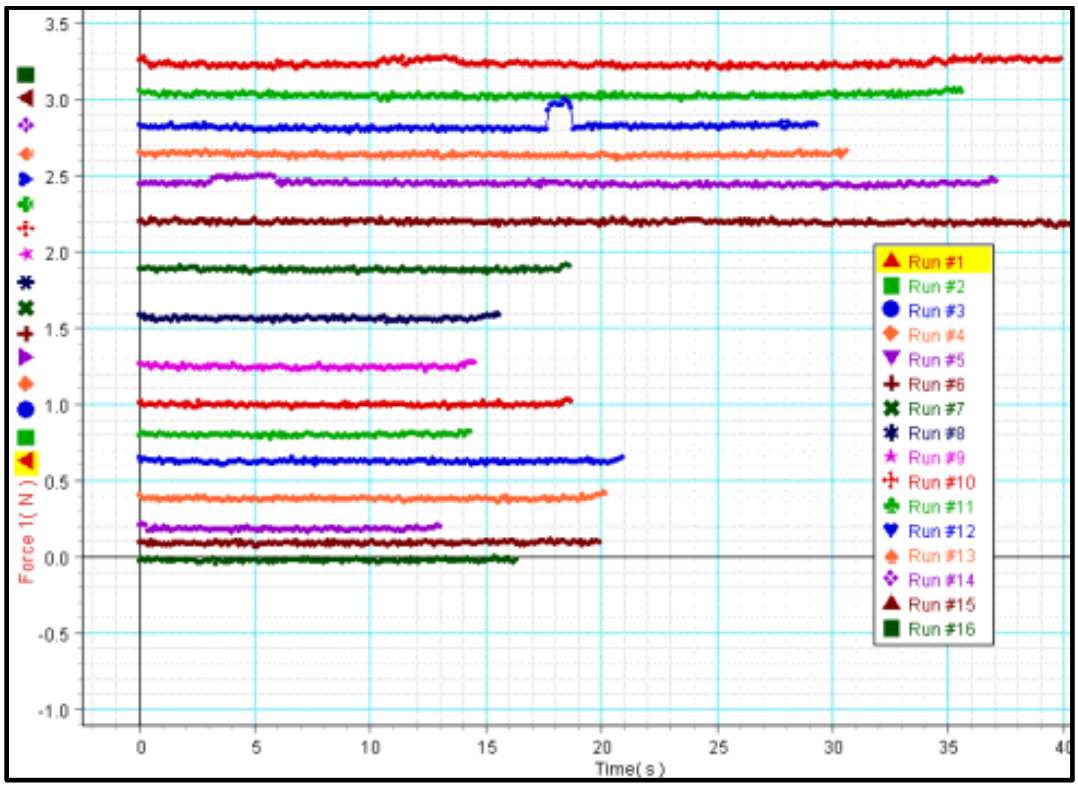


**Figure 5.4: Forces Exerted on Load Cell (Preliminary Test)**

Before continuing, it is necessary to point out a small detail from the graph that may cause confusion. Such detail is that the force generated in test 3 (blue) and test 5 (purple) has inconsistencies on certain time intervals. The reason for this is that the load cell is capable of detecting any slight movement created on the experimental table or any movement generated by the wires. For example, what happens is that the force exerted on the load cell increases as a disturbance is detected, and consequently the data points created on the graph shift from their original position. However, results indicate that after the slight movement vanishes, the force exerted on the load cell becomes constant again. This, in addition, means that such small variations are *not* generated from the inconsistency of the brush-type DC motor. They are instead generated from the unintentional activities that surround the system. For such reason, the variations on the graph are completely ignored and only the constant force is accounted for the computational analysis.

The second observation made from the data is that as the amperes decrease, so does the force exerted on the load cell. This means that the amperes generated on the DC motor and the force exerted on the load cell are proportional to each other. For example, on the first test (4A) a force of 3.2 N is exerted on the load cell, but on the seventh test (2.50A), a force of 1.56 N is generated as the motor intends to rotate. Therefore, it can be understood from the results that the torque on the DC motor increases as the current increases, and similarly, the torque on the DC motor decreases as the current decreases.

Moreover, the third observation made on the preliminary test is that the voltage and current generated by the digital multimeters are similar to each other (Table 5.3), meaning that the highest voltage that can be obtained from the motor is 5V. In particular, the voltage is an extremely important parameter that must be monitored and considered since the DC motors in

Working Model only operate under an input voltage. For instance, in test 1 (4A) the voltage generated on the DC motor is 4.120V, in test 4 (3.25V) the voltage generated is 3.341V, and in test 9 (2.0A) the voltage generated is 2.046V, which means that their ratio is about 1:1. Therefore, it is concluded from these results that the voltage increases as the current increases, and similarly, the voltage decreases as the current decreases.

**Table 5.3: Torque on Brush-Type DC Motor (Preliminary Test)**

| Current (A) | Voltage (V) | Exerted Force (N) | Resistance (Ohms) | Torque (Nm) |
|---|---|---|---|---|
| 4.00 | 4.120 | 3.22 | 1.030 | 0.3272 |
| 3.75 | 3.860 | 3.01 | 1.029 | 0.3058 |
| 3.50 | 3.609 | 2.83 | 1.031 | 0.2875 |
| 3.24 | 3.341 | 2.63 | 1.031 | 0.2672 |
| 3.01 | 3.083 | 2.45 | 1.024 | 0.2489 |
| 2.75 | 2.829 | 2.18 | 1.029 | 0.2215 |
| 2.50 | 2.566 | 1.88 | 1.026 | 0.1910 |
| 2.25 | 2.311 | 1.56 | 1.027 | 0.1585 |
| 2.00 | 2.046 | 1.24 | 1.023 | 0.1260 |
| 1.75 | 1.792 | 0.99 | 1.024 | 0.1006 |
| 1.50 | 1.531 | 0.80 | 1.021 | 0.0813 |
| 1.25 | 1.276 | 0.62 | 1.021 | 0.0630 |
| 1.00 | 1.015 | 0.37 | 1.015 | 0.0376 |
| 0.75 | 0.763 | 0.17 | 1.017 | 0.0173 |
| 0.50 | 0.507 | 0.08 | 1.014 | 0.0081 |

With these observations made, the following step is to take the generated data and calculate the torque on the brush-type DC motor. Such procedure is accomplished by implementing the general torque equation

$$\tau = F \cdot d \tag{5.1}$$

and substituting the respective distance and force values. In this case, however, since the length of the link does not change, the distance value (0.1610 *m*) remains constant throughout the calculation and only the force values change respectively. Therefore, after completing the analysis (Table 5.3), results indicate that the maximum amount of torque generated on the 5A DC motor, according to the specified range (4A – 0.5A), is 0.3272 Nm. This means that only a certain amount of force can be applied on the output displacement element with such maximum torque. If a larger force is applied on the slider, for example, the spring mechanism will not be able to behave accordingly due to a restrained stiffness generated by the torques. However, with such stiffness values, the concept of adjustable springs can be proven without doubt.

The resistance of DC motor is another parameter that is determined from the voltage and current values, and is calculated using the following expression

$$R = \frac{V}{I} \tag{5.2}$$

The reason for determining the resistance is that it is one of the parameters needed for the DC motors in Working Model (see Chapter IV). In this case, results demonstrate that the average value is 1.041 Ω for each respective torque, which means that the ratio between the voltage and current is about 1:1.

Now that the maximum amount of torque has been resolved, the next procedure is to determine the relationship between the current and torque. After graphing the data, results illustrate that the torque is proportional to the armature current, which means that as the torque

increases, so does the current (Figure 5.5), and if the torque decreases, so will the current. This result was expected since the theoretical expression

$$T = k \cdot f \cdot I_a \tag{5.3}$$

states that the torque ($T$) is proportional to the product between the armature current ( $I_a$ ) and the resultant flux ($f$).

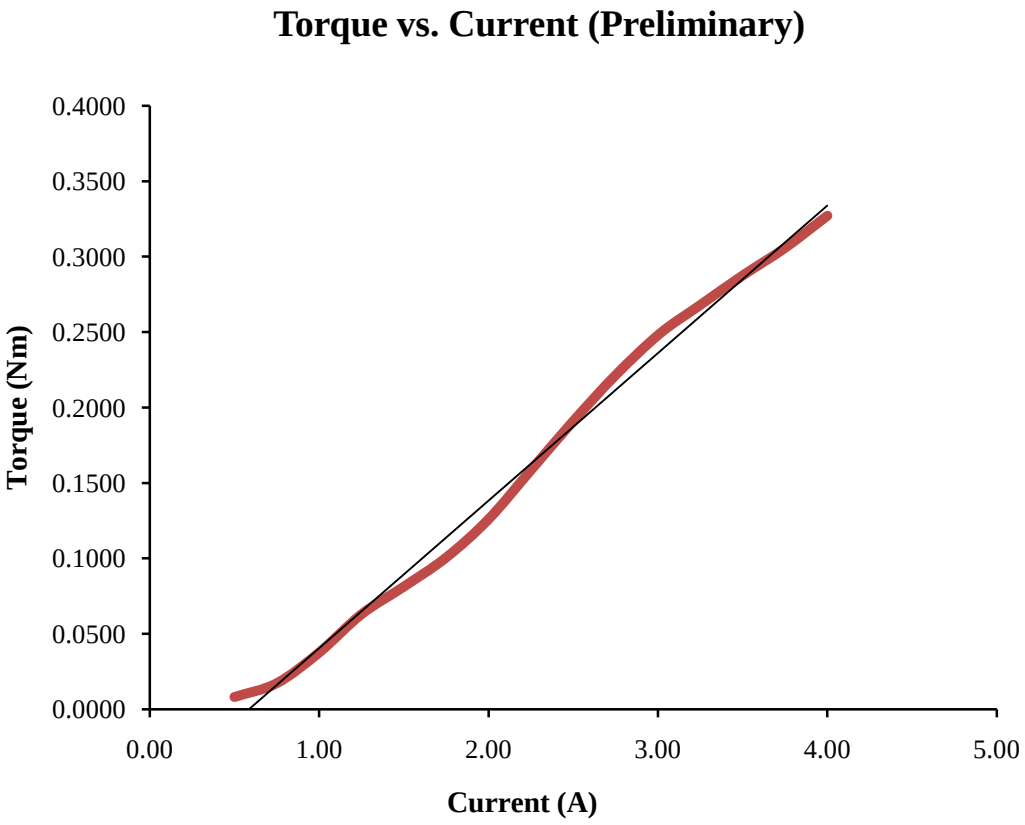


**Figure 5.5: Torque vs. Current (Preliminary Test)**

Having determined the relationship between the torque and armature current concludes the results of the preliminary test (5A brush-type DC motor). In particular, the most important outcome was that the brush-type DC motor was capable of generating a constant torque as it

intended to rotate in a clockwise direction, which means that with such experimental setup, the actively adjustable spring mechanism can definitely be driven. Therefore, all of the equipment needed to assemble and drive the system includes the following:

- 2 - Brush-type DC servo motor with continuous stall torque of 55 oz-in
- 2 - Brush-servo amplifier with analog input, 6A continuous, 10 peak, 9-25 VDC
- 2 - Potentiometer, 10-turn, WWND, 10K ohm
- 2 - Power supply, SW, ENCL, 150W, 24V @ 6 .25A
- 2 - Wire, 18AWG, Black and Red
- 5 - Fuse, Glass, 5A, 1.25 x 0.25, 250V
- 2 - Fuseholder, in-line, 14AWG x 48L, 1.25 x 0.25 Fuse
- 1 - Power supply, SW, ENCL, 15W, 5V @ 3A
- 5 - Digital multimeter
- 1 - Linear displacement potentiometer (5” stroke)
- 3 - Power Cord, 10’, AWG, 18/3, SVT
- 1 - Breadboard
- 2 - Fans
- Alligator cables, cable ties
- Pulley system; rope for pulley system
- Power extension; extension socket
- 5 - Mass
- Greaseless lubricant

Before assembling the spring mechanism, however, it is necessary to measure the torque on each of the two, brand new brush-type DC motors. The idea behind this procedure is to verify that

both motors contain the same torque value. For example, if such analysis is not implemented, what will happen is that the system might not reach equilibrium due to a difference of torque on each motor. Therefore, such procedure *must* be implemented.

In a similar approach as before, the process initiates by connecting the motors to their respective electronic devices (see Figure 5.2). After the test has been conducted on each motor, results indicate that the torque is similar in both cases, meaning that the spring mechanism can be placed in static equilibrium without any problem. In addition, results illustrate that the relationship between the torque and armature current is proportional, meaning that when one increases, so does the other, and vice versa. Such results include the following:

#### 5.3.1.1 DC motor at joint O (motor 2)

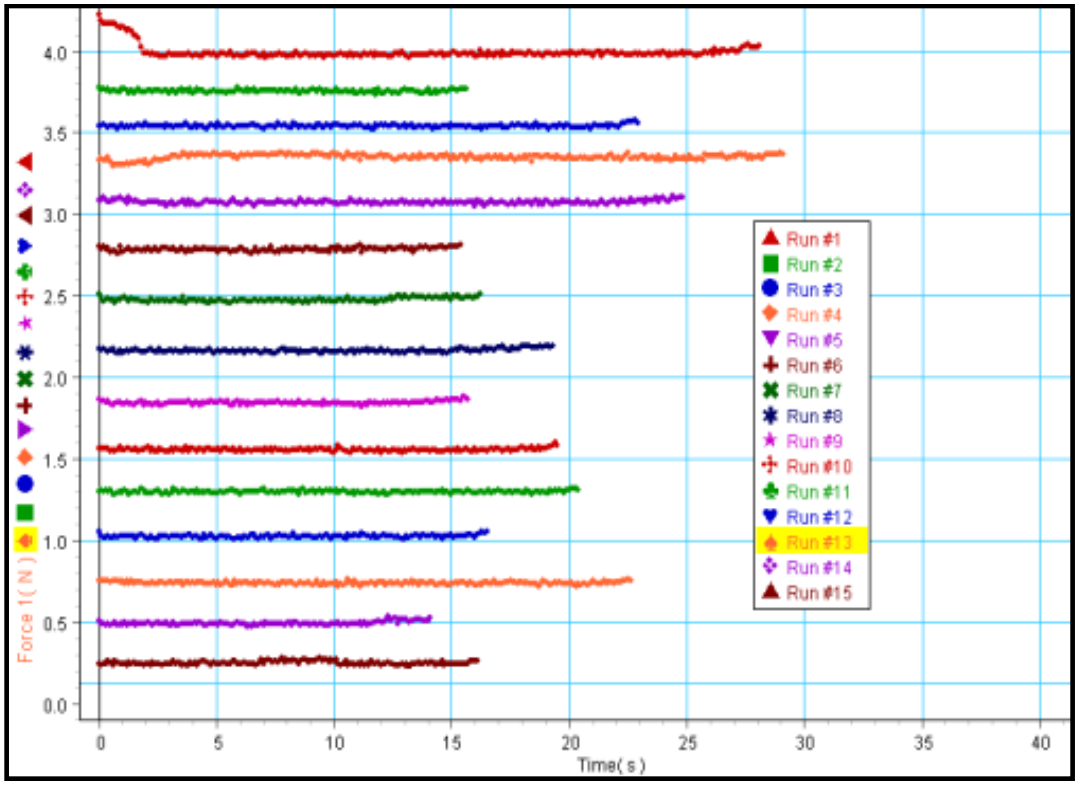


**Figure 5.6: Forces Exerted on Load Cell (Motor 2)**

Results from the constant force generated by the load cell at the end of the link

**Table 5.4: Torque on Brush-Type DC Motor (Motor 2)**

| Current (A) | Voltage (V) | Exerted Force (N) | Resistance (Ohms) | Torque (Nm) |
|---|---|---|---|---|
| 4.000 | 4.150 | 3.980 | 1.038 | 0.4044 |
| 3.750 | 3.900 | 3.750 | 1.040 | 0.3810 |
| 3.500 | 3.637 | 3.540 | 1.039 | 0.3597 |
| 3.250 | 3.383 | 3.350 | 1.041 | 0.3404 |
| 3.000 | 3.117 | 3.070 | 1.039 | 0.3119 |
| 2.750 | 2.862 | 2.740 | 1.041 | 0.2784 |
| 2.500 | 2.600 | 2.460 | 1.040 | 0.2499 |
| 2.250 | 2.332 | 2.160 | 1.036 | 0.2195 |
| 2.000 | 2.077 | 1.840 | 1.039 | 0.1869 |
| 1.750 | 1.816 | 1.550 | 1.038 | 0.1575 |
| 1.500 | 1.557 | 1.300 | 1.038 | 0.1321 |
| 1.250 | 1.302 | 1.020 | 1.042 | 0.1036 |
| 1.000 | 1.045 | 0.740 | 1.045 | 0.0752 |
| 0.750 | 0.785 | 0.490 | 1.047 | 0.0498 |
| 0.500 | 0.528 | 0.290 | 1.056 | 0.0295 |

Results generated from the maximum amount of torque on the brush-type DC motor

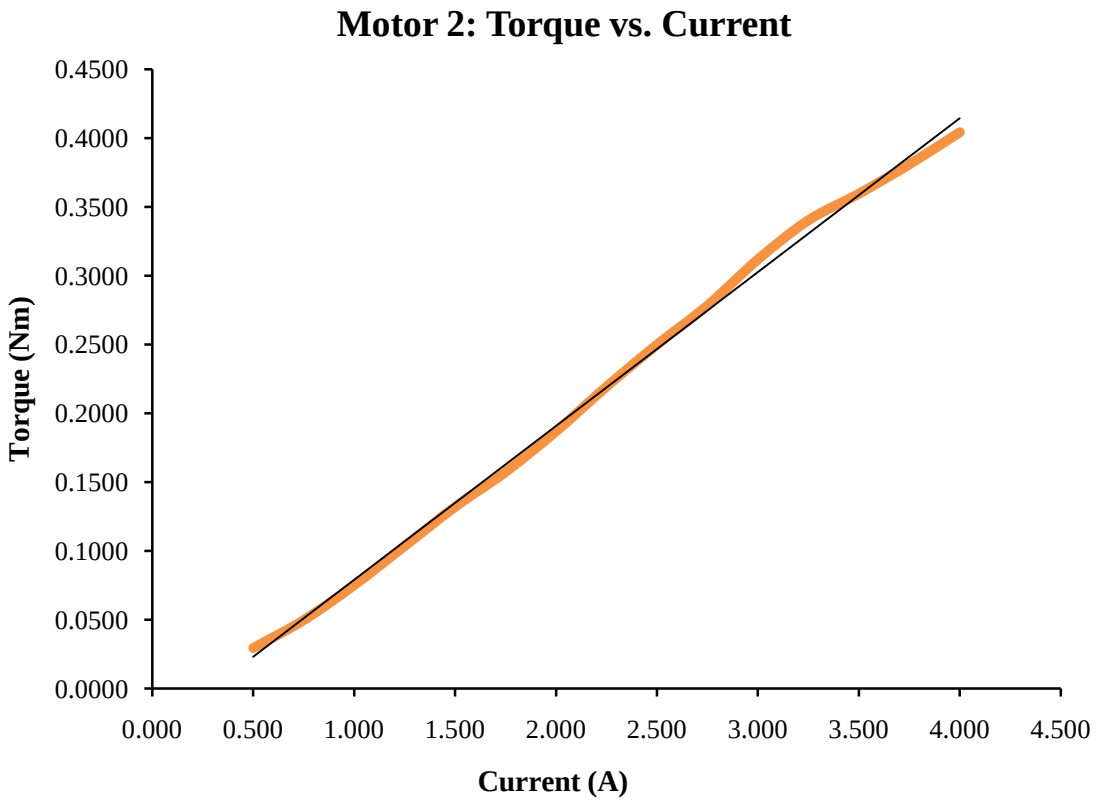


**Figure 5.7: Torque vs. Current (Motor 2)**

### 5.3.1.2 DC motor at joint C (motor 4)

Constant force values obtained during each interval

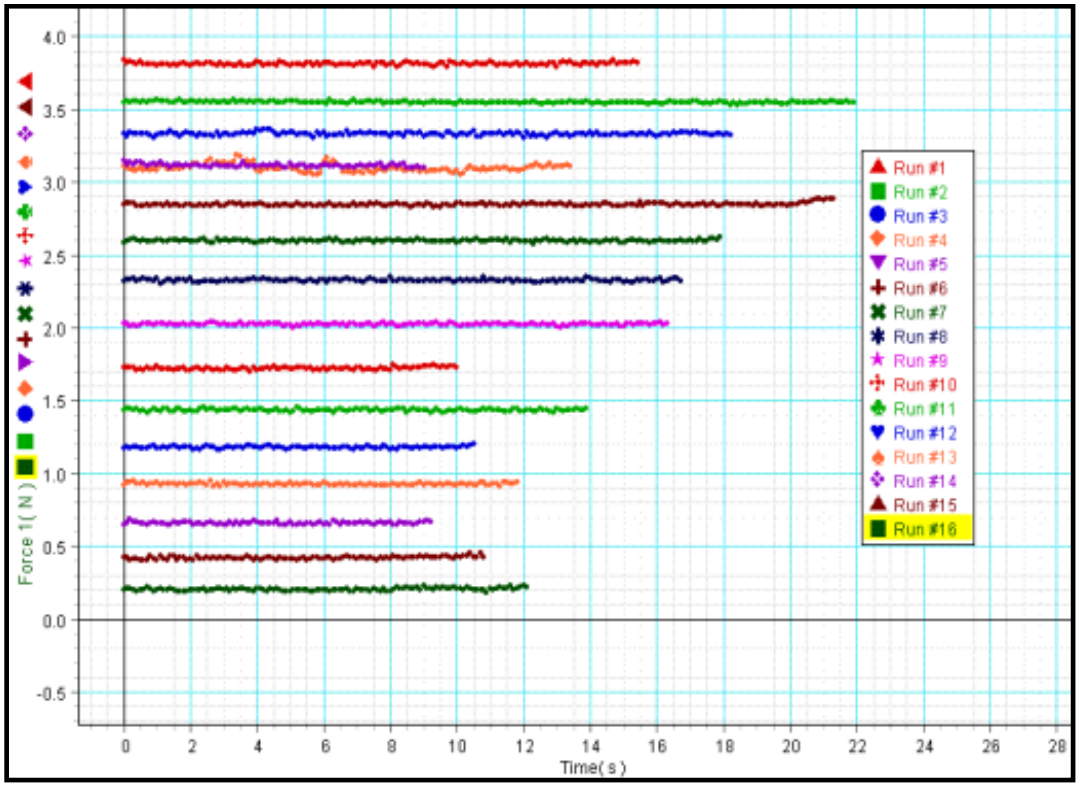


**Figure 5.8: Forces Exerted on Load Cell (Motor 4)**

Results from the constant force generated at the end of the link

**Table 5.5: Torque on Brush-Type DC Motor (Motor 4)**

| Current (A) | Voltage (V) | Exerted Force (N) | Resistance (Ohms) | Torque (Nm) |
|---|---|---|---|---|
| 4.00 | 4.150 | 3.810 | 1.0375 | 0.3871 |
| 3.75 | 3.890 | 3.530 | 1.0373 | 0.3586 |
| 3.50 | 3.630 | 3.330 | 1.0371 | 0.3383 |
| 3.25 | 3.379 | 3.110 | 1.0397 | 0.3160 |
| 3.00 | 3.109 | 2.850 | 1.0363 | 0.2896 |
| 2.75 | 2.852 | 2.590 | 1.0371 | 0.2631 |
| 2.50 | 2.594 | 2.320 | 1.0376 | 0.2357 |
| 2.25 | 2.330 | 2.020 | 1.0356 | 0.2052 |
| 2.00 | 2.073 | 1.720 | 1.0365 | 0.1748 |
| 1.75 | 1.813 | 1.430 | 1.0360 | 0.1453 |
| 1.50 | 1.555 | 1.180 | 1.0367 | 0.1199 |
| 1.25 | 1.305 | 0.920 | 1.0440 | 0.0935 |
| 1.00 | 1.042 | 0.660 | 1.0420 | 0.0671 |
| 0.75 | 0.787 | 0.420 | 1.0493 | 0.0427 |
| 0.50 | 0.528 | 0.200 | 1.0560 | 0.0203 |

Results generated from the maximum amount of torque on the brush-type DC motor

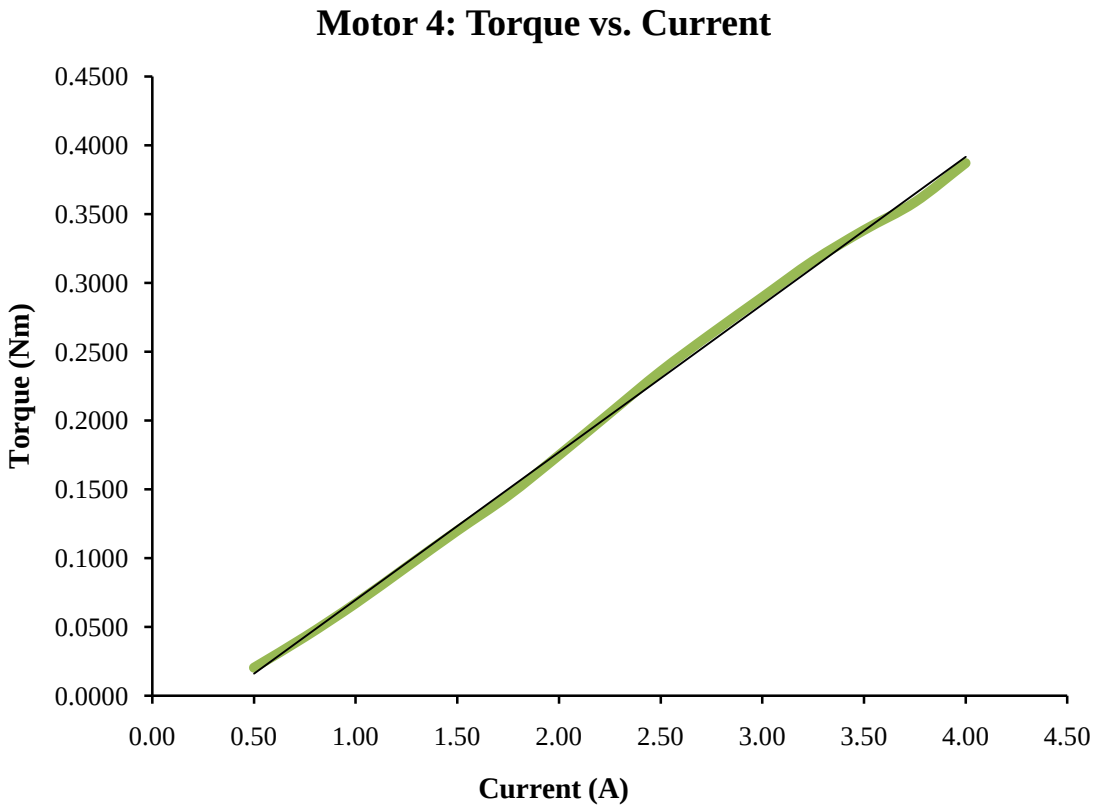


**Figure 5.9: Torque vs. Current (Motor 4)**

### 5.4 Assembly of Actively Adjustable Spring Mechanism

The target of the present section is to take the (previously) listed electrical components and assemble the actively adjustable spring mechanism (Figure 5.10). In particular, there are five steps that need to be implemented in order to obtain the desired motion of the system along the horizontal direction. The first step involves mounting and strapping the brush-type DC motors onto a plywood base with a pair of cable ties. This procedure is carried out in a cautious manner to avoid any type of misalignment between the motors. If the shafts are not parallel to each other,

for example, what will happen is that the output displacement element will not modulate smoothly along the rail system as a result of the friction generated. Therefore, a measuring device is implemented to mark each distance precisely and avoid such scenarios.

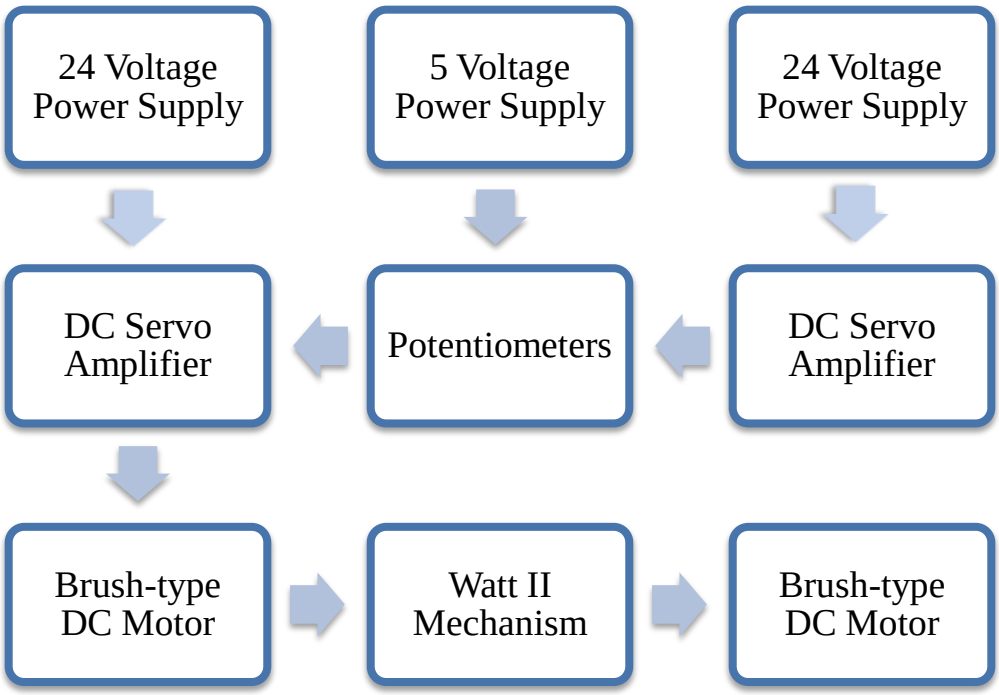


**Figure 5.10: Assembly Configuration of Active Spring Mechanism**

The following step on the assembly process, once the motors have been placed and strapped at their respective location, is to screw down the 24V power supply, the brush-servo amplifier, and the 5V power supply that will be connected to each brush-type DC motor. This procedure is accomplished by neatly distributing the components across the workspace in such manner that they do not interfere with each other. By doing so, it eliminates the possibility of having cables in contact that may damage a component or may cause an accident. On the other hand, the two potentiometers that control the velocity of the motor shafts also need to be attached. These are placed in from of the motors where they can be easily located and easily

operated. However, it is important to mention that both potentiometers are attached to the plywood with the use of an adhesive, not with a screw.

Wiring the devices is the third step that must be implemented to assemble and drive the spring mechanism. The process initiates by connecting a power cord onto the three power sources (2-24V and 1-5V). As done previously, a digital multimeter is used to determine the positive, neutral, and ground of each conductor before any connection can be made. Once the conductors are placed on their respective terminals, the next components to wire are the brush-servo amplifiers and the brush-type DC motors. These components are connected similarly as before, the only difference is that the wiring on Motor 2 is switched to obtain a counterclockwise rotation. In addition, four digital multimeters are placed across the system to measure the current and the voltage generated by the motors. Two of them are connected to Motor 2 while the other two are connected to Motor 4. Moreover, wiring the potentiometers is accomplished by powering a breadboard with 5V and making all of the respective connections. In this case, the advantage of using the breadboard is that it eliminates having cables all over the place that can be difficult to find once the entire system is wired.

Furthermore, the assembly process continues by mounting the rail system besides the grounded revolute joint C. This procedure is carried out in a very cautious manner to attain a precise alignment between the rails and the shafts of the motors. If the rail is misaligned, what will happen is that the mechanism will generate different parameters when placed in static equilibrium, and consequently, the stiffness values will be different from the theoretical stiffness values. Therefore, once the rail system is aligned, the two walls on the outside are strapped using cable ties to avoid any type of movement. This, in addition, allows for the linkage to be mounted on the DC motors and on the rails.

The last step to complete the assembly of the spring mechanism is to attach a linear displacement potentiometer on the output element, connect a fan behind each motor, and mount a pulley system on the base. First of all, what is done to connect the linear potentiometer is that a hole is drilled on the outside wall of the rail system and its shaft is attached to the output slider element. Once the housing and the shaft are attached respectively, it is connected to the 5V power supply and the required voltage is supplied. A digital multimeter is then implemented on the positive terminal to read the displaced length in terms of voltage. In this case, for example, a displacement of 1V is equivalent to 1 inch. Moreover, fans are implemented to blow room temperature air around the motor to keep them from overheating. These fans are connected to the respective 24V power supply and operate constantly as soon as the 24V power supply is connected. Lastly, a pulley system, with a rope attached to the output displacement element, is mounted on the end of the plywood (Figure 5.11). The reason for this step is that several masses will be implemented in order to cause a displacement on the prismatic joint and consequently measure the effective stiffness of the mechanism.

In conclusion, the manufacturing and assembly process of the variable stiffness mechanism was carried out in this chapter. The process initiated by selecting a material that would be able to conserve the aesthetics and functionality during several fabrication conditions and environments. After the selection was made, each component of the spring mechanism was carefully constructed using the required tools and machinery. A preliminary test was then conducted to anticipate how the system would behave in a static situation and consequently anticipate the behavior of the real system in terms of how it would be driven. In addition, the maximum amount of torque generated from the 5A brush-type DC motor was determined as well as a relationship between the torque and the current. As a result, the electronic devices that were

necessary to drive the entire spring mechanism were selected. Once the preliminary test was completed, the actively adjustable system was mounted and assembled.

**Figure 5.11: Assembly of Actively Adjustable Spring Mechanism**

# CHAPTER VI

## RESULTS AND DISCUSSIONS

In Chapter V, before mounting and assembling the adjustable stiffness mechanism, a relationship between the torque and current of each direct brush-type DC motor was determined. From such tests, results indicate that a linearly proportional relationship exists between the generated torque and the input current to the DC motor, which means that a series of equilibrium values can be established to analyze the spring mechanism. Therefore, the objective of the present chapter is to formulate and conduct a test plan that will create experimental information. With such data, consequently, the theoretical values obtained from Working Model will be compared to those obtained experimentally.

In particular, a series of equilibrium torques will be created to measure the effective stiffness of the mechanism in terms of the current generated by the motors (Figure 6.1). For example, determining the effective stiffness of the system will require applying different external (applied) forces on the output slider and measuring its respective displacement with respect to the horizontal global reference frame (Figure 6.2). This process will then be repeated with a different set of input motor torques to form several correlations that will embrace the variation of the mechanism effective stiffness. Once the data is obtained, three graphs will be generated to evaluate the behavior of the actively adjustable spring mechanism. The first graph will represent the effective stiffness of the system as a function of the applied force. The second graph will represent the effective stiffness as a function of the displacement generated on the slider element.

Lastly, the displacement of the will be graphed as a function of the applied force.

## 6.1 Results

**Table 6.1: Test Plan**

| Equilibrium Torque | | | | | |
|---|---|---|---|---|---|
| **Test** | **Current 2 (A)** | **Torque 2 (Nm)** | **Current 4 (A)** | **Torque 4 (Nm)** | **K*(N/m)** |
| 1 | 1.00 | -0.07518 | 1.7290 | 0.14789 | 698.962 |
| 2 | 1.25 | -0.10363 | 2.1613 | 0.19432 | 918.339 |
| 3 | 1.50 | -0.13208 | 2.5935 | 0.24074 | 1137.716 |
| 4 | 1.75 | -0.15748 | 3.0258 | 0.28717 | 1357.439 |
| 5 | 2.00 | -0.18694 | 3.4580 | 0.33359 | 1576.747 |
| 6 | 2.25 | -0.21946 | 3.8903 | 0.38001 | 1796.159 |
| 7 | 2.50 | -0.24994 | 4.3225 | 0.42644 | 2015.225 |
| 8 | 2.75 | -0.27838 | 4.7548 | 0.47286 | 2234.948 |
| 9 | 2.80 | -0.28014 | 4.8412 | 0.48214 | 2278.892 |
| 10 | 2.85 | -0.28573 | 4.9277 | 0.49143 | 2322.802 |

**Table 6.2: Applied Forces on Slider Element (Prismatic Joint)**

| Mass (grams) | Weight (N) |
|---|---|
| 50 | 0.490 |
| 70 | 0.686 |
| 100 | 0.980 |
| 120 | 1.176 |
| 150 | 1.471 |
| 170 | 1.667 |
| 200 | 1.961 |

### 6.1.1 Test 1

#### 6.1.1.1 Theoretical results from Working Model simulation

**Table 6.3: Theoretical Values (Test 1)**

| Theoretical Values from Working Model | | | | |
|---|---|---|---|---|
| **App. Force (N)** | **Xo (m)** | **Xf (m)** | **ΔX (m)** | **K (N/m)** |
| 0.490 | 0.397 | 0.396 | 0.0010 | 490.000 |
| 0.490 | 0.397 | 0.396 | 0.0010 | 490.000 |
| 0.490 | 0.397 | 0.396 | 0.0010 | 490.000 |
| 0.490 | 0.397 | 0.396 | 0.0010 | 490.000 |
| 0.686 | 0.397 | 0.390 | 0.0070 | 98.000 |
| 0.686 | 0.397 | 0.390 | 0.0070 | 98.000 |
| 0.686 | 0.397 | 0.390 | 0.0070 | 98.000 |
| 0.686 | 0.397 | 0.390 | 0.0070 | 98.000 |
| 0.980 | 0.397 | 0.386 | 0.0110 | 89.091 |
| 0.980 | 0.397 | 0.386 | 0.0110 | 89.091 |
| 0.980 | 0.397 | 0.386 | 0.0110 | 89.091 |
| 0.980 | 0.397 | 0.386 | 0.0110 | 89.091 |
| 1.176 | 0.397 | 0.372 | 0.0250 | 47.040 |
| 1.176 | 0.397 | 0.372 | 0.0250 | 47.040 |
| 1.176 | 0.397 | 0.372 | 0.0250 | 47.040 |
| 1.176 | 0.397 | 0.372 | 0.0250 | 47.040 |

### 6.1.1.2 Experimental results

**Table 6.4: Experimental Values (Test 1)**

| Experimental Values | | | | | | | |
|---|---|---|---|---|---|---|---|
| **App. Force (N)** | **Xo (V)** | **Xf (V)** | **Xo (m)** | **Xf (m)** | **ΔX (m)** | **ΔXf (m)** | **K (N/m)** |
| 0.490 | 0.570 | 0.613 | 0.0145 | 0.0156 | 0.0011 | 0.396 | 448.636 |
| 0.490 | 0.570 | 0.608 | 0.0145 | 0.0154 | 0.0010 | 0.396 | 507.667 |
| 0.490 | 0.570 | 0.613 | 0.0145 | 0.0156 | 0.0011 | 0.396 | 448.636 |
| 0.490 | 0.570 | 0.613 | 0.0145 | 0.0156 | 0.0011 | 0.396 | 448.636 |
| 0.686 | 0.570 | 0.720 | 0.0145 | 0.0183 | 0.0038 | 0.393 | 180.052 |
| 0.686 | 0.570 | 0.720 | 0.0145 | 0.0183 | 0.0038 | 0.393 | 180.052 |
| 0.686 | 0.570 | 0.720 | 0.0145 | 0.0183 | 0.0038 | 0.393 | 180.052 |
| 0.686 | 0.570 | 0.722 | 0.0145 | 0.0183 | 0.0039 | 0.393 | 177.683 |
| 0.980 | 0.570 | 1.326 | 0.0145 | 0.0337 | 0.0192 | 0.378 | 51.035 |
| 0.980 | 0.570 | 1.328 | 0.0145 | 0.0337 | 0.0193 | 0.378 | 50.901 |
| 0.980 | 0.570 | 1.333 | 0.0145 | 0.0339 | 0.0194 | 0.378 | 50.567 |
| 0.980 | 0.570 | 1.333 | 0.0145 | 0.0339 | 0.0194 | 0.378 | 50.567 |
| 1.176 | 0.570 | 2.142 | 0.0145 | 0.0544 | 0.0399 | 0.357 | 29.452 |
| 1.176 | 0.570 | 2.138 | 0.0145 | 0.0543 | 0.0398 | 0.357 | 29.528 |
| 1.176 | 0.570 | 2.145 | 0.0145 | 0.0545 | 0.0400 | 0.357 | 29.396 |
| 1.176 | 0.570 | 2.144 | 0.0145 | 0.0545 | 0.0400 | 0.357 | 29.415 |

### 6.1.1.3 Theoretical results vs. experimental results

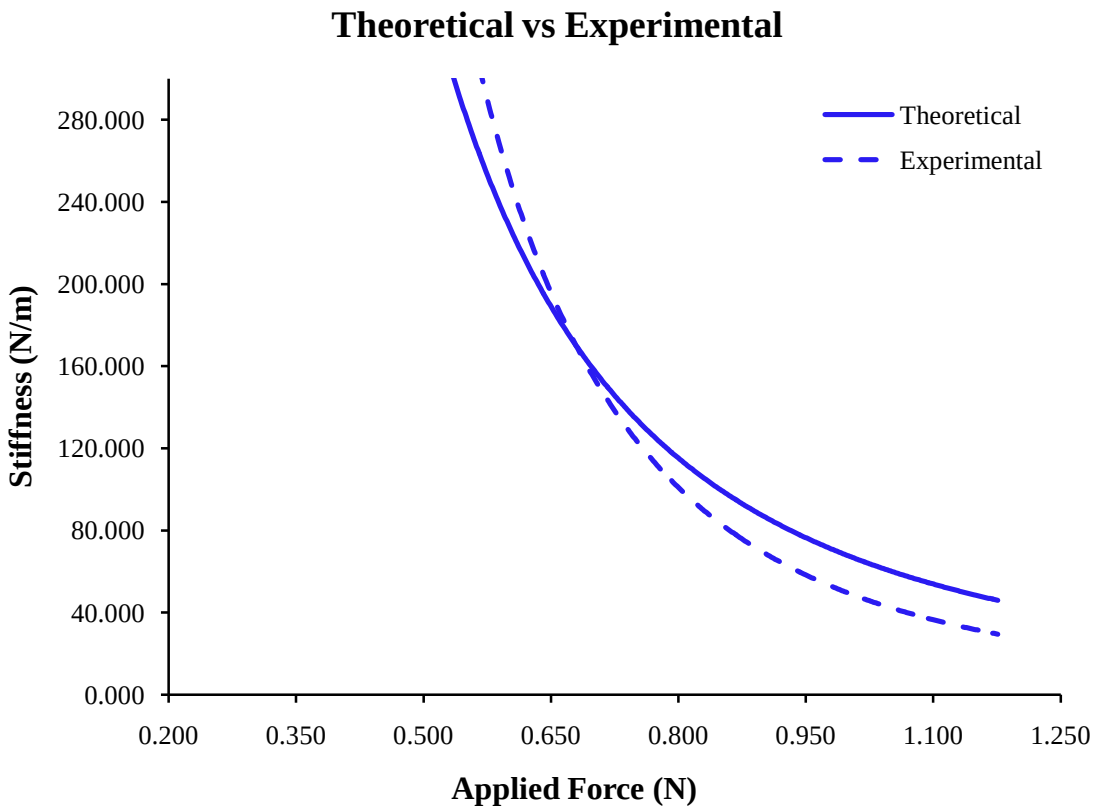


**Figure 6.1: Stiffness vs. Applied Force (Test 1)**

#### 6.1.1.4 Theoretical results vs. experimental results

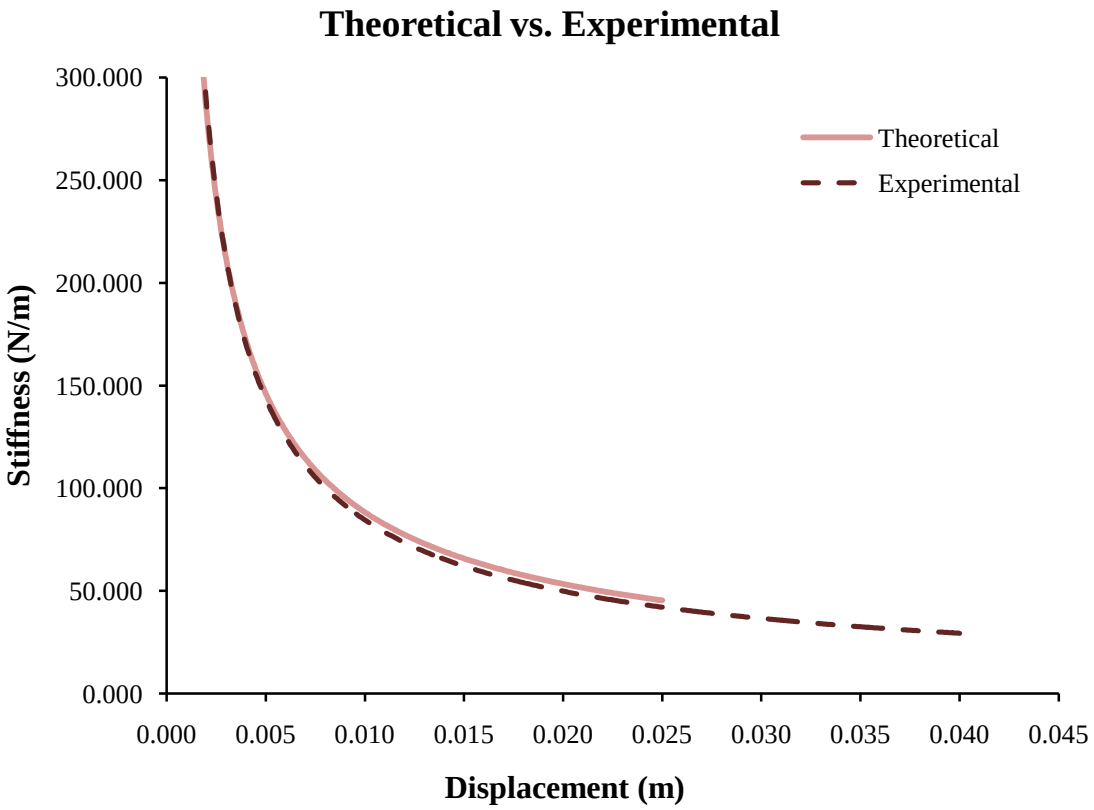


**Figure 6.2: Stiffness vs. Displacement (Test 1)**

### 6.1.2 Test 2

#### 6.1.2.1 Theoretical results from Working Model simulation

**Table 6.5: Theoretical Values (Test 2)**

| Theoretical Values from Working Model | | | | |
|---|---|---|---|---|
| **App. Force (N)** | **Xo (m)** | **Xf (m)** | **ΔX (m)** | **K (N/m)** |
| 0.490 | 0.397 | 0.396 | 0.0008 | 612.500 |
| 0.490 | 0.397 | 0.396 | 0.0008 | 612.500 |
| 0.490 | 0.397 | 0.396 | 0.0008 | 612.500 |
| 0.490 | 0.397 | 0.396 | 0.0008 | 612.500 |
| 0.686 | 0.397 | 0.392 | 0.0050 | 137.200 |
| 0.686 | 0.397 | 0.392 | 0.0050 | 137.200 |
| 0.686 | 0.397 | 0.392 | 0.0050 | 137.200 |
| 0.686 | 0.397 | 0.392 | 0.0050 | 137.200 |
| 0.980 | 0.397 | 0.387 | 0.0100 | 98.000 |
| 0.980 | 0.397 | 0.387 | 0.0100 | 98.000 |
| 0.980 | 0.397 | 0.387 | 0.0100 | 98.000 |
| 0.980 | 0.397 | 0.387 | 0.0100 | 98.000 |
| 1.176 | 0.397 | 0.384 | 0.0130 | 90.462 |
| 1.176 | 0.397 | 0.384 | 0.0130 | 90.462 |
| 1.176 | 0.397 | 0.384 | 0.0130 | 90.462 |
| 1.176 | 0.397 | 0.384 | 0.0130 | 90.462 |
| 1.471 | 0.397 | 0.377 | 0.0200 | 73.550 |
| 1.471 | 0.397 | 0.377 | 0.0200 | 73.550 |
| 1.471 | 0.397 | 0.377 | 0.0200 | 73.550 |
| 1.471 | 0.397 | 0.377 | 0.0200 | 73.550 |
| 1.667 | 0.397 | 0.368 | 0.029 | 57.483 |
| 1.667 | 0.397 | 0.368 | 0.0290 | 57.483 |
| 1.667 | 0.397 | 0.368 | 0.0290 | 57.483 |
| 1.667 | 0.397 | 0.368 | 0.0290 | 57.483 |

### 6.1.2.2 Experimental results

**Table 6.6: Experimental Values (Test 2)**

| Experimental Values | | | | | | | |
|---|---|---|---|---|---|---|---|
| **App. Force (N)** | **Xo (V)** | **Xf (V)** | **Xo (m)** | **Xf (m)** | **ΔX (m)** | **ΔXf (m)** | **K (N/m)** |
| 0.490 | 0.489 | 0.518 | 0.0124 | 0.0132 | 0.0007 | 0.396 | 665.219 |
| 0.490 | 0.489 | 0.517 | 0.0124 | 0.0131 | 0.0007 | 0.396 | 688.976 |
| 0.490 | 0.489 | 0.519 | 0.0124 | 0.0132 | 0.0008 | 0.396 | 643.045 |
| 0.490 | 0.489 | 0.520 | 0.0124 | 0.0132 | 0.0008 | 0.396 | 622.301 |
| 0.686 | 0.489 | 0.570 | 0.0124 | 0.0145 | 0.0021 | 0.395 | 333.431 |
| 0.686 | 0.489 | 0.578 | 0.0124 | 0.0147 | 0.0023 | 0.395 | 303.459 |
| 0.686 | 0.489 | 0.576 | 0.0124 | 0.0146 | 0.0022 | 0.395 | 310.435 |
| 0.686 | 0.489 | 0.572 | 0.0124 | 0.0145 | 0.0021 | 0.395 | 325.396 |
| 0.980 | 0.489 | 0.863 | 0.0124 | 0.0219 | 0.0095 | 0.388 | 103.162 |
| 0.980 | 0.489 | 0.824 | 0.0124 | 0.0209 | 0.0085 | 0.388 | 115.172 |
| 0.980 | 0.489 | 0.825 | 0.0124 | 0.0210 | 0.0085 | 0.388 | 114.829 |
| 0.980 | 0.489 | 0.812 | 0.0124 | 0.0206 | 0.0082 | 0.389 | 119.451 |
| 1.176 | 0.489 | 1.381 | 0.0124 | 0.0351 | 0.0227 | 0.374 | 51.905 |
| 1.176 | 0.489 | 1.375 | 0.0124 | 0.0349 | 0.0225 | 0.374 | 52.256 |
| 1.176 | 0.489 | 1.424 | 0.0124 | 0.0362 | 0.0237 | 0.373 | 49.518 |
| 1.176 | 0.489 | 1.449 | 0.0124 | 0.0368 | 0.0244 | 0.373 | 48.228 |
| 1.471 | 0.489 | 2.258 | 0.0124 | 0.0574 | 0.0449 | 0.352 | 32.738 |
| 1.471 | 0.489 | 2.283 | 0.0124 | 0.0580 | 0.0456 | 0.351 | 32.282 |
| 1.471 | 0.489 | 2.321 | 0.0124 | 0.0590 | 0.0465 | 0.350 | 31.612 |
| 1.471 | 0.489 | 2.383 | 0.0124 | 0.0605 | 0.0481 | 0.349 | 30.577 |
| 1.667 | 0.489 | 3.226 | 0.0124 | 0.0819 | 0.0695 | 0.327 | 23.979 |
| 1.667 | 0.489 | 3.202 | 0.0124 | 0.0813 | 0.0689 | 0.328 | 24.191 |
| 1.667 | 0.489 | 3.207 | 0.0124 | 0.0815 | 0.0690 | 0.328 | 24.146 |
| 1.667 | 0.489 | 3.235 | 0.0124 | 0.0822 | 0.0697 | 0.327 | 23.900 |

### 6.1.2.3 Theoretical results vs. experimental results

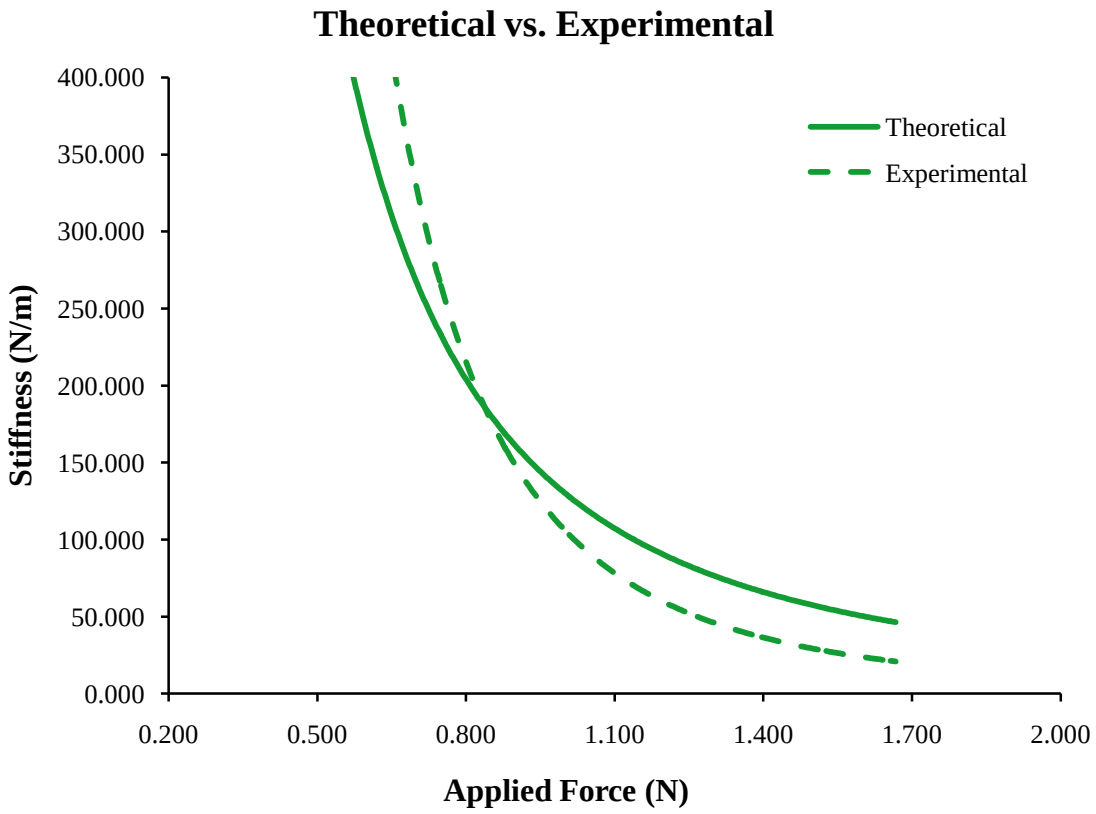


**Figure 6.3: Stiffness vs. Applied Force (Test 2)**

### 6.1.2.4 Theoretical results vs. experimental results

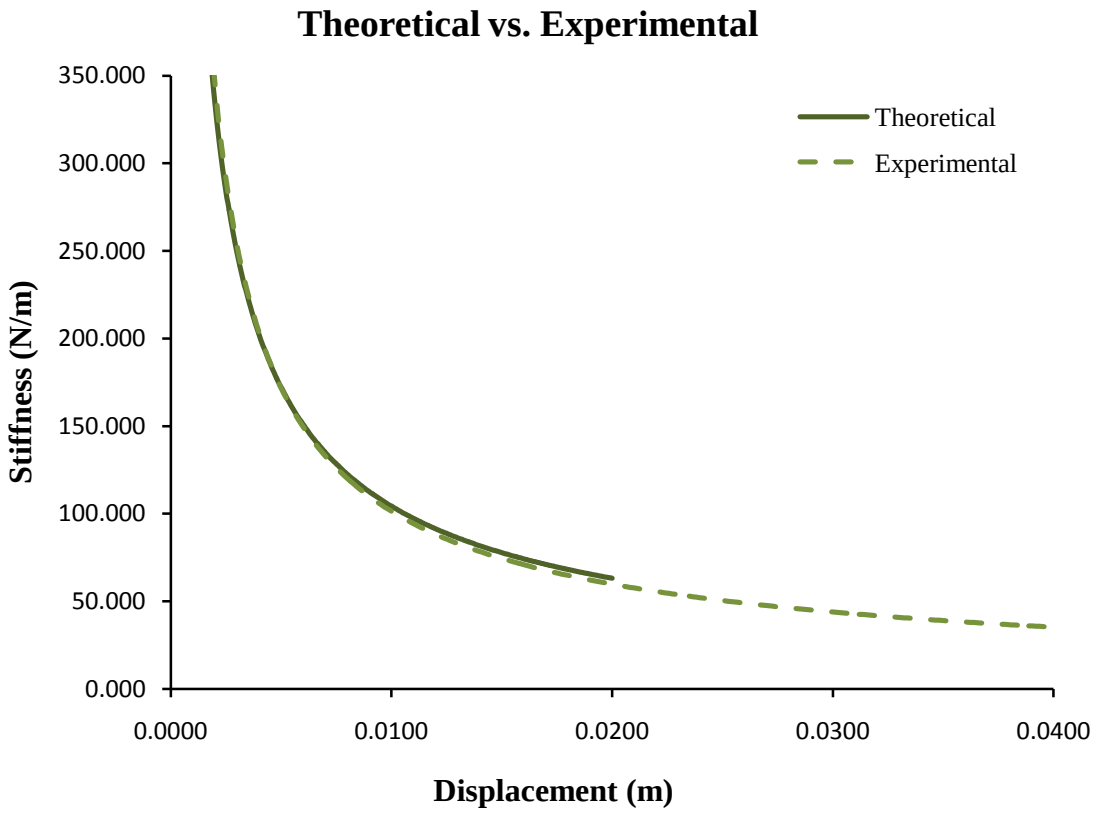


**Figure 6.4: Stiffness vs. Displacement (Test 2)**

### 6.1.3 Test 3

#### 6.1.3.1 Theoretical results from Working Model simulation

**Table 6.7: Theoretical Values (Test 3)**

| Theoretical Values from Working Model | | | | |
|---|---|---|---|---|
| **App. Force (N)** | **Xo (m)** | **Xf (m)** | **ΔX (m)** | **K (N/m)** |
| 0.490 | 0.397 | 0.396 | 0.001 | 612.500 |
| 0.490 | 0.397 | 0.396 | 0.001 | 612.500 |
| 0.490 | 0.397 | 0.396 | 0.001 | 612.500 |
| 0.490 | 0.397 | 0.396 | 0.001 | 612.500 |
| 0.686 | 0.397 | 0.392 | 0.005 | 137.200 |
| 0.686 | 0.397 | 0.392 | 0.005 | 137.200 |
| 0.686 | 0.397 | 0.392 | 0.005 | 137.200 |
| 0.686 | 0.397 | 0.392 | 0.005 | 137.200 |
| 0.980 | 0.397 | 0.387 | 0.010 | 98.000 |
| 0.980 | 0.397 | 0.387 | 0.010 | 98.000 |
| 0.980 | 0.397 | 0.387 | 0.010 | 98.000 |
| 0.980 | 0.397 | 0.387 | 0.010 | 98.000 |
| 1.176 | 0.397 | 0.385 | 0.012 | 98.000 |
| 1.176 | 0.397 | 0.385 | 0.012 | 98.000 |
| 1.176 | 0.397 | 0.385 | 0.012 | 98.000 |
| 1.176 | 0.397 | 0.385 | 0.012 | 98.000 |
| 1.471 | 0.397 | 0.379 | 0.018 | 81.722 |
| 1.471 | 0.397 | 0.379 | 0.018 | 81.722 |
| 1.471 | 0.397 | 0.379 | 0.018 | 81.722 |
| 1.471 | 0.397 | 0.379 | 0.018 | 81.722 |
| 1.667 | 0.397 | 0.372 | 0.025 | 66.680 |
| 1.667 | 0.397 | 0.372 | 0.025 | 66.680 |
| 1.667 | 0.397 | 0.372 | 0.025 | 66.680 |
| 1.667 | 0.397 | 0.372 | 0.025 | 66.680 |

### 6.1.3.2 Experimental results

**Table 6.8: Experimental Values (Test 3)**

| Experimental Values | | | | | | | |
|---|---|---|---|---|---|---|---|
| **App. Force (N)** | **Xo (V)** | **Xf (V)** | **Xo (m)** | **Xf (m)** | **ΔX (m)** | **ΔXf (m)** | **K (N/m)** |
| 0.490 | 0.499 | 0.525 | 0.0127 | 0.0133 | 0.0007 | 0.396 | 741.975 |
| 0.490 | 0.499 | 0.526 | 0.0127 | 0.0134 | 0.0007 | 0.396 | 714.494 |
| 0.490 | 0.499 | 0.528 | 0.0127 | 0.0134 | 0.0007 | 0.396 | 665.219 |
| 0.490 | 0.499 | 0.528 | 0.0127 | 0.0134 | 0.0007 | 0.396 | 665.219 |
| 0.686 | 0.499 | 0.598 | 0.0127 | 0.0152 | 0.0025 | 0.394 | 272.807 |
| 0.686 | 0.499 | 0.605 | 0.0127 | 0.0154 | 0.0027 | 0.394 | 254.791 |
| 0.686 | 0.499 | 0.606 | 0.0127 | 0.0154 | 0.0027 | 0.394 | 252.410 |
| 0.686 | 0.499 | 0.600 | 0.0127 | 0.0152 | 0.0026 | 0.394 | 267.405 |
| 0.980 | 0.499 | 0.881 | 0.0127 | 0.0224 | 0.0097 | 0.387 | 101.002 |
| 0.980 | 0.499 | 0.888 | 0.0127 | 0.0226 | 0.0099 | 0.387 | 99.184 |
| 0.980 | 0.499 | 0.874 | 0.0127 | 0.0222 | 0.0095 | 0.387 | 102.887 |
| 0.980 | 0.499 | 0.896 | 0.0127 | 0.0228 | 0.0101 | 0.387 | 97.186 |
| 1.176 | 0.499 | 1.232 | 0.0127 | 0.0313 | 0.0186 | 0.378 | 63.164 |
| 1.176 | 0.499 | 1.193 | 0.0127 | 0.0303 | 0.0176 | 0.379 | 66.714 |
| 1.176 | 0.499 | 1.283 | 0.0127 | 0.0326 | 0.0199 | 0.377 | 59.055 |
| 1.176 | 0.499 | 1.200 | 0.0127 | 0.0305 | 0.0178 | 0.379 | 66.047 |
| 1.471 | 0.499 | 1.801 | 0.0127 | 0.0457 | 0.0331 | 0.364 | 44.480 |
| 1.471 | 0.499 | 1.834 | 0.0127 | 0.0466 | 0.0339 | 0.363 | 43.381 |
| 1.471 | 0.499 | 1.844 | 0.0127 | 0.0468 | 0.0342 | 0.363 | 43.058 |
| 1.471 | 0.499 | 1.862 | 0.0127 | 0.0473 | 0.0346 | 0.362 | 42.490 |
| 1.667 | 0.499 | 2.676 | 0.0127 | 0.0680 | 0.0553 | 0.342 | 30.147 |
| 1.667 | 0.499 | 2.615 | 0.0127 | 0.0664 | 0.0537 | 0.343 | 31.016 |
| 1.667 | 0.499 | 2.654 | 0.0127 | 0.0674 | 0.0547 | 0.342 | 30.455 |
| 1.667 | 0.499 | 2.660 | 0.0127 | 0.0676 | 0.0549 | 0.342 | 30.370 |

### 6.1.3.3 Theoretical results vs. experimental results

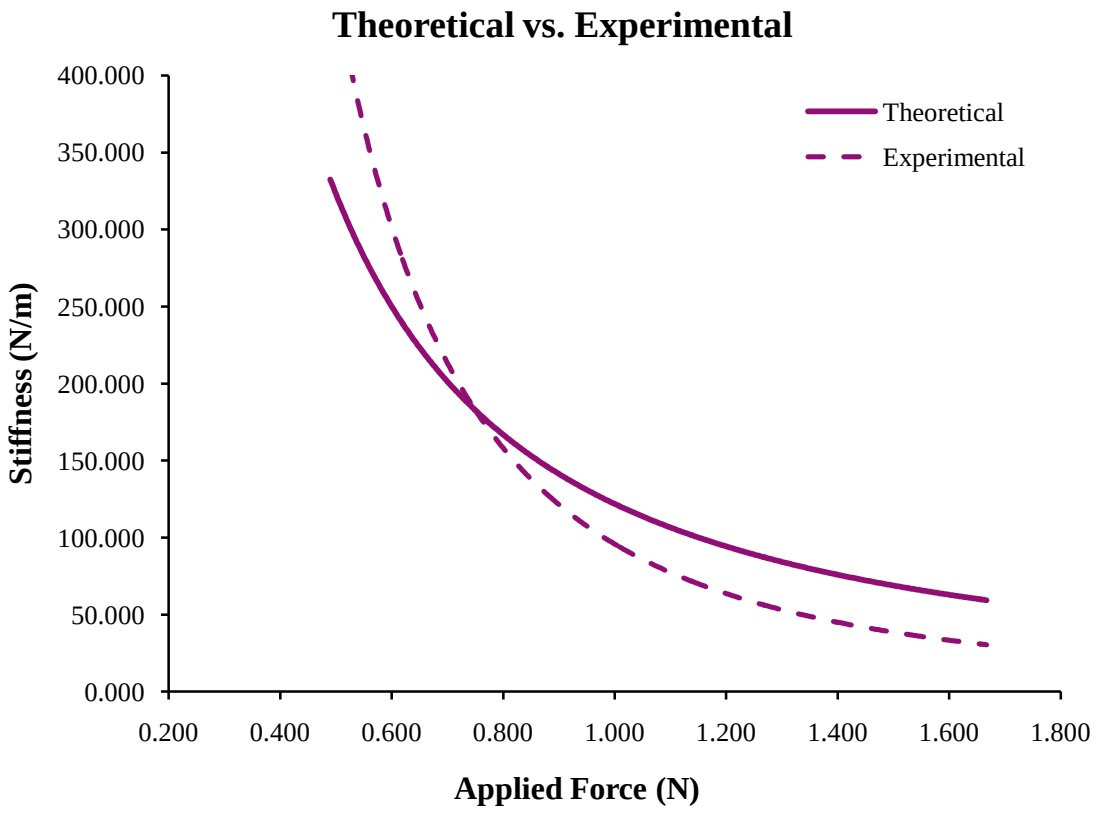


**Figure 6.5: Stiffness vs. Applied Force (Test 3)**

### 6.1.3.4 Theoretical results vs. experimental results

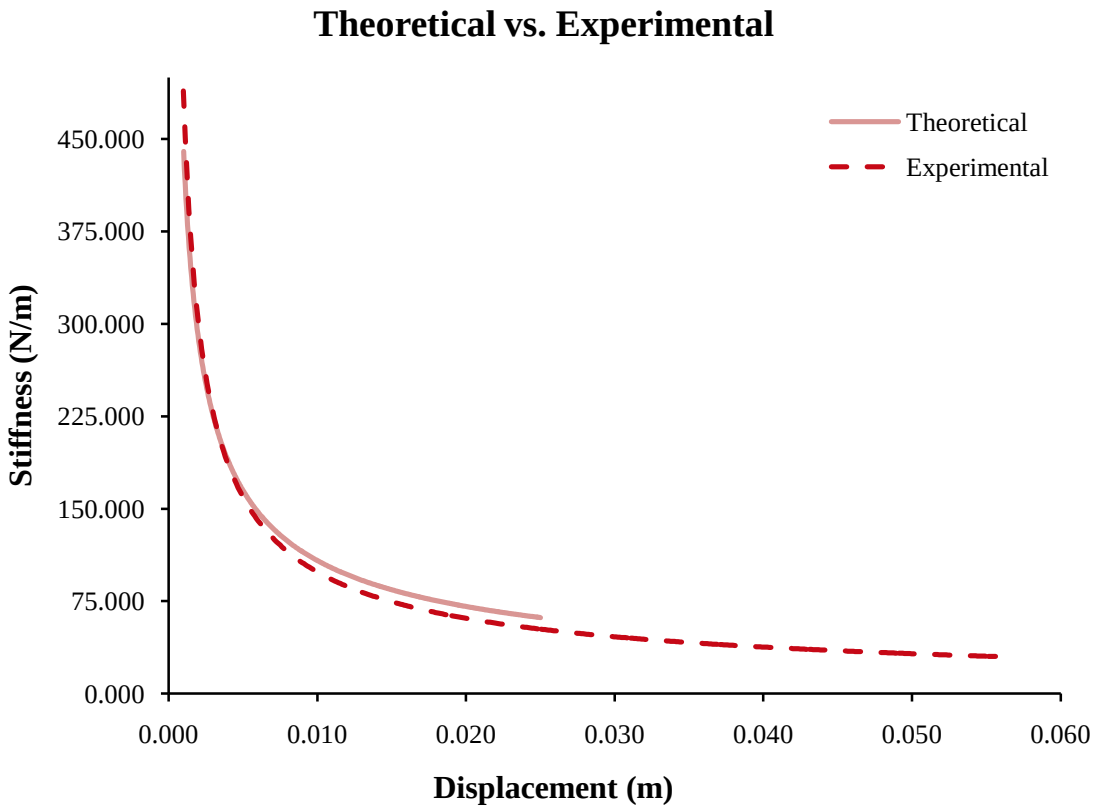


**Figure 6.6: Stiffness vs. Displacement (Test 3)**

### 6.1.4 Test 4

#### 6.1.4.1 Theoretical results from Working Model simulation

**Table 6.9: Theoretical Values (Test 4)**

| Theoretical Values from Working Model | | | | |
|---|---|---|---|---|
| **App. Force (N)** | **Xo (m)** | **Xf (m)** | **ΔX (m)** | **K (N/m)** |
| 0.490 | 0.397 | 0.396 | 0.001 | 816.667 |
| 0.490 | 0.397 | 0.396 | 0.001 | 816.667 |
| 0.490 | 0.397 | 0.396 | 0.001 | 816.667 |
| 0.490 | 0.397 | 0.396 | 0.001 | 816.667 |
| 0.686 | 0.397 | 0.393 | 0.004 | 171.500 |
| 0.686 | 0.397 | 0.393 | 0.004 | 171.500 |
| 0.686 | 0.397 | 0.393 | 0.004 | 171.500 |
| 0.686 | 0.397 | 0.393 | 0.004 | 171.500 |
| 0.980 | 0.397 | 0.390 | 0.007 | 140.000 |
| 0.980 | 0.397 | 0.390 | 0.007 | 140.000 |
| 0.980 | 0.397 | 0.390 | 0.007 | 140.000 |
| 0.980 | 0.397 | 0.390 | 0.007 | 140.000 |
| 1.176 | 0.397 | 0.385 | 0.012 | 98.000 |
| 1.176 | 0.397 | 0.385 | 0.012 | 98.000 |
| 1.176 | 0.397 | 0.385 | 0.012 | 98.000 |
| 1.176 | 0.397 | 0.385 | 0.012 | 98.000 |
| 1.471 | 0.397 | 0.381 | 0.016 | 91.937 |
| 1.471 | 0.397 | 0.381 | 0.016 | 91.937 |
| 1.471 | 0.397 | 0.381 | 0.016 | 91.937 |
| 1.471 | 0.397 | 0.381 | 0.016 | 91.937 |
| 1.667 | 0.397 | 0.376 | 0.021 | 79.381 |
| 1.667 | 0.397 | 0.376 | 0.021 | 79.381 |
| 1.667 | 0.397 | 0.376 | 0.021 | 79.381 |
| 1.667 | 0.397 | 0.376 | 0.021 | 79.381 |

### 6.1.4.2 Experimental results

**Table 6.10: Experimental Values (Test 4)**

| Experimental Values | | | | | | | |
|---|---|---|---|---|---|---|---|
| **App. Force (N)** | **Xo (V)** | **Xf (V)** | **Xo (m)** | **Xf (m)** | **ΔX (m)** | **ΔXf (m)** | **K (N/m)** |
| 0.490 | 0.545 | 0.565 | 0.0138 | 0.0144 | 0.0005 | 0.396 | 964.567 |
| 0.490 | 0.545 | 0.565 | 0.0138 | 0.0144 | 0.0005 | 0.396 | 964.567 |
| 0.490 | 0.545 | 0.567 | 0.0138 | 0.0144 | 0.0006 | 0.396 | 876.879 |
| 0.490 | 0.545 | 0.565 | 0.0138 | 0.0144 | 0.0005 | 0.396 | 964.567 |
| 0.686 | 0.545 | 0.63 | 0.0138 | 0.0160 | 0.0022 | 0.395 | 317.740 |
| 0.686 | 0.545 | 0.646 | 0.0138 | 0.0164 | 0.0026 | 0.394 | 267.405 |
| 0.686 | 0.545 | 0.646 | 0.0138 | 0.0164 | 0.0026 | 0.394 | 267.405 |
| 0.686 | 0.545 | 0.641 | 0.0138 | 0.0163 | 0.0024 | 0.395 | 281.332 |
| 0.980 | 0.545 | 0.904 | 0.0138 | 0.0230 | 0.0091 | 0.388 | 107.473 |
| 0.980 | 0.545 | 0.894 | 0.0138 | 0.0227 | 0.0089 | 0.388 | 110.552 |
| 0.980 | 0.545 | 0.881 | 0.0138 | 0.0224 | 0.0085 | 0.388 | 114.829 |
| 0.980 | 0.545 | 0.842 | 0.0138 | 0.0214 | 0.0075 | 0.389 | 129.908 |
| 1.176 | 0.545 | 1.08 | 0.0138 | 0.0274 | 0.0136 | 0.383 | 86.541 |
| 1.176 | 0.545 | 1.068 | 0.0138 | 0.0271 | 0.0133 | 0.384 | 88.526 |
| 1.176 | 0.545 | 1.121 | 0.0138 | 0.0285 | 0.0146 | 0.382 | 80.381 |
| 1.176 | 0.545 | 1.049 | 0.0138 | 0.0266 | 0.0128 | 0.384 | 91.864 |
| 1.471 | 0.545 | 1.601 | 0.0138 | 0.0407 | 0.0268 | 0.370 | 54.842 |
| 1.471 | 0.545 | 1.673 | 0.0138 | 0.0425 | 0.0287 | 0.368 | 51.342 |
| 1.471 | 0.545 | 1.567 | 0.0138 | 0.0398 | 0.0260 | 0.371 | 56.667 |
| 1.471 | 0.545 | 1.55 | 0.0138 | 0.0394 | 0.0255 | 0.371 | 57.625 |
| 1.667 | 0.545 | 2.148 | 0.0138 | 0.0546 | 0.0407 | 0.356 | 40.942 |
| 1.667 | 0.545 | 2.118 | 0.0138 | 0.0538 | 0.0400 | 0.357 | 41.723 |
| 1.667 | 0.545 | 2.142 | 0.0138 | 0.0544 | 0.0406 | 0.356 | 41.096 |
| 1.667 | 0.545 | 2.152 | 0.0138 | 0.0547 | 0.0408 | 0.356 | 40.840 |

### 6.1.4.3 Theoretical results vs. experimental results

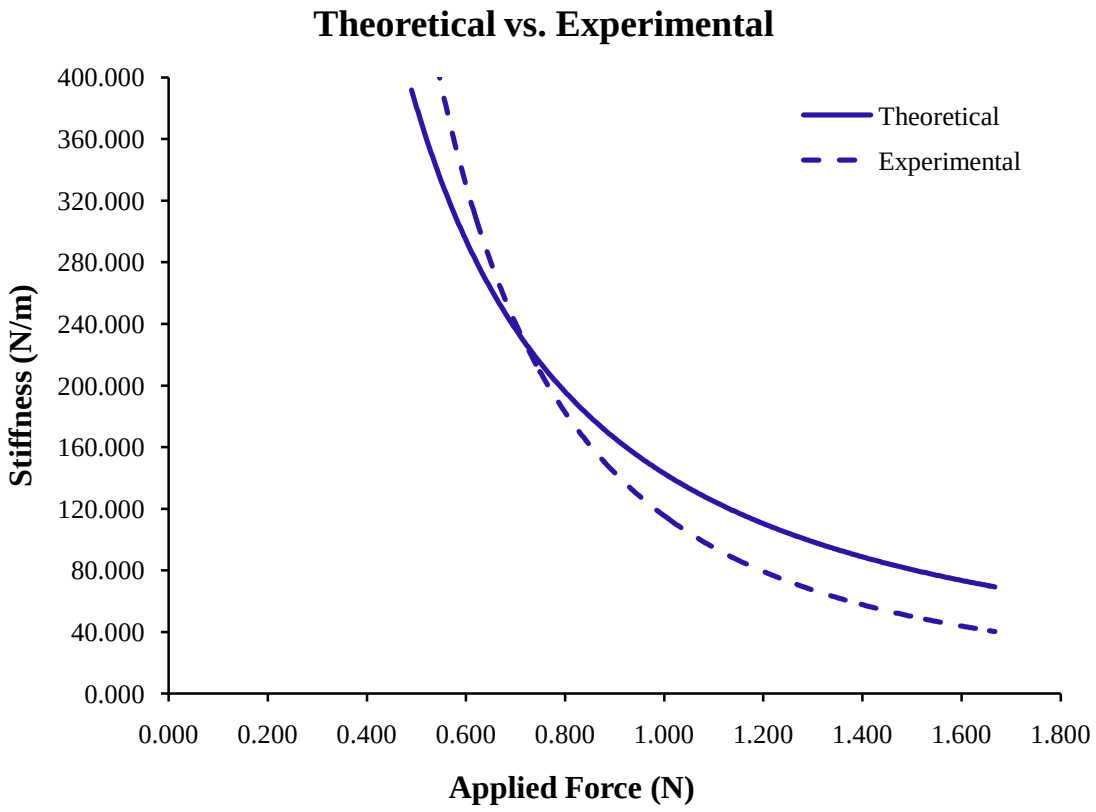


**Figure 6.7: Stiffness vs. Applied Force (Test 4)**

### 6.1.4.4 Theoretical results vs. experimental results

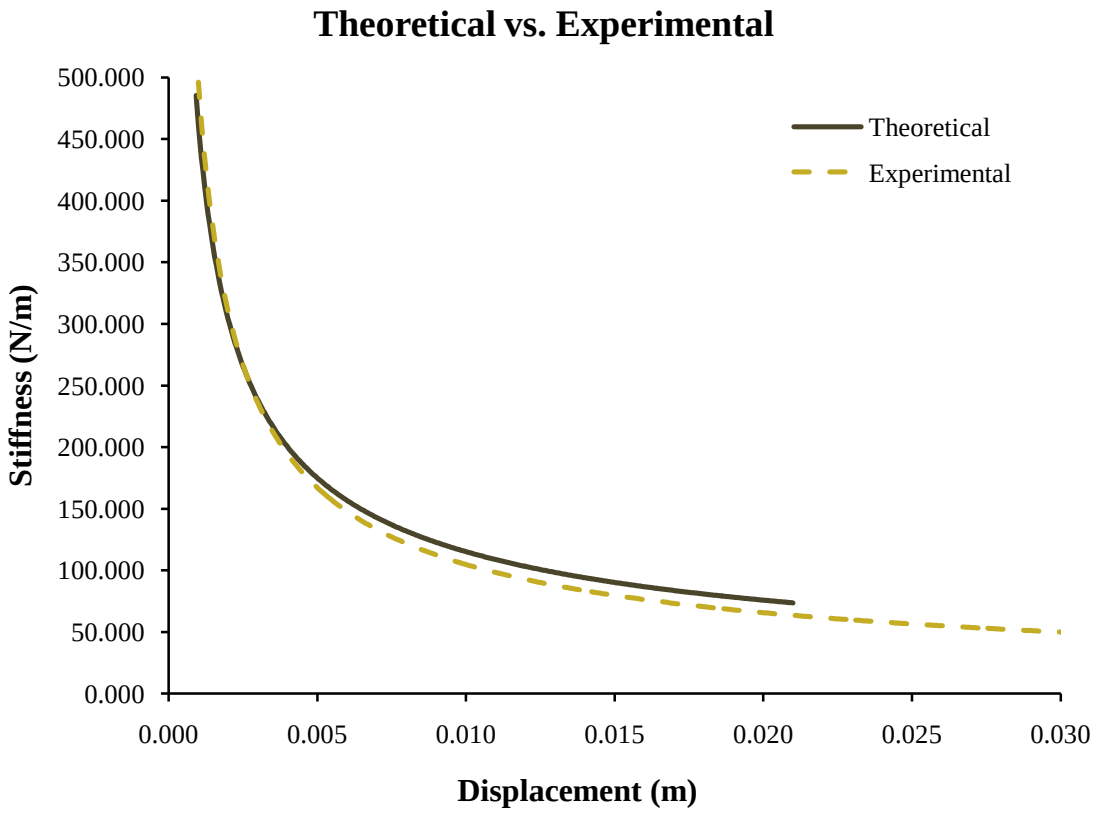


**Figure 6.8: Stiffness vs. Displacement (Test 4)**

### 6.1.5 Test 5

#### 6.1.5.1 Theoretical results from Working Model simulation

**Table 6.11: Theoretical Values (Test 5)**

| Theoretical Values from Working Model | | | | |
|---|---|---|---|---|
| **App. Force (N)** | **Xo (m)** | **Xf (m)** | **ΔX (m)** | **K (N/m)** |
| 0.490 | 0.397 | 0.396 | 0.001 | 924.528 |
| 0.490 | 0.397 | 0.396 | 0.001 | 924.528 |
| 0.490 | 0.397 | 0.396 | 0.001 | 924.528 |
| 0.490 | 0.397 | 0.396 | 0.001 | 924.528 |
| 0.686 | 0.397 | 0.393 | 0.004 | 180.526 |
| 0.686 | 0.397 | 0.393 | 0.004 | 180.526 |
| 0.686 | 0.397 | 0.393 | 0.004 | 180.526 |
| 0.686 | 0.397 | 0.393 | 0.004 | 180.526 |
| 0.980 | 0.397 | 0.388 | 0.009 | 108.889 |
| 0.980 | 0.397 | 0.388 | 0.009 | 108.889 |
| 0.980 | 0.397 | 0.388 | 0.009 | 108.889 |
| 0.980 | 0.397 | 0.388 | 0.009 | 108.889 |
| 1.176 | 0.397 | 0.386 | 0.011 | 106.909 |
| 1.176 | 0.397 | 0.386 | 0.011 | 106.909 |
| 1.176 | 0.397 | 0.386 | 0.011 | 106.909 |
| 1.176 | 0.397 | 0.386 | 0.011 | 106.909 |
| 1.471 | 0.397 | 0.382 | 0.015 | 98.067 |
| 1.471 | 0.397 | 0.382 | 0.015 | 98.067 |
| 1.471 | 0.397 | 0.382 | 0.015 | 98.067 |
| 1.471 | 0.397 | 0.382 | 0.015 | 98.067 |
| 1.667 | 0.397 | 0.378 | 0.019 | 87.737 |
| 1.667 | 0.397 | 0.378 | 0.019 | 87.737 |
| 1.667 | 0.397 | 0.378 | 0.019 | 87.737 |
| 1.667 | 0.397 | 0.378 | 0.019 | 87.737 |
| 1.961 | 0.397 | 0.371 | 0.026 | 75.423 |
| 1.961 | 0.397 | 0.371 | 0.026 | 75.423 |
| 1.961 | 0.397 | 0.371 | 0.026 | 75.423 |
| 1.961 | 0.397 | 0.371 | 0.026 | 75.423 |

### 6.1.5.2 Experimental results

**Table 6.12: Experimental Values (Test 5)**

| Experimental Values | | | | | | | |
|---|---|---|---|---|---|---|---|
| **App. Force (N)** | **Xo (V)** | **Xf (V)** | **Xo (m)** | **Xf (m)** | **ΔX (m)** | **ΔXf (m)** | **K (N/m)** |
| 0.490 | 0.596 | 0.614 | 0.0151 | 0.0156 | 0.0005 | 0.397 | 1071.741 |
| 0.490 | 0.596 | 0.612 | 0.0151 | 0.0155 | 0.0004 | 0.397 | 1205.709 |
| 0.490 | 0.596 | 0.613 | 0.0151 | 0.0156 | 0.0004 | 0.397 | 1134.785 |
| 0.490 | 0.596 | 0.612 | 0.0151 | 0.0155 | 0.0004 | 0.397 | 1205.709 |
| 0.686 | 0.596 | 0.698 | 0.0151 | 0.0177 | 0.0026 | 0.394 | 264.783 |
| 0.686 | 0.596 | 0.694 | 0.0151 | 0.0176 | 0.0025 | 0.395 | 275.591 |
| 0.686 | 0.596 | 0.684 | 0.0151 | 0.0174 | 0.0022 | 0.395 | 306.908 |
| 0.686 | 0.596 | 0.674 | 0.0151 | 0.0171 | 0.0020 | 0.395 | 346.255 |
| 0.980 | 0.596 | 0.891 | 0.0151 | 0.0226 | 0.0075 | 0.390 | 130.789 |
| 0.980 | 0.596 | 0.892 | 0.0151 | 0.0227 | 0.0075 | 0.389 | 130.347 |
| 0.980 | 0.596 | 0.885 | 0.0151 | 0.0225 | 0.0073 | 0.390 | 133.504 |
| 0.980 | 0.596 | 0.872 | 0.0151 | 0.0221 | 0.0070 | 0.390 | 139.792 |
| 1.176 | 0.596 | 1.077 | 0.0151 | 0.0274 | 0.0122 | 0.385 | 96.256 |
| 1.176 | 0.596 | 1.088 | 0.0151 | 0.0276 | 0.0125 | 0.385 | 94.104 |
| 1.176 | 0.596 | 1.042 | 0.0151 | 0.0265 | 0.0113 | 0.386 | 103.810 |
| 1.176 | 0.596 | 1.073 | 0.0151 | 0.0273 | 0.0121 | 0.385 | 97.063 |
| 1.471 | 0.596 | 1.490 | 0.0151 | 0.0378 | 0.0227 | 0.374 | 64.780 |
| 1.471 | 0.596 | 1.446 | 0.0151 | 0.0367 | 0.0216 | 0.375 | 68.133 |
| 1.471 | 0.596 | 1.437 | 0.0151 | 0.0365 | 0.0214 | 0.376 | 68.863 |
| 1.471 | 0.596 | 1.337 | 0.0151 | 0.0340 | 0.0188 | 0.378 | 78.156 |
| 1.667 | 0.596 | 1.838 | 0.0151 | 0.0467 | 0.0315 | 0.365 | 52.842 |
| 1.667 | 0.596 | 1.818 | 0.0151 | 0.0462 | 0.0310 | 0.366 | 53.707 |
| 1.667 | 0.596 | 1.840 | 0.0151 | 0.0467 | 0.0316 | 0.365 | 52.757 |
| 1.667 | 0.596 | 1.844 | 0.0151 | 0.0468 | 0.0317 | 0.365 | 52.588 |
| 1.961 | 0.596 | 2.554 | 0.0151 | 0.0649 | 0.0497 | 0.347 | 39.430 |
| 1.961 | 0.596 | 2.531 | 0.0151 | 0.0643 | 0.0491 | 0.348 | 39.899 |
| 1.961 | 0.596 | 2.543 | 0.0151 | 0.0646 | 0.0495 | 0.348 | 39.653 |
| 1.961 | 0.596 | 2.565 | 0.0151 | 0.0652 | 0.0500 | 0.347 | 39.210 |

### 6.1.5.3 Theoretical results vs. experimental results

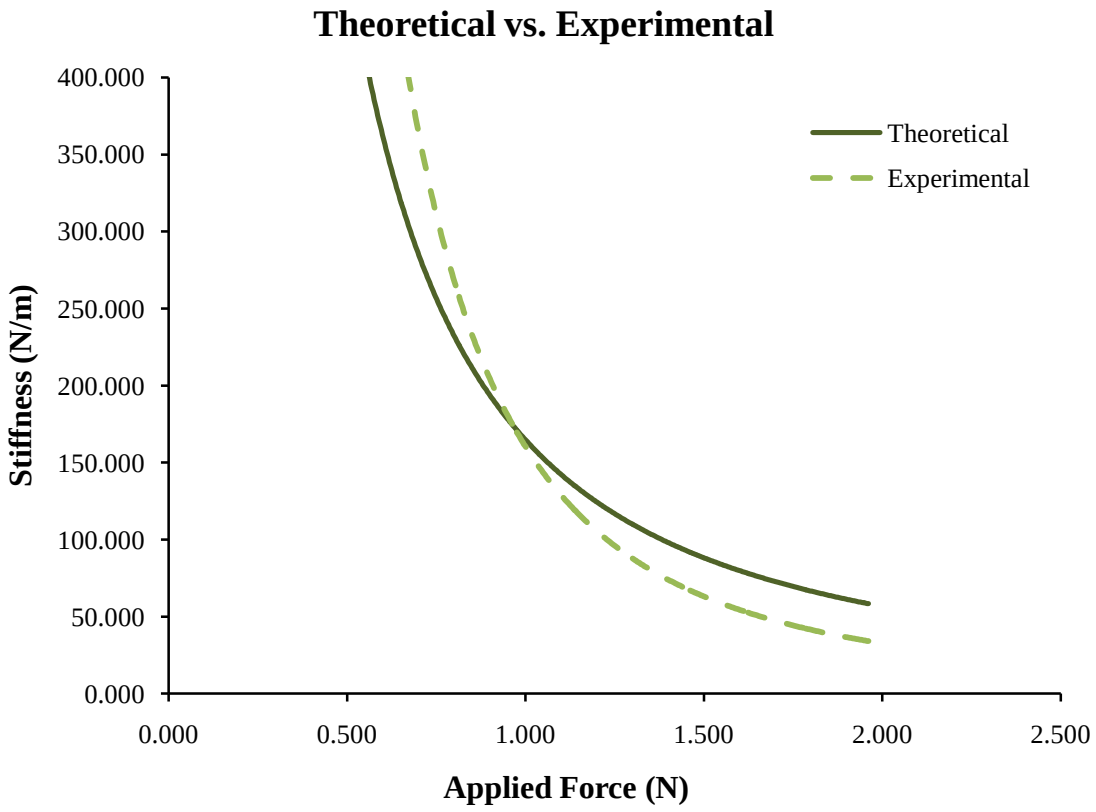


**Figure 6.9: Stiffness vs. Applied Force (Test 5)**

### 6.1.5.4 Theoretical results vs. experimental results

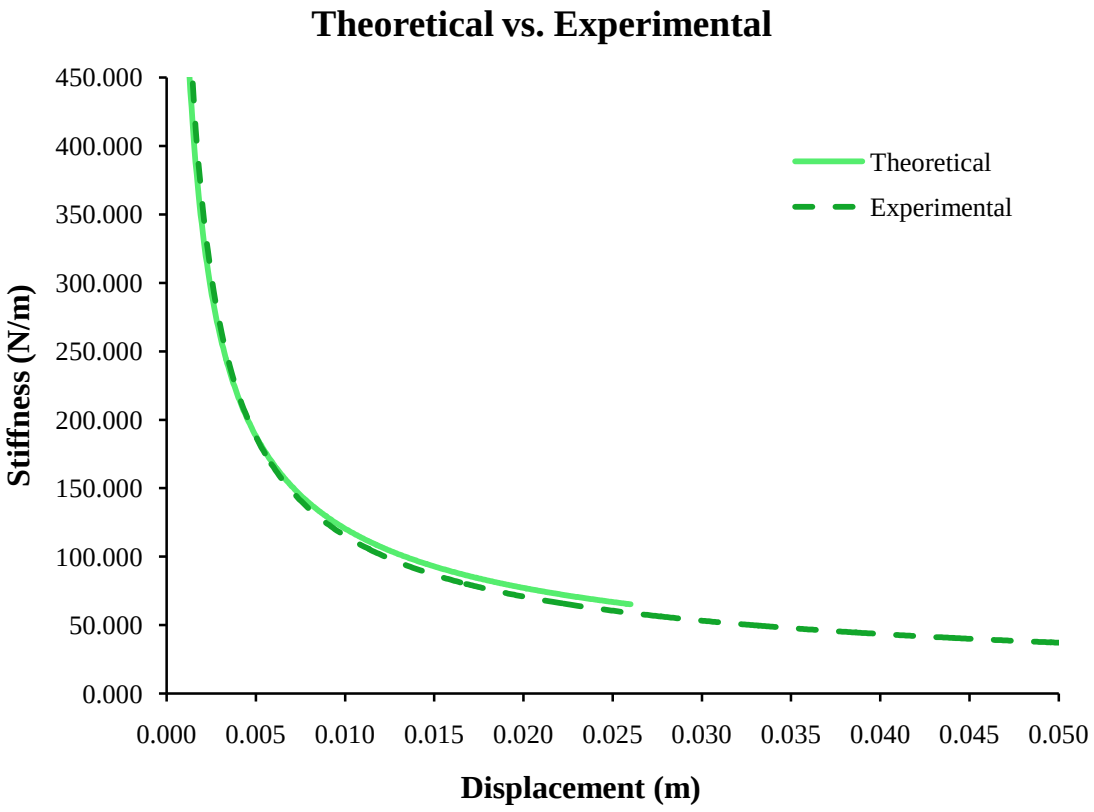


**Figure 6.10: Stiffness vs. Displacement (Test 5)**

### 6.1.6 Test 6

#### 6.1.6.1 Theoretical results from Working Model simulation

**Table 6.13: Theoretical Values (Test 6)**

| Theoretical Values from Working Model | | | | |
|---|---|---|---|---|
| **App. Force (N)** | **Xo (m)** | **Xf (m)** | **ΔX (m)** | **K (N/m)** |
| 0.490 | 0.397 | 0.397 | 0.000 | 1225.000 |
| 0.490 | 0.397 | 0.397 | 0.000 | 1225.000 |
| 0.490 | 0.397 | 0.397 | 0.000 | 1225.000 |
| 0.490 | 0.397 | 0.397 | 0.000 | 1225.000 |
| 0.686 | 0.397 | 0.393 | 0.004 | 171.500 |
| 0.686 | 0.397 | 0.393 | 0.004 | 171.500 |
| 0.686 | 0.397 | 0.393 | 0.004 | 171.500 |
| 0.686 | 0.397 | 0.393 | 0.004 | 171.500 |
| 0.980 | 0.397 | 0.390 | 0.007 | 140.000 |
| 0.980 | 0.397 | 0.390 | 0.007 | 140.000 |
| 0.980 | 0.397 | 0.390 | 0.007 | 140.000 |
| 0.980 | 0.397 | 0.390 | 0.007 | 140.000 |
| 1.176 | 0.397 | 0.387 | 0.010 | 117.600 |
| 1.176 | 0.397 | 0.387 | 0.010 | 117.600 |
| 1.176 | 0.397 | 0.387 | 0.010 | 117.600 |
| 1.176 | 0.397 | 0.387 | 0.010 | 117.600 |
| 1.471 | 0.397 | 0.383 | 0.014 | 105.071 |
| 1.471 | 0.397 | 0.383 | 0.014 | 105.071 |
| 1.471 | 0.397 | 0.383 | 0.014 | 105.071 |
| 1.471 | 0.397 | 0.383 | 0.014 | 105.071 |
| 1.667 | 0.397 | 0.379 | 0.018 | 92.611 |
| 1.667 | 0.397 | 0.379 | 0.018 | 92.611 |
| 1.667 | 0.397 | 0.379 | 0.018 | 92.611 |
| 1.667 | 0.397 | 0.379 | 0.018 | 92.611 |
| 1.961 | 0.397 | 0.373 | 0.024 | 81.708 |
| 1.961 | 0.397 | 0.373 | 0.024 | 81.708 |
| 1.961 | 0.397 | 0.373 | 0.024 | 81.708 |
| 1.961 | 0.397 | 0.373 | 0.024 | 81.708 |

### 6.1.6.2 Experimental results

**Table 6.14: Experimental Values (Test 6)**

| Experimental Values | | | | | | | |
|---|---|---|---|---|---|---|---|
| **App. Force (N)** | **Xo (V)** | **Xf (V)** | **Xo (m)** | **Xf (m)** | **ΔX (m)** | **ΔXf (m)** | **K (N/m)** |
| 0.490 | 0.584 | 0.598 | 0.0148 | 0.0152 | 0.0004 | 0.397 | 1377.953 |
| 0.490 | 0.584 | 0.598 | 0.0148 | 0.0152 | 0.0004 | 0.397 | 1377.953 |
| 0.490 | 0.584 | 0.599 | 0.0148 | 0.0152 | 0.0004 | 0.397 | 1286.089 |
| 0.490 | 0.584 | 0.6 | 0.0148 | 0.0152 | 0.0004 | 0.397 | 1205.709 |
| 0.686 | 0.584 | 0.694 | 0.0148 | 0.0176 | 0.0028 | 0.394 | 245.526 |
| 0.686 | 0.584 | 0.694 | 0.0148 | 0.0176 | 0.0028 | 0.394 | 245.526 |
| 0.686 | 0.584 | 0.694 | 0.0148 | 0.0176 | 0.0028 | 0.394 | 245.526 |
| 0.686 | 0.584 | 0.69 | 0.0148 | 0.0175 | 0.0027 | 0.394 | 254.791 |
| 0.980 | 0.584 | 0.864 | 0.0148 | 0.0219 | 0.0071 | 0.390 | 137.795 |
| 0.980 | 0.584 | 0.885 | 0.0148 | 0.0225 | 0.0076 | 0.389 | 128.182 |
| 0.980 | 0.584 | 0.863 | 0.0148 | 0.0219 | 0.0071 | 0.390 | 138.289 |
| 0.980 | 0.584 | 0.861 | 0.0148 | 0.0219 | 0.0070 | 0.390 | 139.288 |
| 1.176 | 0.584 | 1.065 | 0.0148 | 0.0271 | 0.0122 | 0.385 | 96.256 |
| 1.176 | 0.584 | 1.062 | 0.0148 | 0.0270 | 0.0121 | 0.385 | 96.860 |
| 1.176 | 0.584 | 1.094 | 0.0148 | 0.0278 | 0.0130 | 0.384 | 90.783 |
| 1.176 | 0.584 | 1.047 | 0.0148 | 0.0266 | 0.0118 | 0.385 | 99.998 |
| 1.471 | 0.584 | 1.292 | 0.0148 | 0.0328 | 0.0180 | 0.379 | 81.799 |
| 1.471 | 0.584 | 1.343 | 0.0148 | 0.0341 | 0.0193 | 0.378 | 76.302 |
| 1.471 | 0.584 | 1.308 | 0.0148 | 0.0332 | 0.0184 | 0.379 | 79.991 |
| 1.471 | 0.584 | 1.306 | 0.0148 | 0.0332 | 0.0183 | 0.379 | 80.212 |
| 1.667 | 0.584 | 1.546 | 0.0148 | 0.0393 | 0.0244 | 0.373 | 68.222 |
| 1.667 | 0.584 | 1.553 | 0.0148 | 0.0394 | 0.0246 | 0.372 | 67.730 |
| 1.667 | 0.584 | 1.544 | 0.0148 | 0.0392 | 0.0244 | 0.373 | 68.365 |
| 1.667 | 0.584 | 1.546 | 0.0148 | 0.0393 | 0.0244 | 0.373 | 68.222 |
| 1.961 | 0.584 | 2.09 | 0.0148 | 0.0531 | 0.0383 | 0.359 | 51.265 |
| 1.961 | 0.584 | 2.064 | 0.0148 | 0.0524 | 0.0376 | 0.359 | 52.165 |
| 1.961 | 0.584 | 2.034 | 0.0148 | 0.0517 | 0.0368 | 0.360 | 53.245 |
| 1.961 | 0.584 | 2.105 | 0.0148 | 0.0535 | 0.0386 | 0.358 | 50.759 |

### 6.1.6.3 Theoretical results vs. experimental results

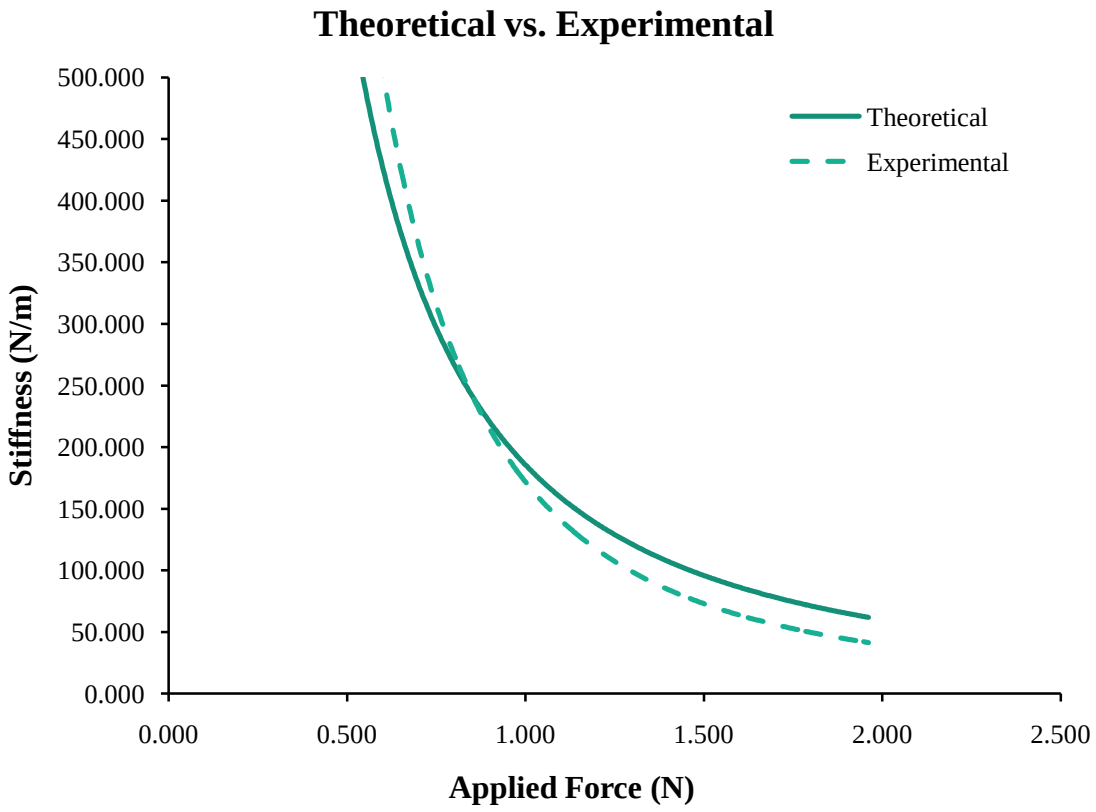


**Figure 6.11: Stiffness vs. Applied Force (Test 6)**

### 6.1.6.4 Theoretical results vs. experimental results

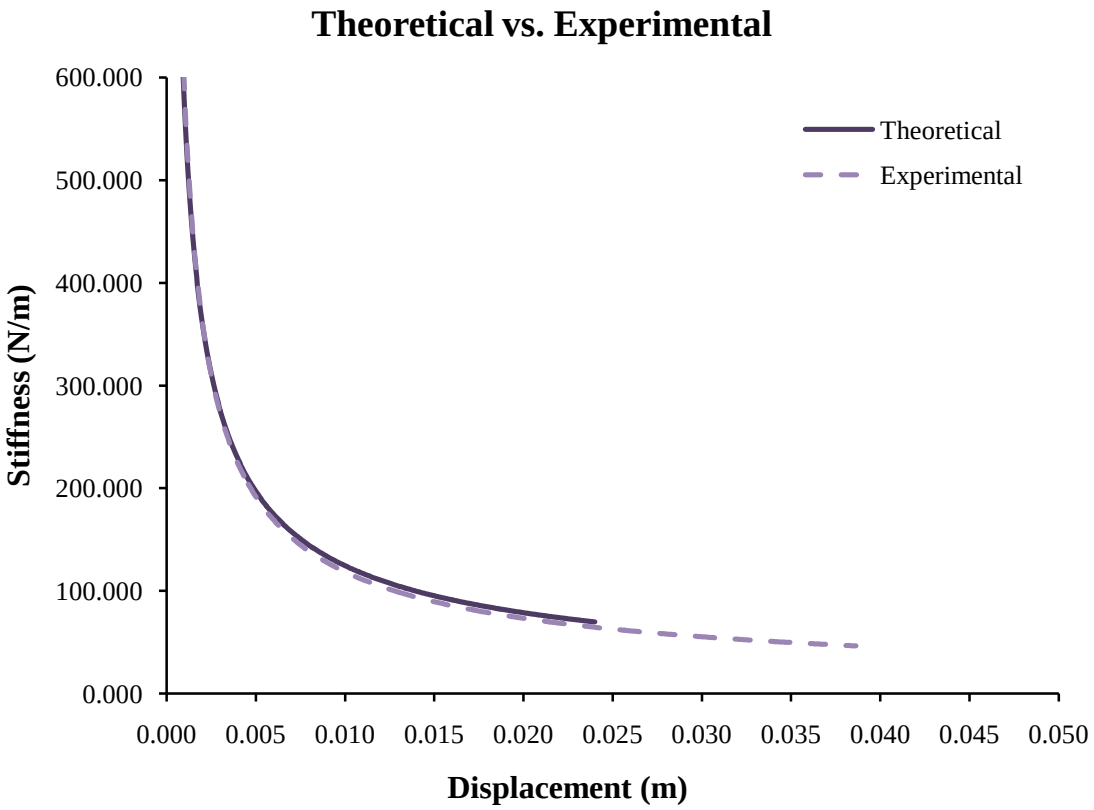


**Figure 6.12: Stiffness vs. Displacement (Test 6)**

### 6.1.7 Test 7

#### 6.1.7.1 Theoretical results from Working Model simulation

**Table 6.15: Theoretical Values (Test 7)**

| Theoretical Values from Working Model | | | | |
|---|---|---|---|---|
| **App. Force (N)** | **Xo (m)** | **Xf (m)** | **ΔX (m)** | **K (N/m)** |
| 0.490 | 0.397 | 0.396 | 0.001 | 816.667 |
| 0.490 | 0.397 | 0.396 | 0.001 | 816.667 |
| 0.490 | 0.397 | 0.396 | 0.001 | 816.667 |
| 0.490 | 0.397 | 0.396 | 0.001 | 816.667 |
| 0.686 | 0.397 | 0.394 | 0.003 | 228.667 |
| 0.686 | 0.397 | 0.394 | 0.003 | 228.667 |
| 0.686 | 0.397 | 0.394 | 0.003 | 228.667 |
| 0.686 | 0.397 | 0.394 | 0.003 | 228.667 |
| 0.980 | 0.397 | 0.390 | 0.007 | 140.000 |
| 0.980 | 0.397 | 0.390 | 0.007 | 140.000 |
| 0.980 | 0.397 | 0.390 | 0.007 | 140.000 |
| 0.980 | 0.397 | 0.390 | 0.007 | 140.000 |
| 1.176 | 0.397 | 0.387 | 0.010 | 117.600 |
| 1.176 | 0.397 | 0.387 | 0.010 | 117.600 |
| 1.176 | 0.397 | 0.387 | 0.010 | 117.600 |
| 1.176 | 0.397 | 0.387 | 0.010 | 117.600 |
| 1.471 | 0.397 | 0.384 | 0.013 | 113.154 |
| 1.471 | 0.397 | 0.384 | 0.013 | 113.154 |
| 1.471 | 0.397 | 0.384 | 0.013 | 113.154 |
| 1.471 | 0.397 | 0.384 | 0.013 | 113.154 |
| 1.667 | 0.397 | 0.381 | 0.016 | 104.188 |
| 1.667 | 0.397 | 0.381 | 0.016 | 104.188 |
| 1.667 | 0.397 | 0.381 | 0.016 | 104.188 |
| 1.667 | 0.397 | 0.381 | 0.016 | 104.188 |

### 6.1.7.2 Experimental results

**Table 6.16: Experimental Values (Test 7)**

| Experimental Values | | | | | | | |
|---|---|---|---|---|---|---|---|
| **App. Force (N)** | **Xo (V)** | **Xf (V)** | **Xo (m)** | **Xf (m)** | **ΔX (m)** | **ΔXf (m)** | **K (N/m)** |
| 0.490 | 0.663 | 0.674 | 0.0168 | 0.0171 | 0.0003 | 0.397 | 1753.758 |
| 0.490 | 0.663 | 0.672 | 0.0168 | 0.0171 | 0.0002 | 0.397 | 2143.482 |
| 0.490 | 0.663 | 0.673 | 0.0168 | 0.0171 | 0.0003 | 0.397 | 1929.134 |
| 0.490 | 0.663 | 0.673 | 0.0168 | 0.0171 | 0.0003 | 0.397 | 1929.134 |
| 0.686 | 0.663 | 0.715 | 0.0168 | 0.0182 | 0.0013 | 0.396 | 519.382 |
| 0.686 | 0.663 | 0.717 | 0.0168 | 0.0182 | 0.0014 | 0.396 | 500.146 |
| 0.686 | 0.663 | 0.716 | 0.0168 | 0.0182 | 0.0013 | 0.396 | 509.583 |
| 0.686 | 0.663 | 0.719 | 0.0168 | 0.0183 | 0.0014 | 0.396 | 482.283 |
| 0.980 | 0.663 | 0.832 | 0.0168 | 0.0211 | 0.0043 | 0.393 | 228.300 |
| 0.980 | 0.663 | 0.898 | 0.0168 | 0.0228 | 0.0060 | 0.391 | 164.182 |
| 0.980 | 0.663 | 0.898 | 0.0168 | 0.0228 | 0.0060 | 0.391 | 164.182 |
| 0.980 | 0.663 | 0.883 | 0.0168 | 0.0224 | 0.0056 | 0.391 | 175.376 |
| 1.176 | 0.663 | 1.083 | 0.0168 | 0.0275 | 0.0107 | 0.386 | 110.236 |
| 1.176 | 0.663 | 1.029 | 0.0168 | 0.0261 | 0.0093 | 0.388 | 126.501 |
| 1.176 | 0.663 | 1.030 | 0.0168 | 0.0262 | 0.0093 | 0.388 | 126.156 |
| 1.176 | 0.663 | 1.020 | 0.0168 | 0.0259 | 0.0091 | 0.388 | 129.690 |
| 1.471 | 0.663 | 1.296 | 0.0168 | 0.0329 | 0.0161 | 0.381 | 91.490 |
| 1.471 | 0.663 | 1.306 | 0.0168 | 0.0332 | 0.0163 | 0.381 | 90.067 |
| 1.471 | 0.663 | 1.283 | 0.0168 | 0.0326 | 0.0157 | 0.381 | 93.409 |
| 1.471 | 0.663 | 1.336 | 0.0168 | 0.0339 | 0.0171 | 0.380 | 86.053 |
| 1.667 | 0.663 | 1.897 | 0.0168 | 0.0482 | 0.0313 | 0.366 | 53.185 |
| 1.667 | 0.663 | 1.923 | 0.0168 | 0.0488 | 0.0320 | 0.365 | 52.087 |
| 1.667 | 0.663 | 1.894 | 0.0168 | 0.0481 | 0.0313 | 0.366 | 53.314 |
| 1.667 | 0.663 | 1.895 | 0.0168 | 0.0481 | 0.0313 | 0.366 | 53.271 |

### 6.1.7.3 Theoretical results vs. experimental results

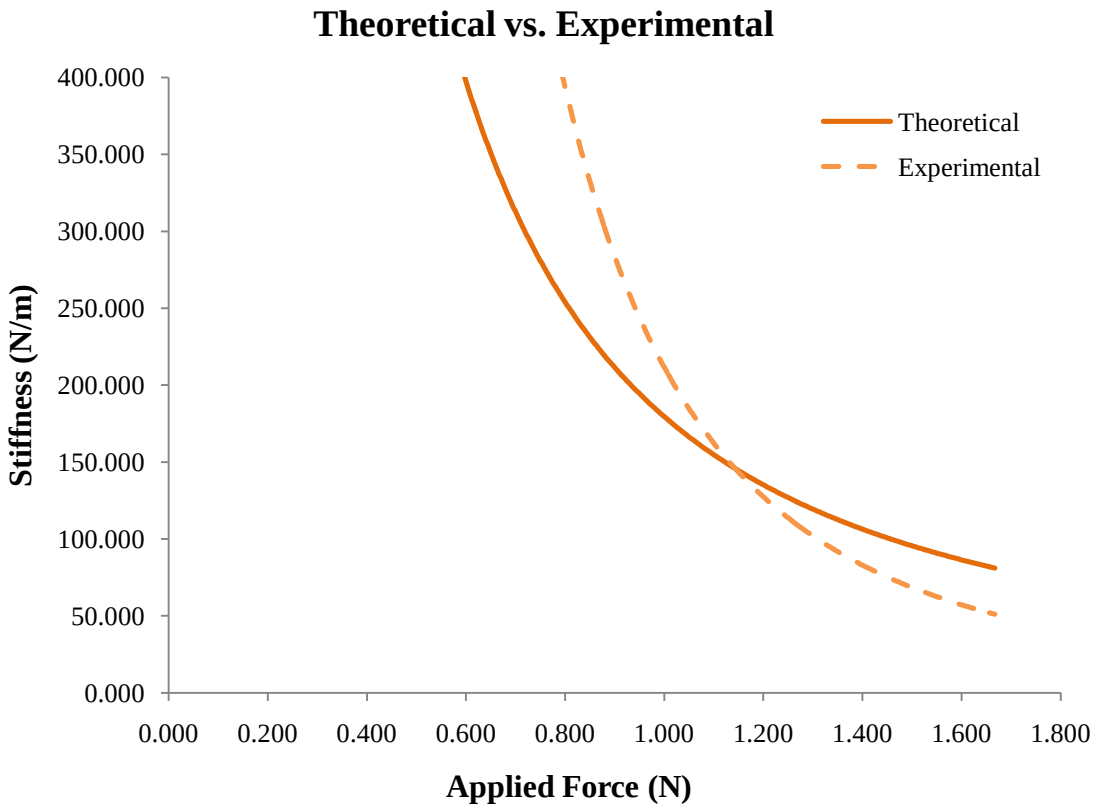


**Figure 6.13: Stiffness vs. Applied Force (Test 7)**

### 6.1.7.4 Theoretical results vs. experimental results

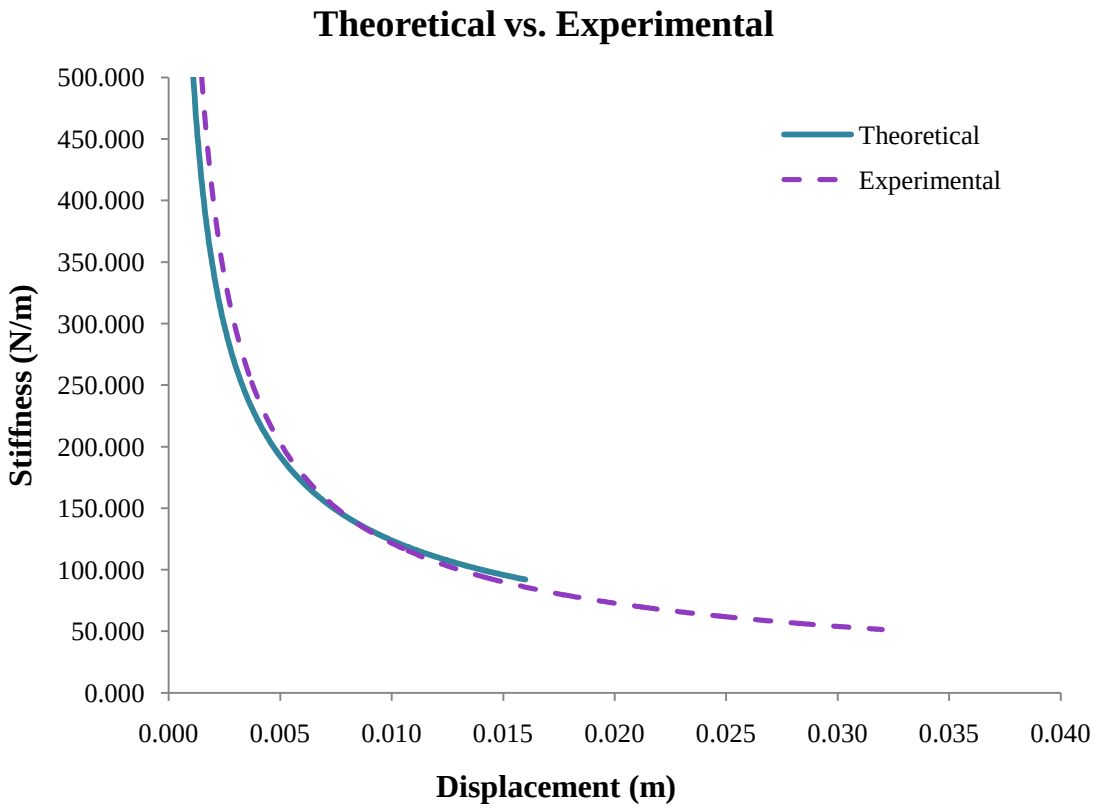


**Figure 6.14: Stiffness vs. Displacement (Test 7)**

### 6.1.8 Test 8

#### 6.1.8.1 Theoretical results from Working Model simulation

**Table 6.17: Theoretical Values (Test 8)**

| Theoretical Values from Working Model | | | | |
|---|---|---|---|---|
| **App. Force (N)** | **Xo (m)** | **Xf (m)** | **ΔX (m)** | **K (N/m)** |
| 0.686 | 0.397 | 0.396 | 0.001 | 890.909 |
| 0.686 | 0.397 | 0.396 | 0.001 | 890.909 |
| 0.686 | 0.397 | 0.396 | 0.001 | 890.909 |
| 0.686 | 0.397 | 0.396 | 0.001 | 890.909 |
| 0.980 | 0.397 | 0.392 | 0.005 | 196.000 |
| 0.980 | 0.397 | 0.392 | 0.005 | 196.000 |
| 0.980 | 0.397 | 0.392 | 0.005 | 196.000 |
| 0.980 | 0.397 | 0.392 | 0.005 | 196.000 |
| 1.176 | 0.397 | 0.389 | 0.008 | 147.000 |
| 1.176 | 0.397 | 0.389 | 0.008 | 147.000 |
| 1.176 | 0.397 | 0.389 | 0.008 | 147.000 |
| 1.176 | 0.397 | 0.389 | 0.008 | 147.000 |
| 1.471 | 0.397 | 0.386 | 0.011 | 133.727 |
| 1.471 | 0.397 | 0.386 | 0.011 | 133.727 |
| 1.471 | 0.397 | 0.386 | 0.011 | 133.727 |
| 1.471 | 0.397 | 0.386 | 0.011 | 133.727 |
| 1.667 | 0.397 | 0.382 | 0.015 | 111.133 |
| 1.667 | 0.397 | 0.382 | 0.015 | 111.133 |
| 1.667 | 0.397 | 0.382 | 0.015 | 111.133 |
| 1.667 | 0.397 | 0.382 | 0.015 | 111.133 |

### 6.1.8.2 Experimental results

**Table 6.18: Experimental Values (Test 8)**

| Experimental Values | | | | | | | |
|---|---|---|---|---|---|---|---|
| **App. Force (N)** | **Xo (V)** | **Xf (V)** | **Xo (m)** | **Xf (m)** | **ΔX (m)** | **ΔXf (m)** | **K (N/m)** |
| 0.686 | 0.665 | 0.694 | 0.0169 | 0.0176 | 0.0007 | 0.396 | 931.306 |
| 0.686 | 0.665 | 0.695 | 0.0169 | 0.0177 | 0.0008 | 0.396 | 900.262 |
| 0.686 | 0.665 | 0.693 | 0.0169 | 0.0176 | 0.0007 | 0.396 | 964.567 |
| 0.686 | 0.665 | 0.693 | 0.0169 | 0.0176 | 0.0007 | 0.396 | 964.567 |
| 0.980 | 0.665 | 0.786 | 0.0169 | 0.0200 | 0.0031 | 0.394 | 318.865 |
| 0.980 | 0.665 | 0.785 | 0.0169 | 0.0199 | 0.0030 | 0.394 | 321.522 |
| 0.980 | 0.665 | 0.784 | 0.0169 | 0.0199 | 0.0030 | 0.394 | 324.224 |
| 0.980 | 0.665 | 0.782 | 0.0169 | 0.0199 | 0.0030 | 0.394 | 329.766 |
| 1.176 | 0.665 | 0.924 | 0.0169 | 0.0235 | 0.0066 | 0.390 | 178.761 |
| 1.176 | 0.665 | 0.929 | 0.0169 | 0.0236 | 0.0067 | 0.390 | 175.376 |
| 1.176 | 0.665 | 0.939 | 0.0169 | 0.0239 | 0.0070 | 0.390 | 168.975 |
| 1.176 | 0.665 | 0.936 | 0.0169 | 0.0238 | 0.0069 | 0.390 | 170.846 |
| 1.471 | 0.665 | 1.133 | 0.0169 | 0.0288 | 0.0119 | 0.385 | 123.747 |
| 1.471 | 0.665 | 1.147 | 0.0169 | 0.0291 | 0.0122 | 0.385 | 120.152 |
| 1.471 | 0.665 | 1.134 | 0.0169 | 0.0288 | 0.0119 | 0.385 | 123.483 |
| 1.471 | 0.665 | 1.146 | 0.0169 | 0.0291 | 0.0122 | 0.385 | 120.402 |
| 1.667 | 0.665 | 1.263 | 0.0169 | 0.0321 | 0.0152 | 0.382 | 109.749 |
| 1.667 | 0.665 | 1.271 | 0.0169 | 0.0323 | 0.0154 | 0.382 | 108.300 |
| 1.667 | 0.665 | 1.284 | 0.0169 | 0.0326 | 0.0157 | 0.381 | 106.026 |
| 1.667 | 0.665 | 1.286 | 0.0169 | 0.0327 | 0.0158 | 0.381 | 105.684 |

### 6.1.8.3 Theoretical results vs. experimental results

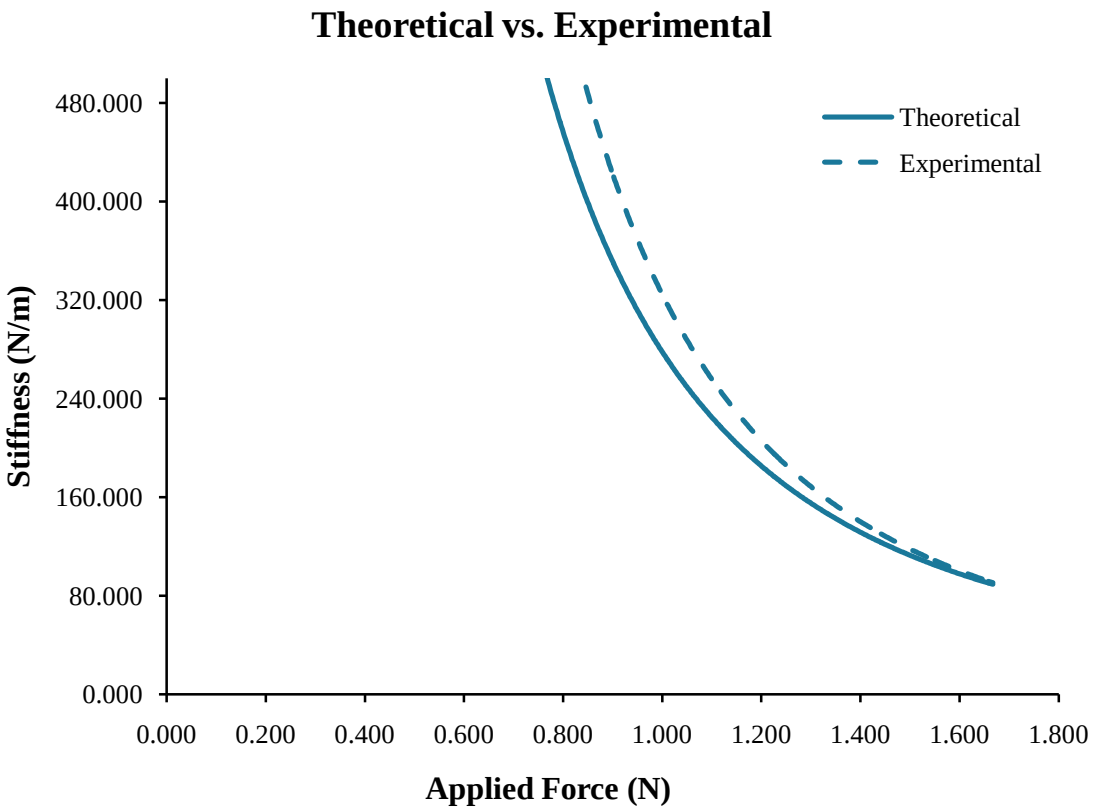


**Figure 6.15: Stiffness vs. Applied Force (Test 8)**

#### 6.1.8.4 Theoretical results vs. experimental results

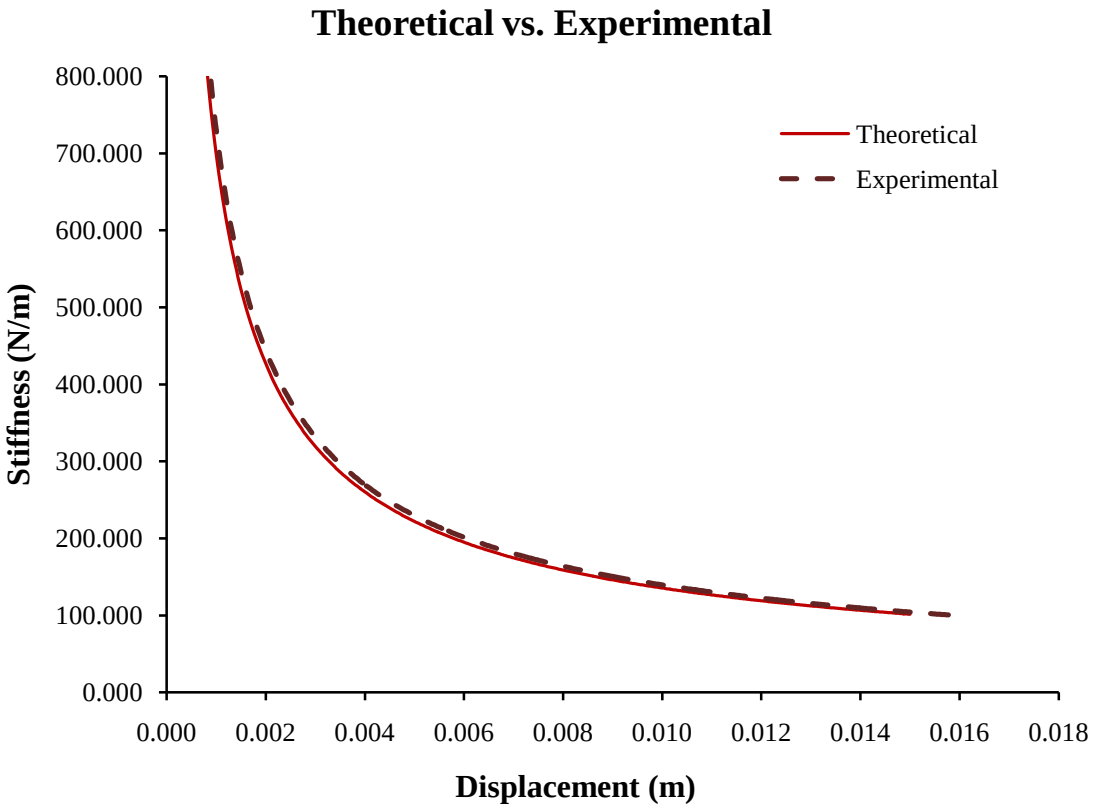


**Figure 6.16: Stiffness vs. Displacement (Test 8)**

### 6.1.9 Test Comparison

#### 6.1.9.1 Stiffness vs. applied force – theoretical

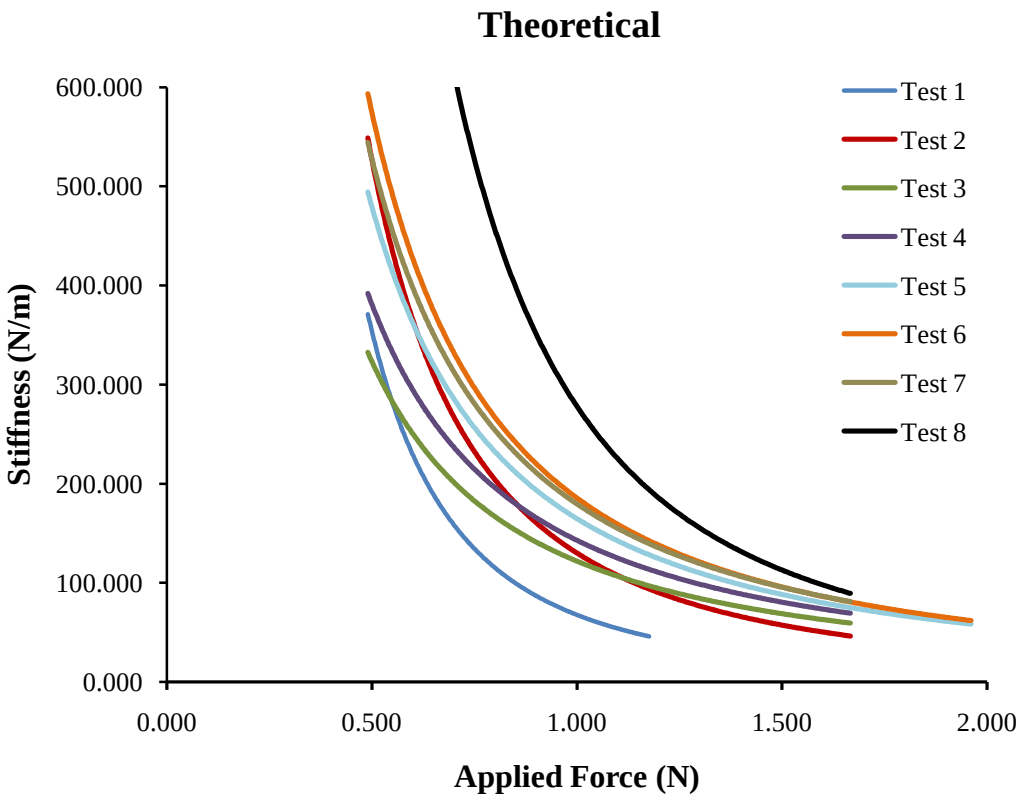


**Figure 6.17: Stiffness vs. Applied Force (Test comparison - theoretical values)**

### 6.1.9.2 Stiffness vs. applied force – experimental

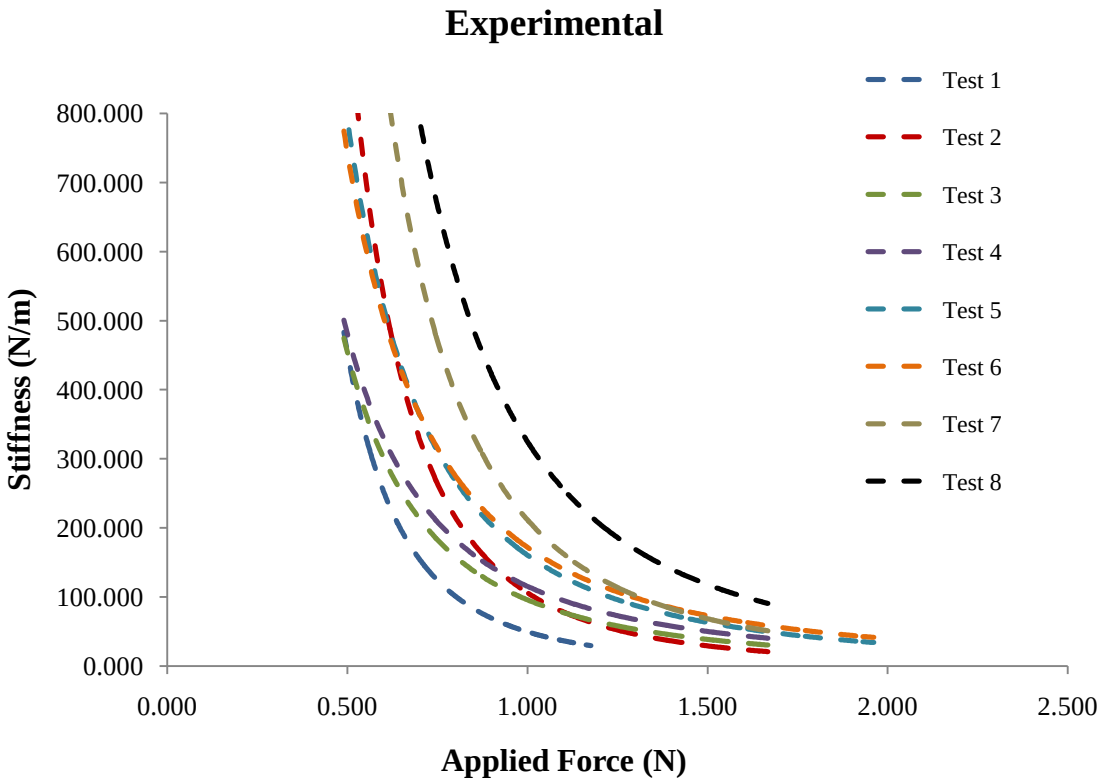


**Figure 6.18: Stiffness vs. Applied Force (Test comparison - experimental values)**

### 6.1.9.3 Stiffness vs. displacement - theoretical

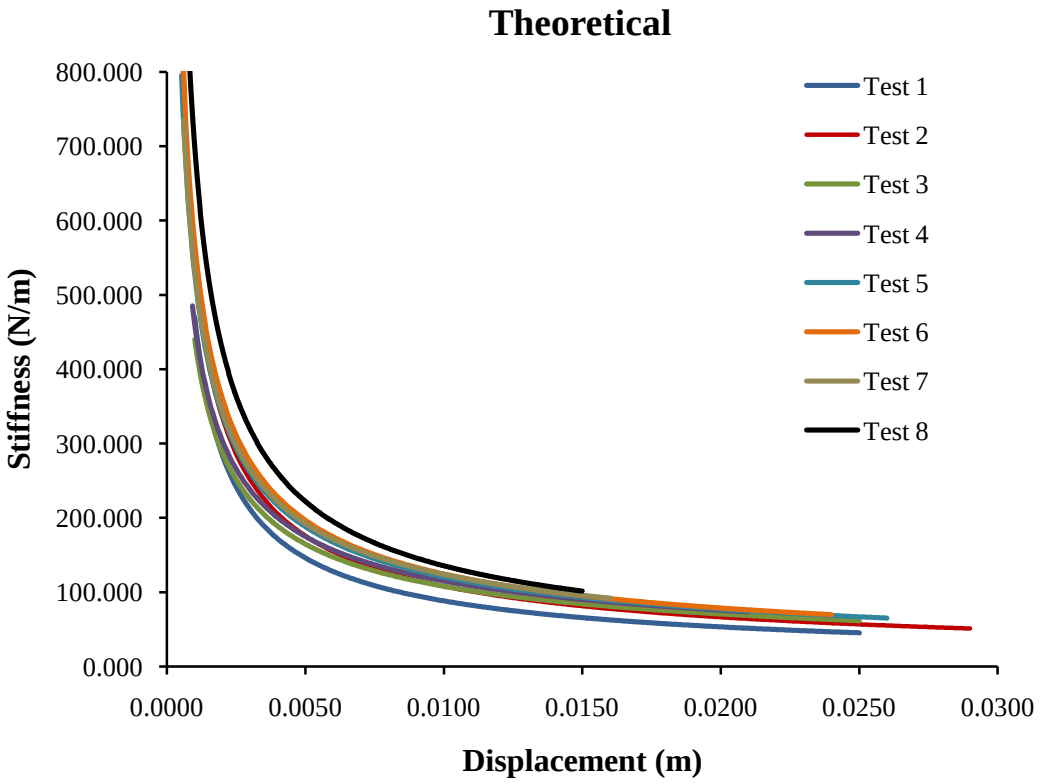


**Figure 6.19: Stiffness vs. Displacement (Test comparison - theoretical values)**

#### 6.1.9.4 Stiffness vs. displacement - experimental

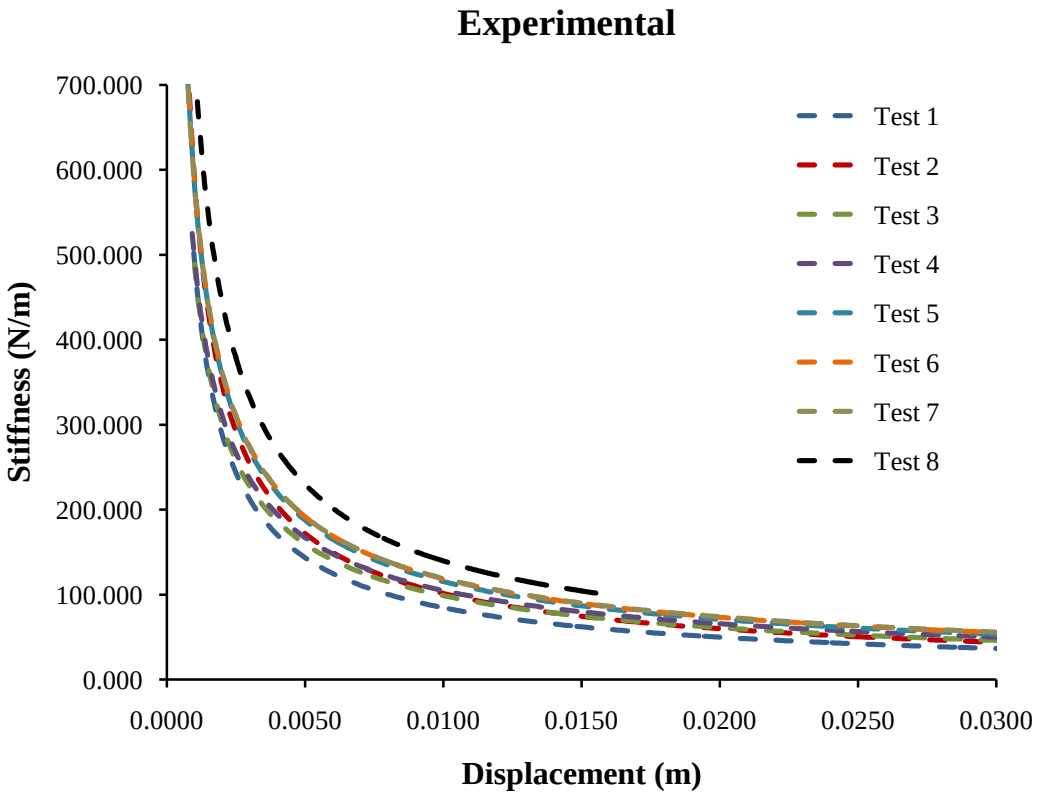


**Figure 6.20: Stiffness vs. Displacement (Test comparison - experimental values)**

### 6.1.9.5 Displacement vs. applied force - theoretical

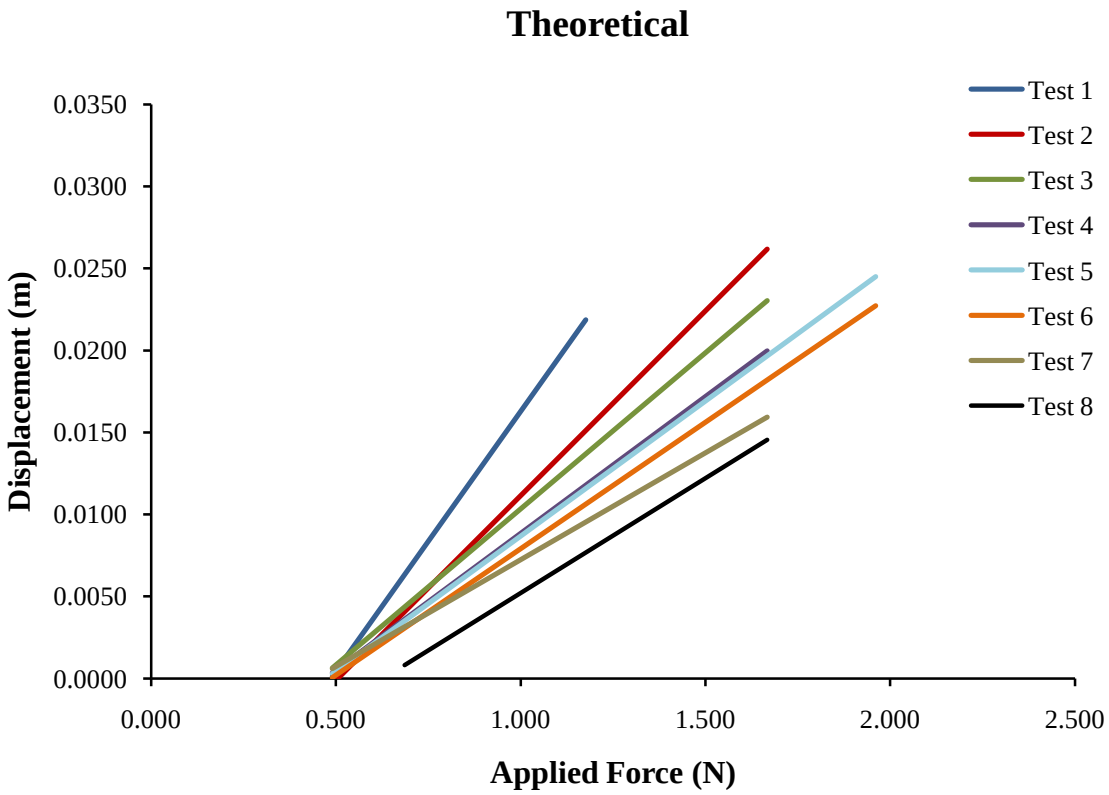


**Figure 6.21: Displacement vs. Applied Force (Test comparison - theoretical values)**

### 6.1.9.6 Displacement vs. applied force - experimental

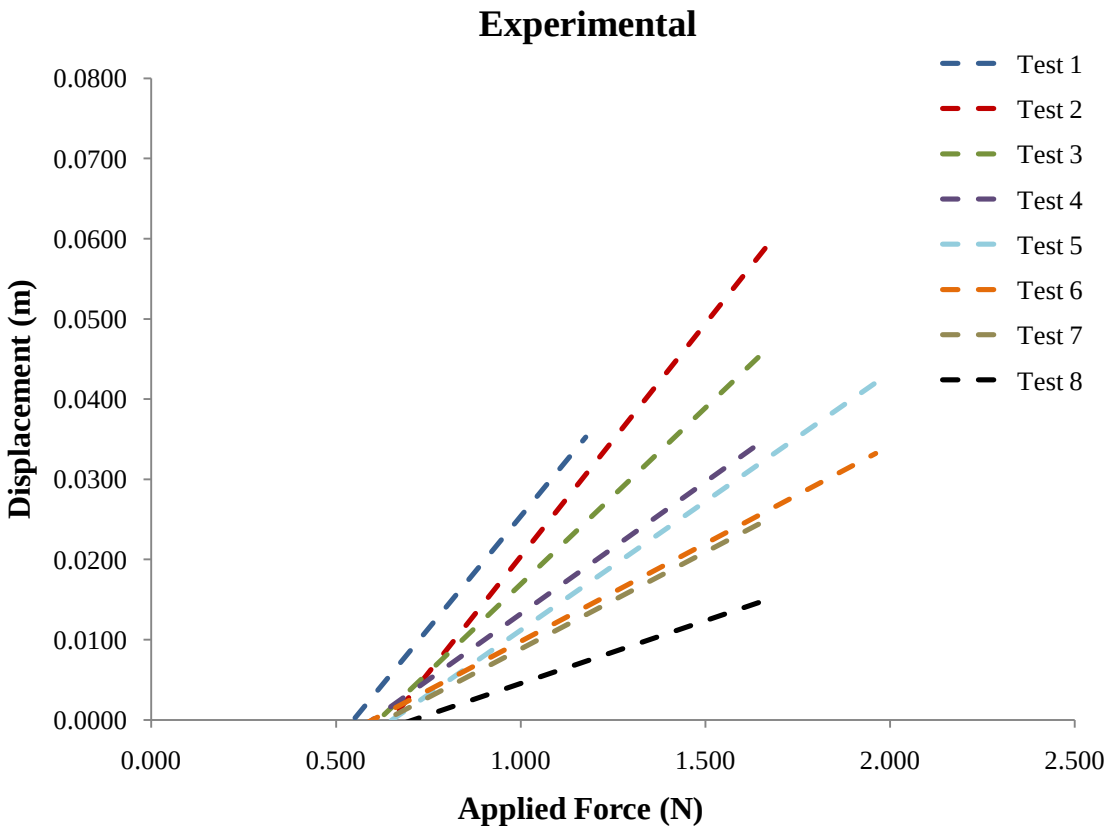


**Figure 6.22: Displacement vs. Applied Force (Test comparison - experimental values)**

### 6.1.9.7 Theoretical and experimental - combined

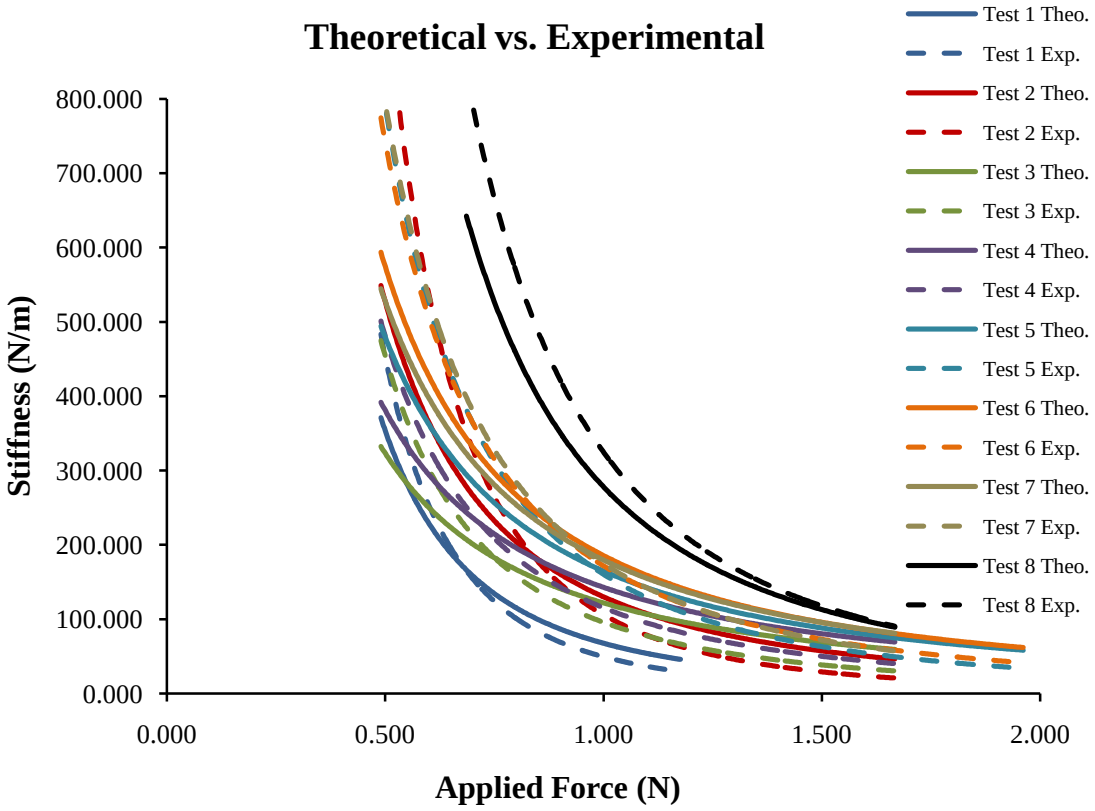


**Figure 6.23: Theoretical vs. Experimental (1)**

### 6.1.9.8 Theoretical and experimental - combined

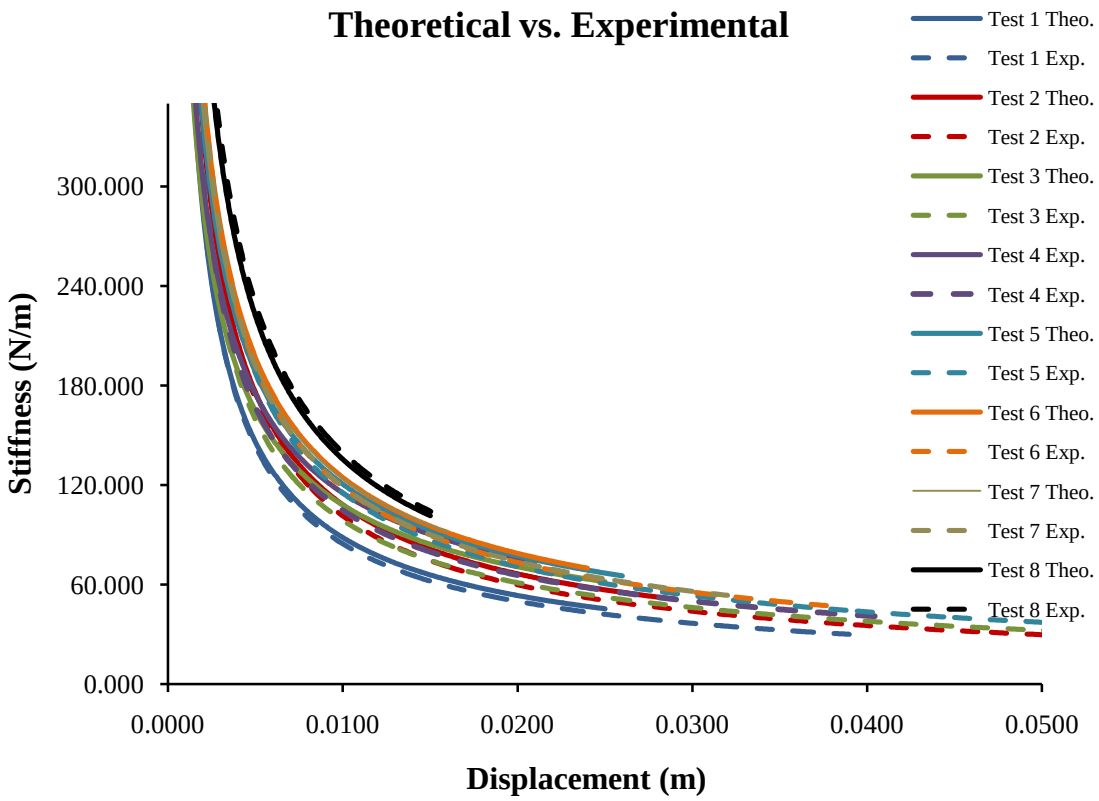


**Figure 6.24: Theoretical vs. Experimental (2)**

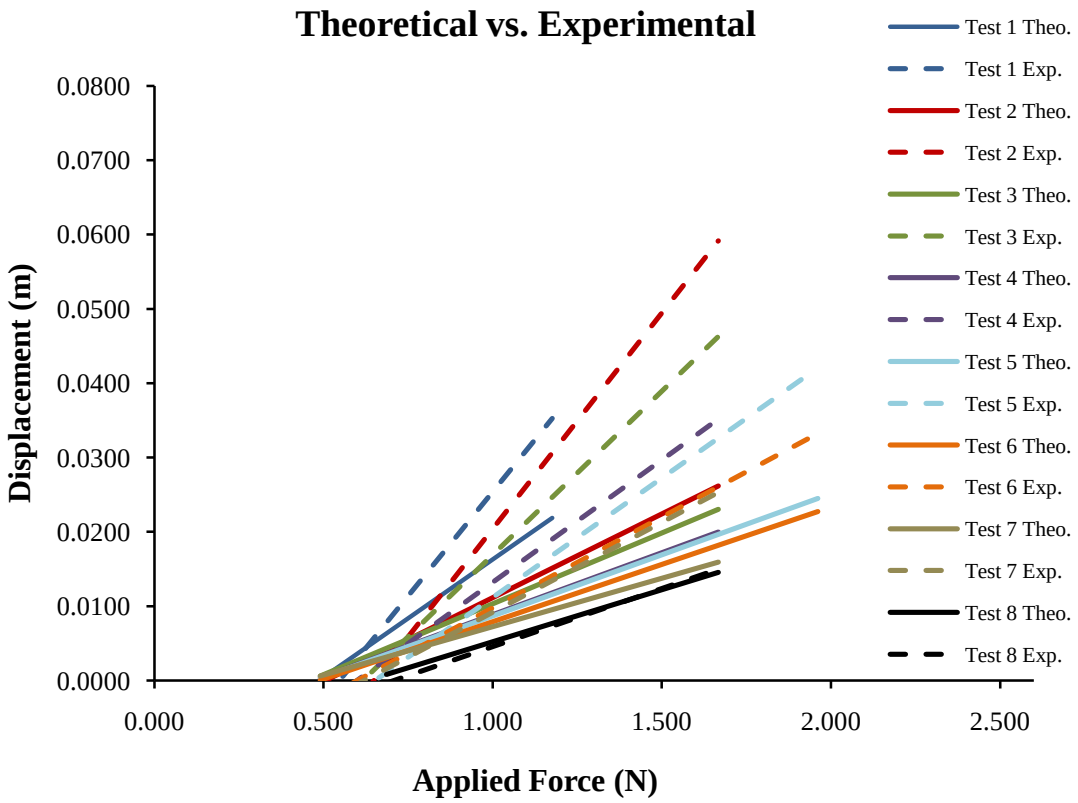


**Figure 6.25: Theoretical vs. Experimental (3)**

## 6.2 Discussion

It is important to mention that the theoretical analyses are based on the development of a frictionless spring mechanism. Such frictionless mechanism, in Working Model, oscillates forever once the equilibrium torques and the respective forces are applied. However, the fabricated prototype, as any real system, has friction effects as a result of the motor bearings, the contact between links, and the contact between the slider and its track. These friction effects cause the variable stiffness mechanism to remain motionless as soon as a minimal amount of force is applied on the output slider element. This means that the experimental results vary slightly with respect to the simulation generated in Working Model 2D.

However, in order to avoid additional discrepancies between the simulation and the experiments, the motor parameters were specified on the Working Model simulation (see Chapter IV, Section 4.3). These parameters, for example, included the resistance of the motor armature, inductance, speed constant, and torque constant. After the experimental and theoretical values were compared, the nonlinear graphical data did not have a similar trajectory (See Appendix A for results). The problem was that the motor inertia was not taken into consideration in Working Model and the simulated spring mechanism was not damping sufficiently as the physical system. It is important to mention that such parameter was not implemented since it was not required on the motor parameters of the software. Therefore, what was done was that the mass of Link 2 and Link 4 was incremented by a total amount of 0.79378 *kg* to match the specified rotor inertia ( $J = 0.008 \frac{oz \cdot in}{s^2}$ ), and the center of mass of both links was lowered one quarter from the center. This procedure was implemented since a large amount of mass is generated from the motor itself when it's trying to rotate in a static situation. Once these parameters were changed and a small amount of friction (0.4) was arbitrarily added on the slot joint, the simulated system was able to damp similarly to the physical system and remain motionless. However, it is important to point out that the majority of the damping came from the motor parameters, and only a very small portion from the friction generated on the slot joint.

Therefore, the first measurement involved analyzing the effective stiffness of the mechanism as a function of the force applied on the linear displacement slider (Figure 6.1). In particular, eight different set of equilibrium torques were tested, even though ten were planned (Table 6.1). The ten experiments were indeed conducted, but the last two were not considered since the results were similar to each other. Therefore, theoretical results (solid lines) indicate that as the force acting on the slider increases, the effective stiffness of the system decreases as a

result of the varying displacement, and thus an inverse proportional relationship is developed. Before continuing, it is important to highlight that the theoretical results are obtained from the Working Model simulation. The same procedures that were implemented on the physical model were implemented on the Working Model simulation. However, as the equilibrium torques (Test 2 (Figure 6.3), Test 3 (Figure 6.5), etc.) increase, the effective stiffness of the linkage increases for every force applied on the output slider. For example, the effective stiffness of the spring mechanism in Test 1 was 89.091 N/m with a force of 0.980 N acting on the output element. In Test 2, the effective stiffness of the mechanism resulted in 98.000 N/m with the same amount of force applied on the slider, but with a different set of equilibrium torques. Furthermore, the effective stiffness of the system resulted in 140.000 N/m in Test 4 (Table 6.9). This means that by applying the same amount of force on the slider element, and varying the equilibrium torques, the effective stiffness can be adjusted respectively (Figure 6.17). Therefore, depending on the application or task addressed, different equilibrium torques can be implemented to meet the required system behavior. On the other hand, experimental results in each case (dotted lines) also indicate that the effective stiffness of the mechanism is inverse proportional to the force applied on the output element (Figure 6.18). As illustrated, the actively adjustable spring mechanism behaves nonlinearly throughout each case, and the generated results are similar to the theoretical results (Figure 6.23). The only factor that keeps both graphs from directly coinciding is the friction.

Furthermore, the second measurement involved evaluating the effective stiffness of the spring mechanism as a function of the displacement caused by the slider. Eight different sets of equilibrium torques were also tested in this case (figures 6.2, 6.4, 6.6, etc.). Theoretical and experimental results indicate that as the displacement increases across the horizontal global

reference frame, the stiffness of the mechanism decreases, denoting that an inverse proportional relationship occurs (Figure 6.19 and Figure 6.20). For example, in Test 7 when the output element displaces a total amount of 0.0018 *m*, the respective effective stiffness is 391.418 N/m, but when it displaces a total amount of 0.0161 *m*, the respective effective stiffness results in 91.490 N/m (Table 6.16). In another words, the increasing force on the slider causes the effective stiffness to decrease. Nonetheless, implementing higher equilibrium input torques reduces the output displacement, and hence the effective stiffness of the mechanism increases (Figure 6.24). From these results, it is important to notice that the theoretical and experimental (nonlinear) results are very similar to each other in all cases, meaning that the concept of adjustable springs is viable and the effective stiffness of the spring mechanism can be predicted.

A third measurement that was carried out to validate the concept of adjustable springs was the displacement of the output element as a function of the force applied on the mechanism (prismatic joint/ slider element). In particular, theoretical and experimental results indicate that the relationship between both parameters is proportional, meaning that as the force increases, the displacement on the slider increases as well (Figure 6.21 and 6.22). For instance, in Test 8 when a 0.686 N force was applied, the slider displaced a total amount of 0.0007 *m*, and when a 1.471 N force was applied, the slider displaced a total amount of 0.0119 *m* (Table 6.18). Therefore, it can be said that depending on the application or task required, different forces can be implemented on the system to obtain the necessary displacement. Moreover, such results also indicate that as the equilibrium torque on each motor increases, the displacement of the output element decreases with the same amount of force applied, and thus the effective stiffness of the system increases. Lastly, one important detail to point out from the generated graphs is that the theoretical and

experimental results are similar to each other, but the friction effects on the real system indeed affect the general outcome.

The desired effective stiffness of the system (Table 6.1), as calculated in Chapter IV, was also compared to the experimental results generated from the eight total experiments. In this study, it is important to emphasize that the desired effective stiffness of the system (equilibrium) was not determined physically due to the limited budget, and consequently the needed device was not purchased. However, an estimation was generated from the experiments to have an idea on how efficient was the concept of redundant actuation. The first step involved determining the effective stiffness of the system at its equilibrium state (Table 6.1, K*). Results indicate that first of all, the desired effective stiffness of the system certainly increases as the equilibrium motor torques are incremented, which means that the kinematic and kinetic equations are valid in this study. Once such calculation was completed, a graph (Figure 6.26) was generated using the effective stiffness of the first measurement on each experimental test, which involves applying a force of 0.490 N on the prismatic joint/slider element.

Results indicate that the (experimental) effective stiffness of the system is lower than the theoretical desired effective stiffness (equilibrium). Such difference is expected since the stiffness of the system is inversely proportional to the force applied on the slider element. However, what is emphasized is that if the (applied) force on the slider element would have been removed, the desired effective stiffness of the spring mechanism would have been larger. The reason for such statement is that when the applied force is removed, the spring mechanism goes back to its equilibrium state, and consequently to its desired effective stiffness. This means that the theoretical and experimental desired effective stiffness results would have been closer to each other, maybe not identical because of the frictional losses, but very close.

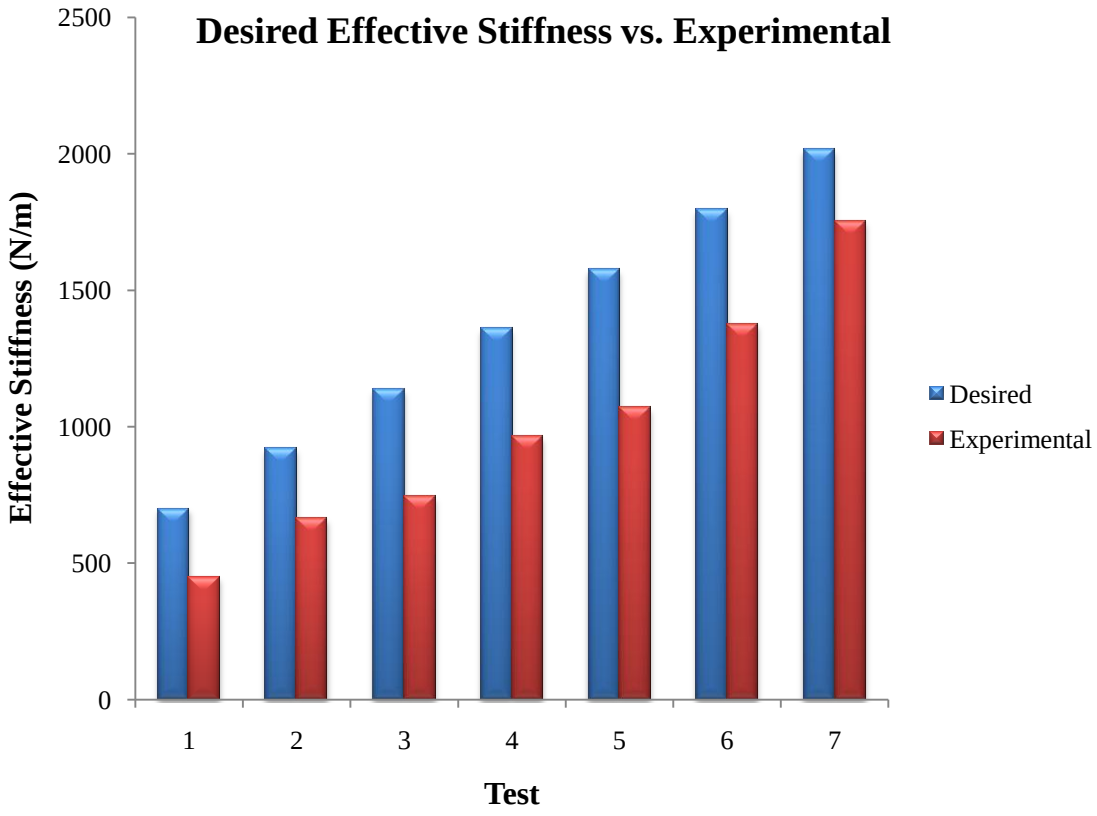


**Figure 6.26: Desired Effective Stiffness Comparison**

Before concluding, it is significant to mention that the configuration of the Watt II linkage plays an important role in the torques needed to drive the actively adjustable spring mechanism. In this case, for example, the initial angle of the input crank (Link 2) was 45° relative to the horizontal axis (Figure 3.1). With such specified angle, a significant set of torque values required for the mechanism to be at its equilibrium state were established in the range of 5A (Table 6.1), which are the amperes on the brush-type DC motor. However, what happens if the specified initial angle is not 45°. Will the equilibrium torques lie in the same range? Will the range increase or decrease? To answer such questions, the initial angle $\theta_2$ of the mechanism was varied (30°, 35°, 40°, 50°, 55°) to determine the equilibrium torques required to satisfy redundant

actuation. Once the torques were calculated, eight different set of torques were determine to see if the values increased or decreased from those of the original configuration (Table 6.1: 45°).

Results indicate that when the initial angle is lower than 45°, the equilibrium motor torques tend to be further apart from each other. For example, the torque at motor 4 is much higher than 5A, this is assuming that the torque values at motor 2 remain the same as all the experiments. It means that a different motor at the grounded revolute joint C would have been required to obtain the necessary amperes and as a result, have a system at equilibrium state (Table 6.19). In most of the cases, a more expensive motor would have to be incorporated. For example, when the initial angle is specified at 30° the values of motor 4 initiate at 5.130A and terminate at 14.621A, which are definitely greater than 5A. As the initial angle is increased to 35° and 40° (Table 6.20, Table 6.21), the torque values on motor 4 tend to decrease, however, such values are slightly greater than 5A. On the other hand, results indicate that when the initial angle is greater than 45°, the equilibrium torques tend to be closer to each other (Table 6.22, Table 6.23).

**Table 6.19: Motor Torques with Initial Input Angle 30°**

| **Theta = 30°** | |
|---|---|
| **Motor 2 (A)** | **Motor 4 (A)** |
| 1.00 | 5.130 |
| 1.25 | 6.413 |
| 1.50 | 7.695 |
| 1.75 | 8.978 |
| 2.00 | 10.260 |
| 2.25 | 11.543 |
| 2.50 | 12.825 |
| 2.75 | 14.108 |
| 2.80 | 14.364 |
| 2.85 | 14.621 |

**Table 6.20: Motor Torques with Initial Input Angle of 35°**

| Theta = 35° | |
|---|---|
| **Motor 2 (A)** | **Motor 4 (A)** |
| 1.00 | 3.030 |
| 1.25 | 3.788 |
| 1.50 | 4.545 |
| 1.75 | 5.303 |
| 2.00 | 6.060 |
| 2.25 | 6.818 |
| 2.50 | 7.575 |
| 2.75 | 8.333 |
| 2.80 | 8.484 |
| 2.85 | 8.636 |

**Table 6.21: Motor Torques with Initial Input Angle of 40°**

| Theta = 40° | |
|---|---|
| **Motor 2 (A)** | **Motor 4 (A)** |
| 1.00 | 2.187 |
| 1.25 | 2.734 |
| 1.50 | 3.281 |
| 1.75 | 3.827 |
| 2.00 | 4.374 |
| 2.25 | 4.921 |
| 2.50 | 5.468 |
| 2.75 | 6.014 |
| 2.80 | 6.124 |
| 2.85 | 6.233 |

**Table 6.22: Motor Torques with Initial Input Angle of 50°**

| Theta = 50° | |
|---|---|
| **Motor 2 (A)** | **Motor 4 (A)** |
| 1.00 | 1.435 |
| 1.25 | 1.794 |
| 1.50 | 2.153 |
| 1.75 | 2.511 |
| 2.00 | 2.870 |
| 2.25 | 3.229 |
| 2.50 | 3.588 |
| 2.75 | 3.946 |
| 2.80 | 4.018 |
| 2.85 | 4.090 |

**Table 6.23: Motor Torques with Initial Input Angle of 55°**

| Theta = 55° | |
|---|---|
| **Motor 2 (A)** | **Motor 4 (A)** |
| 1.00 | 1.222 |
| 1.25 | 1.528 |
| 1.50 | 1.833 |
| 1.75 | 2.139 |
| 2.00 | 2.444 |
| 2.25 | 2.750 |
| 2.50 | 3.055 |
| 2.75 | 3.361 |
| 2.80 | 3.422 |
| 2.85 | 3.483 |

In conclusion, the actively adjustable Watt II linkage was constructed and experimentally tested to compare the theoretical results. Such theoretical and experimental results indicate that the system behaves as a nonlinear system and that in fact, the effective stiffness of the

mechanism can be controlled as different set of equilibrium torques are applied on the grounded revolute joints. However, a mismatch in the frictional effects acting on the system and the model itself produce slightly different results when comparing the Working Model simulation with the experimental data. Although a slight difference occurs due to the frictional effects of the physical system, the results are very similar to each other. In addition, the experimental results were compared to the theoretical desired effective stiffness results. Results indicate that if the applied force on the experimental test is removed from the prismatic joint, the system goes back to its equilibrium state, and consequently, the effective stiffness of the mechanism would have increased. In addition, the initial input angle of the system was changed to observe how the equilibrium input torques were affected in comparison to those established. This means that the concept of adjustable springs, using redundant actuation, has proven to be valid and that the mathematical model that was developed, closely represents the behavior of the real system.

# CHAPTER VII

## SUMMARY AND CONCLUSION

The present study is a comparison of theoretical and experimental results of a variable stiffness mechanism. In particular, a one degree-of-freedom Watt II mechanism was designed and redundantly actuated to achieve the desired effective stiffness. The process began by determining the equilibrium equation of the spring mechanism (unsprung). Such expression was accomplished by equating the virtual work done by the effective load, to that done by the externally applied loads. Based on this expression, consequently, kinematic and kinetic equations were implemented to determine the geometric design of the one degree-of-freedom mechanism and estimate its nonlinear behavior. After describing the motion of the mechanism in terms of position, velocity, and acceleration, the two equilibrium forces (torques) needed to create an effective stiffness on the linkage were calculated. These equations were generated based on the principle of virtual work and were derived using an energy balance approach that relates to Newton's second law of motion.

Developing and testing a physical model was then taken into consideration. For example, the producer began by selecting a material that would be able to conserve the aesthetics and functionality of the system during several fabrication conditions and environments. After the selection was made and each component of the spring mechanism was fabricated, a preliminary test was conducted to anticipate how the system

would behave. Results indicated that a linearly proportional relationship exists between the generated torque and the input current of each brush-type DC motor. With such information, a test plan was developed and a series of experiments were conducted.

Therefore, from the simulations and experiments, it can be concluded that the desired effective stiffness of the spring mechanism can be generated by implementing several parameters. For example, it can be obtained by implementing different types of forces on the linear displacement element, or it can be obtained by modifying the equilibrium torques on the brush-type DC motors, everything depends on the application or task required. In this case, the maximum amount of current that was generated from the DC motors was 5A, but with other motors that can produce higher amperes, greater forces can be applied on the output element and thus greater effective stiffness values.

Additionally, it can be concluded that the adjustable stiffness mechanism produces greater effective stiffness when small forces are applied and less effective stiffness when larger forces are applied. As mentioned previously, additional friction effects were taken into account in the Working Model simulations to match the theoretical and experimental behavior. The results indicated that the theoretical and experimental results are similar to each other, which means that the concept of redundant actuation has been proven to be a way of generating a variable stiffness mechanism.

REFERENCES


[1] Benedict, C.E., & Tesar, D. (1978). Model formulation of complex mechanisms with multiple inputs: Part I-geometry, part II: the dynamic model. *Journal of Mechanical Design*, 100, 747-761.

[2] Cheng, F.T., & Orin, D.E. (1989). Efficient Algorithm for Optimal Force Distribution in Multiple-Chain Robotic Systems-The Compact-Dual LP Algorithm. Proc. IEEE Conference on Robotics and Automation, Scottsdale, AZ, Vol. 1, 943-950.

[3] Conley, W.J. (1975). Integration of Nonlinear Springs into Machines by Analytical Synthesis. Master's Thesis, University of Florida, Gainsville.

[4] Cutkosky, M.R., & Wright, P.K. (1986). Active Control of a Complaint Wrist in Manufacturing Tasks. *ASME Journal of Engineering for Industry*, Vol. 108, No.1 36-43.

[5] Freeman, R.A. (2004). Active Suspension Control via Redundant Actuation. Proc. of the ASME Design Engineering Technical Conference, Vol. 2B, 1043-1054.

[6] Freeman, R.A., & Tesar, D. (1988). Dynamic Modeling of Serial and Parallel Mechanisms/Robotic Systems: Part I-Methodology, Part II-Applications. Proceedings 1988, ASME Mechanisms Conference, DE-Vol. 15-3, 7-27.

[7] Freeman, R.A., & Tesar, D. (1982). The Generalized Coordinate Selection for the Dynamic of Complex Planar Mechanical Systems. *Journal of Mechanical Design*, 104, 206-217.

[8] Griffs, M.W. (1991). Kinestatic Control: A Novel Theory for Simultaneously Regulating Force and Displacement. Ph.D Dissertation, Department of Mechanical Engineering, University of Florida, Gainsville.

[9] Hain, K. (1967). Applied Kinematics. McGraw Hill Book Company, New York.

[10] Hayward, V., & Kurtz, R. (1990). Modeling a Parallel Wrist Mechanism with Actuator Redundancy. Proc. The 2nd International Workshop on Advanced in Robot Kinematics, Linz, Austria.

[11] Hsu, P. (1989). Control of Multi-Manipulator Systems-Trajectory Tracking, Load Distribution, Internal Force Control, and Decentralized Architecture. Proc. IEEE Conf. Robotics and Automation, Scottsdale, AZ, Vol. 2, 1234-1239.

[12] Hogan, N. (1982). Mechanical Impedance Control in Assistive Devices and Manipulators. Robot Motion: Planning and Control, MIT Press, 361-371.

[13] Jacobsen, H.K., Iversen, E.K., & Davis, C.C. (1989). Antagonistic Control of a Tendon Driven Manipulator. Proceedings of the IEEE Conference Robotics and Automation, Scottsdale, AZ, Vol. 3, 1334-1339.

[14] Jobes, C.C. (1987). Synthesis of a Controllable Circuit Breaker Mechanism. Ph.D Dissertation, West Virginia University.

[15] Kumar, V.J., & Gardner, J. (1990). Kinematics of Redundantly Actuated Closed Chains, *IEEE Journal of Robotics and Automation*, Vol. 6, No. 2, 269-273.

[16] Lakshminarayana, K., & Dizioglu, B. (1972). Synthesis of Spring-Restrained Mechanisms for Amplitude-Independent Natural Frequency of Oscillation, Mechanism and Machine Theory, Vol. 7, 167-190.

[17] Matthew, G.K. (1975). The Closed Form Synthesis of Spring Parameters to Balance Given Force Functions in Planar Mechanisms. Ph.D Dissertation, University of Florida, Gainsville.

[18] Meyer, A.N., & Angeles, J. (1989). Force Optimization in Redundantly Actuated Closed Kinematic Chains. Proc. IEEE Conf. on Robotics and Automation, Scottsdale, AZ, Vol. 1 951-956.

[19] Nakamura, Y. (1988). Minimizing Object Strain Energy for Coordination of Multiple Robotic Mechanism. Proc. of American Control Conference, Vol. 1, 499-505.

[20] Nevins, J.L., & Whitney, D.E. (1973) The Force Vector Assembly Concept. Proc. First CISM-IFTOMM Symposium on Theory and Practice of Robots and Manipulators, Udine, Italy.

[21] Pollock, S.F. (1975). Dynamic Model Formulation Programmed for Dyad Based Machines. Master's Thesis, The University of Florida.

[22] Roppen, T., & Nakamura, Y. (1990). Singularity-Free Parameterization and Performance Analysis of Actuation Redundancy. Proceedings of IEEE Conference Robotics and Automation, Cincinnati, OH. 806-811.

[23] Salisbury, J.K. (1985). Kinematic and Force Analysis of Articulated Hands. Recent Advances in Robotics, 1st ed., Wiley, Santa Barbara, CA, 131-174.

[24] Spence, A.P. (1986). Basic Human Anatomy. The Benjamin/Cummings Publishing Co., Inc., 209.

[25] Sreevijayan, D., Tesar, D., & Price, C. (1990). Four-Level Fault-Tolerance in Manipulator Design for Space Orientations. Proc. ISMCR, Johnson Space Center.

[26] Srinath, K., & Karmakar, R. (1988). Vibratory Conveying by Nonsinusoidal Excitation, Proc. The Institution of Mechanical Engineers, Vol. 202, 405-408.

[27] Starr, G.P. (1988). Initial Investigation in Assembly Using a Dexterous Hand. Proc. 1988 Winter Annual Meeting, Chicago, IL, 307-313.

[28] Streit, D.A., & Gilmore, B.J. (1988). Perfect Spring Equilibrators for Rotatable Bodies, 1988 ASME 20th Biannual Mechanism Conf. Kissimmi, FL, 487-496.

[29] Welch, W.A. (1965). Nonlinear Springs. Product Engineering, Oct. 11, 138-141.

[30] West, H.H., & Asada, H. (1985). A Method for the Design of Hybrid Position/Force Controllers for Manipulators Constrained by contact with the Environment. Proc. IEEE Conf. Robotics and Automation, St. Louis, MO, 251-259.

[31] West, H.H. (1980). The Analysis of Structures. McGraw-Hill, New York.

[32] Whitney, D.E., & Nevins, J.L. (1978). What is the Remote Center Compliance and What Can it Do? Internal Report P-728, The Charles Stark Draper Lab., Cambridge, MA.

[33] Zhou, L. (1992). An Actively Adjustable Unidirection Spring Mechanism. Master's Thesis, The University of Texas at Austin.

# APPENDIX A

APPENDIX A

RESULTS WITHOUT MOTOR PARAMETERS

- TEST 1

*Stiffness vs. Applied Force*

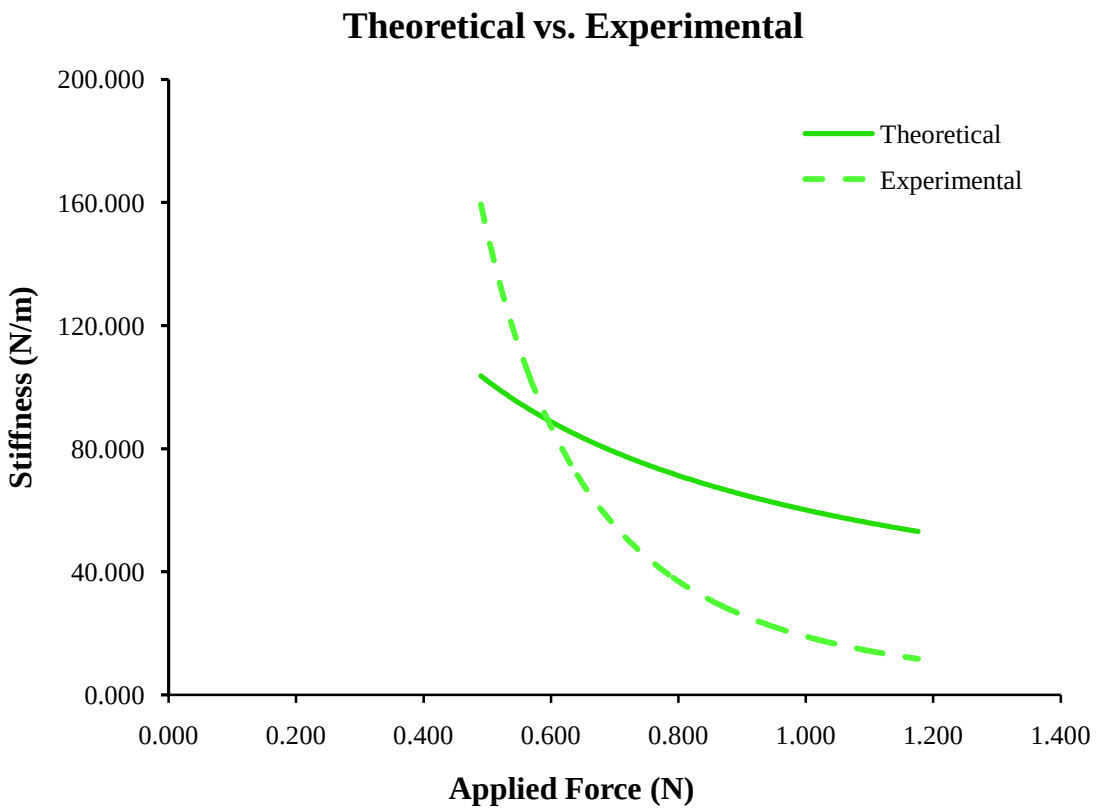


**Figure 1A: Stiffness vs. Applied Force (Test 1)**

*Stiffness vs. Displacement*

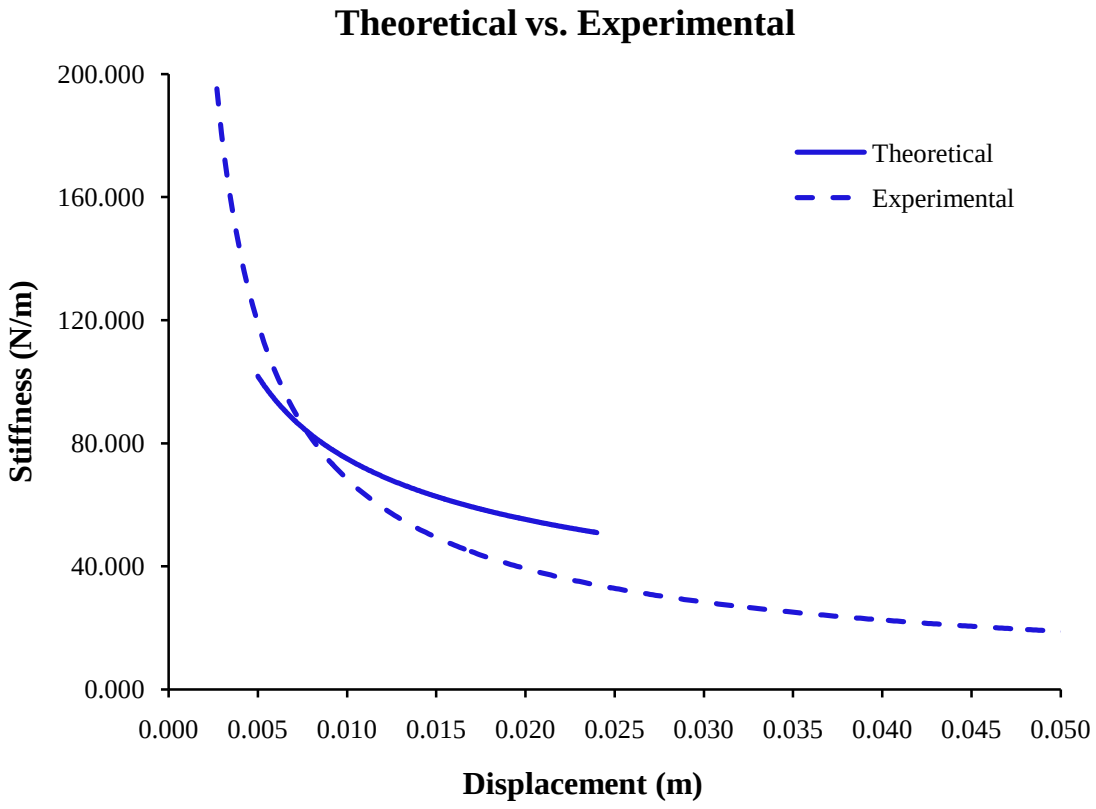


**Figure 2A: Stiffness vs. Displacement (Test 1)**

*Displacement vs. Applied Force*

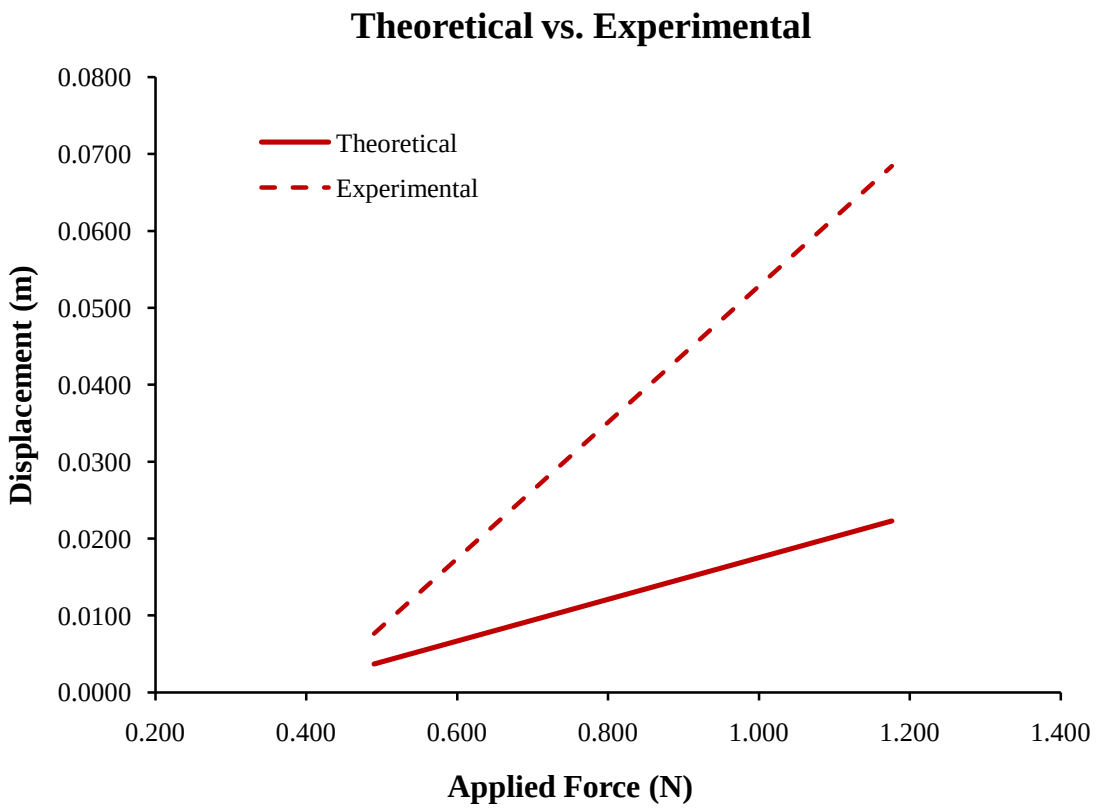


**Figure 3A: Displacement vs. Applied Force (Test 1)**

- TEST 2

*Stiffness vs. Applied Force*

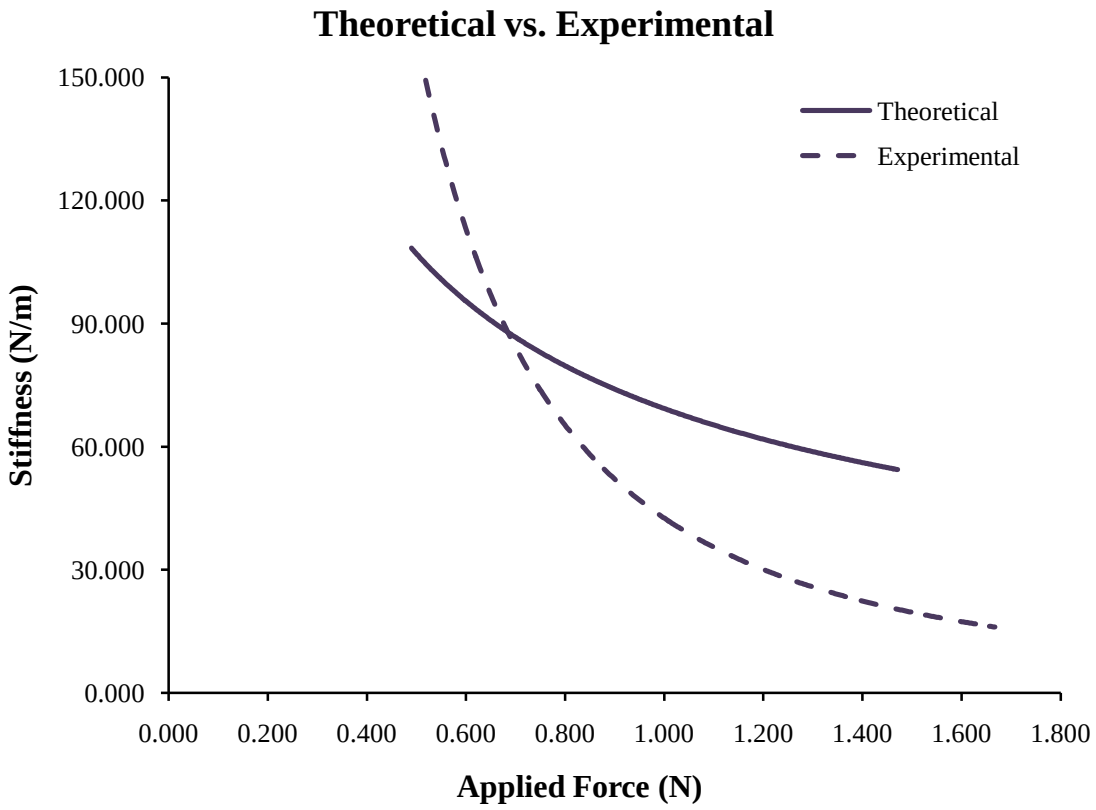


**Figure 4A: Stiffness vs. Applied Force (Test 2)**

*Stiffness vs. Displacement*

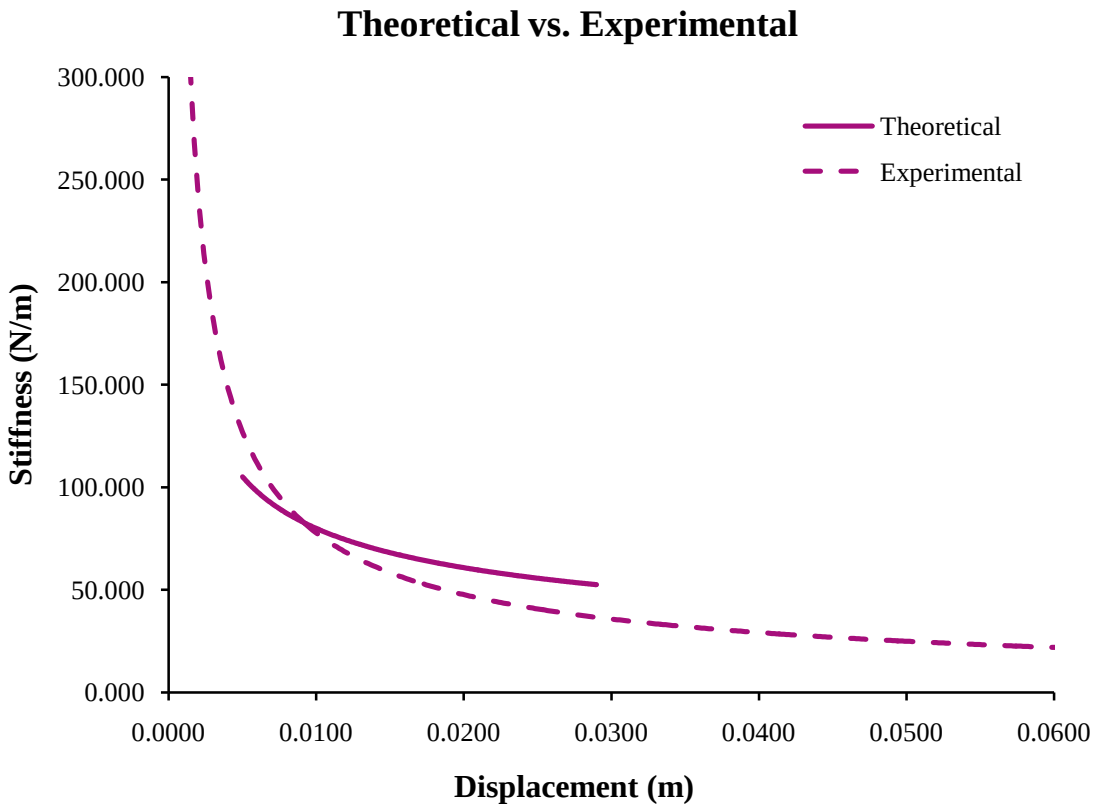


**Figure 5A: Stiffness vs. Displacement (Test 2)**

*Displacement vs. Applied Force*

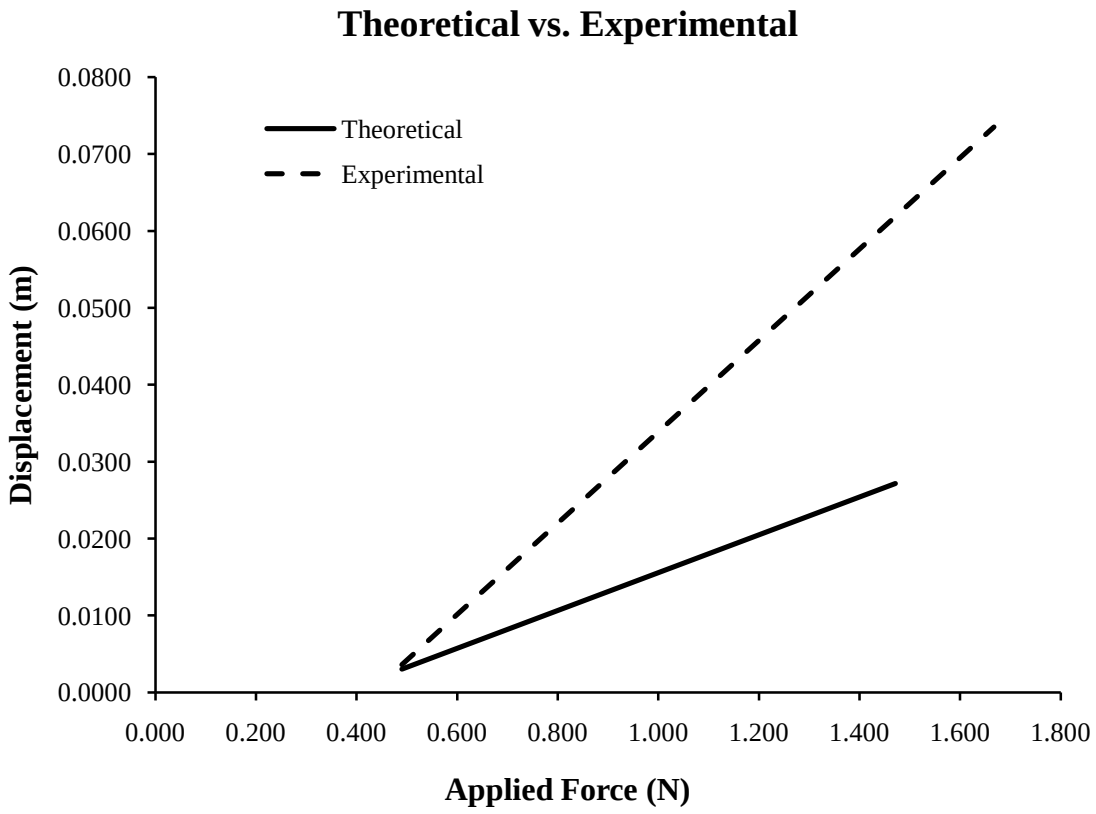


**Figure 6A: Displacement vs. Applied Force (Test 2)**

- TEST 3

*Stiffness vs. Applied Force*

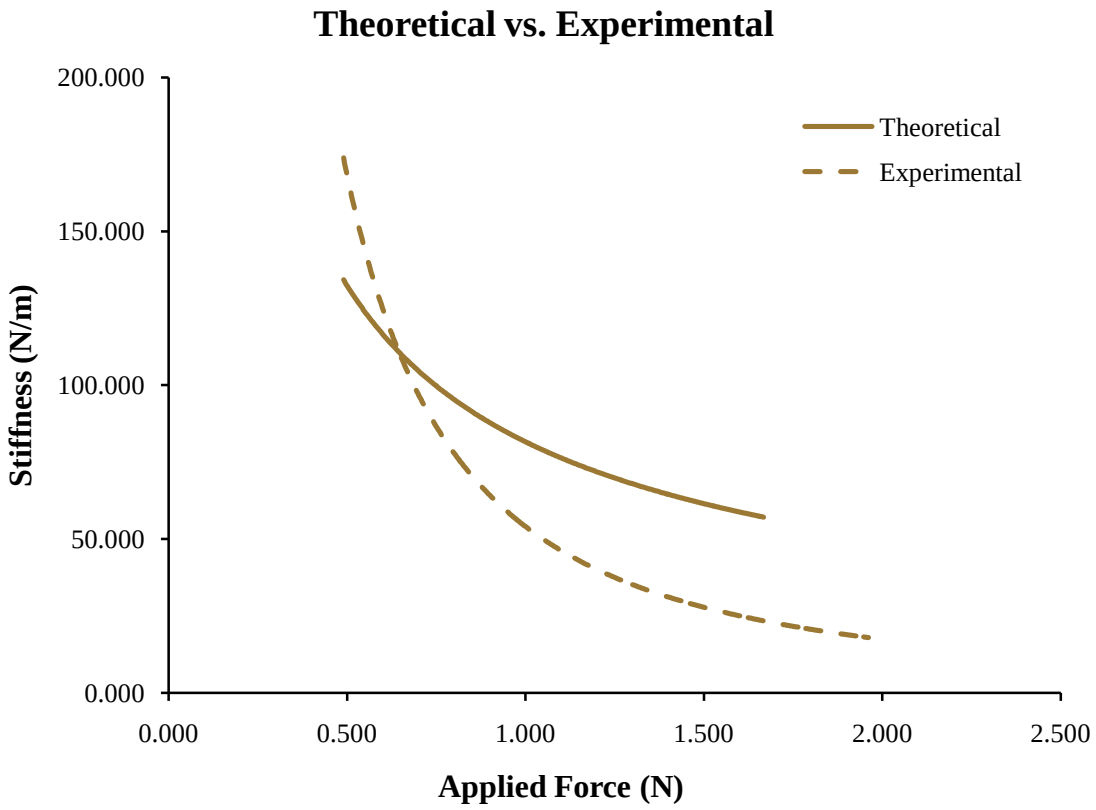


**Figure 7A: Stiffness vs. Applied Force (Test 3)**

*Stiffness vs. Displacement*

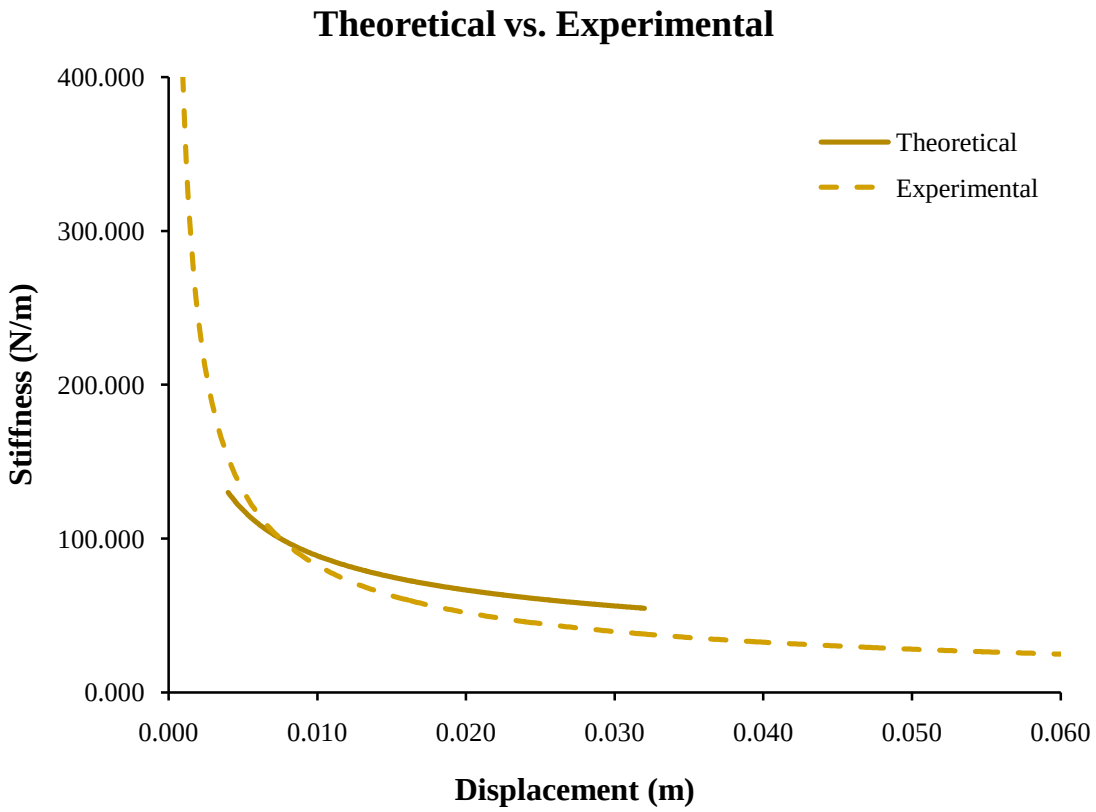


**Figure 8A: Stiffness vs. Displacement (Test 3)**

*Displacement vs. Applied Force*

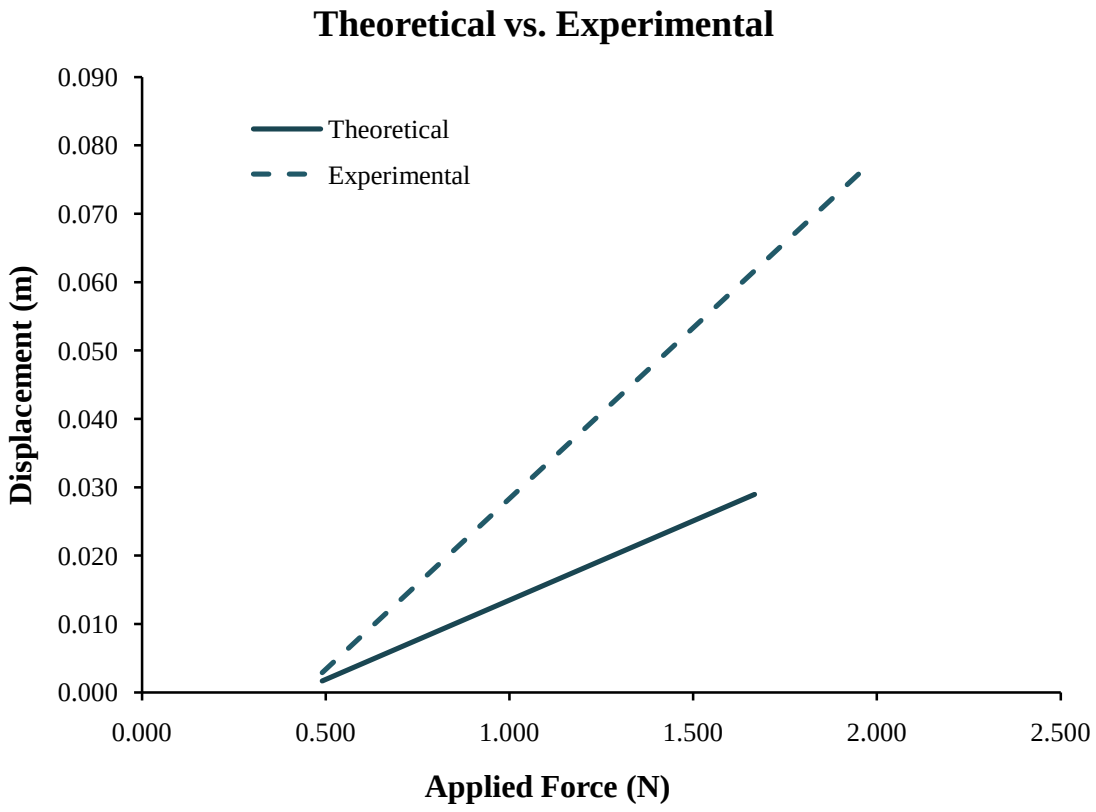


**Figure 9A: Displacement vs. Applied Force (Test 3)**

- TEST 4

*Stiffness vs. Applied Force*

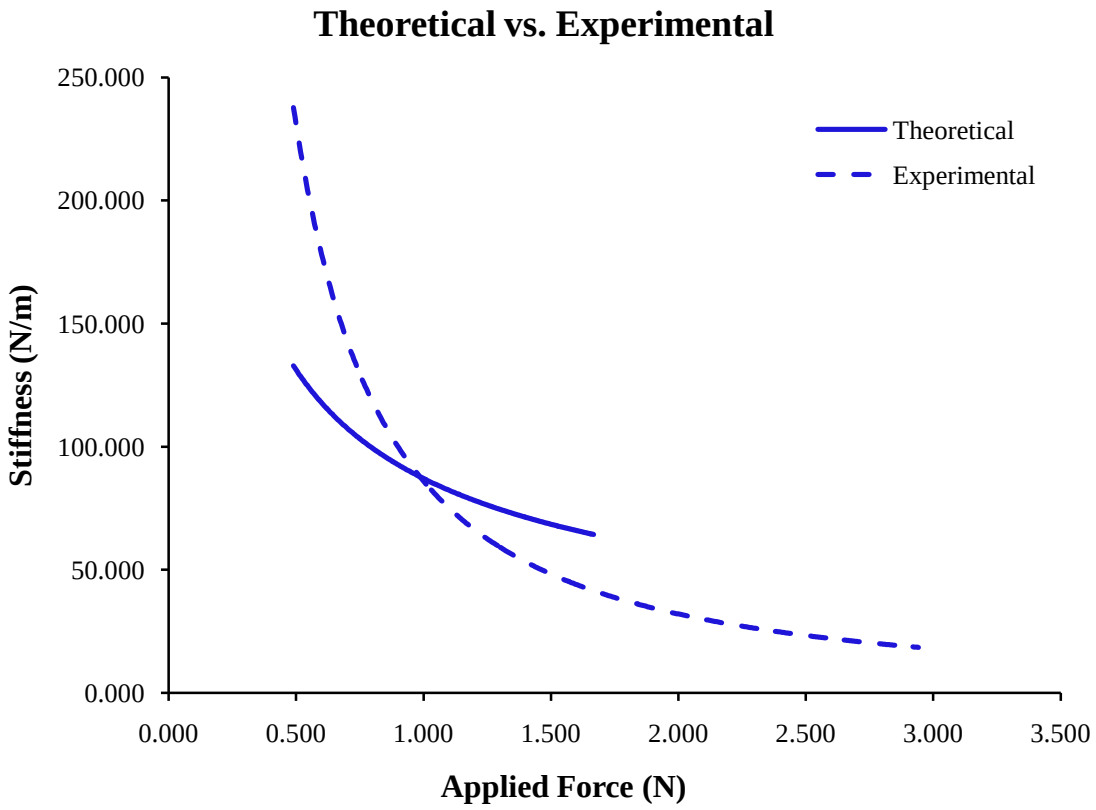


**Figure 10A: Stiffness vs. Applied Force (Test 4)**

*Stiffness vs. Displacement*

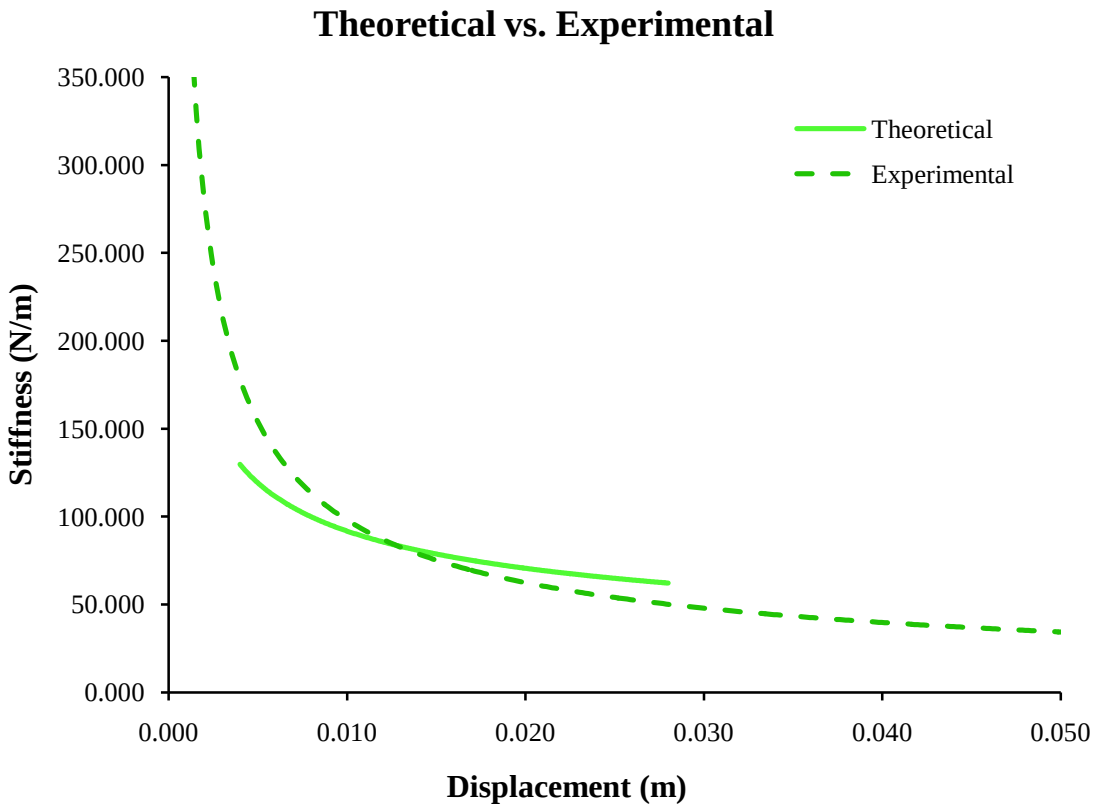


**Figure 11A: Stiffness vs. Displacement (Test 4)**

*Displacement vs. Applied Force*

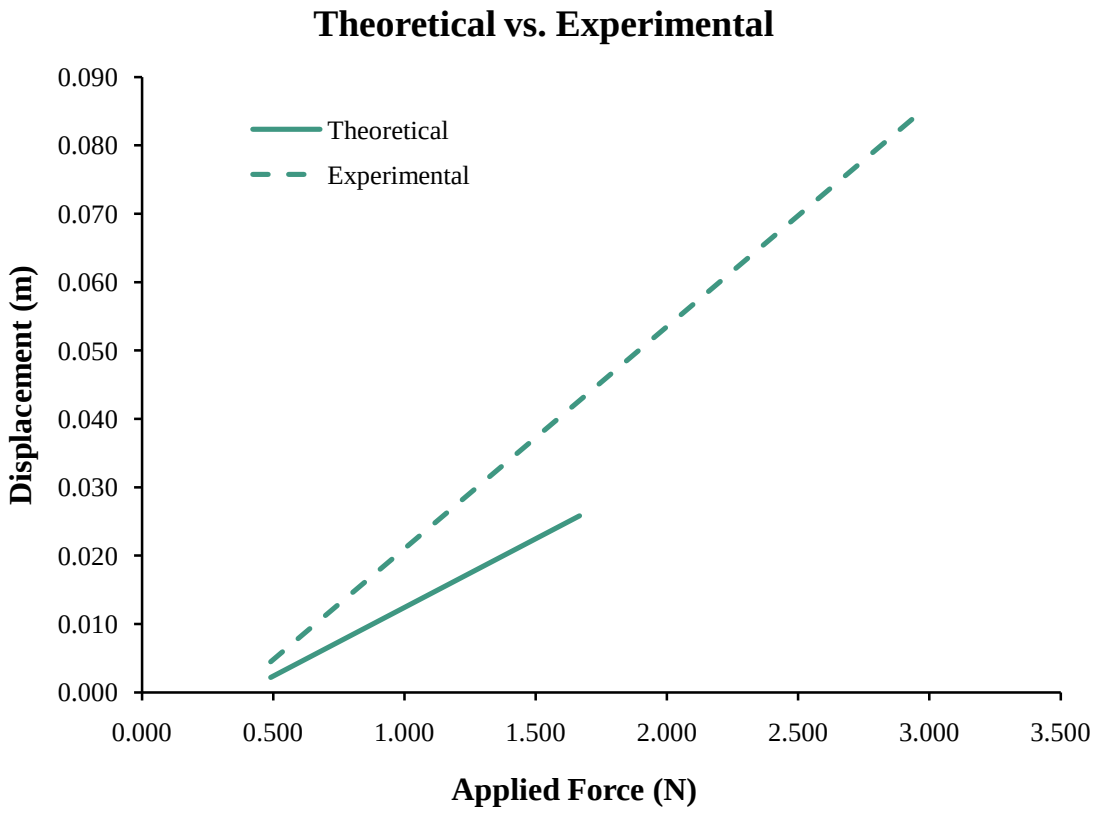


**Figure 12A: Displacement vs. Applied Force (Test 4)**

- TEST 5

*Stiffness vs. Applied Force*

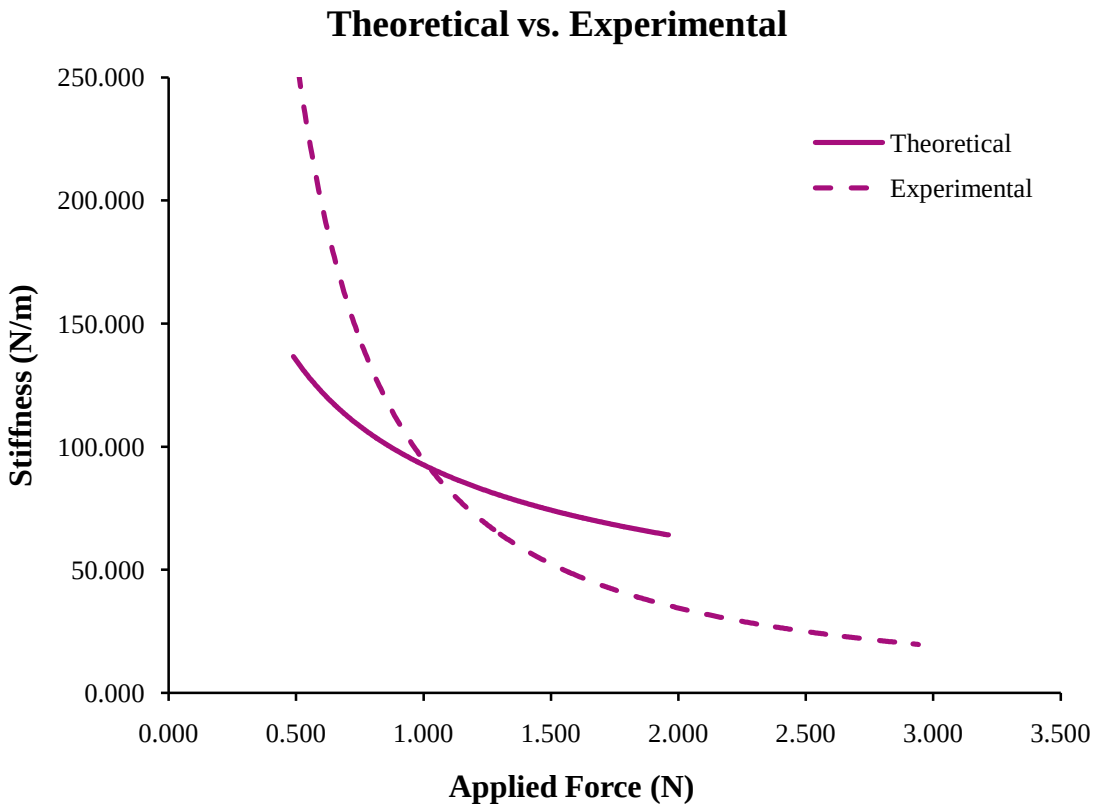


**Figure 13A: Stiffness vs. Applied Force (Test 5)**

*Stiffness vs. Displacement*

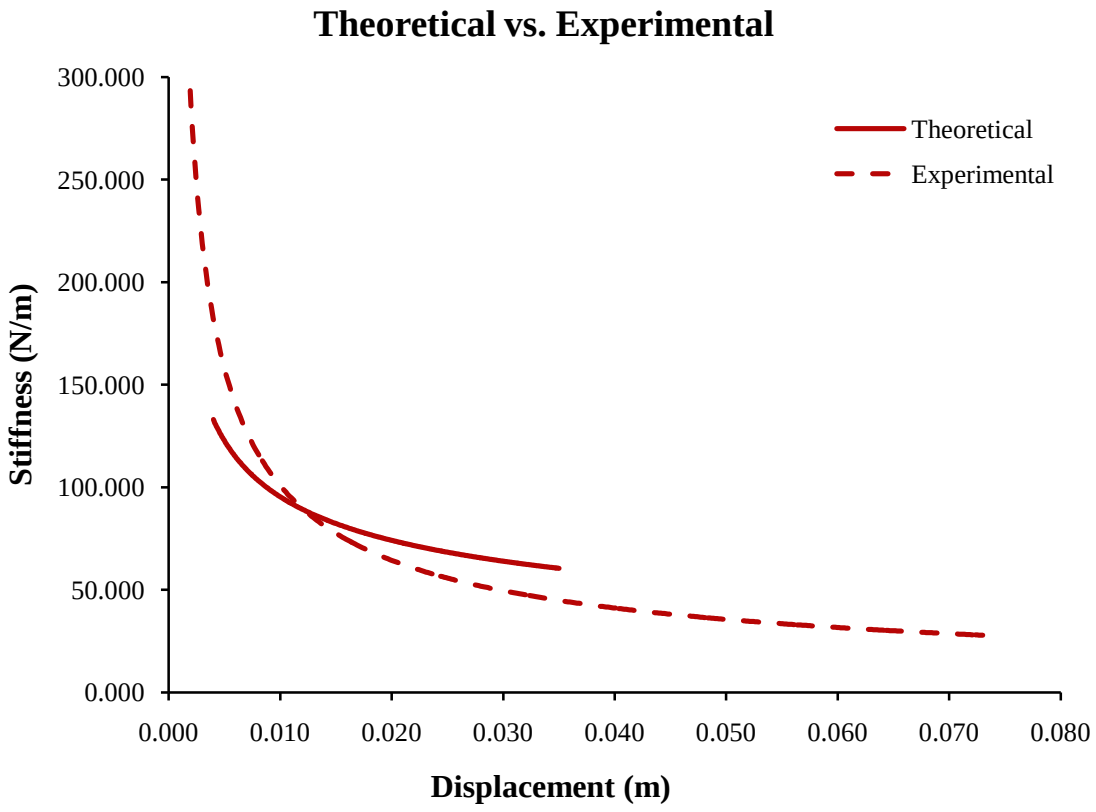


**Figure 14A: Stiffness vs. Displacement (Test 5)**

*Displacement vs. Applied Force*

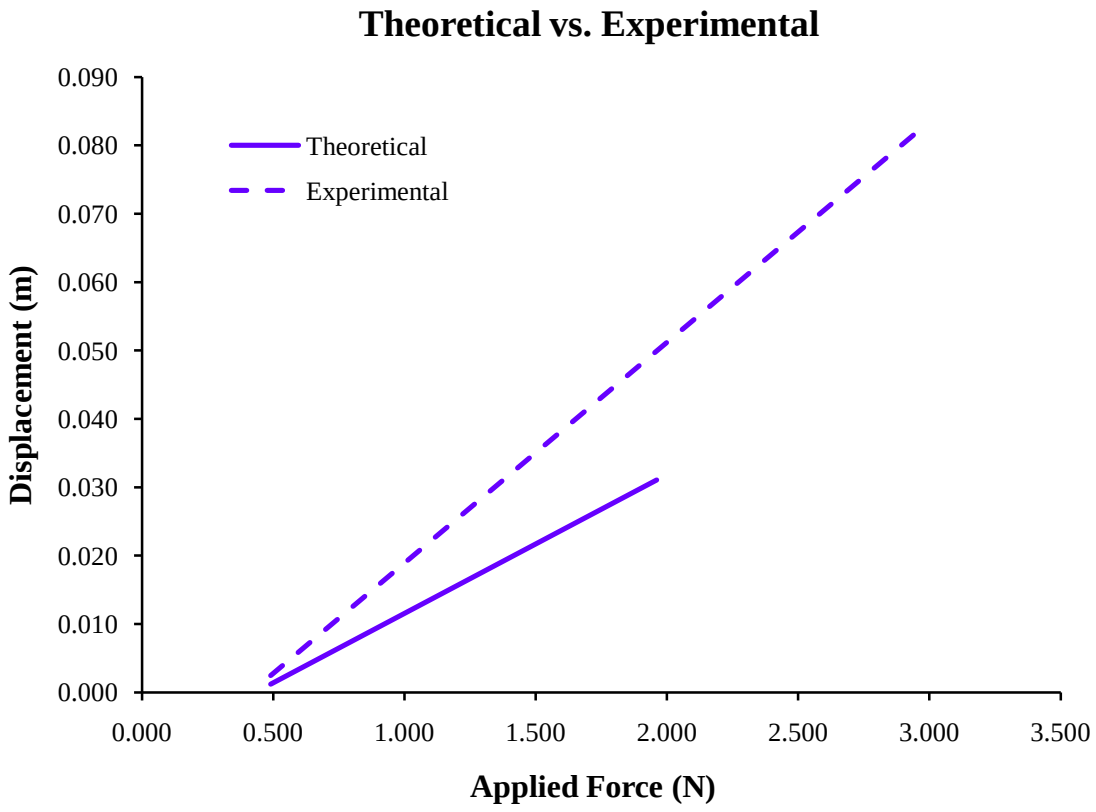


**Figure 15A: Displacement vs. Applied Force (Test 5)**

➢ TEST COMPARISON

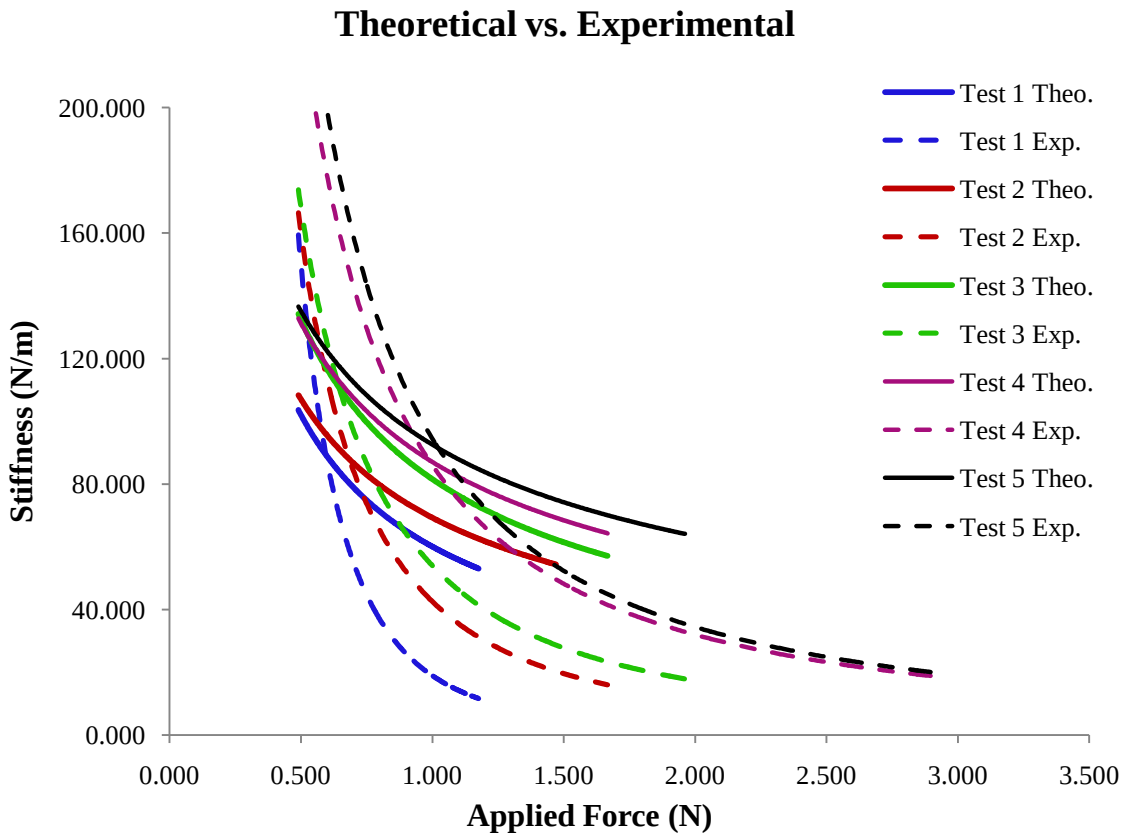


**Figure 16A: Theoretical vs. Experimental (1)**

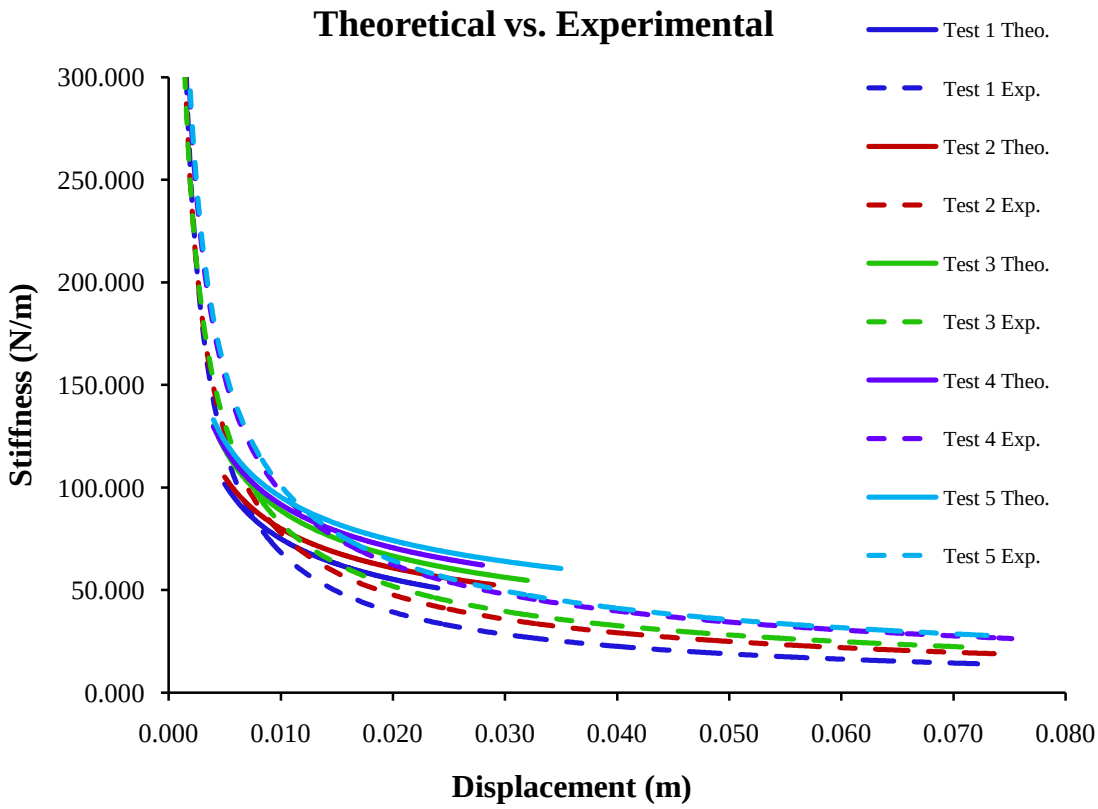


**Figure 17A: Theoretical vs. Experimental (2)**

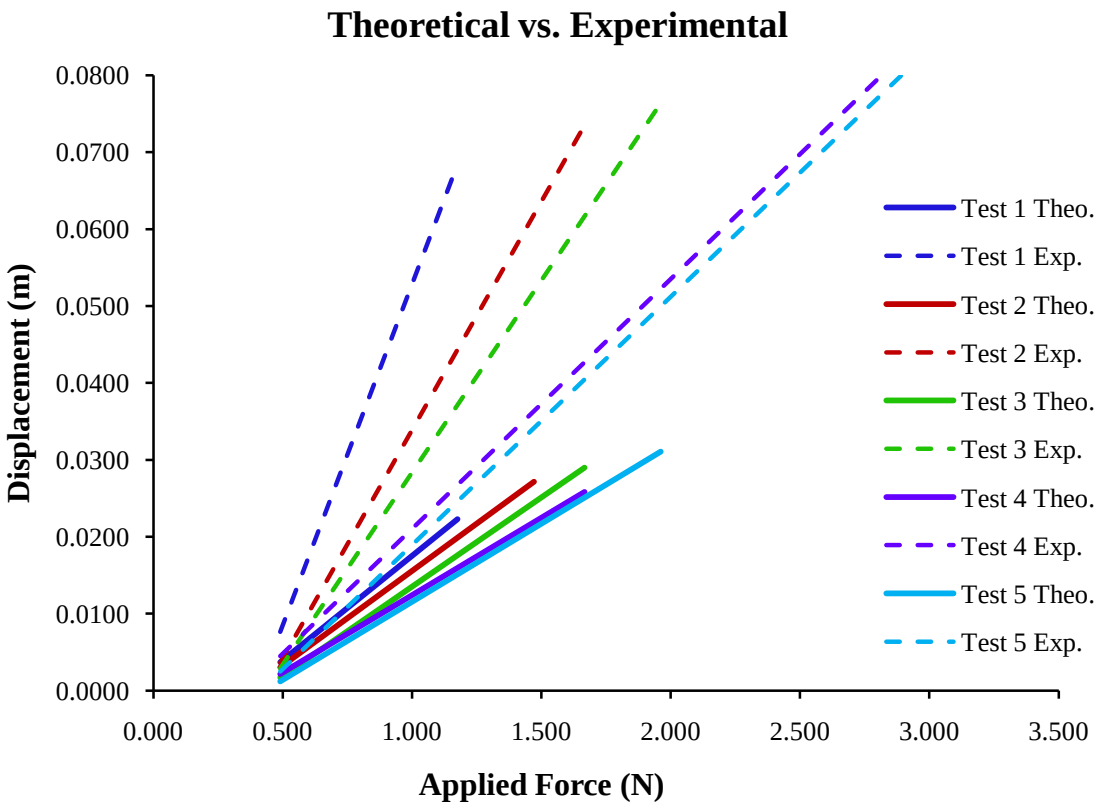


**Figure 18A: Theoretical vs. Experimental (3)**

APPENDIX B

APPENDIX B

DATA FOR APPENDIX A

- TEST 1

**Table B1: Theoretical Results (Test 1)**

| Theoretical Values from Working Model | | | | |
|---|---|---|---|---|
| **App. Force (N)** | **Xo (m)** | **Xf (m)** | **ΔX (m)** | **K (N/m)** |
| 0.490 | 0.397 | 0.392 | 0.0050 | 98.000 |
| 0.490 | 0.397 | 0.392 | 0.0050 | 98.000 |
| 0.490 | 0.397 | 0.392 | 0.0050 | 98.000 |
| 0.490 | 0.397 | 0.392 | 0.0050 | 98.000 |
| 0.686 | 0.397 | 0.389 | 0.0080 | 85.750 |
| 0.686 | 0.397 | 0.389 | 0.0080 | 85.750 |
| 0.686 | 0.397 | 0.389 | 0.0080 | 85.750 |
| 0.686 | 0.397 | 0.389 | 0.0080 | 85.750 |
| 0.980 | 0.397 | 0.382 | 0.0150 | 65.333 |
| 0.980 | 0.397 | 0.382 | 0.0150 | 65.333 |
| 0.980 | 0.397 | 0.382 | 0.0150 | 65.333 |
| 0.980 | 0.397 | 0.382 | 0.0150 | 65.333 |
| 1.176 | 0.397 | 0.373 | 0.0240 | 49.000 |
| 1.176 | 0.397 | 0.373 | 0.0240 | 49.000 |
| 1.176 | 0.397 | 0.373 | 0.0240 | 49.000 |
| 1.176 | 0.397 | 0.373 | 0.0240 | 49.000 |

**Table B2: Experimental Results (Test 1)**

| Experimental Values | | | | | | | |
|---|---|---|---|---|---|---|---|
| **App. Force (N)** | **Xo (V)** | **Xf (V)** | **Xo (m)** | **Xf (m)** | **ΔX (m)** | **ΔXf (m)** | **K (N/m)** |
| 0.490 | 0.786 | 0.853 | 0.0200 | 0.0217 | 0.0017 | 0.395 | 287.930 |
| 0.490 | 0.762 | 0.835 | 0.0194 | 0.0212 | 0.0019 | 0.395 | 264.265 |
| 0.490 | 0.860 | 0.914 | 0.0218 | 0.0232 | 0.0014 | 0.396 | 357.247 |
| 0.490 | 0.838 | 0.895 | 0.0213 | 0.0227 | 0.0014 | 0.396 | 338.445 |
| 0.686 | 0.794 | 2.415 | 0.0202 | 0.0613 | 0.0412 | 0.356 | 16.661 |
| 0.686 | 0.770 | 2.209 | 0.0196 | 0.0561 | 0.0366 | 0.360 | 18.769 |
| 0.686 | 0.862 | 2.031 | 0.0219 | 0.0516 | 0.0297 | 0.367 | 23.103 |
| 0.686 | 0.839 | 2.182 | 0.0213 | 0.0554 | 0.0341 | 0.363 | 20.110 |
| 0.980 | 0.784 | 2.842 | 0.0199 | 0.0722 | 0.0523 | 0.345 | 18.748 |
| 0.980 | 0.775 | 2.543 | 0.0197 | 0.0646 | 0.0449 | 0.352 | 21.823 |
| 0.980 | 0.879 | 2.661 | 0.0223 | 0.0676 | 0.0453 | 0.352 | 21.651 |
| 0.980 | 0.883 | 2.584 | 0.0224 | 0.0656 | 0.0432 | 0.354 | 22.682 |
| 1.176 | 0.774 | 3.615 | 0.0197 | 0.0918 | 0.0722 | 0.325 | 16.297 |
| 1.176 | 0.858 | 3.518 | 0.0218 | 0.0894 | 0.0676 | 0.329 | 17.406 |
| 1.176 | 0.873 | 3.64 | 0.0222 | 0.0925 | 0.0703 | 0.327 | 16.733 |
| 1.176 | 0.874 | 3.443 | 0.0222 | 0.0875 | 0.0653 | 0.332 | 18.022 |

- TEST 2

**Table B3: Theoretical Results (Test 2)**

| Theoretical Values from Working Model | | | | |
|---|---|---|---|---|
| **App. Force (N)** | **Xo (m)** | **Xf (m)** | **ΔX (m)** | **K (N/m)** |
| 0.490 | 0.397 | 0.392 | 0.0050 | 98.000 |
| 0.490 | 0.397 | 0.392 | 0.0050 | 98.000 |
| 0.490 | 0.397 | 0.392 | 0.0050 | 98.000 |
| 0.490 | 0.397 | 0.392 | 0.0050 | 98.000 |
| 0.686 | 0.397 | 0.390 | 0.0070 | 98.000 |
| 0.686 | 0.397 | 0.390 | 0.0070 | 98.000 |
| 0.686 | 0.397 | 0.390 | 0.0070 | 98.000 |
| 0.686 | 0.397 | 0.390 | 0.0070 | 98.000 |
| 0.980 | 0.397 | 0.384 | 0.0130 | 75.385 |
| 0.980 | 0.397 | 0.384 | 0.0130 | 75.385 |
| 0.980 | 0.397 | 0.384 | 0.0130 | 75.385 |
| 0.980 | 0.397 | 0.384 | 0.0130 | 75.385 |
| 1.176 | 0.397 | 0.378 | 0.0190 | 61.895 |
| 1.176 | 0.397 | 0.378 | 0.0190 | 61.895 |
| 1.176 | 0.397 | 0.378 | 0.0190 | 61.895 |
| 1.176 | 0.397 | 0.378 | 0.0190 | 61.895 |
| 1.471 | 0.397 | 0.368 | 0.0290 | 50.724 |
| 1.471 | 0.397 | 0.368 | 0.0290 | 50.724 |
| 1.471 | 0.397 | 0.368 | 0.0290 | 50.724 |
| 1.471 | 0.397 | 0.368 | 0.0290 | 50.724 |

**Table B4: Experimental Results (Test 2)**

| Experimental Values | | | | | | | |
|---|---|---|---|---|---|---|---|
| **App. Force (N)** | **Xo (V)** | **Xf (V)** | **Xo (m)** | **Xf (m)** | **ΔX (m)** | **ΔXf (m)** | **K (N/m)** |
| 0.490 | 0.786 | 0.835 | 0.0200 | 0.0212 | 0.0012 | 0.396 | 393.701 |
| 0.490 | 0.862 | 0.912 | 0.0219 | 0.0232 | 0.0013 | 0.396 | 385.827 |
| 0.490 | 0.852 | 0.904 | 0.0216 | 0.0230 | 0.0013 | 0.396 | 370.987 |
| 0.490 | 0.816 | 0.903 | 0.0207 | 0.0229 | 0.0022 | 0.395 | 221.740 |
| 0.686 | 0.800 | 1.634 | 0.0203 | 0.0415 | 0.0212 | 0.376 | 32.384 |
| 0.686 | 0.858 | 1.402 | 0.0218 | 0.0356 | 0.0138 | 0.383 | 49.647 |
| 0.686 | 0.842 | 1.487 | 0.0214 | 0.0378 | 0.0164 | 0.381 | 41.873 |
| 0.686 | 0.824 | 1.513 | 0.0209 | 0.0384 | 0.0175 | 0.379 | 39.199 |
| 0.980 | 0.797 | 1.979 | 0.0202 | 0.0503 | 0.0300 | 0.367 | 32.642 |
| 0.980 | 0.822 | 1.611 | 0.0209 | 0.0409 | 0.0200 | 0.377 | 48.901 |
| 0.980 | 0.832 | 1.718 | 0.0211 | 0.0436 | 0.0225 | 0.374 | 43.547 |
| 0.980 | 0.891 | 1.819 | 0.0226 | 0.0462 | 0.0236 | 0.373 | 41.576 |
| 1.176 | 0.794 | 3.298 | 0.0202 | 0.0838 | 0.0636 | 0.333 | 18.490 |
| 1.176 | 0.850 | 2.956 | 0.0216 | 0.0751 | 0.0535 | 0.344 | 21.984 |
| 1.176 | 0.816 | 2.945 | 0.0207 | 0.0748 | 0.0541 | 0.343 | 21.747 |
| 1.176 | 0.865 | 3.336 | 0.0220 | 0.0847 | 0.0628 | 0.334 | 18.737 |
| 1.471 | 0.796 | 3.339 | 0.0202 | 0.0848 | 0.0646 | 0.332 | 22.774 |
| 1.471 | 0.860 | 2.980 | 0.0218 | 0.0757 | 0.0538 | 0.343 | 27.318 |
| 1.471 | 0.863 | 3.067 | 0.0219 | 0.0779 | 0.0560 | 0.341 | 26.276 |
| 1.471 | 0.839 | 3.348 | 0.0213 | 0.0850 | 0.0637 | 0.333 | 23.082 |
| 1.667 | 0.794 | 3.693 | 0.0202 | 0.0938 | 0.0736 | 0.323 | 22.639 |
| 1.667 | 0.867 | 3.391 | 0.0220 | 0.0861 | 0.0641 | 0.333 | 26.002 |
| 1.667 | 0.844 | 3.717 | 0.0214 | 0.0944 | 0.0730 | 0.324 | 22.844 |
| 1.667 | 0.829 | 3.637 | 0.0211 | 0.0924 | 0.0713 | 0.326 | 23.372 |

- TEST 3

**Table B5: Theoretical Results (Test 3)**

| Theoretical Values from Working Model | | | | |
|---|---|---|---|---|
| **App. Force (N)** | **Xo (m)** | **Xf (m)** | **ΔX (m)** | **K (N/m)** |
| 0.490 | 0.397 | 0.393 | 0.004 | 122.500 |
| 0.490 | 0.397 | 0.393 | 0.004 | 122.500 |
| 0.490 | 0.397 | 0.393 | 0.004 | 122.500 |
| 0.490 | 0.397 | 0.393 | 0.004 | 122.500 |
| 0.686 | 0.397 | 0.391 | 0.006 | 114.333 |
| 0.686 | 0.397 | 0.391 | 0.006 | 114.333 |
| 0.686 | 0.397 | 0.391 | 0.006 | 114.333 |
| 0.686 | 0.397 | 0.391 | 0.006 | 114.333 |
| 0.980 | 0.397 | 0.386 | 0.011 | 89.091 |
| 0.980 | 0.397 | 0.386 | 0.011 | 89.091 |
| 0.980 | 0.397 | 0.386 | 0.011 | 89.091 |
| 0.980 | 0.397 | 0.386 | 0.011 | 89.091 |
| 1.176 | 0.397 | 0.381 | 0.016 | 73.500 |
| 1.176 | 0.397 | 0.381 | 0.016 | 73.500 |
| 1.176 | 0.397 | 0.381 | 0.016 | 73.500 |
| 1.176 | 0.397 | 0.381 | 0.016 | 73.500 |
| 1.471 | 0.397 | 0.374 | 0.023 | 63.957 |
| 1.471 | 0.397 | 0.374 | 0.023 | 63.957 |
| 1.471 | 0.397 | 0.374 | 0.023 | 63.957 |
| 1.471 | 0.397 | 0.374 | 0.023 | 63.957 |
| 1.667 | 0.397 | 0.365 | 0.032 | 52.094 |
| 1.667 | 0.397 | 0.365 | 0.032 | 52.094 |
| 1.667 | 0.397 | 0.365 | 0.032 | 52.094 |
| 1.667 | 0.397 | 0.365 | 0.032 | 52.094 |

**Table B6 Experimental Results (Test 3)**

| Experimental Values | | | | | | | |
|---|---|---|---|---|---|---|---|
| **App. Force (N)** | **Xo (V)** | **Xf (V)** | **Xo (m)** | **Xf (m)** | **ΔX (m)** | **ΔXf (m)** | **K (N/m)** |
| 0.490 | 0.786 | 0.820 | 0.0200 | 0.0208 | 0.0009 | 0.396 | 567.392 |
| 0.490 | 0.810 | 0.881 | 0.0206 | 0.0224 | 0.0018 | 0.395 | 271.709 |
| 0.490 | 0.818 | 0.885 | 0.0208 | 0.0225 | 0.0017 | 0.395 | 287.930 |
| 0.490 | 0.814 | 0.877 | 0.0207 | 0.0223 | 0.0016 | 0.395 | 306.212 |
| 0.686 | 0.787 | 1.211 | 0.0200 | 0.0308 | 0.0108 | 0.386 | 63.698 |
| 0.686 | 0.814 | 1.375 | 0.0207 | 0.0349 | 0.0142 | 0.383 | 48.142 |
| 0.686 | 0.839 | 1.369 | 0.0213 | 0.0348 | 0.0135 | 0.384 | 50.958 |
| 0.686 | 0.854 | 1.408 | 0.0217 | 0.0358 | 0.0141 | 0.383 | 48.751 |
| 0.980 | 0.786 | 1.377 | 0.0200 | 0.0350 | 0.0150 | 0.382 | 65.284 |
| 0.980 | 0.843 | 1.565 | 0.0214 | 0.0398 | 0.0183 | 0.379 | 53.439 |
| 0.980 | 0.843 | 1.548 | 0.0214 | 0.0393 | 0.0179 | 0.379 | 54.727 |
| 0.980 | 0.824 | 1.492 | 0.0209 | 0.0379 | 0.0170 | 0.380 | 57.758 |
| 1.176 | 0.827 | 2.485 | 0.0210 | 0.0631 | 0.0421 | 0.355 | 27.925 |
| 1.176 | 0.833 | 2.876 | 0.0212 | 0.0731 | 0.0519 | 0.345 | 22.662 |
| 1.176 | 0.886 | 2.905 | 0.0225 | 0.0738 | 0.0513 | 0.346 | 22.932 |
| 1.176 | 0.866 | 2.897 | 0.0220 | 0.0736 | 0.0516 | 0.345 | 22.796 |
| 1.471 | 0.871 | 2.812 | 0.0221 | 0.0714 | 0.0493 | 0.348 | 29.837 |
| 1.471 | 0.865 | 2.969 | 0.0220 | 0.0754 | 0.0534 | 0.344 | 27.525 |
| 1.471 | 0.895 | 3.101 | 0.0227 | 0.0788 | 0.0560 | 0.341 | 26.253 |
| 1.471 | 0.883 | 3.109 | 0.0224 | 0.0790 | 0.0565 | 0.340 | 26.017 |
| 1.667 | 0.784 | 3.357 | 0.0199 | 0.0853 | 0.0654 | 0.332 | 25.507 |
| 1.667 | 0.857 | 3.464 | 0.0218 | 0.0880 | 0.0662 | 0.331 | 25.174 |
| 1.667 | 0.853 | 3.391 | 0.0217 | 0.0861 | 0.0645 | 0.333 | 25.859 |
| 1.667 | 0.877 | 3.482 | 0.0223 | 0.0884 | 0.0662 | 0.331 | 25.194 |
| 1.961 | 0.794 | 3.567 | 0.0202 | 0.0906 | 0.0704 | 0.327 | 27.842 |
| 1.961 | 0.829 | 3.555 | 0.0211 | 0.0903 | 0.0692 | 0.328 | 28.322 |
| 1.961 | 0.822 | 3.608 | 0.0209 | 0.0916 | 0.0708 | 0.326 | 27.712 |
| 1.961 | 0.863 | 3.555 | 0.0219 | 0.0903 | 0.0684 | 0.329 | 28.679 |

- TEST 4

**Table B7: Theoretical Results (Test 4)**

| Theoretical Values from Working Model | | | | |
|---|---|---|---|---|
| **App. Force (N)** | **Xo (m)** | **Xf (m)** | **ΔX (m)** | **K (N/m)** |
| 0.490 | 0.397 | 0.393 | 0.004 | 122.500 |
| 0.490 | 0.397 | 0.393 | 0.004 | 122.500 |
| 0.490 | 0.397 | 0.393 | 0.004 | 122.500 |
| 0.490 | 0.397 | 0.393 | 0.004 | 122.500 |
| 0.686 | 0.397 | 0.391 | 0.006 | 114.333 |
| 0.686 | 0.397 | 0.391 | 0.006 | 114.333 |
| 0.686 | 0.397 | 0.391 | 0.006 | 114.333 |
| 0.686 | 0.397 | 0.391 | 0.006 | 114.333 |
| 0.980 | 0.397 | 0.387 | 0.010 | 98.000 |
| 0.980 | 0.397 | 0.387 | 0.010 | 98.000 |
| 0.980 | 0.397 | 0.387 | 0.010 | 98.000 |
| 0.980 | 0.397 | 0.387 | 0.010 | 98.000 |
| 1.176 | 0.397 | 0.382 | 0.015 | 78.400 |
| 1.176 | 0.397 | 0.382 | 0.015 | 78.400 |
| 1.176 | 0.397 | 0.382 | 0.015 | 78.400 |
| 1.176 | 0.397 | 0.382 | 0.015 | 78.400 |
| 1.471 | 0.397 | 0.376 | 0.021 | 70.048 |
| 1.471 | 0.397 | 0.376 | 0.021 | 70.048 |
| 1.471 | 0.397 | 0.376 | 0.021 | 70.048 |
| 1.471 | 0.397 | 0.376 | 0.021 | 70.048 |
| 1.667 | 0.397 | 0.369 | 0.028 | 59.536 |
| 1.667 | 0.397 | 0.369 | 0.028 | 59.536 |
| 1.667 | 0.397 | 0.369 | 0.028 | 59.536 |
| 1.667 | 0.397 | 0.369 | 0.028 | 59.536 |

**Table B8: Experimental Results (Test 4)**

| Experimental Values | | | | | | | |
|---|---|---|---|---|---|---|---|
| **Force (N)** | **Xo (V)** | **Xf (V)** | **Xo (m)** | **Xf (m)** | **ΔX (m)** | **ΔXf (m)** | **K (N/m)** |
| 0.490 | 0.798 | 0.822 | 0.0203 | 0.0209 | 0.0006 | 0.396 | 803.806 |
| 0.490 | 0.849 | 0.884 | 0.0216 | 0.0225 | 0.0009 | 0.396 | 551.181 |
| 0.490 | 0.856 | 0.877 | 0.0217 | 0.0223 | 0.0005 | 0.396 | 918.635 |
| 0.490 | 0.843 | 0.89 | 0.0214 | 0.0226 | 0.0012 | 0.396 | 410.454 |
| 0.686 | 0.798 | 1.112 | 0.0203 | 0.0282 | 0.0080 | 0.389 | 86.012 |
| 0.686 | 0.833 | 1.173 | 0.0212 | 0.0298 | 0.0086 | 0.388 | 79.435 |
| 0.686 | 0.839 | 1.115 | 0.0213 | 0.0283 | 0.0070 | 0.390 | 97.855 |
| 0.686 | 0.849 | 1.208 | 0.0216 | 0.0307 | 0.0091 | 0.388 | 75.231 |
| 0.980 | 0.784 | 1.211 | 0.0199 | 0.0308 | 0.0108 | 0.386 | 90.358 |
| 0.980 | 0.849 | 1.36 | 0.0216 | 0.0345 | 0.0130 | 0.384 | 75.504 |
| 0.980 | 0.873 | 1.436 | 0.0222 | 0.0365 | 0.0143 | 0.383 | 68.531 |
| 0.980 | 0.865 | 1.368 | 0.0220 | 0.0347 | 0.0128 | 0.384 | 76.705 |
| 1.176 | 0.784 | 1.958 | 0.0199 | 0.0497 | 0.0298 | 0.367 | 39.437 |
| 1.176 | 0.858 | 2.048 | 0.0218 | 0.0520 | 0.0302 | 0.367 | 38.907 |
| 1.176 | 0.857 | 2.002 | 0.0218 | 0.0509 | 0.0291 | 0.368 | 40.436 |
| 1.176 | 0.865 | 2.060 | 0.0220 | 0.0523 | 0.0304 | 0.367 | 38.744 |
| 1.471 | 0.775 | 2.088 | 0.0197 | 0.0530 | 0.0334 | 0.364 | 44.108 |
| 1.471 | 0.879 | 2.183 | 0.0223 | 0.0554 | 0.0331 | 0.364 | 44.412 |
| 1.471 | 0.876 | 2.214 | 0.0223 | 0.0562 | 0.0340 | 0.363 | 43.284 |
| 1.471 | 0.859 | 2.236 | 0.0218 | 0.0568 | 0.0350 | 0.362 | 42.058 |
| 1.667 | 0.784 | 2.859 | 0.0199 | 0.0726 | 0.0527 | 0.344 | 31.629 |
| 1.667 | 0.865 | 3.083 | 0.0220 | 0.0783 | 0.0563 | 0.341 | 29.590 |
| 1.667 | 0.879 | 3.226 | 0.0223 | 0.0819 | 0.0596 | 0.337 | 27.963 |
| 1.667 | 0.874 | 3.249 | 0.0222 | 0.0825 | 0.0603 | 0.337 | 27.634 |
| 1.961 | 0.816 | 3.197 | 0.0207 | 0.0812 | 0.0605 | 0.337 | 32.425 |
| 1.961 | 0.873 | 3.316 | 0.0222 | 0.0842 | 0.0621 | 0.335 | 31.602 |
| 1.961 | 0.853 | 3.320 | 0.0217 | 0.0843 | 0.0627 | 0.334 | 31.295 |
| 1.961 | 0.874 | 3.355 | 0.0222 | 0.0852 | 0.0630 | 0.334 | 31.118 |
| 2.942 | 0.799 | 3.760 | 0.0203 | 0.0955 | 0.0752 | 0.322 | 39.117 |
| 2.942 | 0.821 | 3.693 | 0.0209 | 0.0938 | 0.0729 | 0.324 | 40.330 |
| 2.942 | 0.870 | 3.707 | 0.0221 | 0.0942 | 0.0721 | 0.325 | 40.827 |
| 2.942 | 0.862 | 3.707 | 0.0219 | 0.0942 | 0.0723 | 0.325 | 40.712 |

- TEST 5

**Table B9: Theoretical Results (Test 5)**

| Theoretical Values from Working Model | | | | |
|---|---|---|---|---|
| **App. Force (N)** | **Xo (m)** | **Xf (m)** | **ΔX (m)** | **K (N/m)** |
| 0.490 | 0.397 | 0.393 | 0.004 | 122.500 |
| 0.490 | 0.397 | 0.393 | 0.004 | 122.500 |
| 0.490 | 0.397 | 0.393 | 0.004 | 122.500 |
| 0.490 | 0.397 | 0.393 | 0.004 | 122.500 |
| 0.686 | 0.397 | 0.391 | 0.006 | 114.333 |
| 0.686 | 0.397 | 0.391 | 0.006 | 114.333 |
| 0.686 | 0.397 | 0.391 | 0.006 | 114.333 |
| 0.686 | 0.397 | 0.391 | 0.006 | 114.333 |
| 0.980 | 0.397 | 0.388 | 0.009 | 108.889 |
| 0.980 | 0.397 | 0.388 | 0.009 | 108.889 |
| 0.980 | 0.397 | 0.388 | 0.009 | 108.889 |
| 0.980 | 0.397 | 0.388 | 0.009 | 108.889 |
| 1.176 | 0.397 | 0.384 | 0.013 | 90.462 |
| 1.176 | 0.397 | 0.384 | 0.013 | 90.462 |
| 1.176 | 0.397 | 0.384 | 0.013 | 90.462 |
| 1.176 | 0.397 | 0.384 | 0.013 | 90.462 |
| 1.471 | 0.397 | 0.378 | 0.019 | 77.421 |
| 1.471 | 0.397 | 0.378 | 0.019 | 77.421 |
| 1.471 | 0.397 | 0.378 | 0.019 | 77.421 |
| 1.471 | 0.397 | 0.378 | 0.019 | 77.421 |
| 1.667 | 0.397 | 0.373 | 0.024 | 69.458 |
| 1.667 | 0.397 | 0.373 | 0.024 | 69.458 |
| 1.667 | 0.397 | 0.373 | 0.024 | 69.458 |
| 1.667 | 0.397 | 0.373 | 0.024 | 69.458 |
| 1.961 | 0.397 | 0.362 | 0.035 | 56.029 |
| 1.961 | 0.397 | 0.362 | 0.035 | 56.029 |
| 1.961 | 0.397 | 0.362 | 0.035 | 56.029 |
| 1.961 | 0.397 | 0.362 | 0.035 | 56.029 |

**Table B10: Experimental Results (Test 5)**

| Experimental Values | | | | | | | |
|---|---|---|---|---|---|---|---|
| **Force (N)** | **Xo (V)** | **Xf (V)** | **Xo (m)** | **Xf (m)** | **ΔX (m)** | **ΔXf (m)** | **K (N/m)** |
| 0.490 | 0.798 | 0.814 | 0.0203 | 0.0207 | 0.0004 | 0.397 | 1205.709 |
| 0.490 | 0.861 | 0.900 | 0.0219 | 0.0229 | 0.0010 | 0.396 | 494.650 |
| 0.490 | 0.865 | 0.900 | 0.0220 | 0.0229 | 0.0009 | 0.396 | 551.181 |
| 0.490 | 0.863 | 0.900 | 0.0219 | 0.0229 | 0.0009 | 0.396 | 521.388 |
| 0.686 | 0.798 | 1.046 | 0.0203 | 0.0266 | 0.0063 | 0.391 | 108.903 |
| 0.686 | 0.861 | 1.170 | 0.0219 | 0.0297 | 0.0078 | 0.389 | 87.404 |
| 0.686 | 0.878 | 1.170 | 0.0223 | 0.0297 | 0.0074 | 0.390 | 92.493 |
| 0.686 | 0.879 | 1.170 | 0.0223 | 0.0297 | 0.0074 | 0.390 | 92.811 |
| 0.980 | 0.766 | 1.324 | 0.0195 | 0.0336 | 0.0142 | 0.383 | 69.145 |
| 0.980 | 0.886 | 1.254 | 0.0225 | 0.0319 | 0.0093 | 0.388 | 104.844 |
| 0.980 | 0.883 | 1.247 | 0.0224 | 0.0317 | 0.0092 | 0.388 | 105.996 |
| 0.980 | 0.880 | 1.252 | 0.0224 | 0.0318 | 0.0094 | 0.388 | 103.717 |
| 1.176 | 0.767 | 1.683 | 0.0195 | 0.0427 | 0.0233 | 0.374 | 50.545 |
| 1.176 | 0.880 | 1.805 | 0.0224 | 0.0458 | 0.0235 | 0.374 | 50.053 |
| 1.176 | 0.868 | 1.899 | 0.0220 | 0.0482 | 0.0262 | 0.371 | 44.907 |
| 1.176 | 0.879 | 1.931 | 0.0223 | 0.0490 | 0.0267 | 0.370 | 44.011 |
| 1.471 | 0.758 | 1.885 | 0.0193 | 0.0479 | 0.0286 | 0.368 | 51.387 |
| 1.471 | 0.863 | 2.016 | 0.0219 | 0.0512 | 0.0293 | 0.368 | 50.228 |
| 1.471 | 0.857 | 2.170 | 0.0218 | 0.0551 | 0.0334 | 0.364 | 44.108 |
| 1.471 | 0.857 | 2.208 | 0.0218 | 0.0561 | 0.0343 | 0.363 | 42.867 |
| 1.667 | 0.758 | 2.819 | 0.0193 | 0.0716 | 0.0523 | 0.345 | 31.844 |
| 1.667 | 0.868 | 2.985 | 0.0220 | 0.0758 | 0.0538 | 0.343 | 31.001 |
| 1.667 | 0.857 | 3.058 | 0.0218 | 0.0777 | 0.0559 | 0.341 | 29.818 |
| 1.667 | 0.857 | 3.062 | 0.0218 | 0.0778 | 0.0560 | 0.341 | 29.764 |
| 1.961 | 0.758 | 3.025 | 0.0193 | 0.0768 | 0.0576 | 0.339 | 34.056 |
| 1.961 | 0.868 | 3.127 | 0.0220 | 0.0794 | 0.0574 | 0.340 | 34.177 |
| 1.961 | 0.865 | 3.210 | 0.0220 | 0.0815 | 0.0596 | 0.337 | 32.923 |
| 1.961 | 0.857 | 3.215 | 0.0218 | 0.0817 | 0.0599 | 0.337 | 32.742 |
| 2.942 | 0.758 | 3.632 | 0.0193 | 0.0923 | 0.0730 | 0.324 | 40.302 |
| 2.942 | 0.853 | 3.688 | 0.0217 | 0.0937 | 0.0720 | 0.325 | 40.856 |
| 2.942 | 0.853 | 3.691 | 0.0217 | 0.0938 | 0.0721 | 0.325 | 40.813 |
| 2.942 | 0.843 | 3.692 | 0.0214 | 0.0938 | 0.0724 | 0.325 | 40.655 |

# BIOGRAPHICAL SKETCH

Eleazar Marquez was born in Houston, Texas on September 19th, 1985. A year after he was born, his family moved to Mercedes, Texas, where he was raised and attended school. After graduating as the fourth-top student from Mercedes High School in 2004, he enrolled at The University of Texas-Pan American and received a Bachelor of Science in Mechanical Engineering on December 2008. As an undergraduate student, Eleazar completed an internship with Texas Department of Transportation in the summer of 2006, where he generated several drawings for the Chief Engineer.

Following his graduation, he decided to enter graduate school in the spring of 2009 and pursue a master's degree in Mechanical Engineering. As a graduate student, Eleazar was granted an assistantship to conduct research in the area of Dynamics and Controls. For his research, he completed his master's thesis and wrote a paper called *Development and Testing of an Actively Adjustable Spring Mechanism* which was selected for publication. He graduated on December 2010 with a Master of Science in Mechanical Engineering and is currently pursuing a doctoral degree at Rice University.

Eleazar can be reached at his permanent mailing address: 1104 Valle Verde Dr., Mercedes, TX, 78570.